

INFORMATION TO USERS

This manuscript has been reproduced from the microfilm master. UMI films the text directly from the original or copy submitted. Thus, some thesis and dissertation copies are in typewriter face, while others may be from any type of computer printer.

The quality of this reproduction is dependent upon the quality of the copy submitted. Broken or indistinct print, colored or poor quality illustrations and photographs, print bleedthrough, substandard margins, and improper alignment can adversely affect reproduction.

In the unlikely event that the author did not send UMI a complete manuscript and there are missing pages, these will be noted. Also, if unauthorized copyright material had to be removed, a note will indicate the deletion.

Oversize materials (e.g., maps, drawings, charts) are reproduced by sectioning the original, beginning at the upper left-hand corner and continuing from left to right in equal sections with small overlaps.

Photographs included in the original manuscript have been reproduced xerographically in this copy. Higher quality 6" x 9" black and white photographic prints are available for any photographs or illustrations appearing in this copy for an additional charge. Contact UMI directly to order.

**ProQuest Information and Learning
300 North Zeeb Road, Ann Arbor, MI 48106-1346 USA
800-521-0600**

UMI[®]

University of Alberta

**Estimation of Liquefaction-induced Ground Deformations by CPT&SPT-based
Approaches**

by

Guangwen Zhang ©

**A thesis submitted to the Faculty of Graduate Studies and Research
In partial fulfillment of the requirements for the degree of
Doctor of Philosophy**

in

Geotechnical Engineering

Department of Civil and Environmental Engineering

Edmonton, Alberta

Fall 2001



**National Library
of Canada**

**Acquisitions and
Bibliographic Services**

**395 Wellington Street
Ottawa ON K1A 0N4
Canada**

**Bibliothèque nationale
du Canada**

**Acquisitions et
services bibliographiques**

**395, rue Wellington
Ottawa ON K1A 0N4
Canada**

Your file Votre référence

Our file Notre référence

The author has granted a non-exclusive licence allowing the National Library of Canada to reproduce, loan, distribute or sell copies of this thesis in microform, paper or electronic formats.

The author retains ownership of the copyright in this thesis. Neither the thesis nor substantial extracts from it may be printed or otherwise reproduced without the author's permission.

L'auteur a accordé une licence non exclusive permettant à la Bibliothèque nationale du Canada de reproduire, prêter, distribuer ou vendre des copies de cette thèse sous la forme de microfiche/film, de reproduction sur papier ou sur format électronique.

L'auteur conserve la propriété du droit d'auteur qui protège cette thèse. Ni la thèse ni des extraits substantiels de celle-ci ne doivent être imprimés ou autrement reproduits sans son autorisation.

0-612-69023-7

Canada

University of Alberta

Library Release Form

Name of Author: Guangwen Zhang

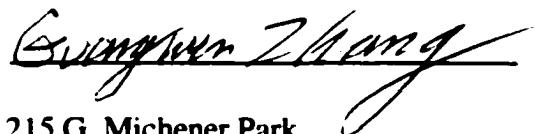
Title of Thesis: Estimation of Liquefaction-induced Ground Deformations by
CPT&SPT-based Approaches

Degree: Doctor of Philosophy

Year this Degree Granted: 2001

Permission is hereby granted to the University of Alberta Library to reproduce single copies of this thesis and to lend or sell such copies for private, scholarly, or scientific research purposes only.

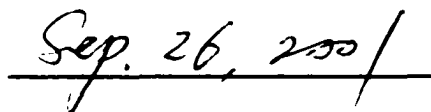
The author reserves all other publication and other rights in association with the copyright in the thesis, and except as herein before provided, neither the thesis nor any substantial portion thereof may be printed or otherwise reproduced in any material form whatever without the author's prior written permission.



215 G, Michener Park

Edmonton, Alberta

Canada, T6H 4M5



Date submitted to the Faculty of
Graduate Studies and Research

University of Alberta

Faculty of Graduate Studies and Research

The undersigned certify that they have read, and recommended to the Faculty of Graduate Studies and Research for acceptance, a thesis entitled **Estimation of Liquefaction-induced Ground Deformations by CPT&SPT-based Approaches** submitted by **Guangwen Zhang** in partial fulfillment of the requirements for the degree of Doctor of Philosophy in Geotechnical Engineering.




Dr. P.K. Robertson (Supervisor)



Dr. R. Brachman (Co-Supervisor)



Dr. D. Chan



Dr. D. Tannant



Dr. K. Fyfe



Dr. T.L. Youd (External Examiner)

September 18, 2001
Date of Approval by Committee

Dedicated to

***The strength of my father,
Liang Zhang***

and

***the everlasting memory of my mother,
Hong-Rong Zheng***

ABSTRACT

Earthquake shaking may result in the liquefaction of saturated sandy soils in the ground. Both ground settlements and lateral spreads are the pervasive types of liquefaction-induced ground deformations for level to gently sloping sites. Currently, the estimations of liquefaction-induced ground deformations are less successful than the evaluations of liquefaction potential. In particular, no CPT-based method is available to estimate ground settlements and lateral displacements.

The objective of this thesis was to develop approaches to estimate liquefaction-induced ground deformations using either CPT or SPT data. First, a CPT-based approach is proposed to estimate liquefaction-induced ground settlements for level ground. The approach combines a CPT-based method to estimate liquefaction resistance with laboratory test results on clean sand to evaluate liquefaction-induced volumetric strains for sandy and silty soils. The approach was used to estimate the ground settlements at two case history sites. Good agreement between the calculated and measured ground settlements was found. Second, three simple, semi-empirical approaches are proposed to estimate lateral displacements in liquefaction-induced lateral spreads for gently sloping ground without a free face, level ground with a free face, and gently sloping ground with a free face respectively. The proposed approaches combine available results from laboratory tests with data from sixteen case histories associated with past thirteen major earthquakes, capture the mechanisms of liquefaction-induced lateral spreads, and characterize the major factors (soil properties, earthquake characteristics, and ground geometry) influencing lateral displacements. Either SPT or CPT data can be used in the

proposed approaches to estimate lateral displacements. Generally, the calculated lateral displacements using the proposed approaches showed variations between 50% and 200% of measured values for the available case histories studied in this research. The proposed approaches may be used to estimate both the magnitude and distribution of liquefaction-induced lateral displacements for gentle slopes and/or ground with a free face for low to medium-risk projects or to provide preliminary estimates for high-risk projects using either SPT or CPT data. The proposed approaches are relatively simple and can be applied with only a few additional calculations following an SPT- or CPT-based liquefaction-potential analysis.

ACKNOWLEDGEMENTS

I would like to express my sincere gratitude to my supervisors, Dr. Peter K. Robertson and Dr. Richard W. I. Brachman, for their guidance and encouragement throughout this work. Their support throughout the research and writing of this thesis is gratefully appreciated. Dr. Robertson understood what I wanted to say long before I did and believed that there was a point in saying it. He possesses a seemingly endless supply of ideas, many of which have been incorporated into this research. Dr. Brachman's inquisitiveness, critical thinking, and high standards greatly enhanced the quality of this work. I was very fortunate to have the privilege of conducting this research under their guidance.

I thank the other staff members in the Geotechnical Group at the University of Alberta for the support that they have provided for this research as well as the wealth of knowledge they have passed on through discussions and class lectures. Special thanks to Dr. Norbert R. Morgenstern for his encouragement at the beginning of my application for this Ph.D. program and for his help during this study and to Sally Petaske for always being helpful.

Collecting data from case histories was an essential task in this study. The lateral spread database compiled by Dr. Steven F. Bartlett and later then published by Dr. T. Leslie Youd of Brigham Young University, Provo, Utah, on his homepage for researchers to download is a highly valuable source of case history data. Their generosity significantly facilitated the collection of the case history data, especially for the case sites in Niigata City during the 1964 Niigata earthquake, for this research. In addition, Dr. Ronaldo Luna of Tulane University provided me with the CPT soundings tested in Treasure Island, and Dr. Jean-Pierre Bardet of the University of Southern California sent me a technical report about the site investigation of the Marina District of San Francisco. The assistance of these individuals is greatly appreciated.

I gratefully acknowledge the financial support provided by the University of Alberta for awarding me an FS Chia PhD Scholarship, which made my study in Canada financially possible and later a Coal Mining Research Company Graduate Scholarship. In addition, research funding provided by the Natural Science and Engineering Research Council of Canada (NSERC) is also greatly appreciated.

I would especially like to recognize the contributions and many helpful suggestions provided by my dissertation examining committee: Professors Richard W. I. Brachman, Dave Chan, Ken R. Fyfe, Peter K. Robertson, Dwayne Tannant, and T. Leslie Youd. Special thanks are extended to my friends and colleagues in China, including Prof. Bihong Chen, Mr. Yujun Chen, Dr. Zhonghua Chen, Dr. Zuyu Chen, Mrs. Shunhua Deng, Dr. Jingshen Jia, Mr. Yishen Li, Dr. Longtan Shao, Mr. Xiaodong Yang, and Prof. Bofang Zhu, for their friendship as well as encouragement. I also thank my fellow graduate students, too numerous to name here individually, for their friendship, challenging discussions, and fresh ideas. Mr. Dave Clyburn of the Academic Support Centre assisted me during the final stages of this work by proofreading this manuscript. His help was highly valuable and is greatly appreciated.

Finally, I would like to express my utmost gratitude and appreciation to all of my family for their understanding and support. I could not have achieved what I have without their sacrifices. The greatest thanks should go to my wife, Wentao Xue, whose love, patience, and support sustained me through the most difficult years of this work. Thanks to my daughter, Marissa, and my son, Derrick, for their cooperation and understanding and for giving me tons of great fun.

CHAPTER 1 INTRODUCTION	1
1.1 General	1
1.2 Scope and Objectives	4
1.3 Thesis Organization.....	5
CHAPTER 2 SOIL LIQUEFACTION AND ITS EVALUATION.....	9
2.1 Definition of Soil Liquefaction	9
2.2 Failures Resulting from Soil Liquefaction	9
2.2.1 <i>Sand boil</i>	10
2.2.2 <i>Ground oscillation</i>	10
2.2.3 <i>Ground settlement</i>	10
2.2.4 <i>Flow failure</i>	11
2.2.5 <i>Lateral spreads</i>	11
2.2.6 <i>Engineered structure failures</i>	12
2.3 Factors Influencing Liquefaction Resistance of Soils.....	12
2.3.1 <i>Soil density</i>	13
2.3.2 <i>Soil composition and grain characteristics</i>	13
2.3.3 <i>In-situ stress condition</i>	14
2.3.4 <i>Soil structure and age</i>	15
2.3.5 <i>Previous strain history</i>	16
2.4 Review of Liquefaction Potential Evaluation	17
2.5 The NCEER SPT-based Method for Liquefaction Potential Analysis	19
2.5.1 <i>Standard penetration test (SPT)</i>	19
2.5.2 <i>The NCEER SPT-based method</i>	19
2.6 The NCEER CPT-based Methods for Liquefaction Potential Analysis	21
2.6.1 <i>Cone penetration test (CPT)</i>	21

2.6.2	<i>The NCEER CPT-based method</i>	22
2.7	Summary	23

CHAPTER 3 ESTIMATION OF LIQUEFACTION-INDUCED GROUND SETTLEMENTS FOR LEVEL GROUND BY A CPT-BASED APPROACH 32

3.1	Introduction	32
3.2	A CPT-based Approach to Estimate Liquefaction-induced Ground Settlements.	33
3.2.1	<i>Post-liquefaction volumetric strain from laboratory tests</i>	33
3.2.2	<i>Relative density from CPT</i>	34
3.2.3	<i>Correction for grain characteristics</i>	35
3.2.4	<i>Calculating ground settlement</i>	36
3.3	Evaluation of the Proposed CPT-based Approach by Case Histories.....	38
3.3.1	<i>Marina District</i>	38
3.3.2	<i>Treasure Island</i>	41
3.4	Effects of Other Major Factors on Calculated Settlements.....	43
3.4.1	<i>Maximum surface acceleration</i>	43
3.4.2	<i>Fines content or mean grain size</i>	44
3.4.3	<i>Transitional zone or thin sandy soil layers</i>	46
3.4.4	<i>The three dimensional distribution of liquefied soil layers</i>	47
3.4.5	<i>Correction factor K_c</i>	49
3.4.6	<i>A cutoff line of I_c equal to 2.6</i>	50
3.5	Recommendations	51
3.6	Summary and Conclusions.....	53

CHAPTER 4 THE MECHANISMS AND MAJOR CONTROLLING FACTORS OF LIQUEFACTION-INDUCED LATERAL SPREADS..... 67

4.1 Introduction	67
4.2 The Mechanisms and Displacement Modes of Liquefaction-induced Lateral Spread	68
4.2.1 <i>Introduction</i>	68
4.2.2 <i>Results from one-g shake-table testing</i>	69
4.2.3 <i>Results from centrifuge modeling</i>	69
4.2.4 <i>Observations from case histories</i>	70
4.2.5 <i>Discussion and Summary</i>	71
4.3 Soil Characteristics.....	72
4.3.1 <i>The effects of soil properties</i>	72
4.3.2 <i>The role of soil-dilative response at large strain</i>	74
4.4 Earthquake Characteristics.....	76
4.4.1 <i>The effects of earthquake characteristics</i>	76
4.4.2 <i>The role of inertial forces</i>	77
4.5 Ground Geometry and In-situ Shear Stress.....	79
4.5.1 <i>The effects of ground geometry</i>	79
4.5.2 <i>The role of in-situ static shear stress</i>	80
4.6 Boundaries and the Three-dimensional Distribution of Liquefied Layers.....	81
4.6.1 <i>The effects of the three-dimensional distribution of liquefied layers</i>	81
4.6.2 <i>The effects of boundaries</i>	82
4.7 Redistribution and Drainage of Excess Pore Pressures.....	83
4.7.1 <i>The effect of the redistribution of pore water in an undrained liquefied layer</i>	83
4.7.2 <i>The effects of the drainage of excess pore pressures in a liquefied layer</i>	84
4.8 Acceleration Isolation due to Liquefaction of Underlying Soils.....	85
4.8.1 <i>Isolation of acceleration</i>	85

4.8.2	<i>The effects of acceleration isolation due to liquefaction of underlying soils</i>	87
4.8.3	<i>The effects of liquefaction sequence of multiple liquefied layers</i>	88
4.9	Conclusions	89

CHAPTER 5 PREVIOUS RESEARCH ON ESTIMATING HORIZONTAL GROUND DISPLACEMENTS ASSOCIATED WITH LIQUEFACTION-INDUCED LATERAL SPREADS..... 108

5.1	Introduction	108
5.2	Laboratory Scale Model Simulations	108
5.2.1	<i>Shake-table modeling</i>	108
5.2.2	<i>Centrifuge modeling</i>	109
5.3	Simplified Analytical Methods	111
5.3.1	<i>Sliding block analysis</i>	111
5.3.2	<i>Towhata's minimum potential energy approach</i>	113
5.3.3	<i>Shamoto's residual shear strain charts</i>	115
5.4	Stress-deformation Analysis	116
5.4.1	<i>The strain potential approach</i>	116
5.4.2	<i>The stiffness or strength reduction approach</i>	116
5.4.3	<i>The nonlinear analysis approach</i>	117
5.4.4	<i>Summary of stress-deformation analysis approaches</i>	118
5.5	Empirical Models	120
5.5.1	<i>Hamada's empirical model</i>	120
5.5.2	<i>Youd and Perkins' LSI model</i>	121
5.5.3	<i>Bartlett and Youd's MLR model</i>	122
5.5.4	<i>The modified Bartlett and Youd's MLR model</i>	124
5.5.5	<i>Rauch and Martin's EPOLLS model</i>	126
5.6	Discussion and Conclusions	128

CHAPTER 6 ESTIMATION OF THE LATERAL DISPLACEMENT INDEX FROM SPT OR CPT DATA	131
6.1 Introduction	131
6.2 Estimation of the Maximum Shear Strains from SPT or CPT Data.....	132
6.2.1 <i>The maximum shear strains of clean sands as determined by laboratory testing</i>	<i>132</i>
6.2.2 <i>Estimation of the maximum shear strains using SPT or CPT data for clean sands</i>	<i>134</i>
6.2.3 <i>Estimation of the maximum shear strains using SPT or CPT data for silty sands or sandy silts</i>	<i>135</i>
6.3 Estimation of the Lateral Displacement Index of Sandy Soils using SPT or CPT Data	137
6.4 Effects of Other Major Factors on Calculated Lateral Displacement Index	138
6.4.1 <i>Maximum surface acceleration.....</i>	<i>138</i>
6.4.2 <i>Transitional zone or thin sandy soil layers.....</i>	<i>139</i>
6.4.3 <i>Correction factor K_c in the NCEER CPT-based method</i>	<i>140</i>
6.4.4 <i>A cutoff line of I_c equal to 2.6 in the NCEER CPT-based method.....</i>	<i>140</i>
6.5 Discussion and conclusions.....	141

CHAPTER 7 ESTIMATION OF LIQUEFACTION-INDUCED LATERAL DISPLACEMENTS FOR GENTLY SLOPING GROUND WITHOUT A FREE FACE USING SPT OR CPT DATA..... 151

7.1 Introduction	151
7.2 Geometric Parameters for Gently Sloping Ground.....	152
7.2.1 <i>Lateral displacement patterns in gently sloping ground.....</i>	<i>152</i>

7.2.2	<i>Selection of a major geometric parameter for gently sloping ground</i>	154
7.3	Case Histories	155
7.3.1	<i>Collection of case histories</i>	155
7.3.2	<i>Case sites in San Francisco during the 1906 San Francisco, California, Earthquake</i>	156
7.3.3	<i>The case site in the Furu-Sumida Creek area, Tokyo during the 1923 Kanto, Japan, Earthquake</i>	158
7.3.4	<i>Case sites in Fukui Plain during the 1948 Fukui, Japan, Earthquake</i>	158
7.3.5	<i>Case sites in Niigata City during the 1964 Niigata, Japan, Earthquake</i>	159
7.3.6	<i>The Juvenile Hall case history during the 1971 San Fernando, California, Earthquake</i>	160
7.3.7	<i>Case sites in Noshiro City during the 1983 Nihonkai-Chubu, Japan, Earthquake</i>	162
7.4	Estimating Equivalent CPT Data from SPT Data	163
7.4.1	<i>The soil behavior type index and fines content</i>	163
7.4.2	<i>Converting SPT data to equivalent CPT data</i>	165
7.5	Establishment of Correlation among Lateral Displacement, Lateral Displacement Index, and Ground Slope for Gently Sloping Ground without a Free Face	166
7.5.1	<i>Correlation between LD/LDI and ground slope using SPT data</i>	167
7.5.2	<i>Correlation between LD/LDI and ground slope using CPT data</i>	168
7.6	An Approach to Estimate Liquefaction-induced Lateral Displacements Using SPT or CPT Data for Gently Sloping Ground without a Free Face	170
7.7	Performance of the Proposed Approach	172
7.7.1	<i>Accuracy of the proposed approach</i>	172
7.7.2	<i>Comparison with the MLR model of Youd et al. (1999)</i>	173
7.8	Discussion	175
7.9	Conclusions	176

CHAPTER 8 ESTIMATION OF LIQUEFACTION-INDUCED LATERAL DISPLACEMENTS FOR LEVEL GROUND WITH A FREE FACE USING SPT OR CPT DATA.....	194
8.1 Introduction	194
8.2 Geometric Parameters for Level Ground with A Free Face.....	194
8.2.1 <i>Lateral displacement patterns in level ground with a free face.....</i>	<i>194</i>
8.2.2 <i>Selection of a major geometric parameter for level ground with a free face</i>	<i>195</i>
8.3 Case Histories.....	196
8.3.1 <i>Portage Creek #1 and Twenty Mile River case sites, Alaska during the 1964 Alaska, Earthquake</i>	<i>196</i>
8.3.2 <i>Case sites in Niigata City during the 1964 Niigata, Japan, Earthquake</i>	<i>197</i>
8.3.3 <i>The Jensen Filtration Plant case site, San Fernando during the 1971 San Fernando, California, Earthquake</i>	<i>199</i>
8.3.4 <i>Case sites in Moss Landing, California during the 1989 Loma Prieta, California, Earthquake</i>	<i>200</i>
8.3.5 <i>Case sites in Dagupan City, Philippines during the 1990 Luzon, Philippines, Earthquake.....</i>	<i>201</i>
8.3.6 <i>Case sites around the Kobe Port during the 1995 Hyogoken-Nanbu (Kobe), Japan, Earthquake</i>	<i>202</i>
8.4 Establishment of the Correlation between LD, LDI, and L/H Using SPT or CPT Data	203
8.4.1 <i>Development of the correlation between LD, LDI, and L/H using SPT data</i>	<i>204</i>
8.4.2 <i>Development of the correlation between LDI, LD, and L/H using CPT data</i>	<i>205</i>
8.5 An Approach to Estimate Liquefaction-induced Lateral Displacements for Level Ground with a Free Face Using SPT or CPT Data	207
8.6 Performance of the Proposed Approach.....	209

8.6.1	<i>Accuracy of the proposed approach.....</i>	209
8.6.2	<i>Comparison with the profile of field lateral displacements measured by inclinometers.....</i>	210
8.6.3	<i>Comparison with the MLR model of Youd et al. (1999).....</i>	212
8.7	Lateral Spreads Restricted by Engineered Structures	213
8.8	Discussion	214
8.9	Conclusions	215

CHAPTER 9 ESTIMATION OF LIQUEFACTION-INDUCED LATERAL DISPLACEMENTS FOR GENTLY SLOPING GROUND WITH A FREE FACE USING SPT OR CPT DATA..... 231

9.1	Introduction	231
9.2	Geometric Parameters for Gently Sloping Ground with A Free Face	231
9.3	Case Histories.....	232
9.3.1	<i>Case sites in Niigata City during the 1964 Niigata, Japan, Earthquake ...</i>	232
9.3.2	<i>The Heber Road case history during the 1979 Imperial Valley, California, Earthquake.....</i>	233
9.3.3	<i>The Wildlife case history during the 1987 Superstition Hills, California, Earthquake.....</i>	234
9.3.4	<i>Case sites in Shiribeshi River area, Japan during the 1993 Hokkaido-nansei-oki, Japan, Earthquake</i>	235
9.4	Evaluation of Superimposition Approach	236
9.5	A Preliminary Approach to Estimate Lateral Displacements for Gently Sloping Ground with A Free Face Using SPT or CPT Data	238
9.6	Performance of the Preliminary Approach.....	241
9.7	Discussion	241

9.8 Conclusions	242
CHAPTER 10 GENERAL DISCUSSION AND CONCLUSIONS	251
10.1 Soil Liquefaction	251
10.2 Estimation of Liquefaction-induced Ground Settlements	252
<i>10.2.1 Overview.....</i>	<i>252</i>
<i>10.2.2 The proposed CPT-based approach.....</i>	<i>253</i>
10.3 The Mechanisms and Controlling Factors of Liquefaction-induced Lateral Spreads	255
10.4 Previous Research on Estimating Liquefaction-induced Lateral Displacements	256
10.5 Estimation of Liquefaction-induced Lateral Displacements Using SPT or CPT Data	259
<i>10.5.1 The proposed approaches for estimating liquefaction-induced lateral displacements using SPT or CPT data</i>	<i>259</i>
<i>10.5.2 Performance of the proposed approaches</i>	<i>261</i>
<i>10.5.3 Advantages of the proposed approaches.....</i>	<i>261</i>
<i>10.5.4 Limitations of the proposed approaches.....</i>	<i>262</i>
<i>10.5.5 Application of the proposed approaches.....</i>	<i>264</i>
10.6 Recommendations for Future Work.....	265
APPENDIX A: LISTING OF THE DATABASES IN THIS RESEARCH.....	290
APPENDIX B: FIGURES SHOWING ESTIMATION LIQUEFACTION-INDUCED LATERAL DISPLACEMENTS WITH DEPTH FOR THE THREE SITES AT THE MOSS LANDING CASE HISTORY.....	310

LIST OF TABLES

Table 2.1 Terminology of liquefaction recommended by Robertson (1994) and Fear (1996)	25
Table 3.1 Comparison of the liquefaction-induced ground settlements measured and calculated using the proposed CPT-based method for the Marina District	54
Table 3.2 Comparison of the liquefaction-induced ground settlements measured and calculated using the SPT based method and the proposed CPT-based method for the Marina District	55
Table 3.3 Comparison of the liquefaction-induced ground settlements measured and calculated using the proposed CPT-based method for Treasure Island	56
Table 3.4 Recorded, calculated, and assumed a_{max} associated with the Marina District during the Loma Prieta earthquake	57
Table 3.5 The ground settlements measured and calculated using the CPT-based approach with and without some modifications for the Marina District and Treasure Island..	58
Table 7.1 Summary of the major parameters for case histories for gently sloping ground without a free face	178
Table 7.2 Boundaries of Soil Behaviour Type.....	179
Table 8.1 Summary of the major parameters for case histories for nearly level ground with a free face	217
Table 9.1 Summary of the major parameters for the available case histories for gently sloping ground with a free face	244
Table A1 A summary of the data used in this thesis for gently sloping ground without a free face.....	279
Table A2 A summary of the data used in this thesis for level ground with a free face...	285
Table A3 A summary of the data used in this research for gently sloping ground with a free face.....	293

LIST OF FIGURES

Figure 1.1 A sketch illustrating the development of liquefaction-induced ground settlements in level ground during earthquake shaking	7
Figure 1.2 A sketch illustrating the development of liquefaction-induced lateral spread in gently sloping ground or ground with a free face during earthquake shaking	8
Figure 2.1 Flowchart for estimating cyclic resistance ratio at earthquake moment magnitude of 7.5, $CRR_{7.5}$, using the NCEER SPT-based method (Youd et al. 2001)	26
Figure 2.2 Flowchart for calculating factor of safety against liquefaction (FS) by the NCEER SPT- or CPT-based method (Youd et al. 2001)	27
Figure 2.3 Example plots illustrating the major steps in evaluating liquefaction potential using the NCEER SPT-based method and SPT data	28
Figure 2.4 A cross section of a typical cone for the electric cone penetration test (CPT)	29
Figure 2.5 Flowchart for estimating $CRR_{7.5}$ using the NCEER CPT-based method	30
Figure 2.6 Example plots illustrating the major steps in evaluating liquefaction potential using the NCEER CPT-based method with CPT data	31
Figure 3.1 Curves for estimating post-liquefaction volumetric strain of clean sands	59
Figure 3.2 Relationship between ϵ_v and $(q_{c1N})_{cs}$ for different factor of safety (FS)	60
Figure 3.3 A flowchart illustrating the application of the proposed CPT-based approach to estimate liquefaction-induced ground settlement on level ground	61
Figure 3.4 Example plots illustrating the major steps in performing liquefaction potential analysis using the NCEER CPT-based method	62
Figure 3.5 Example plots illustrating the major steps in estimating liquefaction-induced ground settlements using the proposed CPT-based approach	63
Figure 3.6 Plan view of the geologic units and CPT locations at the Marina District	64
Figure 3.7 Typical geological profile at Treasure Island	64
Figure 3.8 Effect of inputted peak surface acceleration on calculated settlements for some CPTs at the Marina District	65

Figure 3.9 Sketches illustrating three-dimensional distribution of liquefied layers (a) deep liquefied soil layer (b) shallow liquefied soil layer (c) multiple liquefied layers (d) localized liquefied layer.....	66
Figure 4.1 An example of time history of lateral displacement in one of the one-g shake-table tests by Sasaki et al (1991).....	92
Figure 4.2 Relationship between thickness of loose sand layer and average displacement in one-g shake-table test by Miyajima et al. (1991).....	93
Figure 4.3 An example of lateral displacements in one-g shake-table test by Yasuda et al. (1992).....	94
Figure 4.4 An example of the model setup and measured lateral displacements in one of the centrifuge model tests by Abdoun (1997).....	95
Figure 4.5 An example of the profiles of the measured lateral displacements and shear strains in one of the centrifuge model tests by Taboada and Dobry (1998).....	96
Figure 4.6 Patterns of lateral displacements in centrifuge modeling tests by Fiegel and Kutter (1994b).....	97
Figure 4.7 Filed measurements of lateral displacements with depth by the inclinometers at one of the Moss Landing case history sites during the 1989 Loma Prieta earthquake (modified from Boulanger et al. (1995)).....	98
Figure 4.8 Axial strain vs. number of cycles for a sand with different relative density, D_r , in cyclic triaxial tests by Seed and Lee (1966).....	99
Figure 4.9 Time histories of strain, stress, and excess pore pressure (EPP) for an undrained stress-controlled cyclic triaxial test of Nevada Sand ($D_r = 40\%$) with an imposed static (initial) deviatoric stress tested by Arulmoli et al. (1992).....	99
Figure 4.10 Liquefaction-induced permanent lateral displacement vs. prototype slope angle for sloping ground in centrifuge model tests by Taboada and Dobry (1996)	100
Figure 4.11 Sketches illustrating the potential vertical distribution of a liquefied sand later in a sloping ground.....	100
Figure 4.12 Sketches illustrating the potential vertical distribution of a liquefied sand layer in ground with a free face.....	101
Figure 4.13 An example of non-homogenous soil layers and related liquefaction-induced	

lateral displacements in the field (Section S-1 in Noshira City under the 1983 Nihonkai-Chubu earthquake).....	102
Figure 4.14 Recorded seismic motions in the vertical array of seismometers at Kobe Port Island during the 1995 Hyogoken-Nambu earthquake	103
Figure 4.15 Time histories of the acceleration at the different depths in a loose sand in a large shake-table test by Kanatani et al. (1995)	103
Figure 4.16 Lateral accelerations at the different depths in a sloping ground with the field slope angle of 1.3° in a cyclic centrifuge model test by Taboada (1995)	104
Figure 4.17 Acceleration time histories recorded at the ground surface for level and sloping grounds with the different slope angles in cyclic centrifuge model tests by Taboada (1995)	105
Figure 4.18 Profiles of liquefaction-induced lateral displacements at the end of shaking for sloping grounds with the different slope angles (or slope) in the field, α_{field} , in cyclic centrifuge model tests by Taboada (1995).....	106
Figure 4.19 Sketches illustrating the potential vertical distribution of two liquefiable layers in a sloping ground	107
Figure 6.1 A flowchart illustrating the components dominating magnitude of lateral displacements in a liquefaction-induced lateral spread.....	143
Figure 6.2 Cyclic shear stress-strain curves and the maximum shear strain from an undrained cyclic simple shear test for a clean sand without biased static shear stresses.....	144
Figure 6.3 Relationships between factor of safety and maximum shear strain for clean sands from laboratory tests.....	145
Figure 6.4 Limiting shear strains in laboratory cyclic simple shear tests	145
Figure 6.5 Relationships between maximum shear strain and factor of safety for different relative densities (D_r) for clean sands	146
Figure 6.6 A flowchart illustrating the major procedures in calculating lateral displacement index (LDI).....	147
Figure 6.7 Example plots illustrating major procedures in calculating lateral displacement index (LDI) using the SPT-based approach with SPT data	148

Figure 6.8 Example plots illustrating major procedures in calculating lateral displacement index (LDI) using the CPT-based approach with CPT data.....	149
Figure 7.1 Conceptual flow chart for developing an empirical correlation between LD, LDI, and S for gently sloping ground without a free face.....	180
Figure 7.2 Lateral displacement patterns observed in a gently sloping ground with various slopes in a case site under the 1983 Nihonkai-Chubu earthquake	181
Figure 7.3 A sketch illustrating (a) geometric parameters and (b) lateral displacement patterns in a gently sloping ground	182
Figure 7.4 Definition of ground slope, S, in gentle slope ground: (a) single slope (b) multiple slopes.....	183
Figure 7.5 Relationship between the soil behaviour type index (I_c) calculated from CPT and fines content (FC).....	184
Figure 7.6 CPT - SPT correlations with mean grain size.....	185
Figure 7.7 Relationship between the ratio of measured lateral displacement (LD) to lateral displacement index (LDI) and ground slope for the data of which the values of LDI were calculated using SPT data for five case histories for gently sloping ground without a free face.....	186
Figure 7.8 Relationship between the ratio of measured lateral displacement (LD) and lateral displacement index (LDI) and ground slope for the data of which the values of LDI were calculated using in-situ CPT data for two case histories for gently sloping ground without a free face.....	187
Figure 7.9 Relationship between the ratio of measured lateral displacement (LD) and lateral displacement index (LDI) and ground slope for the data of which the values of LDI were calculated using the equivalent CPT data that were converted from SPT data for four case histories for gently sloping ground without a free face.....	188
Figure 7.10 A flow chart illustrating the application of the proposed approach to estimate lateral displacements in a liquefaction-induced lateral spread for gently sloping ground without a free face using SPT or CPT data.....	189
Figure 7.11 Comparison of the values of lateral displacements measured at sites for the five case histories and calculated using the proposed approach with SPT data for	

gently sloping ground without a free face	190
Figure 7.12 Comparison of the values of lateral displacements measured at sites for six case histories and calculated by the proposed approach using in-situ or equivalent CPT data for gently sloping ground without a free face	191
Figure 7.13 Comparison of lateral displacements measured at sites for the Niigata case history and calculated by the proposed approach and by the MLR model of Youd et al. (1999) for gently sloping ground without a free face.....	192
Figure 7.14 Comparison of lateral displacements calculated by the proposed approach and by the MLR model of Youd et al. (1999) for different ground slope for the Niigata case history for gently sloping ground without a free face	193
Figure 8.1 A sketch illustrating (a) geometric parameters and (b) lateral displacement patterns on level ground with a free face	218
Figure 8.2 Definition of free face height (H) and the distance to a free face (L) for level ground with a free face.....	219
Figure 8.3 Conceptual flow chart for developing an empirical correlation between LD/LDI and L/H for level ground with a free face	220
Figure 8.4 Relationship between LD/LDI and L/H for the data of which the values of LDI were calculated using SPT data for the available four case histories for level ground with a free face	221
Figure 8.5 Relationship between LD/LDI and L/H for the data of which the values of LDI were calculated using in-situ CPT data for the Moss Landing case history for level ground with a free face.....	222
Figure 8.6 Relationship between LD/LDI and L/H for the data of which the values of LDI were calculated using the equivalent CPT data that were converted from SPT data for the four case histories where only SPT data were available for level ground with a free face	223
Figure 8.7 A flowchart illustrating major steps in the application of the proposed approach to estimate lateral displacements in a liquefaction-induced lateral spread for level ground with a free face using SPT or CPT data	224
Figure 8.8 Comparison of lateral displacements measured at sites for the four case	

histories and calculated by the proposed approach using SPT data for level ground with a free face	225
Figure 8.9 Comparison of lateral displacements measured at sites for the five case histories and calculated by the proposed approach using in-situ or equivalent CPT data for level ground with a free face.....	226
Figure 8.11 Comparison of lateral displacements measured at sites for two case histories and calculated by the proposed approach and by the MLR model of Youd et al. (1999) for level ground with a free face.....	228
Figure 8.12 Comparison of lateral displacements calculated by the proposed approach and by the MLR model of Youd et al. (1999) for different L/H ratios for two case histories for level ground with a free face.....	229
Figure 8.13 Relationship between ratio of measured lateral displacement (LD) to the lateral displacement index (LDI) and L/H for the Kobe Port case history where quay walls restricted the lateral displacements of the ground	230
Figure 9.1 A sketch illustrating geometric parameters in different zones for gently sloping ground with a free face.....	245
Figure 9.2 Comparison of lateral displacements measured at case history sites and calculated using the superimposition approach for gently sloping ground with a free face	246
Figure 9.3 Relationship between the ratio of measured lateral displacement (LD) to the lateral displacement index (LDI) and L/H for the available four case histories for gently sloping ground with a free face.....	247
Figure 9.4 Relationship between ground slope and its effect on LD/LDI for the available four case histories for gently sloping ground with a free face	248
Figure 9.5 A flow chart illustrating the application of the preliminary approach to estimate lateral displacements in a liquefaction-induced lateral spread using SPT or CPT data for gently sloping ground with a free face	249
Figure 9.6 Comparison of lateral displacements measured at the available four case history sites and calculated using the preliminary approach for gently sloping ground with a free face	250

CHAPTER 1 INTRODUCTION

1.1 General

It is widely recognized that earthquakes are among the most severe natural disasters. For instance, in 1976, the Tangshan, China earthquake resulted in the collapse of and severe damage to many buildings and in the death of several hundred thousand people (NRC 1982). The 1995 Hyogoken-Nanbu (Kobe), Japan earthquake caused more than one hundred billion dollars in total damage (Hamada et al. 1995). Nevertheless, earthquakes cannot be prevented from occurring and will remain one of the major natural hazards in the world.

Earthquake shaking may cause a loss of strength or stiffness in a saturated sandy soil in the ground. The process leading to such a loss of strength or stiffness is called soil liquefaction. The consequences of soil liquefaction can be enormous, with significant financial and environmental implications and risks to human safety. During past major earthquakes, enormous damage to engineered structures and lifelines has been caused by liquefaction-induced ground failures (Hamada and O'Rourke 1992; O'Rourke and Hamada 1992). For instance, liquefaction-induced lateral spreads spawned by the 1964 Alaska earthquake caused \$80 million damage to 266 bridges and numerous sections of embankments along the Alaska Railroad and Highway (McCulloch and Bonilla 1970; Bartlett 1991). Liquefaction-induced ground settlements that occurred in the Marina District and Treasure Island, California, as a result of the 1989 Loma Prieta earthquake, caused significant damage to buildings and lifelines (Bennett 1990; Egan and Wang 1991). Generally, liquefaction-induced ground failures include flow slides, lateral spreads, ground oscillation, ground settlements, and sand boils. In this thesis, research will focus on liquefaction-induced ground settlements and lateral spreads only.

Both ground settlements and lateral spreads are the pervasive types of liquefaction-

induced ground failures for level to gently sloping sites. Ground settlements may occur in both level and sloping ground and generally are major deformation failures for level ground. Figure 1.1 is a sketch illustrating the development of liquefaction-induced ground settlement in level ground during and after an earthquake. When saturated sandy soils are subjected to shaking during an earthquake, excess pore water pressures are known to build up, leading to liquefaction or loss of strength in sandy soils. With the dissipation of the pore water pressure during and after an earthquake, some volume change in the sandy soils will occur, which is manifested on the ground surface as settlements.

Lateral spreads are the most common type of ground failure caused by soil liquefaction during earthquakes and usually occur on gentle slopes ranging from 0.3 to 5 percent (Youd 1978) or on level (or gently inclined) ground with a free face (e.g., river banks, sea walls, road cuts). Figure 1.2 is a sketch illustrating the development of liquefaction-induced lateral spread in gently sloping ground or ground with a free face during an earthquake. With the development of excess pore water pressure in saturated sandy soils during seismic loading, the stiffness of the soils is reduced, and shear strains are induced in the soils as well. Due to the presence of biased static driving shear stresses in the soils in gentle slopes or ground with a free face, residual shear strains are then accumulated in the down-slope direction or in the direction towards the free face. These residual shear strains result in lateral spreading of the ground. Different from flow failures, the ultimate undrained shear strengths in the soils are greater than the static driving shear stresses in the soils for lateral spreads. As a result, displacements associated with lateral spreads are finite and seldom catastrophic, yet still can be very damaging.

Several groups of methods have been proposed to estimate liquefaction-induced ground settlements or lateral displacements, including numerical and analytical models, laboratory modeling approaches, and field-data-based methods. The expense and difficulty associated with obtaining and testing high quality samples of loose sandy soils significantly limit the applications of numerical and analytical models and laboratory testing approaches in the routine practice of geotechnical engineering. Therefore, field-

data-based methods are likely best suited to provide simple, reliable and direct methods to estimate liquefaction-induced ground deformations (i.e. settlements and lateral displacements) for low to medium risk projects and to provide preliminary estimates for high risk projects.

Several field tests are commonly used for the evaluation of liquefaction resistance of sandy soils, including the cone penetration test (CPT), the standard penetration test (SPT), shear-wave velocity measurement, and the Becker penetration test. Recently, the CPT has become very popular because of its greater repeatability and reliability and the continuous nature of its profile as compared with other field tests. The CPT has also been widely and successfully used in evaluating liquefaction potential in geotechnical practice.

To date, an SPT-based method (Tokimatsu and Seed 1987) and an SPT&CPT-based method (Ishihara and Yoshimoni 1992) have been used to calculate liquefaction-induced ground settlements for clean sand only. A method to estimate liquefaction-induced ground settlements based on the CPT for all sandy soils has not yet been developed. Therefore, a simple CPT-based approach to estimate liquefaction-induced ground settlements is needed in the practice of geotechnical engineering.

Several field-data-based empirical methods (Hamada et al. 1986; Youd and Perkins 1987; Bartlett and Youd 1995; Youd et al. 1999; Rauch and Martin 2000) are available for estimating lateral displacements in a liquefaction-induced lateral spread. It is difficult to choose one empirical model over another since they all seem to give similar results within a factor of two or three. Generally, both Hamada's model and Youd and Perkins' model characterize only partial controlling factors that influence the magnitude of lateral spreading displacements and therefore are useful only in specific geological regions and for certain kinds of earthquakes. Rauch and Martin's SPT-based model is a useful tool for predicting average surface horizontal movements on a potential lateral spread. It is believed that Bartlett and Youd's SPT-based model provides better results since it takes into account all the major physical concepts that control displacement. The SPT-based

model of Youd et al. (1999), which is an updated version of Bartlett and Youd's SPT-based model, may be the best of the available empirical models to estimate lateral displacements in a liquefaction-induced lateral spread at this stage even though it still has some limitations. In summary, the available field-data-based methods are empirical and do not incorporate the extensive knowledge gained from laboratory studies of soil liquefaction. In addition, none of them can be used to estimate the distribution of lateral displacements with depth below the ground surface. Furthermore, no CPT-based method to estimate liquefaction-induced lateral displacements is currently available even though the CPT has greater repeatability and reliability, and provides a continuous profile compared with other field tests. Therefore, there is a need for simple, semi-empirical SPT- and CPT-based approaches to estimate both the magnitude and distribution of lateral displacements in a liquefaction-induced lateral spread on the basis of both laboratory test results and case history data.

1.2 Scope and Objectives

One of the objectives of this research is to develop a CPT-based approach to estimate liquefaction-induced ground settlements at sites with essentially level ground during earthquakes. The performance of the proposed CPT-based approach will then be evaluated by comparing calculated and measured ground settlements for available case histories. The major factors that influence the estimation of liquefaction-induced ground settlements using CPT data will also be discussed in detail. Guidance for taking the effects of these factors into account in estimating liquefaction-induced ground settlements using the proposed CPT-based approach will be provided as well.

Another objective of this research is to develop several semi-empirical SPT- and CPT-based approaches for estimating both the magnitude and distribution of lateral displacements in liquefaction-induced lateral spreads during earthquakes. Lateral spreads can occur in gently sloping ground without a free face, nearly level ground with a free face, and gently sloping ground with a free face. In this research, the three types of

ground geometry are studied separately in developing the SPT- and CPT-based approaches.

Before the development of the semi-empirical SPT- and CPT-based approaches, the mechanisms and major controlling factors for liquefaction-induced lateral spreads will be investigated based mainly on the available results from one-g shake table and geotechnical centrifuge modeling tests and the observations from available case histories associated with past major earthquakes. To understand the current research status in estimating lateral displacements, previous research on estimating horizontal ground displacements associated with liquefaction-induced lateral spreads will also be reviewed.

Finally, a set of simple, semi-empirical SPT- and CPT-based approaches for estimating lateral displacements in liquefaction-induced lateral spreads during earthquakes will be developed on the basis of laboratory testing results and case history data. The performance of the proposed approaches will be preliminarily examined using available case history data. General recommendations for the applications of the proposed approaches will be presented as well.

1.3 Thesis Organization

This thesis contains ten chapters. An overview of the research in this thesis as well as its objectives has been explained in the previous two sections. Chapter 2 briefly reviews the definition of soil liquefaction, liquefaction-induced ground failures, liquefaction potential evaluation, and the NCEER SPT- and CPT-based simplified methods recommended by Youd et al. (2001) for the evaluation of liquefaction potential. A CPT-based approach to estimate liquefaction-induced ground settlements at sites with essentially level ground during earthquakes is developed in Chapter 3. The performance of the proposed CPT-based method is then evaluated by comparing the calculated and measured ground settlements at sites for two available case histories. The major factors that influence the estimation of liquefaction-induced ground settlements using CPT data are also discussed

in detail in Chapter 3. Mainly based on the available results from one-g shaking table and geotechnical centrifuge modeling tests and the observations from available case histories associated with past major earthquakes, the mechanisms and major controlling factors of liquefaction-induced lateral spreads are investigated in Chapter 4. A general review of previous research on estimating horizontal ground displacements associated with liquefaction-induced lateral spreads is conducted in Chapter 5. The review is mainly focused on the strengths and limitations of each of the available methods. Chapter 6 defines a new parameter, the lateral displacement index (LDI), and presents CPT- and SPT-based procedures to estimate the lateral displacement index. The lateral displacement index is then used as one of the major parameters in developing several approaches to estimate lateral displacements. A simple, semi-empirical approach for estimating lateral displacements in liquefaction-induced lateral spreads during earthquakes for gently sloping ground without a free face using SPT or CPT data is developed in Chapter 7 on the basis of available case history data. The performance and application of the proposed approach are also investigated in Chapter 7. Similarly, a simple, semi-empirical approach for estimating liquefaction-induced lateral displacements during earthquakes for level ground with a free face using SPT or CPT data is developed in Chapter 8 on the basis of available case history data. Its performance and application are also studied. Liquefaction-induced lateral spreads for gently sloping ground with a free face are investigated in Chapter 9, and an approach to estimate lateral displacements for gently sloping ground with a free face using SPT or CPT data is then developed. Its evaluation and application are also discussed in the chapter. Finally, Chapter 10 presents the summary and conclusions of the research in this thesis.

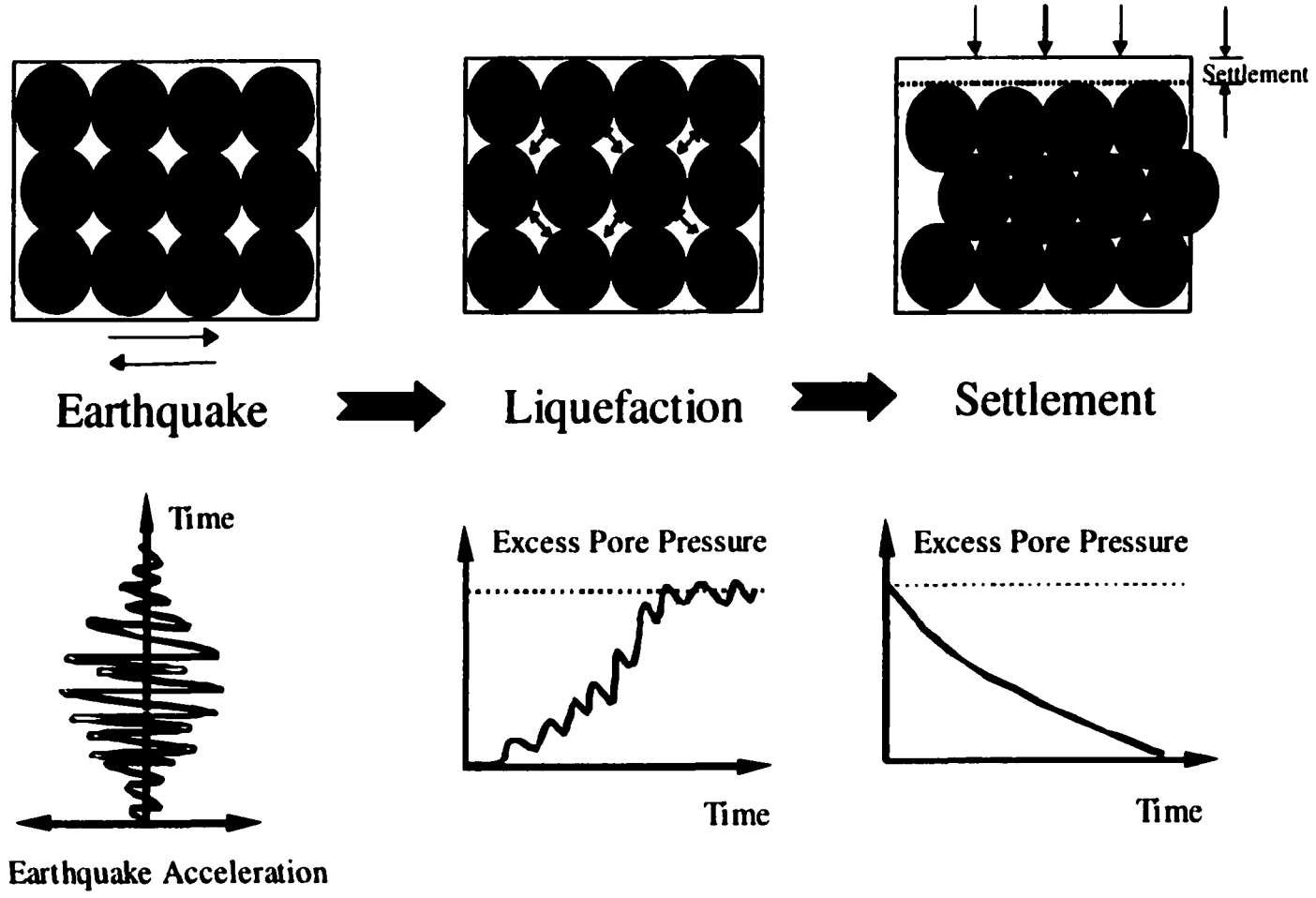


Figure 1.1 A sketch illustrating the development of liquefaction-induced ground settlements in level ground during earthquake shaking

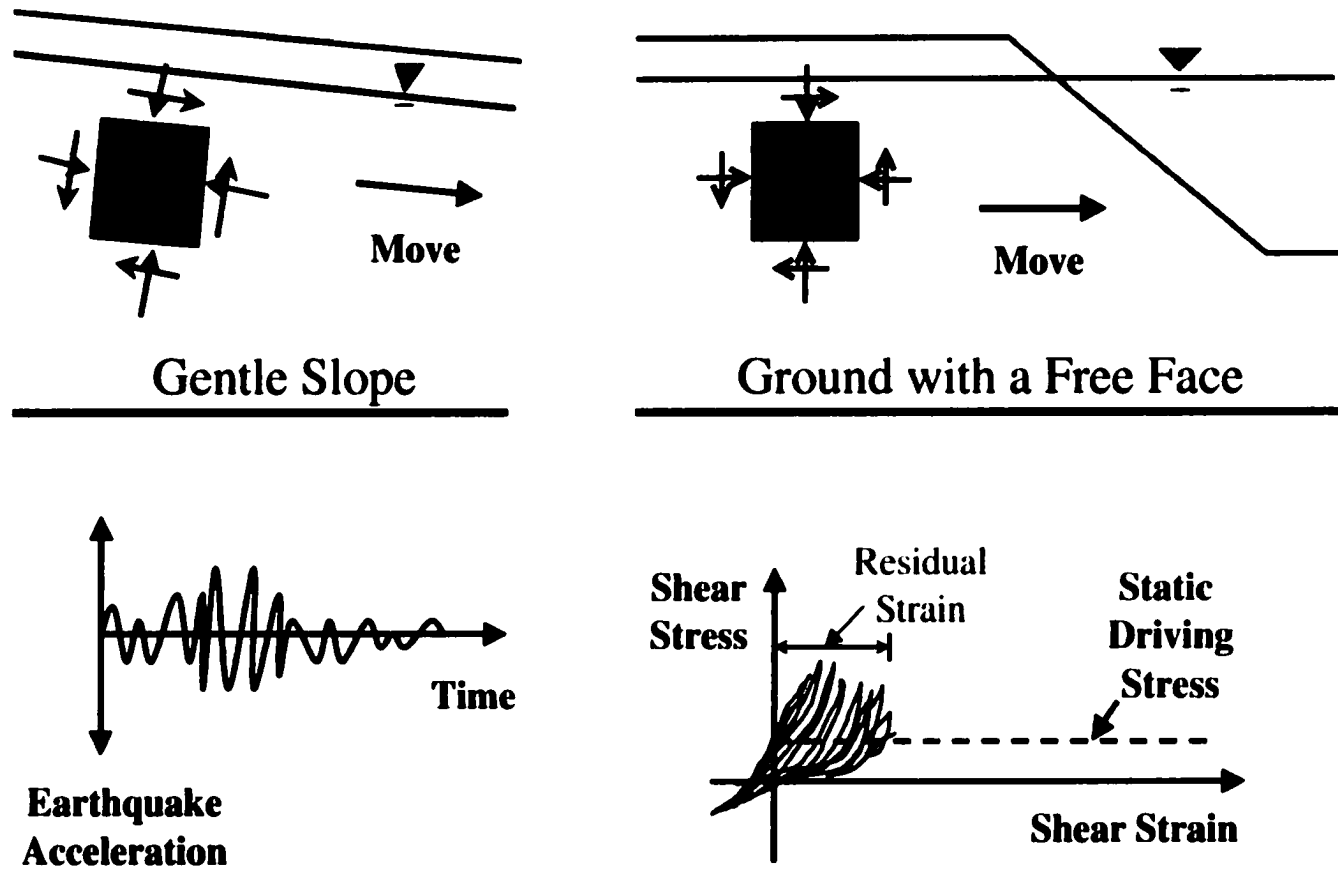


Figure 1.2 A sketch illustrating the development of liquefaction-induced lateral spread in gently sloping ground or ground with a free face during earthquake shaking

CHAPTER 2 SOIL LIQUEFACTION AND ITS EVALUATION

2.1 Definition of Soil Liquefaction

The term “liquefaction” has been used to describe a number of different, though related phenomena concerning the fact that the strength and stiffness of a soil are reduced by earthquake shaking or other rapid loading. Fear (1996) conducted an historical review of the definitions of liquefaction and found that there has been confusion (over the years, even amongst the most well-known leaders in soil mechanics) about what terminology should be used to describe the observed phenomena when a soil is subjected to undrained static or cyclic loading. Following the work of Robertson (1994), Fear (1996) proposed the following new terminology with respect to soil liquefaction to distinguish among the phenomena that have frequently been lumped together under the heading of liquefaction. Fear used two terms to describe soil liquefaction: *flow liquefaction* and *cyclic softening*. Cyclic softening is separated into *cyclic liquefaction* and *cyclic mobility*. These terms are distinguished in Table 2.1. This study focuses on cyclic softening only, specifically on cyclic liquefaction at sites with level ground and gentle slopes.

2.2 Failures Resulting from Soil Liquefaction

The consequences of liquefaction can be enormous, with significant financial and environmental implications and risks to human safety. Soil liquefaction can result in both ground failures and engineered structure failures. Generally, ground failures include sand boils, ground oscillation, deformation failures (ground settlements and lateral spreads), and flow failures. Engineered structure failures include the bearing capacity failure of buildings, the buoyant rise of buried structures, the failure of retaining walls, and other structure failures caused by ground failures.

2.2.1 Sand boil

On level ground, the high pore water pressure caused by soil liquefaction can cause pore water to flow rapidly to the ground surface. This flow can occur both during and after an earthquake. If the flowing pore water rises quickly enough, it can carry sand particles through cracks up to the surface, where they are deposited in the form of sand volcanoes or sand boils. Because of the dissipation of the excess pore pressure with the development of sand boils, sand boils are usually accompanied by subsidence of the ground. Generally, the damage associated with sand boils is relatively minor. Sand boils are of little engineering significance by themselves, but they are useful indicators of high excess pore pressure generation (Kramer 1996).

2.2.2 Ground oscillation

The occurrence of liquefaction at depth beneath a flat ground surface can decouple the liquefied soils from the surficial soils and produce large, transient ground oscillations (Kramer 1996). The surficial soils are often broken into blocks separated by fissures that can open and close during an earthquake. Ground waves with amplitudes of up to one meter have been observed during ground oscillation, but permanent displacements are usually small. Prediction of the amplitude of ground oscillation at a particular site is very difficult; even detailed non-linear ground response analyses can provide only crude estimates.

2.2.3 Ground settlement

Liquefaction-induced ground settlements are essentially vertical deformations of surficial soil layers caused by the densification and compaction of loose granular soils following earthquake loading. When saturated sandy soils are subjected to shaking during an earthquake, pore water pressures are known to build up, leading to liquefaction or loss of strength in sandy soils. With the dissipation of the pore water pressure during and after an earthquake, some volume change in the sandy soils will occur, which is manifested on

the ground surface as settlements. The settlements may occur in both level and sloping ground. However, they are the major deformation failures in level ground. In this research, the settlements in essentially level ground which is far away from a free face (e.g., river banks, sea walls, and road cuts) are termed liquefaction-induced ground settlements. An integrated CPT-based approach to estimate liquefaction-induced ground settlements will be proposed in Chapter 3 of this thesis.

2.2.4 Flow failure

Flow failures are the most catastrophic ground failures caused by liquefaction and very destructive to constructed works. Flows can move relatively long distances (many tens of meters) at relatively high speeds (several tens of kilometers per hour) (Youd 1978). Flow failure generally occurs on steep slopes (greater than 6%) where in-situ static driving shear stresses in a soil are greater than the reduced shear strength of the soil because of a large reduction in soil strength in the strain softening response soil during liquefaction. During flow failure, a liquefied soil mass is subjected to a very large and continuous shear deformation until the flow is arrested by a sudden decrease in the ground slope or by some other impediments. Different from liquefaction-induced deformation failures, flow failure can be triggered by either rapid static loading or dynamic loading such as earthquake acceleration. Estimation of the deformations produced by liquefaction-induced flow failures is extremely difficult.

2.2.5 Lateral spreads

Liquefaction-induced lateral spreads, the most common type of ground failures caused by liquefaction during earthquakes, are finite, lateral ground movements resulting from pore pressure build-up or liquefaction in an underlying granular deposit during an earthquake. Damage caused by lateral spreading, though not always spectacular and seldom catastrophic, is severely disruptive and often pervasive. Different from flow failure, lateral spreads occur on gentle slopes ranging from 0.3 to 5 percent (Youd 1978) or on level (or gently inclined) ground with a free face (e.g., river banks, sea walls, road cuts)

where in-situ static driving shear stresses are smaller than the shear strength of the liquefied soil during an earthquake. During lateral spreading of the ground, blocks of intact, surficial soil displace horizontally in a down-slope direction or in the direction towards a free face as a result of seismic and gravitational forces. Lateral spreads characteristically produce a zone of displaced soil having graben or extensional fissures at the head of the failure, shear deformations along the side margins, and compression or buckling of the soil near the toe (Bartlett 1991). Lateral spreads produce less severe displacements (ranging from a few centimeters to several meters), yet still can be very damaging. In this thesis, several CPT- and SPT-based approaches to estimate lateral displacements in a liquefaction-induced lateral spread will be developed.

2.2.6 Engineered structure failures

When liquefaction in a soil supporting the foundations of structures such as buildings and bridges occurs, the strength of the soil decreases. If the strength is reduced enough, the bearing capacity failure of the structures may occur, which can cause tilting or sinking of the structures. The buoyant rise of buried structures such as tanks may also occur because of high pore water pressure and reduced shear strength in the liquefied soil surrounding the structures during an earthquake. Furthermore, failures of retaining walls may result from the increased lateral loads from liquefied backfill soils or loss of support from liquefied foundation soils. In addition, the ground failures discussed above may also result in damage to the structures or facilities within or above the liquefied soils. For example, liquefaction-induced ground settlements may cause cracking of pavements or buildings; liquefaction-induced lateral spread may damage piles, pipelines, or the foundations of bridges.

2.3 Factors Influencing Liquefaction Resistance of Soils

A number of factors influence liquefaction resistance of soils, including soil density, soil composition and grain characteristics, in-situ stress condition, soil structure and age, and

previous strain history. Several researchers (e.g. Seed 1976, 1979; Finn 1981, 1995; Ishihara 1996) have discussed in detail the influences of these factors. The major factors will be briefly reviewed and summarized in the next few sections.

2.3.1 Soil density

Soil density (or relative density) is one of the most important factors that influence the liquefaction resistance of soils. Since the earliest studies of soil liquefaction under cyclic loading conditions were done, it has been recognized that the cyclic stresses required to develop peak cyclic pore pressure ratios of 100% or a given amount of strain are profoundly influenced by the relative density of the soil (Seed 1979). The denser the soil, the higher the soil resistance to liquefaction.

2.3.2 Soil composition and grain characteristics

The liquefaction susceptibility of a soil is influenced by its compositional characteristics that influence the development of excess pore pressure. While liquefaction is usually associated with sands or non-plastic silts, gravelly soils have also been known to liquefy. Clays are generally not prone to pore pressure generation and liquefaction. Plastic fines in sandy soils usually create sufficient adhesion between the sand grains to limit the ability of larger particles to move into a denser arrangement. Consequently, soils with a significant plastic fines content are rarely observed to liquefy in earthquakes. Based on laboratory test results, Ishihara (1996) observed that the cyclic resistance of a fines-containing sand did not change much for the low plasticity range (plasticity index below 10), but increased thereafter linearly with increasing plasticity index. Consequently, as discussed by Ishihara (1996), non-plastic soil fines with a dry surface texture (such as rock flour) do not create adhesion and do not provide significant resistance to the liquefaction susceptibility of a soil.

Liquefaction susceptibility is also influenced by grain characteristics (particle size, gradation, and particle shape). Particle size in a soil relates to soil composition, and its

influence on liquefaction susceptibility has been discussed above. Well-graded soils are generally less susceptible to liquefaction than poorly graded soils. Field evidence indicates that most liquefaction failures have involved uniformly graded soils (Kramer 1996). Soils with rounded particle shapes are known to be densified more easily than soils with angular grains. Consequently, they are usually more susceptible to liquefaction than angular-grained soils. Rounded soil particles of uniform size are generally the most susceptible to liquefaction (Poulos et al. 1985).

Soil composition and grain characteristics also affect soil permeability, which plays an important role in the liquefaction characteristics of a soil deposit. Generally, coarser-grained soils with high permeability are considered too permeable to sustain any generated pore pressure long enough for liquefaction to develop. In addition, the liquefaction vulnerability of a soil deposit is affected by the permeability of surrounding soils. Less pervious clayey soils can prevent the rapid dissipation of excess pore pressures generated in an adjacent deposit of saturated gravelly soils. On the other hand, sufficient drainage above or below a saturated deposit may prevent the accumulation of pore pressure and liquefaction.

2.3.3 In-situ stress condition

Cyclically loaded, isotropically consolidated triaxial compression tests performed on sands have indicated that while the liquefaction resistance of a soil increases with increasing confining pressure, the resistance, as measured by the cyclic stress ratio, is a non-linear function that decreases with increased normal stress (NCEER 1997). The correction factor K_{σ} was developed by Seed (1983) and then updated by Seed and Harder (1990) to allow using the simplified procedure for confining pressures greater than 100 kPa. Recent research (Arango 1996; Harder and Boulanger 1997; Vaid and Sivathayalan 2000) shows that K_{σ} also depends on relative density. Youd et al (2001) recommended an equation for estimating K_{σ} values for engineering practice.

Sloping ground induces static shear within the body of a soil mass before the onset of

earthquake shaking. The presence of static shear at a given confining stress may either increase or decrease the measured cyclic resistance of sand depending upon its initial state (Vaid and Sivathayalan 2000). Generally, the presence of a static shear stress will improve the cyclic resistance of dense soils under relatively low confining pressures. However, loose soils and some soils under high confining pressures have lower liquefaction resistance under the influence of initial static shear stresses than in the absence of these stresses. Seed (1983) recommended the use of a correction factor, K_α , to correct results obtained from the simplified procedure for level ground to sloping ground sites. However, the participants of NCEER (1997) concluded that a general recommendation for use of K_α by the engineering profession is not advisable at present.

Both theory and experimental data show that the stress ratios required to cause cyclic liquefaction are significantly influenced by the coefficient of earth pressure at rest, K_0 , in a soil deposit (Seed 1979). If the cyclic resistance ratio is defined as the cyclic resistance divided by the vertical effective confining stress at the time of consolidation, the larger the K_0 value at the time of consolidation, the greater the cyclic resistance ratio. Interestingly, Ishihara (1996) found that the effects of the K_0 condition can be properly evaluated by taking the cyclic resistance ratio with respect to the initial mean effective stress rather than the vertical effective confining stress.

2.3.4 Soil structure and age

The characteristics of saturated sands under cyclic loading are significantly influenced by the method of sample preparation in laboratory testing and soil structure in the field. Laboratory test results reported by Mulilis et al. (1975) indicated that, depending on the method of sample preparation, the cyclic resistance ratio required to cause a peak cyclic pore pressure ratio of 100% in a given number of stress cycles for samples of the same sand having the same density may vary by as much as 200%. Vaid et al. (1995) also conducted undrained direct simple shear tests of a sand reconstituted by water-pluviated, air-pluviated, and moist-tamped methods. They found that significant differences in the undrained behavior were observed for the different methods of sample reconstitution that

control the ensuing fabric. Furthermore, it is reasonable to expect that cemented sands would have higher cyclic resistance to initial liquefaction due to the “adhesion” in the field.

Several investigators have shown that liquefaction resistance of soils increases with age (NCEER 1997). Seed (1979) observed significant increases in liquefaction resistance associated with the age of reconstituted sand specimens tested in the laboratory. Youd and Hoose (1977) noted that liquefaction resistance increases markedly with geologic age. Sediments deposited within the past few hundred years are generally much more susceptible to liquefaction than older Holocene sediments (Youd and Hoose 1977; NCEER 1997). Yoshimi et al. (1989) conducted cyclic triaxial tests using undisturbed samples by means of the ground freezing technique. They found that the cyclic resistance of undisturbed samples from the in-situ deposit in Niigata was about twice as great as the cyclic resistance of the samples from the newly deposited sand fill with a similar relative density. Generally, the age of naturally sedimented deposits increases with depth.

2.3.5 Previous strain history

Seed (1979) summarized the previous laboratory test results and found that the cyclic resistance ratios that cause 100% a pore pressure response for a freshly deposited sand and for a similar deposited sand that had previously been subjected to a strain history representative of several very small earthquake shocks were quite different. Although the prior strain history caused no significant densification of the sand, it increased the resistance ratio required to cause a peak cyclic pore pressure ratio of 100% in the sand by a factor of about 1.5. However, Vaid and Sivathayalan (2000) found that a sand with a strain softening response before a small pre-strain still had strain-softening response on reloading. On the other hand, if the pre-strain is large, they found that the behavior of the pre-strained sand on reloading depends on both the magnitude and direction of pre-strain relative to the reloading direction. For reloading in the same direction as the pre-strain, the virgin strain-softening response may be eliminated. In contrast, for reloading in the

direction opposite to that of pre-strain, the sand may be transformed into an increasing strain-softening type.

2.4 Review of Liquefaction Potential Evaluation

A number of approaches to evaluate the potential for initiation of liquefaction have been developed over the years. They include the cyclic stress approach (e.g., Seed and Idriss 1971), the cyclic strain approach (e.g., Dobry et al. 1982), the nonlinear effective stress-based response analysis approach (e.g., Finn et al. 1977), the Arias intensity approach (e.g., Kayen and Mitchell 1997), the critical-state approach for sands (e.g., Jefferies 1999), and others. Each has advantages and limitations, and each is preferred by different groups of engineers. In general, the most common approach of those used by engineers is the cyclic stress approach.

The cyclic stress approach is conceptually quite simple: the earthquake-induced loading, expressed in terms of cyclic stress ratio (CSR), is compared with the liquefaction resistance of the soil, expressed in terms of the cyclic resistance ratio (CRR). At locations where the CSR exceeds the CRR, liquefaction is expected to occur. The CSR can be estimated by ground response analyses or by a simplified procedure (Seed and Idriss 1971). The CRR can be characterized using either laboratory test data or field test data. Initial studies of liquefaction involved laboratory tests of reconstituted specimens (Seed and Lee 1966). Since the effects of structure, aging, cementation, and strain history cannot be replicated in these “disturbed” specimens and obtaining “undisturbed” specimens using the ground freezing technique is costly and difficult, the use of field test results has become a popular means of evaluating the CRR. The field tests include the standard penetration test (SPT), cone penetration test (CPT), flat dilatometer test (DMT), shear wave velocity (V_s) measurement, and Becker penetration test (BPT). A number of field-test-based methods, including the SPT-based methods (e.g., Seed et al. 1983), the CPT-based methods (e.g., Robertson and Campanella 1985), the DMT-based methods (e.g., Robertson and Campanella 1986), the V_s -based methods (e.g., Stokoe et al. 1988),

and the BPT-based methods (e.g., Harder and Seed 1986), have been developed to evaluate the CRR. The advantages and limitations of each of the field tests will be briefly reviewed below.

Shear wave velocity (V_s) has been recognized as a useful measure of liquefaction resistance. The use of V_s as a field index of liquefaction resistance is justified because both the V_s and cyclic resistance ratio are similarly influenced by void ratio, effective confining stresses, stress history, and geologic age. However, the observation that the V_s of sand is insensitive to factors (e.g., soil fabric, overconsolidation ratio, prior cyclic straining) that are known to influence liquefaction resistance suggests that V_s measurements alone may not be sufficient to evaluate the liquefaction potential of all soil deposits (Jamiolkowski and LoPresti 1992). Another significant limitation of using V_s in liquefaction hazard evaluations is that V_s measurements are made at small strains, whereas liquefaction is a large strain phenomenon.

The Becker penetration test (BPT) has become one of the most effective and widely-used tools for gravelly soils (Harder and Seed 1986). A major source of variation in BPT blow counts is deviations in hammer energy. In addition, friction along the driven casing also influences penetration resistance.

Correlations for liquefaction potential with the horizontal stress index of the dilatometer test (DMT) have also been proposed (Marchetti 1982; Robertson and Camponella 1986). However, their use in geotechnical practice is still very limited.

Currently, the CPT and SPT are the primary field tests used in liquefaction potential evaluation of non-gravelly soils. The advantages and limitations of the SPT and CPT and two of the updated SPT- and CPT-based methods will be briefly reviewed in Sections 2.5 and 2.6.

2.5 The NCEER SPT-based Method for Liquefaction Potential Analysis

2.5.1 Standard penetration test (SPT)

The standard penetration test (SPT) is carried out in a borehole by driving a standard split spoon sampler down a distance of 450 mm into soils using repeated blows of a 63.5 kg (140lb.) hammer falling through 762 mm (30in.) (Clayton et al. 1995). The penetration resistance (N) is the number of blows required to drive the split spoon for the last 300 mm of penetration.

The SPT has several advantages. The test equipment is simple and is available almost worldwide. The test procedure is easy to carry out, and the cost of the test is relatively low. A sample of the tested soils is usually obtained with the test. In addition, many useful correlations have been developed. In the United States and most other countries, the SPT has been the most commonly used in-situ test for characterizing liquefaction resistance because of its simplicity. Factors that tend to increase liquefaction resistance (e.g., density, prior seismic straining, over-consolidation ratio, lateral earth pressures, and time under sustained pressure) also tend to increase SPT resistance (Kramer 1996). An updated SPT-based method for evaluating the liquefaction resistance of sandy soils will be briefly reviewed in Section 2.5.2.

The SPT has many problems such as test equipment and procedure dependence, low repeatability, low reliability, discontinuity of measurements, and so on. The main factors affecting the SPT have been reviewed, and a number of correction measures have been proposed by a few researchers (e.g., Seed et al. 1985; Skempton 1986; Robertson et al. 1983).

2.5.2 The NCEER SPT-based method

Youd et al. (2001) presented an updated SPT-based method (which will be referred to as the NCEER SPT-based method hereafter) that was recommended by about 20

participants of the NCEER (the National Center for Earthquake Engineering Research) (1997) Workshop for liquefaction potential evaluation. In this thesis, the NCEER SPT-based method was applied in evaluating the liquefaction potential of sandy soils for sites with SPT data. Figures 2.1 and 2.1 are the flowcharts showing the equations and procedures to calculate the cyclic resistance ratio at earthquake moment magnitude of 7.5, $CRR_{7.5}$, and the factor of safety against liquefaction using the NCEER SPT-based method respectively.

Figure 2.3 illustrates the major procedures to evaluate the liquefaction potential of sandy soils using the NCEER SPT-based method by a working example. Figure 2.3a shows the SPT N values according to depth for a standard penetration test (SPT) conducted at a site. With the SPT, soil samples are usually obtained and fines contents (FC) in the soils were measured, as shown in Figure 2.3b. $(N_1)_{60}$, as shown in Figure 2.3c, is the SPT blowcount normalized to an overburden pressure of 100 kPa and to a hammer energy ratio or hammer efficiency of 60 percent. The equivalent clean sand normalized SPT N value, $(N_1)_{60cs}$, can be calculated using the data for $(N_1)_{60}$ and FC, as shown in Figure 2.3d. The seismic demand placed on a soil layer by a given earthquake, expressed in terms of cyclic stress ratio (CSR) that is a function of earthquake magnitude, peak surface acceleration, vertical total stress, and vertical effective stress, is shown as a dashed line in Figure 2.3e. The capacity of the soil to resist liquefaction, expressed in terms of cyclic resistance ratio (CRR) that is a function of $(N_1)_{60cs}$, is presented as a solid line in Figure 2.3e. If CSR exceeds CRR, liquefaction of the soil is highly likely during the earthquake. The factor of safety against liquefaction (FS), Figure 2.3f, is a ratio of CRR to CSR. If FS is equal to or less than 1.0, liquefaction of the soil is highly expected during the earthquake. In the liquefaction potential analysis, soils with more than 15% clay content or soils above the ground water table are assumed to be non-liquefiable.

2.6 The NCEER CPT-based Methods for Liquefaction Potential Analysis

2.6.1 Cone penetration test (CPT)

The first Dutch (mechanical) cone penetrometer was made in 1932 in Holland and it provided only one measurement – cone resistance (Lunne et al. 1997). Begemann (1969) significantly improved the Dutch (mechanical) cone penetration test by adding an “adhesion jacket” behind the cone. With this new device, the local skin friction could be measured in addition to the cone resistance but the two measurements were made in two test steps. Although several improvements have been added to the original design, mechanical cone penetrometers still have some obvious disadvantages compared with the electric ones.

The first electrical cone penetrometer, called the Rotterdam cone, was developed in Holland and patented in 1948 (Lunne et al. 1997). Delft Soil Mechanics Laboratory produced the first electrical cone penetrometer in which the local side friction could also be measured separately with the cone tip resistance. A large number of different electric cone penetrometers have been developed in many countries around the world. Generally, the reference test equipment consists of a 60° cone with 10 cm² base area and a 150 cm² friction sleeve located above the cone, as shown in Figure 2.4. In this study, the soundings from the electrical CPT using the reference equipment were used.

In the cone penetration test (CPT), a cone on the end of a series of rods is pushed hydraulically into the ground without the need for a soil boring at a constant rate (usually, 20 mm/s \pm 5 mm/s for an electric CPT). Continuous or intermittent measurements are made of the resistance to the cone. Measurements are also made of either the combined resistance to penetration of the cone and the outer surface of a sleeve or the resistance of a surface sleeve (Lunne et al. 1997). Electric cone penetrometers produce continuous analogue data. Most systems convert the data to digital form at selected intervals that are in the range of 10 - 50 mm in general.

A primary advantage of the CPT is that a nearly continuous profile of penetration resistance is developed for stratigraphic interpretation (NCEER 1997). Generally, the CPT has greater repeatability and reliability in its testing data as compared with other field tests mentioned above. The continuous profile of the CPT measurements also allows for a more detailed interpretation of soil layers and soil types than the other tools. In recent years, the CPT has been widely and successfully used in evaluating liquefaction potential in geotechnical practice. An updated CPT-based method for evaluating liquefaction resistance of sandy soils will be briefly reviewed in Section 2.6.2.

2.6.2 The NCEER CPT-based method

Several CPT-based methods have been proposed for predicting liquefaction resistance of sandy soils (NCEER 1997). Most require the fines content and/or the mean grain size, D_{50} , and/or plasticity index of the fine fraction to be known for silty sands or sandy silts. Soil samples are therefore needed from a location close to the CPT position. To overcome the disadvantages of the previous CPT-based methods, Robertson and Wride (1998) developed an integrated procedure to evaluate the liquefaction resistance of sandy soils based solely on CPT data. A comparison of Robertson and Wride's CPT-based method with SPT-based methods and other CPT-based methods has demonstrated that Robertson and Wride's method is reliable and convenient (Gilstrap 1998; Juang et al. 1999a). In addition, Juang et al. (1999b) found that the degree of conservatism in the Robertson and Wride method is comparable to that in Seed and Idriss' (1971, 1982) SPT-based method, which has been widely used in geotechnical practice around the world for more than twenty years.

The method of Robertson and Wride (1998) (referred as the NCEER CPT-based method hereafter) was recommended by Youd et al. (2001) to evaluate the liquefaction resistance of sandy soils. The NCEER CPT-based method was used to evaluate the CRR of sandy soils for sites with CPT sounding in this thesis. Figure 2.5 is a flowchart showing the equations and procedures to calculate the cyclic resistance ratio at earthquake moment magnitude of 7.5, $CRR_{7.5}$ using the NCEER CPT-based method. The factor of safety

against liquefaction can be calculated by following the flowchart in Figure 2.2.

The major procedures to evaluate the liquefaction potential of sandy soils using the NCEER CPT-based method with CPT data are illustrated in Figure 2.6 by using a working example. The CPT tip resistance q_c and sleeve friction f_s , as shown in Figures 2.6a and 2.6b, can be directly calculated from the CPT soundings. The soil behavior type index I_c , as presented in Figure 2.6c, is a key parameter used in the NCEER CPT-based method. It is a function of q_c , f_s , vertical total stress, and vertical effective stress. Figure 2.6d shows the $(q_{c1N})_{cs}$ vs. depth plot. The equivalent clean sand normalized CPT penetration resistance, $(q_{c1N})_{cs}$, is a function of I_c , q_c , vertical total stress, and vertical effective stress. The cyclic stress ratio (CSR) and cyclic resistance ratio (CRR) are shown in Figure 2.3e. The cyclic stress ratio (CSR) is a function of earthquake magnitude, peak surface acceleration, vertical total stress, and vertical effective stress. The cyclic resistance ratio (CRR) is a function of $(q_{c1N})_{cs}$ only. If CSR exceeds CRR, liquefaction of the soil is highly likely during the earthquake. The factor of safety against liquefaction (FS), as shown in Figure 2.6f, is a ratio of CRR to CSR. If FS is equal to or less than 1.0, liquefaction of the soil is highly expected during an earthquake. Soils with an I_c greater than 2.6 are generally clayey soils and are assumed to be non-liquefiable in the NCEER CPT-based method. In addition, soils above the ground water table are also assumed to be non-liquefiable.

2.7 Summary

Soil liquefaction is a complex phenomenon that can be affected by a variety of factors that control either the liquefaction resistance of soils or the cyclic stresses induced by a given earthquake. A number of factors influence the liquefaction resistance of soils including soil density, soil composition and grain characteristics, in-situ stress conditions, soil structure and age, and previous strain history. The cyclic stresses induced by a given earthquake are mainly controlled by the magnitude of a given earthquake, the peak surface acceleration, and in-situ stress conditions in soils.

A number of approaches to evaluate the liquefaction potential of sandy soils have been developed over the years. In general, the most common approach used by engineers is the cyclic stress approach (e.g., Seed and Idriss 1971). Currently, the use of in-situ testing results and field performance data has become a popular means of assessing liquefaction susceptibility in the cyclic stress approach. Several field tests are commonly used for the evaluation of the liquefaction resistance of sandy soils including the cone penetration test (CPT), the standard penetration test (SPT), shear-wave velocity measurement, and the Becker penetration test (BPT). In the United States and most other countries, the standard penetration test (SPT) has been the most commonly used in-situ test for characterizing the liquefaction resistance of sandy soils because of the simplicity of the SPT. However, the SPT has many limitations, such as test equipment and procedure dependence, low repeatability, low reliability, the discontinuity of measurements, and so on. Recently, the CPT has become popular for site characterization because of its greater repeatability and reliability and the continuous nature of its profile as compared with other field tests. The CPT has also been increasingly used in evaluating liquefaction potential for sandy soils in geotechnical practice. In this thesis, the NCEER SPT- or CPT- based methods, as summarized by Youd et al. (2001), were used to evaluate the liquefaction resistance of saturated sandy soils.

Soil liquefaction can result in both engineered structure failures and ground failures. Engineered structure failures include bearing capacity failures of buildings, the buoyant rise of buried structures, failures of retaining walls, and other structural failures caused by ground failures. Generally, liquefaction-induced ground failures include flow slides, lateral spreads, ground oscillation, ground settlements, and sand boils. Research in this thesis focuses on liquefaction-induced ground settlements and lateral spreads only.

Table 2.1 Terminology of liquefaction recommended by Robertson (1994) and Fear (1996)

Terminology	Flow Liquefaction	Cyclic Liquefaction	Cyclic Mobility
Loading Conditions	Static or cyclic	Cyclic with shear stress reversal	Cyclic without shear stress reversal
Soil Response to Shear	Strain softening	Strain softening or strain hardening	Strain softening or strain hardening
Induced Stress State	In-situ shear stresses greater than minimum undrained shear strength	Effective stress state reaches essentially zero	Zero effective stress does not develop
Failure or Deformation Potential	Sufficient volume of soil must strain soften. Failure can result in slide or flow depending upon geometry and stress state.	Strain softened shear modulus can lead to large deformations during cyclic loading. Soils will tend to stabilize upon termination of cyclic loading.	Limited deformations, unless very loose soil results in flow liquefaction
Soil Types	Any metastable saturated soil; very loose granular deposits, very sensitive clays, and loess deposits.	Almost all saturated sands, with limited deformations in clayey soils.	Almost all saturated sands, with limited deformations in clayey soils.

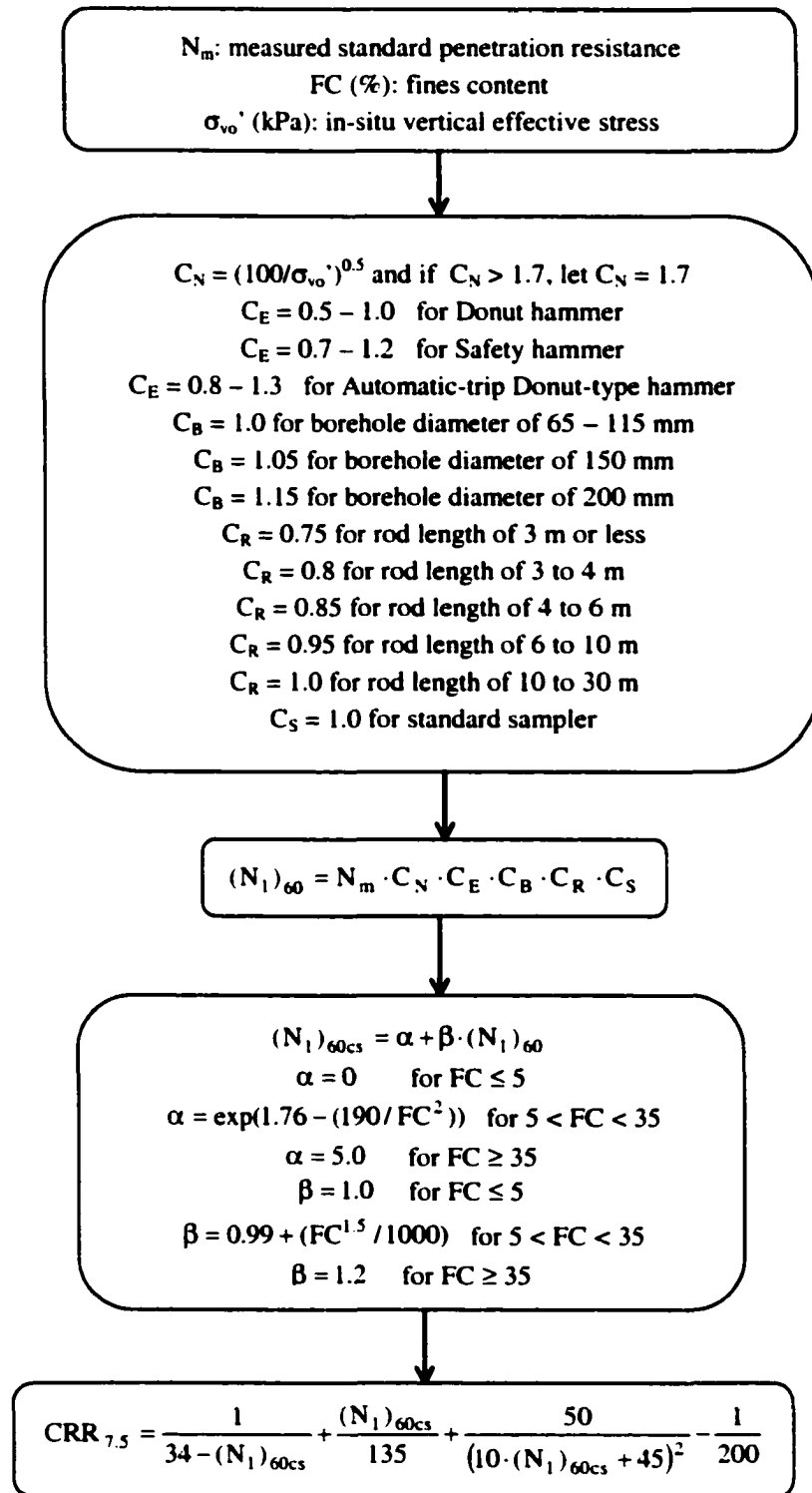


Figure 2.1 Flowchart for estimating the cyclic resistance ratio at earthquake moment magnitude of 7.5, $CRR_{7.5}$, using the NCEER SPT-based method (Youd et al. 2001)

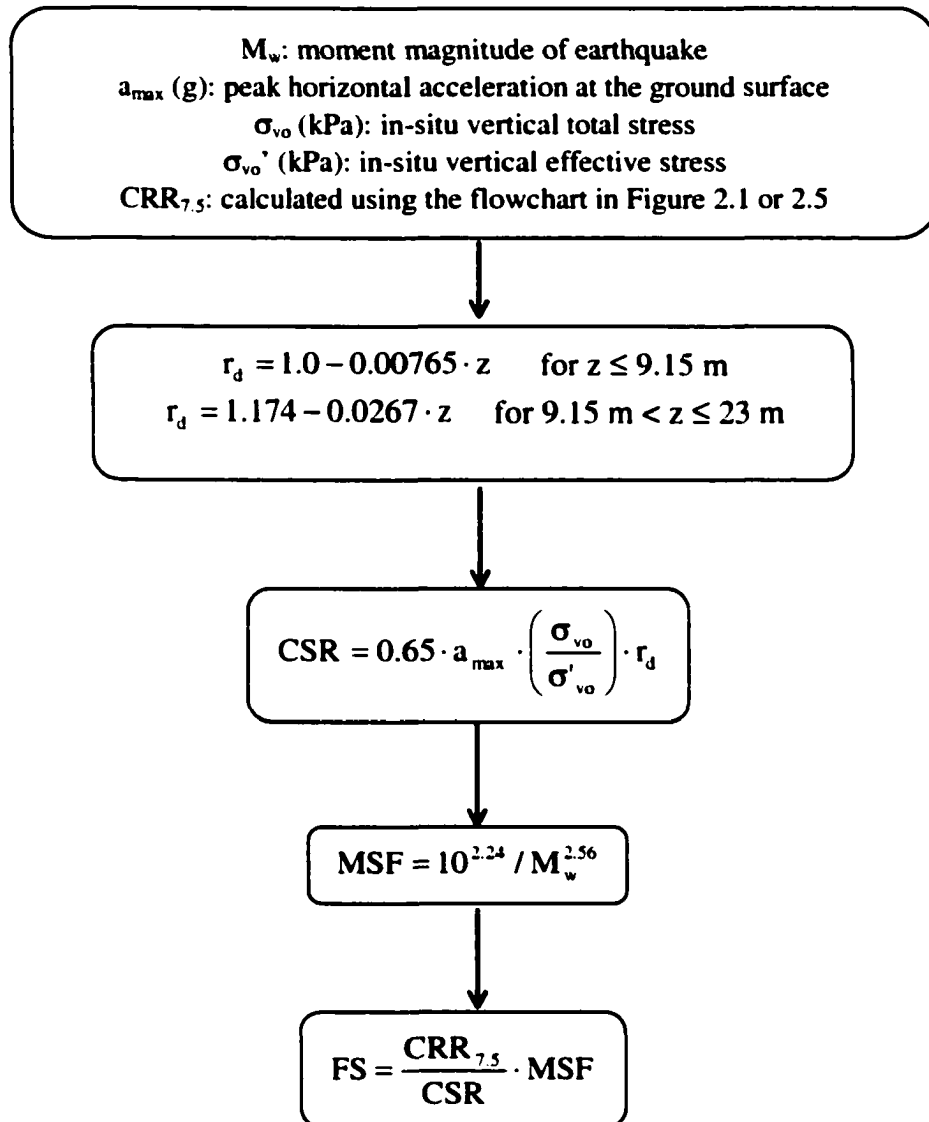


Figure 2.2 Flowchart for calculating factor of safety against liquefaction (FS) by the NCEER SPT- or CPT-based method (Youd et al. 2001)

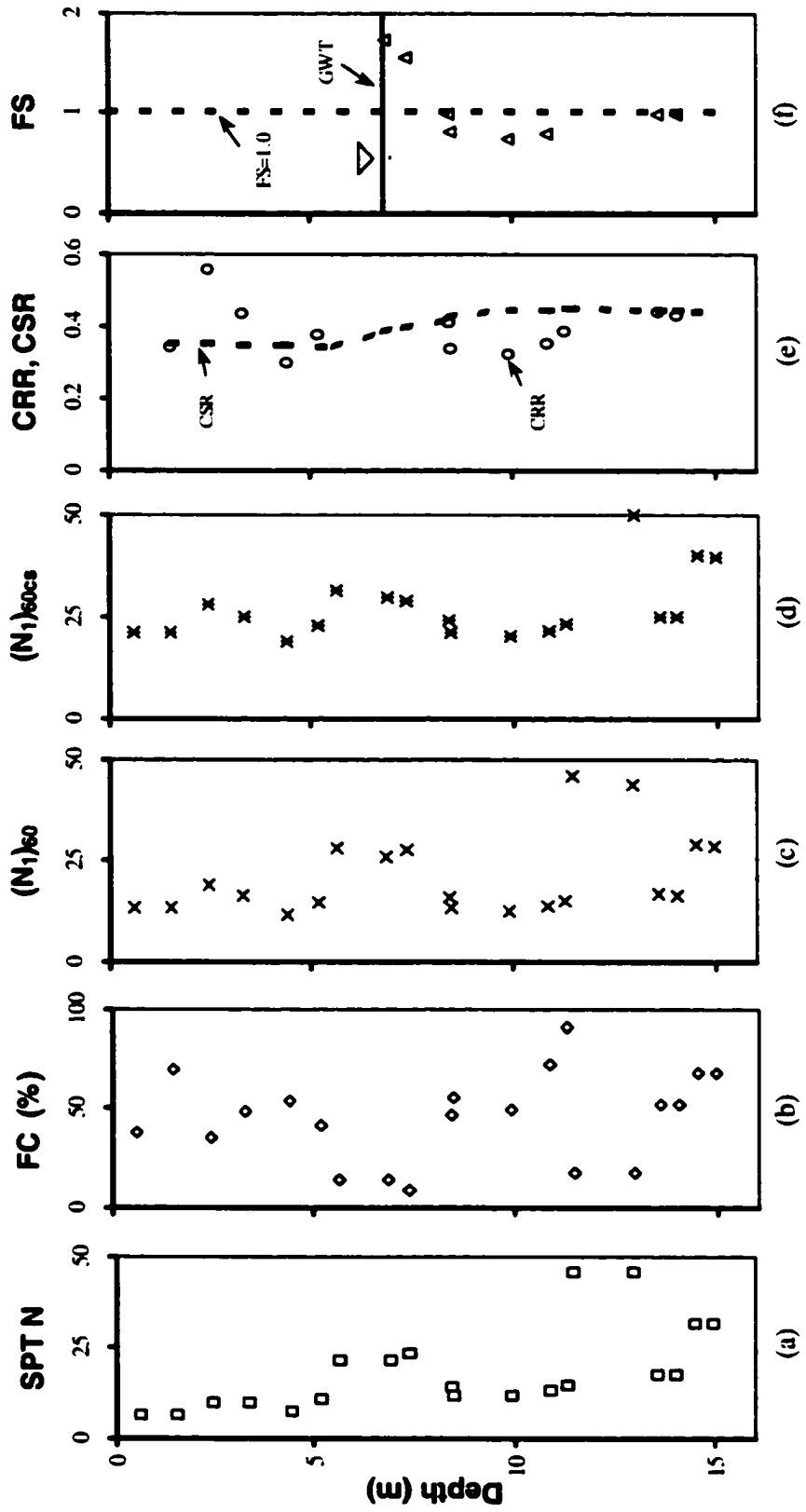


Figure 2.3 Example plots illustrating the major steps in evaluating liquefaction potential using the NCEER SPT-based method and SPT data

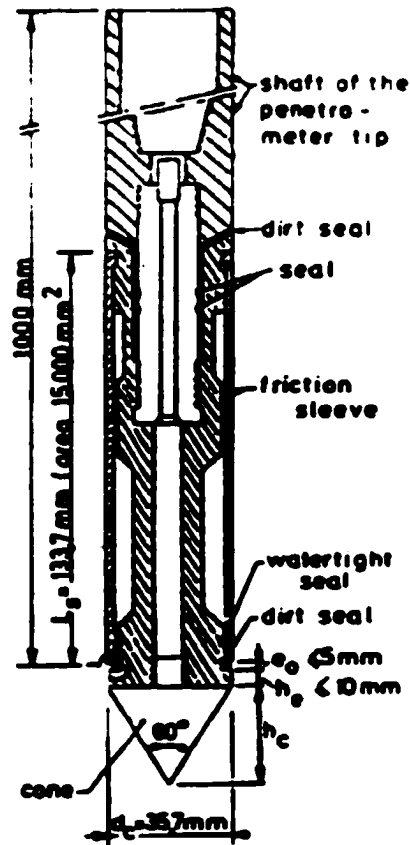


Figure 2.4 A cross section of a typical cone for the electric cone penetration test (CPT)

(modified from Lunne et al. (1997))

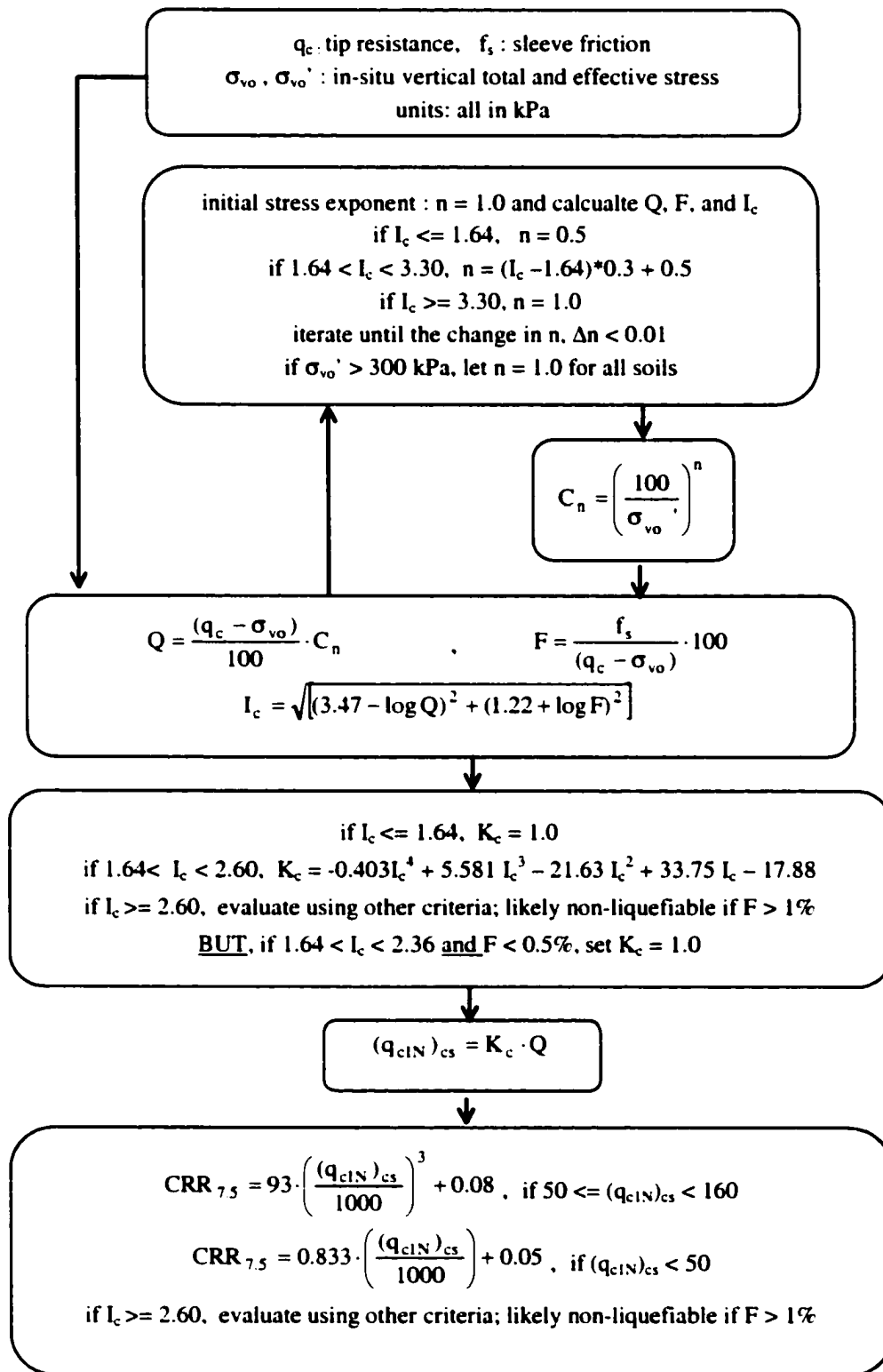


Figure 2.5 Flowchart for estimating $CRR_{7.5}$ using the NCEER CPT-based method
 (modified from Robertson and Wride (1998))

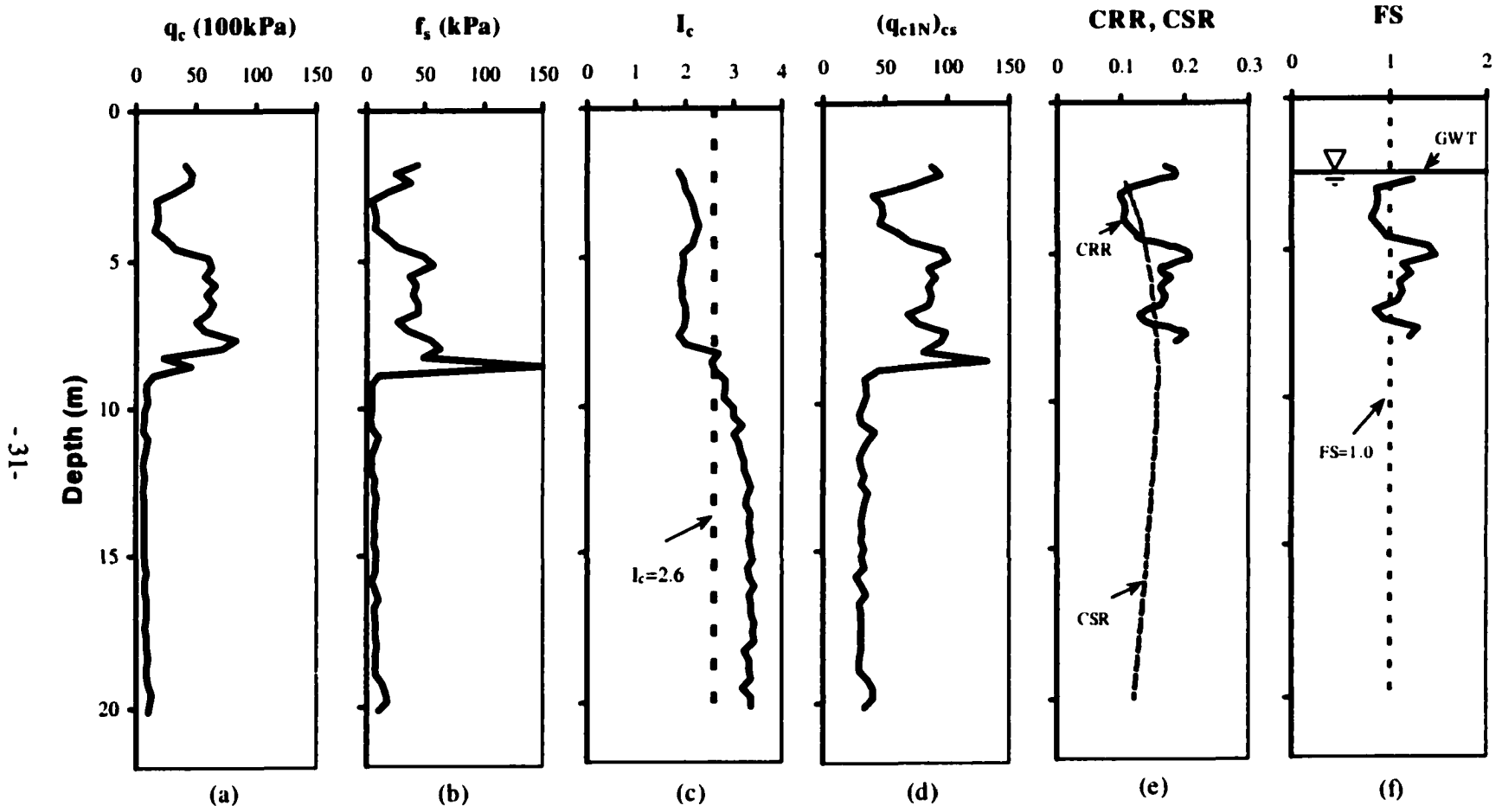


Figure 2.6 Example plots illustrating the major steps in evaluating liquefaction potential using the NCEER CPT-based method with CPT data

CHAPTER 3 ESTIMATION OF LIQUEFACTION-INDUCED GROUND SETTLEMENTS FOR LEVEL GROUND BY A CPT-BASED APPROACH

3.1 Introduction

Liquefaction of loose, saturated granular soils during earthquakes is a major hazard for construction of facilities in many regions. Both ground settlements and lateral spreads are the pervasive types of liquefaction-induced ground deformations for level to gently sloping sites. This chapter focuses on estimating liquefaction-induced ground settlements. Liquefaction-induced ground settlements are essentially vertical deformations of surficial soil layers caused by the densification and compaction of loose granular soils following earthquake loading. They may occur in both level and sloping ground during an earthquake and generally are major deformation failures with level ground. During past major earthquakes, significant damage to engineered structures and lifelines has been caused by liquefaction-induced ground settlements.

Several methods have been proposed to estimate liquefaction-induced lateral ground displacements, including numerical models, laboratory testing approaches, and field-test-based methods. Challenges associated with sampling loose sandy soils limit the applications of numerical and laboratory testing approaches in routine practice. Field-test-based methods are likely best suited to provide simple, reliable, and direct methods to estimate liquefaction-induced ground deformations for low- to medium-risk projects and to provide preliminary estimates for high-risk projects.

To date, an SPT-based method (Tokimatsu and Seed 1987) and an SPT&CPT-based method (Ishihara and Yoshimoni 1992) have been used to calculate liquefaction-induced ground settlements for clean sands only. A method to estimate liquefaction-induced ground settlements based on the CPT for all sandy soils has not yet been developed even though the CPT has greater reliability and a nearly continuous profile of test data compared with other field tests and has been increasingly used in evaluating liquefaction

potential in geotechnical practice. Therefore, a simple CPT-based approach to estimate liquefaction-induced ground settlements is needed in the practice of geotechnical engineering.

The objective of the research in this chapter is to develop a CPT-based approach to estimate liquefaction-induced ground settlements at sites with essentially level ground during earthquakes. The performance of the proposed CPT-based method will be then evaluated by comparing the calculated and measured ground settlements at available case history sites. The major factors that affect estimation of liquefaction-induced ground settlements using CPT data will also be discussed in detail in this chapter. Guidance for taking the effects of these factors into account in estimating liquefaction-induced ground settlements using the proposed CPT-based approach will be provided as well.

3.2 A CPT-based Approach to Estimate Liquefaction-induced Ground Settlements

3.2.1 Post-liquefaction volumetric strain from laboratory tests

Nagase and Ishihara (1988) conducted cyclic simple shear tests on saturated loose, medium-dense and dense samples of Fuji River sand. Both uni-directional and multi-directional loading conditions were simulated by employing irregular time histories of motions observed during major earthquakes in Japan between 1964 and 1983. Following the undrained application of the irregular loading, pore water pressures were allowed to dissipate and the resulting volumetric strains of the samples were measured. The amount of re-consolidation volumetric strain found from the tests provides a measure of the volumetric strain that may occur for in-situ deposits of sands following liquefaction during earthquakes.

Based mainly on the laboratory results of Nagase and Ishihara (1988), Ishihara and Yoshimine (1992) established a family of curves, as shown in Figure 3.1, from which the

volumetric strain resulting from dissipation of pore water pressures was correlated with relative density (or density index) and the factor of safety against liquefaction (FS) for clean sands. These curves are used to estimate post-liquefaction volumetric strain for clean sands in this study.

3.2.2 Relative density from CPT

Relative density (D_r) was used by Ishihara and Yoshimine (1992) to quantify the state of density of a sand. However, D_r can not be measured directly from the CPT. Several empirical correlations between D_r and cone tip resistance (q_c) have been proposed (e.g., Jamiokowski et al. 1985; Tatsuoka et al. 1990).

The curves proposed by Ishihara and Yoshimine (1992) were based mainly on results from laboratory tests conducted on Fuji River sand. However, no calibration chamber testing has been carried out to establish the relationship between D_r and q_c for Fuji River sand. Ishihara and Yoshimine (1992) recommended use of the correlation proposed by Tatsuoka et al. (1990) for Toyoura sand.

It is known that grain characteristics of sands may affect the correlation between D_r and q_c . Grain characteristics of Fuji River sand are similar to those of the five sands used by Jamiolkowski et al. (1985) and the sand used by Tatsuoka et al. (1990). Hence, the correlation (Equation [3.1]) by Tatsuoka et al. (1990) is used in this study since this method provides slightly smaller and more conservative estimates of relative density than the correlation by Jamiolkowski et al. (1985) when q_{c1N} is less than about 10 MPa.

$$[3.1] \quad D_r = -85 + 76 \log(q_{c1N})$$

where D_r is the relative density of a clean sand as a percentage, and q_{c1N} is the normalized CPT tip resistance corrected for effective overburden stresses corresponding to 100 kPa.

3.2.3 Correction for grain characteristics

The curves of Figure 3.1 proposed by Ishihara and Yoshimine (1992) were based on laboratory test results on clean sand. If these curves are used to estimate the post-liquefaction volumetric strains of silty sands using the CPT, some modifications for grain characteristics or fines content on the CPT soundings and their interpretations must be made.

There are two potential approaches to account for the effect of grain characteristics. One approach is to use the equivalent clean sand normalized CPT penetration resistance, $(q_{c1N})_{cs}$, defined by Robertson and Wride (1998) to account for the effect of grain characteristics or fines content on CPT soundings. The parameter, $(q_{c1N})_{cs}$, can then be treated as the cone tip resistance for a clean sand and used directly to estimate the post-liquefaction volumetric strain at certain values of factor of safety (FS).

An alternate approach is to estimate the relative density (D_r) of silty soils using the CPT and then use D_r and FS to evaluate the post-liquefaction volumetric strain based on the curves by Ishihara and Yoshimine (1992). This implicitly assumes that silty soils with the same D_r and FS may result in the same post-liquefaction volumetric strains under cyclic loading. Unfortunately, no generally accepted correlation between D_r and CPT data is available for silty soils.

One major advantage of the first approach is that it is convenient to get both FS and $(q_{c1N})_{cs}$ from the liquefaction potential analysis and then estimate the post-liquefaction volumetric strain. The proposed CPT-based method in this study uses the first approach to estimate post-liquefaction volumetric strains for sandy and silty soils. The correlations between $(q_{c1N})_{cs}$ and post-liquefaction volumetric strain (ϵ_v) for different FS were developed on the basis of the curves of Ishihara and Yoshimine (1992), as shown in Figure 3.2. Equation [3.2] is the mathematical expressions for the curves in Figure 3.2.

[3.2a]	if FS ≤ 0.5,	$\varepsilon_v = 102 \cdot (q_{c1N})_{cs}^{-0.82}$	for $33 \leq (q_{c1N})_{cs} \leq 200$
[3.2b]	if FS = 0.6,	$\varepsilon_v = 102 \cdot (q_{c1N})_{cs}^{-0.82}$	for $33 \leq (q_{c1N})_{cs} \leq 147$
[3.2c]	if FS = 0.6,	$\varepsilon_v = 2411 \cdot (q_{c1N})_{cs}^{-1.45}$	for $147 \leq (q_{c1N})_{cs} \leq 200$
[3.2d]	if FS = 0.7,	$\varepsilon_v = 102 \cdot (q_{c1N})_{cs}^{-0.82}$	for $33 \leq (q_{c1N})_{cs} \leq 110$
[3.2e]	if FS = 0.7,	$\varepsilon_v = 1701 \cdot (q_{c1N})_{cs}^{-1.42}$	for $110 \leq (q_{c1N})_{cs} \leq 200$
[3.2f]	if FS = 0.8,	$\varepsilon_v = 102 \cdot (q_{c1N})_{cs}^{-0.82}$	for $33 \leq (q_{c1N})_{cs} \leq 80$
[3.2g]	if FS = 0.8,	$\varepsilon_v = 1690 \cdot (q_{c1N})_{cs}^{-1.46}$	for $80 \leq (q_{c1N})_{cs} \leq 200$
[3.2h]	if FS = 0.9,	$\varepsilon_v = 102 \cdot (q_{c1N})_{cs}^{-0.82}$	for $33 \leq (q_{c1N})_{cs} \leq 60$
[3.2i]	if FS = 0.9,	$\varepsilon_v = 1430 \cdot (q_{c1N})_{cs}^{-1.48}$	for $60 \leq (q_{c1N})_{cs} \leq 200$
[3.2j]	if FS = 1.0,	$\varepsilon_v = 64 \cdot (q_{c1N})_{cs}^{-0.93}$	for $33 \leq (q_{c1N})_{cs} \leq 200$
[3.2k]	if FS = 1.1,	$\varepsilon_v = 11 \cdot (q_{c1N})_{cs}^{-0.65}$	for $33 \leq (q_{c1N})_{cs} \leq 200$
[3.2l]	if FS = 1.2,	$\varepsilon_v = 9.7 \cdot (q_{c1N})_{cs}^{-0.69}$	for $33 \leq (q_{c1N})_{cs} \leq 200$
[3.2m]	if FS = 1.3,	$\varepsilon_v = 7.6 \cdot (q_{c1N})_{cs}^{-0.71}$	for $33 \leq (q_{c1N})_{cs} \leq 200$
[3.2n]	if FS = 2.0,	$\varepsilon_v = 0.0$	for $33 \leq (q_{c1N})_{cs} \leq 200$

With the CPT sounding, the design earthquake (M and a_{max}) and other input parameters (e.g., ground water table, unit weight), the equivalent clean sand normalized CPT penetration resistance, $(q_{c1N})_{cs}$, and FS for sandy and silty soils can be obtained from the CPT-based liquefaction potential analysis proposed by Robertson and Wride (1998) (or the NCEER CPT-based method). The post-liquefaction volumetric strain can then be estimated using Figure 3.2 for every reading in the CPT sounding.

3.2.4 Calculating ground settlement

For sites with level ground, far from any free face (e.g., river banks, seawalls), it is reasonable to assume that little or no lateral displacement occurs after the earthquake, such that the volumetric strain will be equal or close to the vertical strain. If the vertical

strain in each soil layer is integrated with depth using Equation [3.3], the result should be an appropriate index of potential liquefaction-induced ground settlement at the CPT location due to the design earthquake.

$$[3.3] \quad S_L = \sum_{i=1}^n \epsilon_{v_i} \Delta z_i$$

where S_L is the calculated liquefaction-induced surface ground settlement at the CPT location; ϵ_{v_i} is the post-liquefaction volumetric strain for the soil sub-layer i ; Δz_i is the thickness of the sub-layer i ; and n is the number of soil sub-layers.

Figure 3.3 is a flowchart showing the procedures to estimate liquefaction-induced ground settlements using the proposed CPT-based method. These procedures can be illustrated in Figures 3.4 and 3.5 using a CPT profile from the Marina District site in California. This site is discussed in detail in the next section. Figure 3.4 illustrates the major steps in evaluating liquefaction potential using the NCEER CPT-based method (or Robertson and Wride's (1998) method) and shows the profiles of measured CPT tip resistance q_c , sleeve friction f_s , soil behavior type index I_c , cyclic resistance ratio CRR & cyclic stress ratio CSR, and factor of safety against liquefaction FS, respectively. Data in Figures 3.4a and 3.4b can be directly obtained from the CPT sounding. Figures 3.4c, 3.4d and 3.4e show the results calculated based on the NCEER CPT-based method as discussed in Section 2.6. Note that, according to Robertson and Wride's approach, CRR is not calculated when the soil behavior type index is greater than 2.6. These soils are assumed to be non-liquefiable in Robertson and Wride's approach.

The four key plots for estimating liquefaction induced ground settlements by the proposed CPT-based method are presented in Figure 3.5. Figures 3.5a to 3.5d show the profiles of equivalent clean sand normalized tip resistance $(q_{c1N})_{cs}$, factor of safety FS, post-liquefaction volumetric strain ϵ_v , and liquefaction induced ground settlement S_L , respectively. Data in Figures 3.5a and 3.5b are from the liquefaction potential analysis. Figure 3.5c shows post-liquefaction volumetric strains ϵ_v , which were calculated based

on the curves in Figure 3.2, with depth. The settlement shown in Figure 3.5d is obtained using Equation [3.3] and the volumetric strains from Figure 3.5c.

3.3 Evaluation of the Proposed CPT-based Approach by Case Histories

In the past 20 years, a number of post-liquefaction CPTs have been conducted at sites around the world, especially in the USA. In addition, earthquake-induced ground deformations have also been measured at some of these sites. These case histories provide an opportunity to evaluate the proposed CPT-based method for estimating liquefaction-induced ground settlements by comparing estimated settlements with those measured in the field.

One hundred and thirty three CPT soundings have been collected from fifteen case history sites in the USA. Eight case history sites are associated with lateral spreads and five case history sites have post-liquefaction phenomena of sand boils and cracks but no reported values of liquefaction induced ground settlements. Hence, only two case history sites (Marina District and Treasure Island) are available to evaluate the proposed CPT-based liquefaction-induced ground settlement method.

3.3.1 Marina District

The Marina District is located on the north side of San Francisco, California. During the 1989 Loma Prieta earthquake the area was significantly damaged, even though it was more than 100 km from the epicenter. Liquefaction induced sand boils, ground fissures, and ground settlements were observed and recorded.

Following the 1989 earthquake, several groups conducted post-earthquake investigations in the area. A subsurface investigation that included five CPT soundings were performed and vertical settlements caused by the earthquake were measured by the US Geological Survey (Bennett 1990). Bardet and Kapuskar (1991) also conducted a

subsurface investigation including nine CPTs in the Marina District. Two of these CPTs only penetrated into soils down to 2 to 3 m and thus can not be used in this study. Three of the CPTs were conducted at locations near the seawall where both lateral spreads and ground settlements occurred during the earthquake due to the adjacent free face. A total of nine CPTs (M1, M2, M3, M4, M6, C-2, C-8, C-9, C-12) were used to evaluate the proposed CPT-based method.

The stratigraphy in the Marina District generally consists of three distinct sand deposits overlying the San Francisco Bay Mud or bedrock (Holzer and O'Rourke 1990). Figure 3.6 is a plan showing the general locations of the geologic units in the Marina District. The western part of the district in the upper 8 m contains mainly beach sand deposits. CPT soundings M1, M2, M3, C-8, and C-9 penetrated in this material. The central part of the district is underlain by sand to silty sand fill in the upper 8 m. Much of this fill was placed back hydraulically in 1912 as a slurry with no compaction (Rollins and McHood 1998). CPT soundings M4, C-2, and C-12 penetrated this sediment. Both the beach sand and the hydraulic fill overlie bay mud. The eastern part of the district is underlain by dune sand in the upper 11 m and no bay mud is beneath the dune sand. CPT M6 penetrated the dune sand sediment.

The input data for the proposed CPT-based method include: CPT soundings (cone tip resistance and sleeve friction) with depth, moment magnitude of the earthquake, maximum surface acceleration during the earthquake, depth to ground water table, and the unit weights of the soils.

No accelerograph was located in the Marina District before the earthquake. The closest site that recorded main-shock accelerograms was located on bedrock of the Pacific Heights, approximately 1.5 km south of the Marina District (Boatwright et al. 1992). As a result, many researchers (Bardet et al. 1992; Bennett 1990; Boatwright et al. 1992; Holzer and O'Rourke 1990; O'Rourke et al. 1991; Rollins and McHood 1998; Taylor et al. 1992) have conducted studies to estimate the maximum surface acceleration (a_{max}) at the Marina District during the Loma Prieta earthquake. The variation of the maximum

surface accelerations either calculated or assumed ranged from 0.12g to 0.32g for the Marina District during the Loma Prieta earthquake.

There are generally three distinct geological zones in the Marina District area, which are different in soil type, soil compressibility, and soil thickness of each layer. It is reasonable to assume that they had a different response to the earthquake and thus the different values of a_{max} . Based on the work by Idriss (1990), Seed et al. (1994), and others, values of a_{max} of 0.12g, 0.16g, and 0.24g were used in this work for the eastern (dune sand, no bay mud), western (beach sand over thinner bay mud), and central zones (hydraulic fill over thicker bay mud) of the Marina District.

The depth to the ground water table varied between 2.3 m and 5.5 m within the Marina District during the earthquake (Bonilla 1992). A moment magnitude of 7.0 was used to model the 1989 Loma Prieta earthquake (Boulanger et al. 1995; Gilstrap 1998). Average total unit weights of 15.0 kN/m^3 and 19.4 kN/m^3 were assumed for soil above and below the ground water table, respectively.

Table 3.1 presents the liquefaction-induced ground settlements measured and calculated using the proposed CPT-based method for the Marina District. The calculated settlements are quite similar to the measured/estimated settlements. In general, the calculated settlements are slightly larger than the actual values.

O'Rourke et al. (1991) used the SPT based method of Tokimatsu and Seed (1987) to estimate the liquefaction-induced settlement at the Marina District. They assumed a peak ground acceleration of 0.2 g and an earthquake magnitude of 7.1 in their analyses. The calculated settlements by O'Rourke et al. (1991) are presented in Table 3.2. Rollins and McHood (1998) also computed the settlements at six SPT locations in the Marina District using the SPT based method of Tokimatsu and Seed (1987). However, they adopted a peak ground acceleration of $0.15 \pm 0.05\text{g}$ and an earthquake magnitude of 6.75 as the input. Although Tokimatsu and Seed (1987) did not specify a procedure for correcting for fines content in the settlement computation, Rollins and McHood (1998) corrected for

finer content by adjusting the volumetric-strain curves in a manner consistent with the correction of Seed et al. (1985) for liquefaction triggering. The ranges of settlements calculated by Rollins and McHood (1998) are also presented in Table 3.2.

The results in Table 3.2 show that the calculated settlements using the proposed CPT-based method are much closer to the measured values than those calculated using the SPT based method for the Marina District site. This is especially the case for the hydraulic fill zone where large settlements occurred due to the earthquake and where the SPT based approaches overestimate the settlements by up to a factor of two. The discontinuous nature in a SPT and low resolution with its readings in a very loose or loose sandy soil layer may partially contribute to the bad performance of the SPT-based method.

3.3.2 Treasure Island

Treasure Island is a 400 acre man-made island situated in San Francisco Bay approximately midway between the cities of San Francisco and Oakland, California. During the 1989 Loma Prieta earthquake, liquefaction-related phenomena, including sand boils, ground surface settlements, and lateral spreading movements, were evident at many locations across the island. The buildings and underground utilities on/in the island were damaged by the ground settlements and lateral displacements (Egan and Wang 1991).

Following the 1989 earthquake, several groups conducted post-earthquake investigations in the area (Power et al. 1998; Hryciw 1991). Liquefaction-induced ground settlements and lateral movements were recorded at nine existing benchmarks on the island. The liquefaction-induced differential settlements between the ground and piled buildings on the island were also observed (Bennett 1998). CPT data were collected at forty-two locations around the island (Power et al. 1998; Hryciw 1991). However, only twelve of the CPT soundings can be used to evaluate the proposed CPT-based method for this case history site since the majority of the CPT locations were close to the perimeter of the island where both lateral spreads and ground settlements occurred.

Subsurface materials at Treasure Island can generally be divided into four strata: hydraulically placed sand fill, native shoal sand and clay, recent bay sediments, and older bay sediments (Power et al. 1998) as shown in Figure 3.7. The hydraulically placed sand fill was dredged from various borrow sources located within San Francisco Bay during filling operations and consisted of mostly fine-to-medium-grained sand material containing different amounts of gravel, silt and clay depending on the location. The sand fill is supported by a rock mound placed on either the native soil or fill materials to act as a retaining dike along the island's perimeter. The shoal sand is similar to the fill deposit but with higher density and shell content. The sand fill and shoal sand range in combined thickness from approximately 7.5 m to 15 m. The recent bay mud consists primarily of soft to stiff silty clay and range in thickness from about 4.5 m to 40.5 m. The older bay sediments consist of very stiff sandy, silty, and/or peaty clay and dense sand and overlie the bedrock that is about 85 m below the ground surface.

Treasure Island is relatively flat. The ground water levels in the island are typically at depths of 1.5 to 2.4 m below the ground surface. In this study, the ground water table was assumed to be 2.0 m below the ground surface. Ground motion was recorded at the fire station on Treasure Island during the 1989 Loma Prieta earthquake. The recorded peak acceleration was 0.16 g (Hryciw et al. 1991). The ground response analyses (Hryciw et al. 1991; Power et al. 1998) had shown that the intensity of ground shaking did not vary greatly in different places on the island. Consequently, a peak acceleration of 0.16 g was used in this study. A moment magnitude of 7.0 was used to model the 1989 Loma Prieta earthquake. Average total unit weights of 15.0 kN/m³ and 19.4 kN/m³ were assumed for soil above and below the ground water table, respectively.

No measured values of liquefaction-induced ground settlements are available at the locations where the CPTs used in this study were penetrated. However, the pre-earthquake and post-earthquake data from nine survey benchmarks in the island indicated that the total settlements generally ranged from 5 to 15 cm (2 to 6 inches) (Power et al. 1998). Furthermore, observations of the ground-surface settlements adjacent to piled structures also indicated that the settlements were generally as much as approximately 15

cm (6 inches) (Power et al. 1998).

The calculated settlements and the ranges of observed liquefaction-induced ground settlements for Treasure Island are shown in Table 3.3. In general, the calculated settlements are larger than the observed values. This implies that the proposed method appears to be conservative for this case history site. The possible reasons for this conservativeness will be discussed in detail in next few sections. However, it is useful to reflect on the accuracy of our calculation of ground settlements in sand for the simple case of static vertical loading. For example, Tan and Duncan (1991) proposed that the most accurate static-loading settlement predictions should be multiplied by 1.7 to ensure that 85 percent of the measured settlements would be less than the computed settlements (Rollins and McHood 1998). Thus, considering the complexity involved in the estimation of liquefaction-induced ground settlements under earthquake loading, the agreement here between observed and calculated settlements is encouraging.

3.4 Effects of Other Major Factors on Calculated Settlements

3.4.1 Maximum surface acceleration

The amplification of earthquake motions is a complex process and is dependent on soil properties, thickness, frequency content of motions and local geological settings. For a given earthquake and geological setting, the amplification increases with the increase of soil compressibility and with soil thickness (Law 1990).

Maximum surface acceleration at a site is one important parameter used in evaluating liquefaction potential of sandy soils. However, its determination is difficult without recorded accelerographs for a given earthquake because it may vary with soil stratigraphy, soil properties, earthquake properties, the relative location of the site to the epicenter and even ground geometry. Ground response analysis may help to solve the problem but still leave some uncertainty in the results.

As an example, Table 3.4 shows the different values of maximum surface acceleration estimated or assumed by the different researchers for the Marina District site under the 1989 Loma Prieta earthquake. The values vary from 0.12 g to 0.32 g. Obviously, this wide range of the values will produce uncertainty in evaluating liquefaction potential and estimating liquefaction-induced ground settlements. The effects of these variations on the calculated settlements may be much different for the different CPT soundings as illustrated in Figure 3.8. The calculated settlement for the CPT M6 is very sensitive to the peak surface acceleration for values less than 0.2 g. A change of the peak surface acceleration from 0.12 g to 0.20 g would cause the calculated ground settlement increasing from 2 cm to 20 cm for the CPT M6. On the contrary, a variation in the peak surface acceleration from 0.12 g to 0.20 g only causes slightly change of the calculated settlement for the CPT M2. And for all three CPT soundings studied, the calculated ground settlements almost does not change if the peak surface acceleration is greater than 0.20 g at which the calculated volumetric strains have reached their maximums.

3.4.2 Fines content or mean grain size

Lee and Albaisa (1974) conducted laboratory cyclic triaxial tests to study earthquake induced settlements in saturated sands with different grain sizes. They found that grain size has a significant effect on the re-consolidation volumetric strains when "initial liquefaction" occurs or the peak pore pressure ratio reaches to 100% in soils. Their test results indicated that volumetric strains would increase with increasing mean grain size at a given relative density. Generally, increase of fines content in sands will result in decreasing mean grain size of the sands. Therefore, it can be concluded that post-liquefaction volumetric strains would decrease with increasing fines content in sands at a given relative density.

Both Tokimatsu and Seed (1987) and Ishihara and Yoshimine (1992) methods are applicable to saturated clean sands only. However, it is a practical necessity to include sands having fines content greater than five percent, ranging from sands with little silt to

silty sands.

Seed and Harder (1990) stated that "triggering" (i.e. initial liquefaction) and "post-triggering" (i.e. liquefaction induced deformations) analyses for liquefaction are inherently different as they relate to different phenomena. Unfortunately, at present there are no systematic laboratory "post-triggering" testing data available on silty sands as reported for clean sands. Equally, there are no systematic field "post-triggering" data accumulated on liquefaction induced volumetric strains relating to silty sands. As a result, a compromised alternative procedure is to adopt similar approaches with "post-triggering" (i.e. liquefaction induced volumetric strains) analysis for sands with fines as with "triggering" (i.e. liquefaction resistance) analysis.

The effect of fines content on liquefaction resistance of sand had been investigated by several researchers (Iwasaki et al. 1978; Tatsuoka et al. 1980; Tokimatsu and Yoshimi 1981; Zhou 1981). They found that silty sands are considerably less vulnerable to liquefaction than clean sands with similar SPT blow-counts. Based on this observation, "correction factors" of SPT blow-counts or "corrected" cyclic resistance ratio for sands with different fines contents or mean grain sizes had been widely used in liquefaction potential analyses using SPT or CPT based methods (Seed and Idriss 1982; Robertson and Campanella 1985; Seed et al. 1985; Robertson and Wride 1998). Robertson and Wride (1998) used $(q_{c1N})_{cs}$ to incorporate the effect of sand grain characteristics on cyclic resistance ratio in liquefaction potential analysis.

$(q_{c1N})_{cs}$ is the value with consideration of the appropriate "correction" values for the apparent fines content in liquefaction potential analysis. In this study, $(q_{c1N})_{cs}$ is also used to estimate post-liquefaction volumetric strains for sands with fines. This approach is based on an assumption that both liquefaction resistance and post-liquefaction deformation properties of sandy soils including silty sands can be quantified using the same method and formula as clean sands if equivalent clean sand normalized cone penetration resistance, $(q_{c1N})_{cs}$, is used. This implies that no further correction procedure is needed for the effect of fines content or mean grain size if $(q_{c1N})_{cs}$ is used to estimate

the liquefaction induced settlements of sandy soils including silty sands. Because $(q_{c1N})_{cs}$ will increase with increase of fines content with sands for a given cone tip resistance, the resultant calculated post-liquefaction volumetric strains will decrease with increase of fines content for a given factor of safety. Therefore, in general, this approach appears to indirectly account partially or wholly for the effect of grain characteristics on post-liquefaction volumetric strains and cast the same trend as observed by Lee and Albaisa (1974).

3.4.3 Transitional zone or thin sandy soil layers

Many researchers (Sanglerat 1972; Campanella and Robertson 1988; Berg 1994; Vreugdenhil 1995; Robertson and Fear 1995; Robertson and Wride 1998) have recognized the influence of soil layering on CPT cone resistance. Based on the results of the experiments and numerical analyses for a two layered system, Berg (1994) concluded that the thickness of at least 40 – 50 cm is required to ensure reaching full tip resistance in a CPT for a stiff frictional deposit (e.g., sand) sandwiched by softer soil layers. Vreugdenhil (1995) also concluded that the error in the measured cone resistance within a thin stiff layer is a function of the thickness of the layer as well as the stiffness of the layer relative to that of the surrounding softer soil.

It is also recognized that transitional zones between soft clay layers and stiff sandy soil layers or thin sandy layers surrounding by thick soft soil layers have an influence on the results of a liquefaction potential analysis and calculated liquefaction-induced settlements in this study. However, it should be noted that the influence of the transitional zones or thin sandy layers on calculated $(q_{c1N})_{cs}$, and FS has been partially counteracted implicitly in Robertson and Wride's method. Generally, the measured tip resistance in a sandy soil layer close to a soft soil layer (usually a clayey soil layer) is smaller than the "actual" tip resistance and the resultant friction ratio is greater than the "actual" friction ratio due to the influence of the soft soil layer. As a result, the calculated I_c will increase, therefore, the correction factor K_c , $(q_{c1N})_{cs}$, and FS will increase as well. So, finally, the $(q_{c1N})_{cs}$ and FS may be close to the "true" values in a same sandy soil layer that is not influenced by

the soft soil layer. Therefore, the calculated ground settlements would be close the “actual” values because of this implicit correction incorporated with Robertson and Wride’s method.

In this study, no further correction is taken to quantify the influences of both the transitional zones and thin sandy layers on the tip resistance of a sandy soil layer because of its complexity. This is on the conservative side in estimating liquefaction potential and liquefaction related deformations. Further research is needed to quantify the influence of transitional zones or thin sandy soil layers on calculated FS and liquefaction-induced ground settlements.

3.4.4 The three dimensional distribution of liquefied soil layers

Both Tokimatsu & Seed (1987) and Ishihara & Yoshimine (1992) suggested that the surface ground settlements could be calculated by multiplying the volumetric strain by the thickness of the liquefied layer and adding them together through the depth. However, the three-dimensional distribution of liquefied soil layers may affect ground surface settlements.

The vertical distribution of liquefied layers may play a role on ground surface settlements. Liquefaction of a relatively thick but deep sandy soil (Figure 3.9a) may have minimal effect on the performance of an overlying structure founded on shallow foundations. However, liquefaction of a near surface thin layer of soil (Figure 3.9b) may have major implications on the performance of the same structure. Ishihara (1985) investigated the effect of thickness of liquefiable soil and non-liquefied surface layer on liquefaction-induced damage. He used observations from case history sites affected by the 1983 Nihonkai-Chubu earthquake and 1976 Tangshan earthquake to develop boundary curves for site identification of liquefaction-induced damage with different peak ground acceleration levels. A study to evaluate and verify Ishihara’s (1985) criteria was performed by Youd and Garris (1995) using the data calculated from a wide range of earthquakes and site conditions. Youd and Garris found that the thickness bounds

proposed by Ishihara appear to be valid for sites not susceptible to ground oscillation or lateral spread, however, the bounds suggested by Ishihara are not valid for the prediction of ground-surface disruption for sites susceptible to ground oscillation (includes ground settlements) or lateral spread. O'Rourke and Pease (1997) also evaluated Ishihara's (1985) criteria by using the data from the Marina, South of Market and Mission Creek case sites. They generally agreed with the conclusions of Youd and Garris (1995). Gilstrap (1998) concluded that Ishihara's (1985) relationships for predicting liquefaction-induced surface effects may be over-simplified on the basis of his case history studies. Furthermore, the application of Ishihara's criteria in practice for cases with multiple liquefied layers (Figure 3.9c) is not clear.

Besides the effect of vertical distribution of liquefied layers, the horizontal extent of liquefied layers may also have effect on ground surface settlements. A small locally liquefied soil zone with limited horizontal extent (Figure 3.9d) would have limited extent of surface manifestation than that for a horizontally extensive liquefied soil zone with the same soil properties and vertical distribution of the liquefied layer. On the other hand, the locally liquefied soil zone may be more damaging to the engineered structures and facilities due to the potential large differential settlements. However, no quantitative study has been reported for the effect of horizontal extent of liquefied layers on ground surface settlements.

Ignoring the effect of three-dimensional distribution of liquefied layers on ground surface settlements may result in over-estimating liquefaction-induced ground settlements for some sites. Engineering judgement is needed to consider the effect to avoid an overly conservative design. Case histories from previous earthquakes have indicated that little or no surface manifestation was observed for cases where the depth from ground surface to the top of the liquefied layer was greater than 20 m. Based on this observation, it may be reasonable to expect that a liquefied layer beneath a thick non-liquefied layer of 20 m would not contribute to the surface ground settlement. On the other hand, caution should be paid to locally liquefied soil zones since potential differential settlements around the zones may be more significant even though the total ground settlements are same as those

for horizontally extensive liquefied soil zones.

3.4.5 Correction factor K_c

Robertson and Wride (1998) recommended that the correction factor K_c is set to be equal to one instead of using K_c of 1.0 to 2.14 when the CPT data plot in the zone defined by $1.64 < I_c < 2.36$ and $F < 0.5\%$. The purpose of this recommendation was to avoid confusing very loose clean sands with denser sands containing fines because both very loose clean sands and denser sands containing fines may fit in the same zone. As a result, if a soil with its CPT data fitted in the zone is a denser sand containing fines, the calculated $(q_{c1N})_{cs}$ for the soil with this recommendation may be reduced to only 50% of the “real” value calculated without the recommendation. This recommendation is on the conservative side in evaluating liquefaction potential of sandy soils. However, on the other hand, this recommendation may result in over-estimating of liquefaction-induced ground settlements for sites with denser sands containing fines fitted in that zone.

This seems to be true for some of the CPT soundings in the two case histories studied in this research. For example, based on soil profiles, CPT profiles, and engineering judgement, the soil should be assessed as a denser sand containing fines, but a portion of the soil was evaluated as a very loose clean sand with K_c set to be one due to the recommendation. To investigate the effect of this recommendation on the calculated settlements for these two case history sites, the settlements were re-calculated without this recommendation and are shown in Table 3.5. The effect can be seen from the differences between the values calculated with and without this recommendation in Table 3.5. The differences are up to 14% for several CPT soundings tested in Treasure Island and negligible for the soundings tested in the Marina District. It is understandable that the effect of this recommendation on calculated ground settlements may vary with sites and will depend on the amount of the soils fitted in the zone defined by $1.64 < I_c < 2.36$ and $F < 0.5\%$ within a soil profile for a site studied. If a large amount of the soils is fitted in the zone for the site, the effect would be much more significant than that for the two case history sites studied above. Therefore, soil sampling is recommended to further

clarify soil properties for the specific sites where a large amount of the soils are fitted in the zone defined by $1.64 < I_c < 2.36$ and $F < 0.5\%$.

3.4.6 A cutoff line of I_c equal to 2.6

A cutoff line of I_c equal to 2.6 is set in the Robertson and Wride (1998) to distinguish the sandy and silty soils with clayey soils which are believed non-liquefiable in general. Gilstrap (1998) studied the case histories by using Robertson and Wride's method and compared the I_c calculated using the CPT soundings with the index test results of the samples that were taken from the boreholes close to the CPT locations at the case history sites. He found that more than 95% of the samples that had the associated CPT soundings with calculated I_c greater than 2.6 were classified as clayey soils based on the index test results. He then concluded that the I_c cutoff line of 2.6 is generally reliable for identifying clayey soils. However, he also noticed that 20% to 50% of the samples that had the associated CPT soundings with calculated I_c ranging from 2.4 to 2.6 were classified as clayey soils as well based on the index test results. This implies that the cutoff line of I_c equal to 2.6 appears slightly conservative for clayey soils.

To investigate the sensitivity of the calculated settlements to this cutoff line for the two case histories studied in this research, a cutoff line of I_c equal to 2.5 was also tested. The calculated settlements using the new cutoff line are shown in Table 3.5. The differences between the calculated settlements for the cutoff lines of I_c equal to 2.6 and 2.5 are up to about 17% for several CPT soundings tested in Treasure Island and minor for the soundings tested the Marina District. It is understandable that the effect of the cutoff line with I_c equal to 2.6 on calculated ground settlements may vary with sites and will depend on the amount of the soils having calculated I_c ranging from 2.5 to 2.6 within a soil profile for a site studied. If a large amount of the soils has the calculated I_c ranging from 2.5 to 2.6 for the site, the effect would be much greater than that for the two case history sites studied above.

The combined influence of the recommendation for K_c and the cutoff line of I_c equal to

2.6 on the calculated settlements for the two case history sites was also investigated. The differences in the calculated settlements for the cases with and without the combined influence are up to 25% as shown in Table 3.5 for some of the CPT soundings in Treasure Island and minor for all the CPT soundings in the Marina District. As mentioned above, the effect may vary with sites and will depend on the amount of the soils having calculated I_c ranging from 2.5 to 2.6 or/and fitted in the zone defined by $1.64 < I_c < 2.36$ and $F < 0.5\%$ within the sites studied.

Ignoring influence of the recommendation for K_c and the cutoff line of I_c equal to 2.6 on the calculated ground settlements is on the conservative side. However, it may cause over-estimation of liquefaction-induced ground settlements for some sites where a large amount of the soils have a calculated I_c close to 2.6 or/and are fitted in the zone defined by $1.64 < I_c < 2.36$ and $F < 0.5\%$. Therefore, soil sampling is recommended to further clarify soil properties for the specific sites mentioned above.

3.5 Recommendations

Reasonable agreement between calculated settlements by the proposed CPT-based method and measured settlements at the two case history sites provides encouragement that the proposed methodology captures the dominant factors influencing liquefaction-induced ground settlements. Although further evaluations are required with future case history data, the proposed method appears to provide a satisfactory estimate of liquefaction-induced ground settlements, should be useful for low to medium risk projects and also provide preliminary estimation for higher risk projects.

A number of factors may affect the accuracy of calculated settlements in estimating liquefaction-induced ground settlements. The maximum surface acceleration is one of the major factors. Its determination is difficult without measured values at a studied site and rough estimates using available simple correlations often create much uncertainty concerning the estimated liquefaction-induced ground settlements. For important

projects, a site specific response analysis is required to determine maximum surface accelerations.

Fines content or mean grain size of sandy soils may affect liquefaction-induced ground settlements. However, their effects on the calculated settlements may be partially included in the proposed CPT-based approach. More studies are required to investigate these effects, and no further correction is recommended at this stage.

The effects of a transitional zone between a sandy soil and a clayey soil or thin sandy soil sandwiched between two soft clayey soil layers on cone tip resistance are obvious. They may also affect the estimation of liquefaction-induced ground settlements when using CPT data. However, these effects on the calculated settlements may also be partially incorporated with the proposed CPT-based approach. More studies are also required for the effects and no further correction is recommended at this stage.

Both vertical and horizontal distribution of liquefied layers in a site may play a role in ground surface settlements. Ignoring the effect of the three-dimensional distribution of liquefied layers on ground surface settlements may result in over-estimating liquefaction-induced ground settlements for some sites. Unfortunately, no reliable measure is available to quantify this effect at this stage. Therefore, engineering judgement is needed to consider the effect in order to avoid an overly conservative design.

Robertson and Wride's method may be conservative in evaluating liquefaction potential and estimating liquefaction-induced ground settlements for some sites where a large amount of the soils are fitted in the zone defined by $1.64 < I_c < 2.36$ and $F < 0.5$. Therefore, soil sampling with some index tests is strongly recommended to further clarify soil properties for the specific sites mentioned above.

3.6 Summary and Conclusions

A CPT-based approach has been presented to estimate liquefaction-induced ground settlements for sites with level ground using CPT data. The approach combines an established CPT-based method for liquefaction potential analysis with laboratory test results to estimate the liquefaction-induced volumetric strains for sandy and silty soils.

The proposed methodology was used to estimate the liquefaction-induced ground settlements at the Marina District and Treasure Island case history sites devastated by liquefaction during the 1989 Loma Prieta earthquake. Good agreement between the calculated and measured liquefaction-induced ground settlements was found. The proposed CPT-based method provided better results when compared with the existing SPT-based method. It is suggested that the proposed CPT-based method may be used to estimate liquefaction-induced settlements for low to medium risk projects and also provide preliminary estimates for higher risk projects.

The major factors that affect estimation of liquefaction-induced ground settlements using CPT were also discussed in detail in this chapter. These factors include maximum surface acceleration, fines content or mean grain size, the transitional zone or thin sandy soil layers, three-dimensional distribution of liquefied soil layers, the correction factor K_c , and the cutoff line of I_c equal to 2.6. The recommendations for taking the effects of these factors into account in estimating liquefaction-induced ground settlements using the proposed CPT-based approach were also presented.

Table 3.1 Comparison of the liquefaction-induced ground settlements measured and calculated using the proposed CPT-based method for the Marina District

CPT	a_{max}	Ground water level (Bonilla 1992) (m)	Calculated settlement using proposed CPT- based method (cm)	Measured settlement (Bennett 1990) (cm)
M6	0.12	5.5	2.3	0.0 – 1.6
M1	0.16	2.3	5.9	0.0 – 3.4
M2	0.16	2.7	1.9	0.0 – 3.4
M3	0.16	2.7	1.0	1.1
C-8	0.16	2.7	3.0	1.9
C-9	0.16	2.6	0.1	0.0 – 3.4
M4	0.24	2.4	11.2	9.6
C-2	0.24	2.3	12.1	9.6 – 10.7
C-12	0.24	2.3	9.4	7.0 – 10.7

Table 3.2 Comparison of the liquefaction-induced ground settlements measured and calculated using the SPT based method and the proposed CPT-based method for the Marina District

Soil type at the Marina District	Liquefaction-induced ground settlement (cm)			
	Measured (Bennett 1990)	SPT-based method (O'Rourke et al. 1991)	SPT-based method (Rollins and McHood 1998)	Proposed CPT-Based Method
Dune sand at the lower eastern part	0 – 2.0	3.0 – 4.0	0.5 – 1.5	2.3
Beach sand or old fill at the western part	0.1 – 4.0	5.0 – 6.0	0.5 – 8.0	0.1 – 5.9
Hydraulic fill at the central part	7.0 – 12.0	17.0 – 24.0	12.5 – 24.5	9.4 – 12.1

Table 3.3 Comparison of the liquefaction-induced ground settlements measured and calculated using the proposed CPT-based method for Treasure Island

Zone	CPT	Calculated settlement using proposed CPT-based approach (cm)	Observed settlement (Power et al. 1998) (cm)
Zone one	C-28	15.9	5 to 10 cm (about 2 to 4 inches)
	C-32	14.4	
	C-33	15.3	
	C-34	12.2	
	C-35	10.7	
	C-37	11.8	
	C-42	17.2	
Zone two	C-29A	18.8	10 to 15 cm (about 4 to 6 inches)
	C-30	27.0	
	C-31	33.3	
	C-39	23.6	
	UM10	25.8	

Table 3.4 Recorded, calculated, and assumed a_{max} associated with the Marina District during the Loma Prieta earthquake

a_{max} (g)	Method	Reference	Comments
0.05 – 0.11	Recorded	Bardet et al. 1992	at five bedrock sites within 7 km from the Marina District
0.13 – 0.17	Recorded	Bardet et al. 1992	at three artificial fill sites within 7 km from the Marina District
0.12 – 0.15	Calculated	Bardet et al. 1992	one-dimensional site response analysis
0.20 – 0.23	Calculated	Bardet et al. 1992	two-dimensional site response analysis
0.15 ± 0.05	Calculated	Rollins and McHood 1998	one-dimensional site response analysis
0.16 – 0.32	Estimated	Holzer and O'Rourke 1990	possible acceleration range
0.12 – 0.17	Estimated	Taylor et al. 1992	possible acceleration range
≥ 0.25	Estimated	Boatwright et al. 1992	possible acceleration in the central part (hydraulic fill)
0.16 and 0.32	Assumed	Bennett 1990	liquefaction potential analysis using SPT data
0.2	Assumed	O'Rourke et al. 1991	liquefaction potential analysis using SPT data
0.24	Assumed	Gilstrap 1998	liquefaction potential analysis using CPT data

Table 3.5 The ground settlements measured and calculated using the CPT-based approach with and without some modifications for the Marina District and Treasure Island

Site	Zone	Liquefaction-induced ground settlement (cm)				
		Calculated ⁽¹⁾ (basic procedure)	Calculated ⁽²⁾ (without the recommendation for K_c)	Calculated ⁽³⁾ (with the cutoff line of $I_c = 2.5$)	Calculated ⁽⁴⁾ (without the recommendation for K_c and with the cutoff line of $I_c = 2.5$)	Observed ⁽⁵⁾
Marina District	Eastern Part	2.3	0.9	2.3	0.9	0.0 – 1.6
	Western Part	0.1 – 5.9	0.1 – 5.3	0.1 – 5.4	0.1 – 4.8	0.0 – 3.4
	Central Part	9.4 – 12.1	9.4 – 11.8	8.8 – 10.0	8.6 – 9.4	7.0 – 10.7
Treasure Island	Zone one	10.7 – 17.2	10.7 – 16.4	9.8 – 15.5	9.7 – 14.7	5.0 – 10.0
	Zone two	18.8 – 33.3	18.1 – 30.6	17.3 – 27.4	16.5 – 24.8	10.0 – 15.0

Note:

- (1) Calculated settlement by using the basic CPT-based approach (with the caution recommendation of K_c and the cutoff line of $I_c = 2.6$).
- (2) Same as (1) but without the caution recommendation of setting K_c to be one for the soils fitted in the zone defined by $1.64 < I_c < 2.36$ and $F < 0.5\%$.
- (3) Same as (1) but set the cutoff line of $I_c = 2.5$ instead of using the cutoff line of $I_c = 2.6$
- (4) Same as (1) but without the caution recommendation of setting K_c to be one and with the cutoff line of $I_c = 2.5$
- (5) Measured or observed ground settlements in the Marina District (Bennett 1990) and Treasure Island (Power et al. 1998)

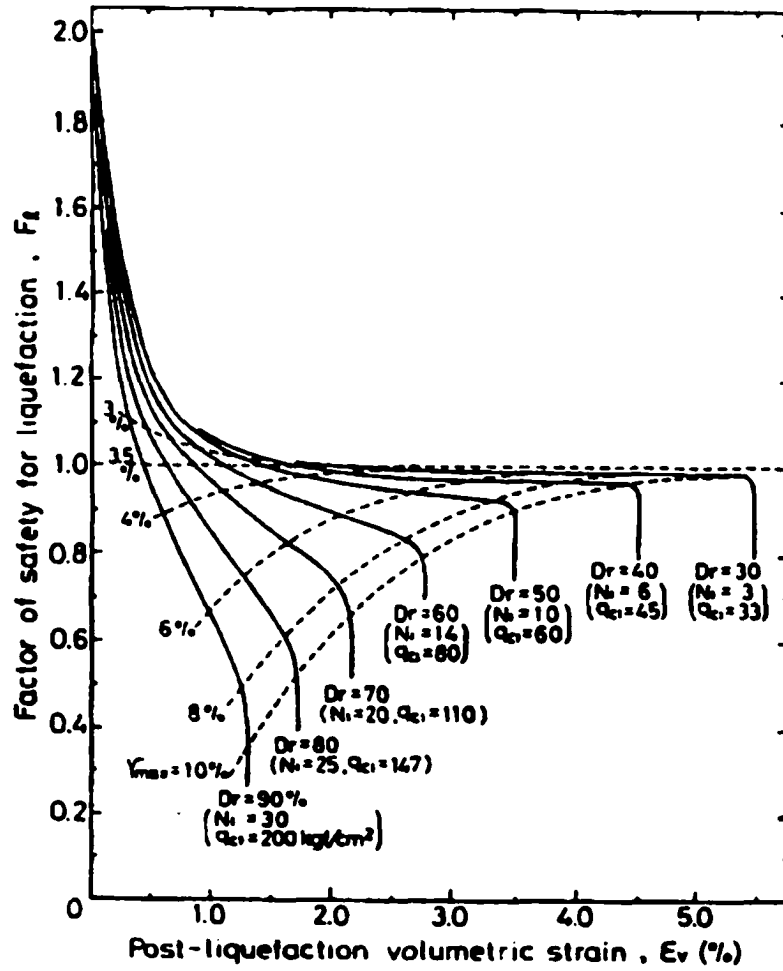


Figure 3.1 Curves for estimating post-liquefaction volumetric strain of clean sands

(after Ishihara and Yoshimine 1992)

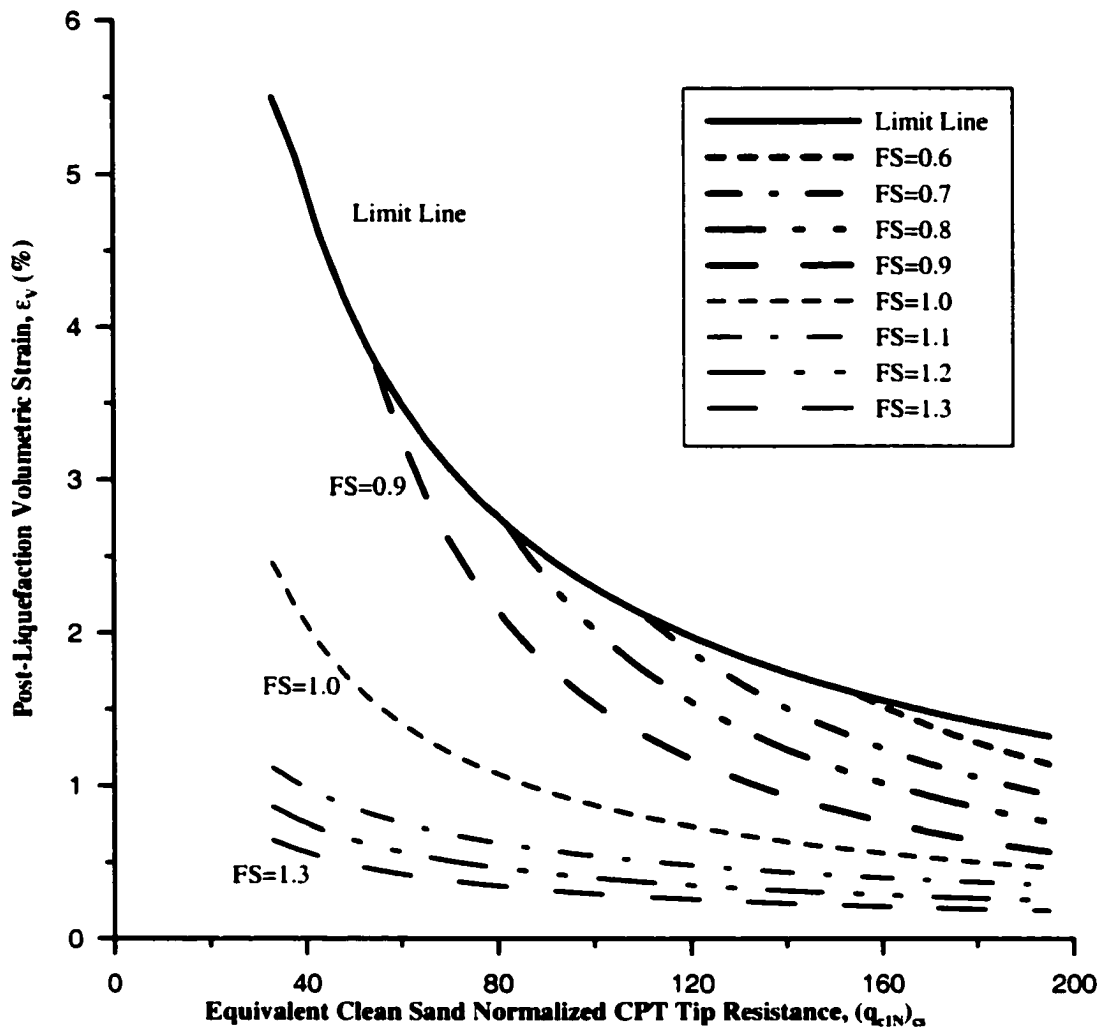


Figure 3.2 Relationship between ϵ_v and $(q_{c1N})_{cs}$ for different factor of safety (FS)
 (data from Ishihara and Yoshimine (1992))

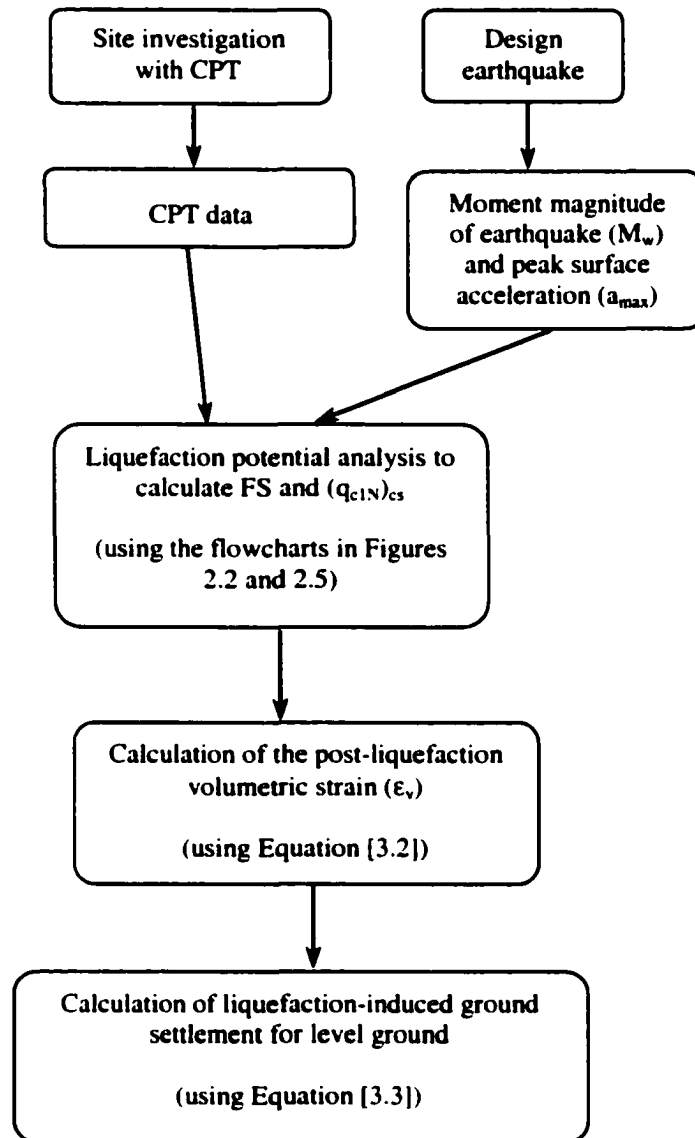


Figure 3.3 A flowchart illustrating the application of the proposed CPT-based approach to estimate liquefaction-induced ground settlement on level ground

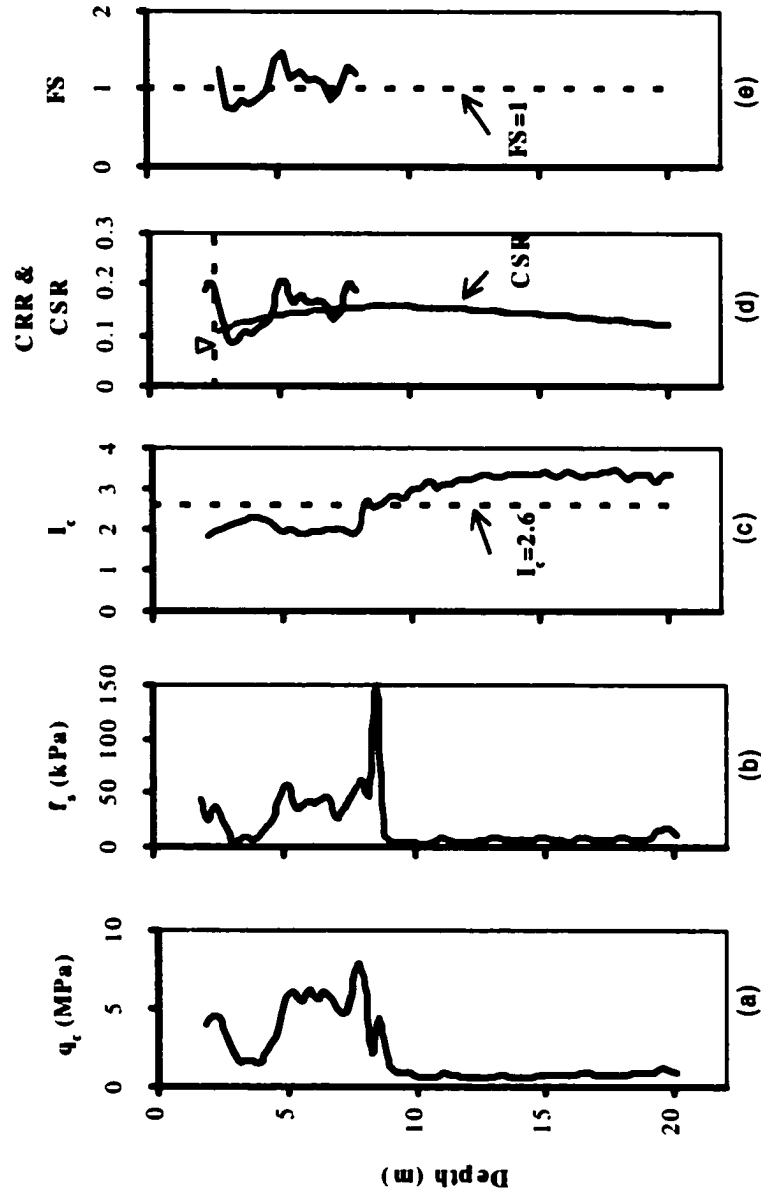


Figure 3.4 Example plots illustrating the major steps in performing liquefaction potential analysis using the NCEER CPT-based method

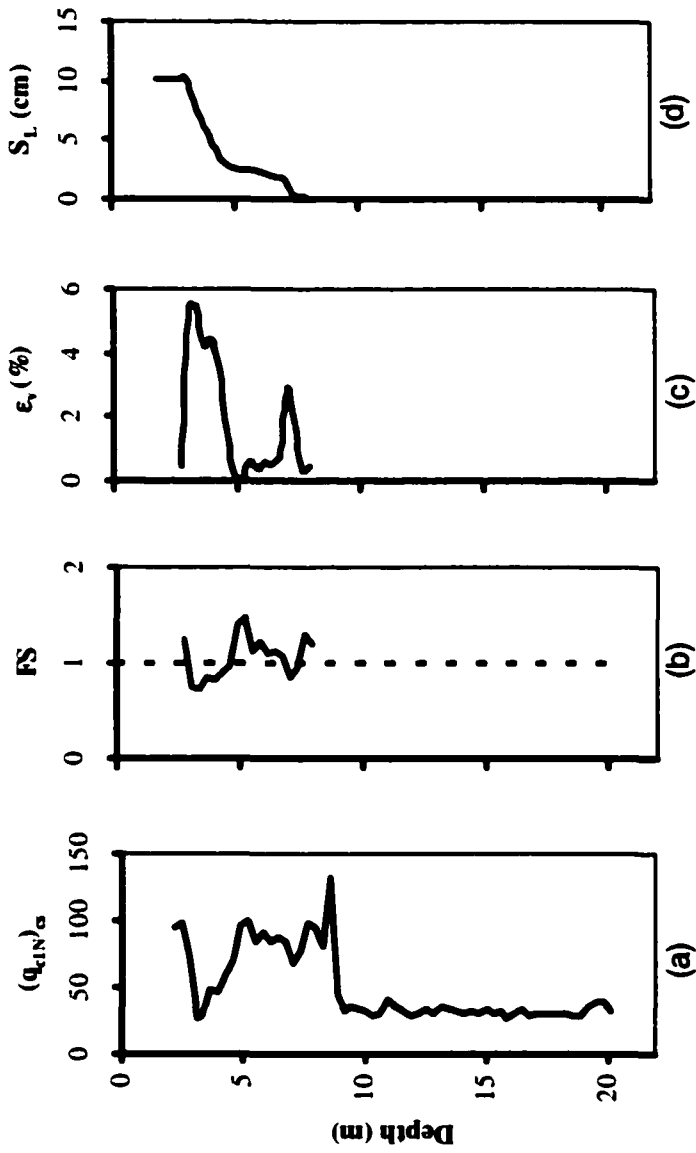


Figure 3.5 Example plots illustrating the major steps in estimating liquefaction-induced ground settlements using the proposed CPT-based approach

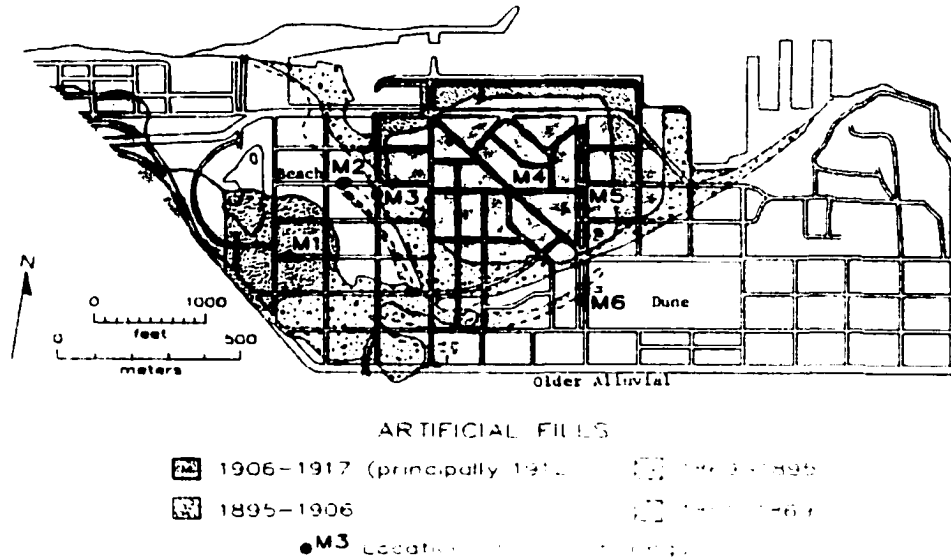


Figure 3.6 Plan view of the geologic units and CPT locations at the Marina District

(modified from Bennett 1990)

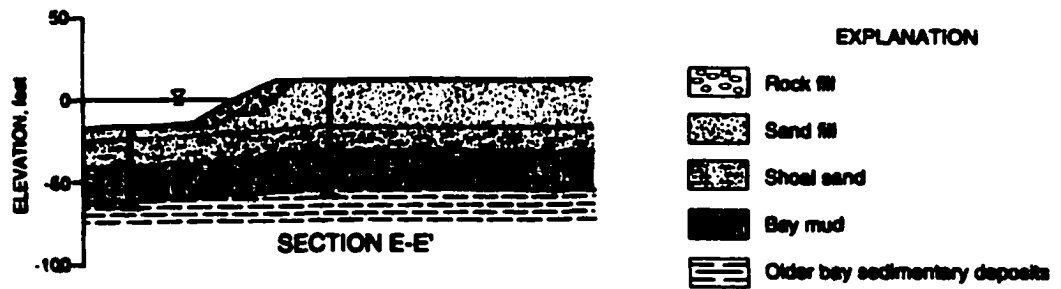


Figure 3.7 Typical geological profile at Treasure Island

(modified from Power et al. 1998)

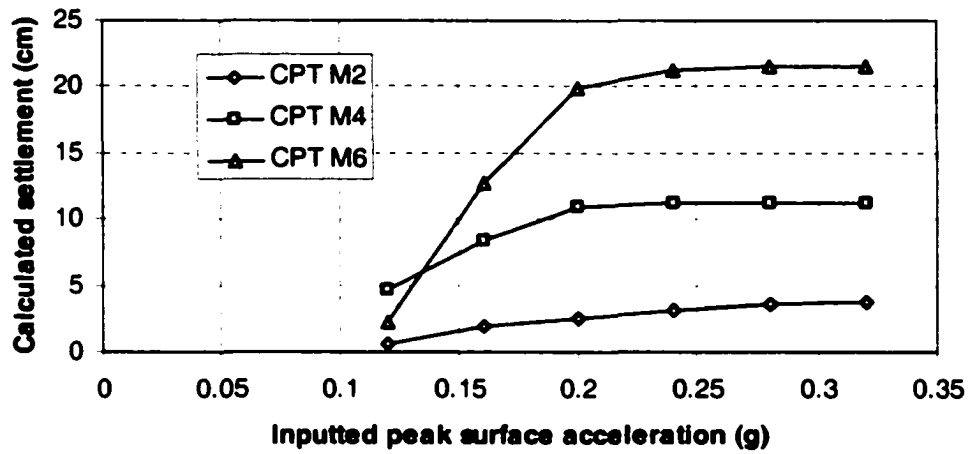


Figure 3.8 Effect of inputted peak surface acceleration on calculated settlements for some CPTs at the Marina District

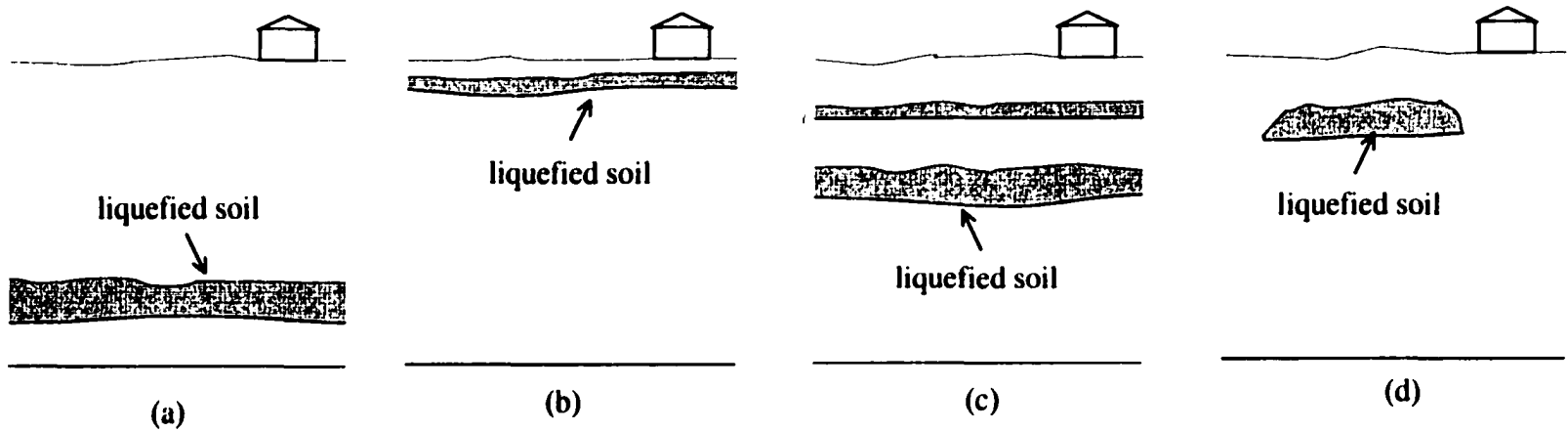


Figure 3.9 Sketches illustrating three-dimensional distribution of liquefied layers (a) deep liquefied soil layer (b) shallow liquefied soil layer (c) multiple liquefied layers (d) localized liquefied layer

CHAPTER 4 THE MECHANISMS AND MAJOR CONTROLLING FACTORS OF LIQUEFACTION-INDUCED LATERAL SPREADS

4.1 Introduction

Historically, liquefaction research focused first on excess pore pressure buildup due to the seismically-induced shear stresses and strains in the ground and on the triggering of liquefaction in horizontal or mildly sloping deposits. While new tools and refinements continue to be developed on the subjects of pore pressure buildup and liquefaction triggering, these aspects are reasonably well understood and reliable evaluation methods already exist (Dobry and Abdoun 1998). On the other hand, the response of soils after the triggering of liquefaction remains poorly understood.

Large lateral ground deformation, which induces severe damage to various infrastructure and lifeline systems, has been observed during past earthquakes in liquefied sandy soil deposits with level ground close to free faces or gently inclined surfaces. However, estimation of the ground deformation is much more difficult and depends in a complex way on a number of factors. In the last two decades, several groups of researchers (e.g., De Alba et al. 1976; Sasaki et al. 1992; Taboada 1995) have conducted laboratory cyclic triaxial or simple shear, one-g shake-table, and dynamic geotechnical centrifuge model tests to investigate the mechanisms of the liquefaction-induced ground deformations associated with lateral spreading of ground during earthquakes. Great strides have also been made in the last decade toward empirically determining and correlating these factors with ground deformation (e.g., Hamada et al. 1986; Bartlett and Youd 1995; Rauch and Martin 2000) on the basis of available case histories. Nevertheless, there are still uncertainties and disagreements between researchers about basic aspects of the mechanisms of liquefaction after triggering (Dobry and Abdoun 1998). These uncertainties currently pose a major hurdle in the development of reliable analytical techniques for evaluating more precisely liquefaction-induced deformations. Therefore,

the understanding of the mechanisms of liquefaction-induced lateral spreads is a prerequisite to estimate correctly liquefaction-induced lateral displacements.

In this chapter, the mechanisms and controlling factors for liquefaction-induced lateral spreads will be reviewed and discussed based mainly on testing results in laboratory cyclic triaxial or simple shear, one-g shake-table, and dynamic geotechnical centrifuge model tests and field observations during past earthquakes.

4.2 The Mechanisms and Displacement Modes of Liquefaction-induced Lateral Spread

4.2.1 Introduction

There are generally two different opinions among researchers about the displacement modes associated with liquefaction-induced lateral spreads. One opinion (e.g., Dobry and Baziar 1992) generally contends that the lateral displacement mainly occurs along a failure surface with concentrated strains, that the displacement is independent of the thickness of liquefied layers, and that one of the major factors controlling lateral spreads is the minimum undrained shear strength of the soil within the failure zone. An alternate hypothesis (e.g., Sasaki et al. 1992; Yasuda et al. 1992) is that the lateral displacement is contributed to by distributed residual shear strains throughout liquefied layers because of a decrease in shear strength and shear modulus due to liquefaction, and that the thickness of liquefied layers plays an important role in the mode of lateral displacement. In the following several sections, the displacement modes associated with liquefaction-induced lateral spreads will be discussed along with a review of the available results from one-g shake-table testing and dynamic centrifuge modeling and observations from case histories.

4.2.2 Results from one-g shake-table testing

Sasaki et al. (1991) carried out a series of one-g shake-table tests to study lateral displacements of gently sloping (2.5% to 7.5%) ground due to soil liquefaction during earthquakes. Typical results from their tests are shown in Figure 4.1. Figure 4.1 indicates that the surface lateral displacements resulted from distributed residual shear strains within the layers rather than from concentrated strains along a failure surface. Miyajima et al. (1991) also conducted nine one-g shake-table tests to investigate the major factors that affect liquefaction-induced lateral displacements. Figure 4.2 shows the relationship between the thickness of loose sand layers and average displacement for the different ground slopes from the test results of Miyajima et al. (1991) and indicates that the average displacement increased with an increase in the thickness of the loose sand layers. To study the mechanism for permanent ground displacement due to soil liquefaction, shake-table tests on twenty-four soil models were conducted by Yasuda et al. (1992). They found that liquefaction-induced ground displacements did not occur at the boundary between the liquefied layer and the lower non-liquefied layer but in the whole liquefied layer with an almost constant residual shear strain (see Figure 4.3). Figure 4.3 illustrates the configuration of one of their tested models, Model B, and its displacement mode during the test.

4.2.3 Results from centrifuge modeling

Abdoun (1997) conducted thirteen centrifuge model tests of sand liquefaction with and without pile foundations for multi-layered soil deposits to study the performance of both the ground and piles under liquefaction-induced lateral spreads. Figure 4.4 (a) provides a sketch of his Model 4 (one of the models used in his tests) setup and instrumentation location and Figure 4.4 (b) shows the soil lateral displacement profiles of the Model 4 at different times during shaking. The results plotted in Figure 4.4 (b) suggest that no concentrated shear strain occurred at the interfaces between the liquefied soil (Nevada sand) and the non-liquefied soil (cemented sand), and near uniform residual shear strain was triggered throughout the liquefied layer. Taboada and Dobry (1998) also performed

eleven centrifuge tests of liquefaction-induced lateral spreading in sand using a laminar box similar to that of Abdoun (1997). Figure 4.5 is an example of the profiles of the measured lateral displacements and shear strains in one of the centrifuge model tests by Taboada and Dobry (1998). Although the induced residual shear strains shown in Figure 4.5 in the liquefied layer were not uniform, the lateral displacement did occur through out the whole liquefied layer.

To study the behavior of the mildly sloping ground subjected to earthquake loading and liquefaction, Fiegel and Kutter (1994b) carried out two centrifuge modeling tests. The first model consisted of a uniform layer of saturated sand, while the second consisted of a layer of sand overlain by a relatively impermeable layer of non-plastic silt; both model slopes were constructed at an angle of 2.6° . In the uniform sand model, the lateral displacement was distributed throughout much of the layer (see Figure 4.6 (a)); however, in the layered model, displacement was concentrated along the interface between the two layers (see Figure 4.6 (b)). They found that the concentration displacement was consistent with a reduction in the shear resistance between the silt layer and the sand layer due to the redistribution of voids at the interface. This phenomenon will be discussed further in Section 4.7.

4.2.4 Observations from case histories

Moss Landing is one of two case history sites where liquefaction-induced lateral displacements were measured by slope inclinometers that were installed before earthquakes. Three slope inclinometers labeled SI-2, SI-4, and SI-5 were installed along the shoreline edge of Sandholdt Road at Moss Landing prior to the 1989 Loma Prieta earthquake (Boulanger et al. 1997). Readings were made before and after the earthquake. The differences in the readings were attributed to liquefaction-induced lateral displacements due to the earthquake. The measured lateral displacements according to depth for the three inclinometers are shown in Figure 4.7. No evidence of concentrated strains along a failure surface was found, however some non-uniform residual shear strains did take place throughout one or two soil layers.

Permanent ground displacements during the 1964 Niigata earthquake and the 1983 Nihonkai-Chubu earthquake caused enormous damage to houses, buildings, and lifeline facilities due to soil liquefaction. Based on studies of the measured permanent ground displacements (using pre- and post-earthquake photographs) caused by the two earthquakes, Hamada et al. (1986) found that the ground displacement was generally proportional to a power of 0.48 of the thickness of the relevant liquefied layers for each of the studied case history sites.

Based on the work of Bartlett and Youd (1992, 1995), Youd et al. (1999) developed an empirical model from multiple linear regression analyses of U.S. and Japanese case histories of liquefaction-induced lateral spreads during previous earthquakes. They found that the thickness of a liquefied layer was an important factor controlling the magnitude of liquefaction-induced lateral displacements in their studies. The calculated lateral displacement was proportional to a power of 0.547 of the thickness of saturated cohesionless soils with normalized SPT values, $(N1)_{60}$, equal to or less than 15.

4.2.5 Discussion and Summary

Uncertainties concerning the displacement modes associated with liquefaction-induced lateral spreads remain at present. However, the available data from one-g shake-table tests and centrifuge modeling tests, and the observations from previous case histories generally support that lateral displacements in a liquefaction-induced lateral spread result from the accumulation of residual shear strains that were distributed throughout liquefied layers. Consequently, one would expect that the magnitude of liquefaction-induced lateral displacements should be dominated by the distributed residual shear strains in liquefied layers and the thickness of liquefied layers.

The residual shear strains in liquefied layers are primarily a function of two parameters: 1) the maximum shear strains under loading conditions without biased static shear stresses, and 2) the biased (driving) in-situ static shear stresses. The biased in-situ static

shear stresses are mainly controlled by geometric parameters (e.g., ground slope, free face height, and the distance to a free face) characterising ground geometry at the site. The thickness of liquefied layers also influences the magnitude of liquefaction-induced lateral displacements with greater lateral displacements for thicker liquefied layers. Therefore, the three major components controlling the magnitude of liquefaction-induced lateral displacements are the maximum shear strains in liquefied layers, the thickness of liquefied layers, and geometric parameters at a studied site.

4.3 Soil Characteristics

4.3.1 The effects of soil properties

A number of soil properties influence the susceptibility of a soil to liquefaction. They include soil density, composition, gradation, particle shape, structure and age. The effects of these factors on soil liquefaction susceptibility have been discussed in Section 2.2. Generally, these factors also affect liquefaction-induced lateral displacements.

It is understandable that soil density (or relative density) is one major factor controlling the potential lateral displacement of a soil in a lateral spread. Seed and Lee (1966) conducted cyclic triaxial tests to study the behavior of sands after initial liquefaction and found that relative density influenced the rate of increase of strain amplitude, with an increasing number of stress cycles following liquefaction. The slower rate of strain increased with increasing density, and the gradual transition in behavior from loose to dense sand was readily apparent, as shown in Figure 4.8.

Soil composition and grain characteristics affect both the liquefaction characteristics of a soil as noted earlier in Section 2.2.2 and lateral displacements in lateral spreads. Currently, most studies focus on the effects of fines (particles smaller than 0.075 mm in size) in sand on the liquefaction resistance of the sand only. Koester (1994) has found that the fines content (percent by weight finer than 0.075 mm) had a more pronounced

effect on the liquefaction resistance, at a given void ratio, than the plasticity of the fines for soils with less than 30% fines. On the other hand, Ishihara (1996) found that the most important index property influencing the cyclic resistance was the plasticity index of the fines contained in sand. Generally, researchers agree that both fines content and the plasticity of the fines play important roles in the soil liquefaction resistance. This also appears to be true for the effects of fines on the liquefaction-induced lateral displacements, although their effects on lateral displacements have not been fully evaluated at present.

Note that the fines content also affects the in-situ penetration resistance as measured by penetration tests (SPT or CPT). That is, for soils with the same cyclic resistance, the penetration resistance is lower in soils with a higher proportion of fines. Consequently, soils with the same penetration resistance are compared, the cyclic resistance is greater for soils having more fines. This phenomenon is evident in the widely-used empirical methods for evaluating liquefaction potential based on SPT data (Seed et al. 1985), where, for a given SPT value, the liquefaction resistance increases with fines content.

Research has indicated that both the structure and age of a soil may significantly influence the liquefaction resistance of the soil as discussed in Section 2.2.4. For cohesionless material, the older the deposit, the greater the resistance to liquefaction. It is also reasonable to expect that cemented sands will have higher cyclic resistance to initial liquefaction due to the “adhesion”. However, the post-liquefaction behavior of cemented or aged sands may be different due to the breakdown of the bondage during liquefaction. So the effects of structure and age on post-liquefaction behavior may be different from those on liquefaction potential. As well, penetration resistance in the SPT or CPT also increases when the soil is cemented or aged. If two sands have the same value of penetration resistance and are in other ways the same except that one is cemented or aged and the other is non-cemented or recently deposited, it is expected that the potential lateral displacement as a result of an earthquake could be larger for the cemented or aged sand than for the non-cemented or recently deposited sand.

4.3.2 The role of soil-dilative response at large strain

The restraint on shear strain due to soil-dilative response at large shear strains has been noted and referred to as a form of cyclic-mobility in several pioneering liquefaction studies (e.g., Seed and Lee 1966; Casagrande 1975). Elgamal et al. (1998) presented a comprehensive summary of the available research on soil-dilative response at large shear strains and concluded that this response appears to have a dominant impact on the magnitude of liquefaction-induced accumulated deformations in clean sands. The evidence for soil-dilative response was observed in undrained cyclic laboratory tests, one-g shake-table studies, centrifuge experiments, and in-situ seismic responses. A brief summary of this evidence is given below, based mainly on the work of Elgamal et al. (1998).

De Alba et al. (1976) conducted large-scale simple shear tests and found that specimens tended to dilate as shear strain increased for medium and dense sands. They concluded that there was a limited amount of shear strain that could be developed regardless of the applied stress ratio or the number of stress cycles for sands with relative densities greater than about 45% and without the presence of a biased-driving shear stress. Similar responses were also observed and documented in cyclic laboratory tests for numerous sands (Seed and Lee 1966; Ishihara 1985; Arulmoli et al. 1992; Shamoto et al. 1997). In addition, soil-dilative response has been observed as well in cyclic laboratory tests in the presence of a biased-driving shear stress (Arulmoli et al. 1992; Taboada et al. 1996). Although cycle-by-cycle accumulation of permanent strain increments in a biased preferred direction was observed in these tests, it is clear that a drop in excess pore pressure and an increase in shear stress were observed at each of large shear strain amplitudes in a biased direction for a cyclic triaxial test with an imposed initial deviatoric stress, as shown in Figure 4.9.

Dilative soil behavior has been frequently observed in shake-table studies. Most of these studies were conducted in Japan (Koga and Matsuo 1990; Sasaki et al. 1992; Towhata and Toyota 1994; Shamoto et al. 1996), as summarized by Elgamal et al. (1998). The

common feature during these shake-table tests is that the acceleration spikes corresponding to instants of reduction in excess pore pressure and an increase in shear stress at large shear strain amplitudes were observed in a down-slope direction for the tested models with an inclined ground surface.

The occurrence of a similar spiky acceleration response was also reported in a large number of centrifuge studies (Lee and Schofield 1988; Arulmoli et al. 1992; Tobaada 1995; Abdoun 1997; Zeghal et al. 1999). For instance, Tobaada (1995) conducted ten centrifuge model tests of liquefaction-induced lateral spreading to simulate a horizontal or sloping 10 m thick layer of water-saturated coarse sand of infinite lateral extent on an impervious rigid base. The slope angle simulated in the field ranged from 0° to 10°. He found that the solid skeleton of the soil tries to dilate and induces an instantaneous reduction in pore pressure and a corresponding increase in soil shear strength at large cyclic strains of about 1% to 2% in the ground with a ground slope greater than about two percent. He also concluded that this dilative response, which was found to become more prominent as the slope angle and the input acceleration increased and as the input frequency decreased, limited the downslope strain accumulation and thus the value of the final lateral displacement.

Furthermore, recent records of field seismic site response (Holzer et al. 1989; Zeghal and Elgamal 1994) during liquefaction also displayed peculiar acceleration spikes associated with simultaneous instants of excess pore-pressure drop.

All the evidence mentioned above suggests that the soil-dilative response at large strains may result in a significant regaining of shear stiffness and strength at a large cyclic shear strain, which may lead to a strong restraining effect on the magnitude of accumulated permanent shear strains in lateral spreads. This dilative response is believed to be more prominent in denser soils and as the slope angle and the input acceleration increase and as the input frequency decreases.

4.4 Earthquake Characteristics

4.4.1 The effects of earthquake characteristics

The “size” of an earthquake is obviously a very important parameter for both the evaluation of liquefaction potential and the estimation of liquefaction-induced lateral displacements during the earthquake. Earthquake magnitude is a quantitative measurement of earthquake size. Large magnitude earthquakes are capable of producing large and widespread ground failure in moderately to highly liquefiable soils that are located near the seismic source. In contrast, lateral spread displacement tends to be smaller and more limited for moderate to smaller earthquakes.

The distance to a seismic energy source or fault rupture is another important parameter in evaluating liquefaction potential and estimating liquefaction-induced lateral displacements. During large earthquakes, severe and damaging lateral spreads occur close to the seismic energy source. The amount of liquefaction-induced ground displacement tends to diminish logarithmically with increasing distance from the fault rupture (Youd and Perkins 1987).

The peak horizontal ground acceleration (a_{max}) is often used to characterize the intensity of strong ground motion. Earthquake shaking must have a sufficient amplitude to generate excess pore pressure and initiate liquefaction. Once the soil has liquefied, the resulting ground displacement also increases with increasing values of a_{max} (Bartlett 1991). This idea is supported by the centrifuge test results of Taboada and Dobry (1998). The value of a_{max} can be related to the magnitude of an earthquake and the distance to the seismic energy source through empirical attenuation relationships (e.g., Joyner and Boore 1988). However, the determination of a_{max} is difficult without having recorded accelerographs for a given earthquake because a_{max} varies with soil stratigraphy, soil properties, other earthquake properties, and even ground geometry.

The duration of strong motion can influence the severity of earthquake damage. Long-

lived strong ground motion tends to increase the extent of liquefaction in the soil and prolongs the time that the mobilized soil mass is subjected to downslope translation by earthquake and gravitational forces (Bartlett 1991). It has been observed in both one-g shake-table tests (e.g., Sasaki et al. 1992) and centrifuge experiments (e.g., Taboada 1995) that permanent deformations in a lateral spread after liquefaction of the soils in the lateral spread accumulated on a cycle by cycle basis. Therefore, it is understandable that the liquefaction-induced lateral displacement increases with increased durations of strong ground motion. Generally, the duration of strong motion increases with increasing earthquake magnitude. There are also available empirical relationships (e.g., Krinitzsky et al. 1988) to estimate the duration using the magnitude and distance to the epicenter of the earthquake.

Earthquakes produce complicated loading with components of motion that span a broad range of frequencies (Kramer 1996). Tatsuoka et al. (1986) conducted cyclic undrained triaxial tests to study the effect of loading frequencies on liquefaction resistance of clean sands and found that the effect of loading frequency between 0.05 Hz and 1.0 Hz was very small. The same conclusions were reached by Peacock and Seed (1968) based on the results of simple shear tests at frequencies between 1/6 and 4 Hz, and by Yoshimi and Oh-oka (1975) based on the results of ring shear tests at frequencies ranging from 1 to 12 Hz. Taboada and Dobry (1998) conducted centrifuge tests to investigate the effect of loading frequency on the magnitude of lateral displacements in a lateral spread. They found that the final permanent shear strains for the experiment run at input frequency of 1 Hz were about twice those of the experiment run at 2 Hz after 20 cycles of shaking. Nevertheless, the duration of the shaking for the experiment run at 1 Hz was also exactly twice that of the experiment at 2 Hz. Therefore, it appears that the duration rather than the loading frequency is the key parameter that contributes to the difference in the measured shear strains.

4.4.2 The role of inertial forces

Cyclic liquefaction or cyclic mobility of a saturated sandy soil can be triggered by the

inertial forces (manly cyclic horizontal shear stress) produced by an earthquake if the cyclic loading is sufficiently large in magnitude and duration. However, the role of the inertial forces in the post-liquefaction phenomena (e.g., liquefaction-induced lateral spreading) during an earthquake may be quite different from that in the triggering of soil liquefaction. To assess the relative influence of static and inertial forces on a lateral spread, Sasaki et al. (1991) conducted a special model test on a one-g shake-table. In this test, a conical embankment was liquefied with unidirectional base motions. The resulting slope movements were generally radially outward from the slope and were not significantly greater in the direction of the shaking. Sasaki et al. (1991) concluded that the influence of the inertial forces was indirect, determining the extent of soil liquefaction and possibly controlling the rate of development of the lateral soil movement.

On the other hand, the inertial forces in soils during an earthquake appear to play a direct role in governing the ground movement in a liquefaction-induced lateral spread. Castro (1987) suggested that the lateral spreading of a gentle slope is not likely to continue after earthquake motions cease because the static shear stresses in a lateral spread are relatively low. On the basis of all available evidence from one-g shake-table and centrifuge model tests, Dobry and Abdoun (1998) also supported the idea that lateral ground deformation in lateral spreads stops when the shaking stops, except where liquefied layers are in a very steep slope or very close to a steep free face, where large static driving shear stresses exist. Although eyewitness' accounts of lateral spreads in past earthquakes confirmed that liquefaction-induced lateral movements might continue for some time after an earthquake, Dobry and Abdoun (1998) believed that the continued ground deformations were probably caused by shaking due to after-shocks that were too weak to be felt by the witnesses, but strong enough to cause significant strains and displacements in the already liquefied soil.

The role of inertial forces in a lateral spread is not quite clear at present. More research is required to assess the role of inertial forces in liquefaction-induced lateral displacement. Generally, it is believed that both static and inertial forces may play some role in driving the down-slope movements in a lateral spread.

4.5 Ground Geometry and In-situ Shear Stress

4.5.1 The effects of ground geometry

As described in Section 2.3.4, lateral spreads generally occur on gentle slopes ranging from 0.3 to 5 percent (Youd 1978) or on level/inclined ground with a free face. A free face is any abrupt topographical depression such as an escarpment, river channel, canal, or road cut. The results of one-g shake-table tests and centrifuge model tests and field observations from case histories indicate that ground geometry has a major effect on the magnitude of lateral displacements in a lateral spread.

Miyajima et al. (1991) conducted one-g shake-table tests to study the effect of the slope of a loose sand layer on the average lateral displacement and found that the average displacement increased with increasing ground slope. They also observed that the velocity of ground displacement increased with ground slope.

Taboada et al. (1996) investigated the effect of ground slope on the lateral displacement in a lateral spread. Seven centrifuge tests were conducted with the same input motion but with various prototype ground slopes ranging from 0° to 10°. They found that the measured permanent lateral displacement increased with increasing prototype slope angle, as shown in Figure 4.10.

Based on U.S. and Japanese case histories of liquefaction-induced lateral spreads during previous earthquakes, Youd et al. (1999) developed an empirical model from multiple linear regression analyses. In their model, the magnitude of lateral displacement is proportional to a power of 0.343 of the ground slope (in percent) for sites with gently sloping ground. In addition, they found that lateral spread displacement markedly increased with the proximity of a free face and decayed logarithmically when the distance to the free face increased. This phenomenon was also clearly observed in the lateral

spreads that occurred during the 1995 Hyogoken-Nambu earthquake, as reported by Ishihara et al. (1996). Bartlett and Youd (1995) also observed that the height of the free face (i.e., the depth of a channel) influenced displacement as well. The higher the height of the free face, the larger the lateral displacement, if other factors are the same.

Rauch (1997) also conducted multiple regression analyses on the basis of case history lateral displacement data obtained during 16 major previous earthquakes throughout the world. He found that the square root of the average lateral displacement was linearly proportional to the ground slope and the height of the free face in a lateral spread.

4.5.2 The role of in-situ static shear stress

As discussed in Section 4.5.1, ground geometry (ground slope, distance to a free face, free face height) has a significant effect on lateral displacements in a lateral spread. Nevertheless, its effect can be partially or wholly explained as the effect of in-situ static shear stress on the lateral displacements. For example, the effect of ground slope on liquefaction-induced lateral displacements for sloping ground can be partially or fully explained as the effect of the static shear stresses in a direction parallel to the ground surface on the lateral displacements. This is because the static shear stresses are proportional to the ground slope. Although more complicated stress distributions likely exist in the vicinity of a free face for ground with a free face, generally the static shear stresses in a direction parallel to the ground surface decrease with increasing distance to a free face. This trend is similar to that for lateral displacements that decrease with increasing distance to a free face. Therefore, the effect of ground geometry can be explained partially as the effect of the static shear stresses. Of course, a free face provides an unrestricted boundary, leading to greater horizontal displacements of the ground during an earthquake, and this may not be accounted for by the static shear stresses.

Local slide failures may occur in the vicinity of a free face where high static shear stresses usually exist because of the steep slope of the free face. Local slide failure may

cause large deformations in the vicinity of the free face. The large deformations cannot be accounted for by the liquefaction-induced lateral spread discussed previously. In these cases, slope stability analysis may need to be conducted to evaluate the stability. Furthermore, if local slide failure occurs in the vicinity of a free face, retroactively progressive slide failures may also be triggered at the site, the mechanism of which is quite different from that of liquefaction-induced lateral spreads.

4.6 Boundaries and the Three-dimensional Distribution of Liquefied Layers

4.6.1 The effects of the three-dimensional distribution of liquefied layers

The vertical distribution of liquefied soil layers in a lateral spread may have an effect on the magnitude of the lateral displacement. For instance, consider two sites with the same ground slope and with liquefied layers with the same soil conditions (e.g., same thickness of liquefied layers and the same factor of safety against liquefaction) but having different vertical positions. The liquefied layer is close to the ground surface in one site as shown in Figure 4.11 (a) but at a deep depth in the other site, as shown in Figure 4.11 (b). Logically, it is expected that the magnitude of the lateral displacements resulting from the same earthquake for these two sites may be different due to the different effects of the upper non-liquefied layers. The same comments may be made for a lateral spread that occurs in ground with a free face. For the three cases, as shown in Figure 4.12, other conditions remain the same, but the vertical position of the liquefied layer is different. It is also envisaged that the magnitude of the lateral displacements resulting from the same earthquake for these three cases may be different and would be the largest for the case shown in Figure 4.12 (a) and the smallest for the case in Figure 4.12 (c) because of the different effects of lateral confinement. The soil profile for each of the hypothetical cases discussed above is only with one layer of liquefied soils. In fact, multiple liquefied layers may exist for some of sites in the field, thus making the effect of the vertical distribution of liquefied layers even more complicated.

A horizontally continuous and uniform sandy soil layer rarely exists in the field even for man-made soil structures. Figure 4.13 is one example that illustrates the lateral variation of the thickness of the liquefied layers and the liquefaction-induced lateral displacements at a site in Noshiro City where extensive lateral spreads occurred during the 1983 Nihonkai-Chubu earthquake. Figure 4.13 shows that both the thickness of the liquefied layers and the liquefaction-induced lateral displacements at the site changed dramatically in the horizontal direction. The variation of the properties and thickness of the liquefied layers in the horizontal direction creates more difficulties in estimating liquefaction-induced lateral displacements.

4.6.2 The effects of boundaries

The magnitude and direction of displacements in a lateral spread may be affected by natural or constructed features in the vicinity. For example, O'Rourke and Lane (1989) reported that a lateral spread in San Francisco was strongly influenced by the underlying topography. Hamada et al. (1986) found that the slope of the bottom non-liquefied layer beneath a liquefied later affects the direction and magnitude of the lateral displacements if the slope of the bottom non-liquefied layer is greater than the surface slope. In contrast, Yasuda et al. (1992) and Sasaki et al. (1992) found that almost no displacement occurred for level ground with an inclined bottom in their shake-table tests. They also observed that the direction of lateral displacements was controlled by the direction of the inclined ground surface and not by that of the inclined bottom when the ground surface and the bottom non-liquefied layer inclined in the opposite direction. Rauch (1997) thought that a level surface over a liquefied deposit of variable thickness would become sloped as a result of greater settlements in the thicker sections, and consequently, displacements might occur in the direction towards greater thickness of the liquefied soil. Nevertheless, the role of the bottom geometry of a liquefied soil layer is not clear at the current stage.

Retaining walls, quay walls, piles, piers, tunnels, pipelines, and other structures can constrict the movement of a lateral spread. This was evidenced in many case history sites

(e.g., some sites in Niigata City (Hamada 1992b)). On the other hand, local large ground deformation caused by the failure of retaining structures such as quay walls and retaining walls may not be interpreted as liquefaction-induced lateral spreads.

The lateral displacements in a lateral spread are not uniform even for a sloping ground with a uniform sandy soil in shake-table tests. Sasaki et al. (1992) observed that the lateral displacement is at its maximum at the top of a slope but negligible at the toe of a slope in their shake-table tests. Besides the lateral displacements, subsidence occurred near the top, while heaving was evident near the toe.

The boundaries of a lateral spread are usually defined by the general limits of the liquefied deposit. Ground surface failures can also extend for some distance beyond the boundary edges. O'Rourke and Lane (1989) named this feature marginal slumping. Marginal slumping occurs when movement of the soil blocks in a lateral spread releases the lateral supports to the soil further up the slope. Ground deformations may then occur beyond the zone of liquefied soil.

4.7 Redistribution and Drainage of Excess Pore Pressures

4.7.1 The effect of the redistribution of pore water in an undrained liquefied layer

Shake-table (Liu and Qiao 1984) and centrifuge (Fiegel and Kutter 1994a) tests have shown that pore water draining from the voids of loose layers can accumulate beneath the less permeable layers and form water interlayers (Kramer 1996). Kokusho (1999) also observed that a water film developed beneath the silt layer overlaying a loose sand layer in his shake-table tests. He also found that the maximum thickness and duration of a water film were approximated as being inversely proportional to the sand density, indicating that the effect of a water film will be more pronounced for looser soils. If a water film is formed in a sand layer continuously along a potential slip surface due to a less permeable upper soil layer, the upper soil might move as a block along the water

film. This may explain the observation by Fiegel and Kutter (1994b) as discussed in Section 4.2.3 that the lateral displacement was concentrated along the interface between an upper silt layer and a lower sand layer in one of their centrifuge model tests. Based on the above-mentioned observations, it is probable that the water film effect has an important role in lateral spread for a liquefied, very loose sand layer overlaid by an impervious soil layer in the field.

In addition, even if a water film is not formed, the upward migration of pore water and the tendency for soil grains to settle will probably result in a weaker sandy layer beneath a low permeability layer. Below a clayey, surficial soil at the site studied by Youd and Bennett (1983), the penetration resistance was significantly lower in the upper one to two meters of thick sand deposit that was liquefied.

4.7.2 The effects of the drainage of excess pore pressures in a liquefied layer

The migration of pore water in partially drained conditions can have a significant impact on the magnitude of displacements in a lateral spread since some degree of pore water drainage almost always occurs in nature (Rauch 1997). Stark and Mesri (1992) noted that partial drainage of excess pore pressures can produce an increase in shear resistance as sliding progresses and therefore reduce the magnitude of lateral displacements in a lateral spread.

On the other hand, excess pore pressures generated in a liquefied soil deposit can increase the pore pressures in adjacent soils. Seed and Lee (1966) pointed out that the migration of excess pore pressures might cause liquefaction of adjacent soils even when the adjacent soil would not otherwise be subject to liquefaction in a given seismic event. Upward movement of pore water can even induce liquefaction or softening of the sandy soil in the capillary zone just above the ground water level. One piece of field evidence is that a permanent lateral strain of about 3% in the sandy soil above the ground water level in one of the Moss Landing case history sites during the 1989 Loma Prieta earthquake was measured by an inclinometer that was installed before the earthquake, as

shown in Figure 4.7 (c).

4.8 Acceleration Isolation due to Liquefaction of Underlying Soils

4.8.1 Isolation of acceleration

The development of positive excess pore pressures leading to soil liquefaction causes soil stiffness to decrease during an earthquake. With the decrease in soil stiffness, the amplitude and frequency content of the surface motion may change considerably throughout an earthquake (Kramer 1996). In the most extreme case, the development of liquefaction in even a thin very loose sandy soil layer can cause the stiffness of the soil layer to be so low that the high-frequency components of bedrock motion cannot be transmitted to the upper soil layers above the liquefied layer. This phenomenon has been observed in the recorded accelerograms from several past earthquakes and measurements of accelerations in both centrifuge and shake-table tests.

In the 1964 Niigata earthquake, an accelerogram (Aki 1988) recorded at a building resting on liquefiable soil shows that both the acceleration amplitude and frequency were reduced after about 7 seconds since the motion began when the soil was liquefied. Compared with the recorded accelerogram on the bedrock close to Treasure Island, O'Rourke and Pease (1992) also noticed that the recorded surface acceleration experienced a sudden drop after about 15 seconds on Treasure Island where the loose hydraulic fill was liquefied during the 1989 Loma Prieta earthquake. Furthermore, a vertical array of seismometers was installed at depths of 83m, 32mm 16m and 0m from the ground surface at Port Island in Kobe, Japan before the 1995 Hyogoken-Nambu (Kobe) earthquake (Iwasaki and Tai 1996). Figure 4.14 shows the recorded motions of EW components at the different depths at the Port Island during the 1995 Kobe earthquake. It can be seen that both the magnitude and frequency of the motion at the ground surface are much smaller than those at deep depth. Iwasaki and Tai (1996) concluded that the fill material within the top 15 m in the Port Island may have liquefied

during the earthquake and the liquefaction caused de-amplification of the higher frequency components of the earthquake acceleration.

Kanatani et al. (1995) studied the behavior of saturated sand subject to earthquake excitation through large shake-table tests. They found that the response acceleration near the ground surface (A1) was almost zero after 2 seconds in the tested loose sand ($D_r = 57\%$), as shown in Figure 4.15, and concluded that the dramatic decreases in the response accelerations in the loose sand were caused by a high pore pressure ratio of about 0.84.

Taboada (1995) conducted ten centrifuge model tests of liquefaction-induced lateral spreading to simulate a horizontal or sloping 10 m thick uniform layer of water-saturated coarse sand ($D_r = 45\%$) of infinite lateral extent on an impervious rigid base. The slope angle simulated in the field ranged from 0° to 10° . Figure 4.16 shows the recorded lateral accelerations at depths of 0.0 m, 2.6 m, 7.5 m, and 10 m (base) in one of Taboada's tests with a field ground slope of 1.3° (a 2.3% slope). Note that the accelerations were dramatically reduced after 3 seconds at the ground surface and 6 seconds at a depth of 2.6 m. Interestingly, the pore pressure measurements indicated that the times for the changes of accelerations exactly coincided with the times of the occurrence of pore pressure ratios reaching one (fully liquefied) at the surface and a depth of 2.6 m. However, there was almost no change in the acceleration at a depth of 7.5 m because the sand at a depth of 7.5 m was not fully liquefied (the pore pressure ratio was much less than one) during the test. These observations further support the idea that a liquefied zone may isolate the upper zones from further seismic excitation during earthquakes.

Another interesting observation from Taboada (1995) is that the isolation of acceleration by liquefied layers plays less of a role with an increase in ground slope for sloping ground. Figure 4.17 compares the recorded accelerations at the ground surface for ground with the different field slope angles of 0° , 1.3° , 4.8° , and 10° under a similar base acceleration. Figure 4.17 shows that a sudden drop in accelerations for ground with the slope angles of 0° and 1.3° was clearly observed but no obvious reduction in

accelerations for ground with the slope angles of 4.8° and 10° occurred even though the sand at the shallow depth was fully liquefied during all the tests. Instead, large upslope acceleration spikes were observed for ground with the slope angles of 4.8° and 10° , which were due to the dilative shear-strain response as discussed in Section 4.3.2. However, Abdoun (1997) conducted several centrifuge tests using the same equipment but for the models with three layers of soils (non-liquefiable layer, liquefiable layer, and non-liquefiable) and with a field ground slope angle of 4.8° . The measurements in his tests indicated that the recorded accelerations in the top non-liquefiable layer dropped dramatically after the liquefaction of the underlying liquefiable sand even for ground with a slope angle of 4.8° .

On the other hand, the effect of the liquefaction of underlying soils on the acceleration of upper soil layers also depends on the horizontal extent of the liquefied layers. In real situations, seismic energy will be transmitted to the liquefiable site both through its base and through non-liquefied soil at the edges of the liquefiable deposit. This has an important influence on site response since the relatively stiff soils at the edges have a greater potential for transmission of forces in comparison with the semi-fluid nature and low stiffness of the liquefied soil. Pease and Bureau (1998) concluded that most of the energy transmitted into the surface non-liquefied layer over a narrow liquefied site appears to occur through the horizontal boundaries (or edges), and the characteristics of the liquefied soil have little influence on the observed behavior.

4.8.2 The effects of acceleration isolation due to liquefaction of underlying soils

Seismic acceleration of a soil layer in level ground or in gentle slopes (less than 5%) may be reduced due to the liquefaction of the underlying soil layers as discussed above. This reduction in acceleration may also influence the development of shear strains in the upper layers and therefore may limit resultant lateral displacements in a liquefaction-induced lateral spread.

Figure 4.18 shows the profiles of permanent lateral displacement at the end of shaking for

different slope angles in the field, α_{field} , in the centrifuge model tests conducted by Taboada (1995). Figure 4.18 indicates that the top layer of about 2.0 m in the models with slope angles equal or less than 4.8° did not contribute much to the lateral displacements at the ground surface. The reduction in acceleration in the upper zone due to liquefaction of the underlying soil zones appears to be a major reason for this phenomenon. Similar phenomena were also observed in centrifuge tests performed by Abdoun (1997) as shown in Figure 4.4 and in the shake-table tests conducted by Sasaki et al. (1991) as shown in Figure 4.1. In addition, based mainly on the observations in shake-table tests, Towhata et al. (1991, 1992, 1999) used a sinusoidal function to simulate the distribution of horizontal permanent displacement along a vertical cross section of a uniform liquefied soil layer. This implies that they assumed that the upper zone in the liquefied layer contributes much less to the permanent displacement at the ground surface than the lower zone of the liquefied zone does.

4.8.3 The effects of liquefaction sequence of multiple liquefied layers

The effect of the acceleration reduction in the upper zone by liquefaction of the underlying soil zones on lateral displacements in a liquefaction-induced lateral spread for a uniform liquefied layer has been discussed in Section 4.8.2. The effect is more complicated for ground with multiple liquefied layers as shown in Figure 4.19.

For example, consider that two gently sloping grounds are with two similar liquefiable layers and experience the same earthquake but are with reverse vertical distribution of the two liquefiable layers, as shown in Figures 4.19 (a) and (b). For the case in Figure 4.19 (a), the soil liquefaction in the upper very loose sand layer may not affect the triggering of liquefaction in the lower medium dense sand layer. If the earthquake loading is strong enough, soil liquefaction can be triggered in the lower medium dense sand layer as well. As a result, both layers may contribute to the lateral displacement of the ground. On the other hand, for the case in Figure 4.19 (b), because soil liquefaction may be triggered first in the lower very loose sand layer and thus isolate the upper medium dense sand layer from further seismic acceleration, the upper medium dense sand layer may not be

liquefied during the same earthquake. Therefore, it seems that the liquefaction sequence of multiple liquefied layers may also influence the liquefaction-induced lateral displacements.

4.9 Conclusions

Liquefaction-induced lateral spreads are a pervasive type of liquefaction-induced ground failures for gentle slopes or on level (or gently inclined) ground with a free face (e.g., river banks, sea walls, road cuts). During past major earthquakes, enormous damage to engineered structures and lifelines has been caused by liquefaction-induced ground lateral spreads. A lot of research has been conducted to investigate the mechanisms and controlling factors of lateral spreads by means of laboratory cyclic triaxial or simple shear tests, one g shake table tests, and dynamic geotechnical centrifuge model tests. The review of the available testing results of these tests and the studies of case histories associated with past earthquakes generally suggest the following observations and conclusions:

- Test results from one g shake table and centrifuge model tests and observations from case histories generally support the hypothesis that lateral displacements in a liquefaction-induced lateral spread result from distributed residual shear strains throughout liquefied layers. Three major components controlling the magnitude of liquefaction-induced lateral displacements are the maximum shear strains in liquefied layers, the thickness of liquefied layers, and geometric parameters characterising ground geometry (e.g., ground slope, free face height, and the distance to a free face) at a studied site.
- Soil properties (e.g., soil density, soil composition, grain characteristics, as well as structure and age), earthquake characteristics (e.g., earthquake magnitude, the distance to seismic energy or fault rupture, peak horizontal ground acceleration, the duration of strong motion), and ground geometry are three of the most important

factors influencing liquefaction-induced ground lateral spreads. Two of the three major components controlling the magnitude of liquefaction-induced lateral displacements, the maximum shear strains in liquefied layers and the thickness of liquefied layers, are mainly determined by soil properties and earthquake characteristics.

- The restraint on shear strain due to soil dilative response at large strain has been observed in laboratory cyclic triaxial/simple shear tests, shake table tests, and centrifuge model tests. The soil dilative response may lead to a strong restraining effect on the magnitude of cyclic and accumulated residual shear strains of soils in a lateral spread.
- Both boundaries and the three-dimensional distribution of liquefied layers may have effects on lateral displacements in lateral spreads. The effect will be on a case-by-case basis.
- The seismic acceleration of a soil layer in level ground or gentle slopes (less than 5%) may be reduced due to the liquefaction of the underlying loose soil layers. This reduction of acceleration may also influence the development of shear strains in the upper layers and, therefore, may limit the resulting lateral displacements in a liquefaction-induced lateral spread. This phenomenon is supported by an approximate sinusoidal function distribution of horizontal permanent displacement along a vertical cross section of a uniform liquefied soil layer in shake-table and centrifuge model tests.
- Redistribution (including the development of a water film beneath a low permeability layer) and drainage of excess pore pressures in liquefied layers during earthquakes may also play some role in a lateral spread. However, it is very difficult to quantify their effects.
- A water film may be formed at the top of a liquefied, very loose thick sand layer

beneath a soil layer with a very low permeability. This film may either lead to the potential for large and concentrated displacements occurring along the film because of its very low shear strength and stiffness or may possibly isolate the upper layers from further seismic acceleration and thus limit the lateral displacement at the ground surface if static driving shear stresses at a given site are low enough and a flow slide will not be triggered.

Although the mechanisms and controlling factors of liquefaction-induced lateral spreads are complex and have not been fully understood currently, there is a need for tools to estimate the magnitude and distribution of lateral displacements in lateral spreads. In Chapters 7, 8, and 9 of this thesis, a set of new semi-empirical approaches to estimate the magnitude and distribution of lateral displacements in lateral spreads will be developed.

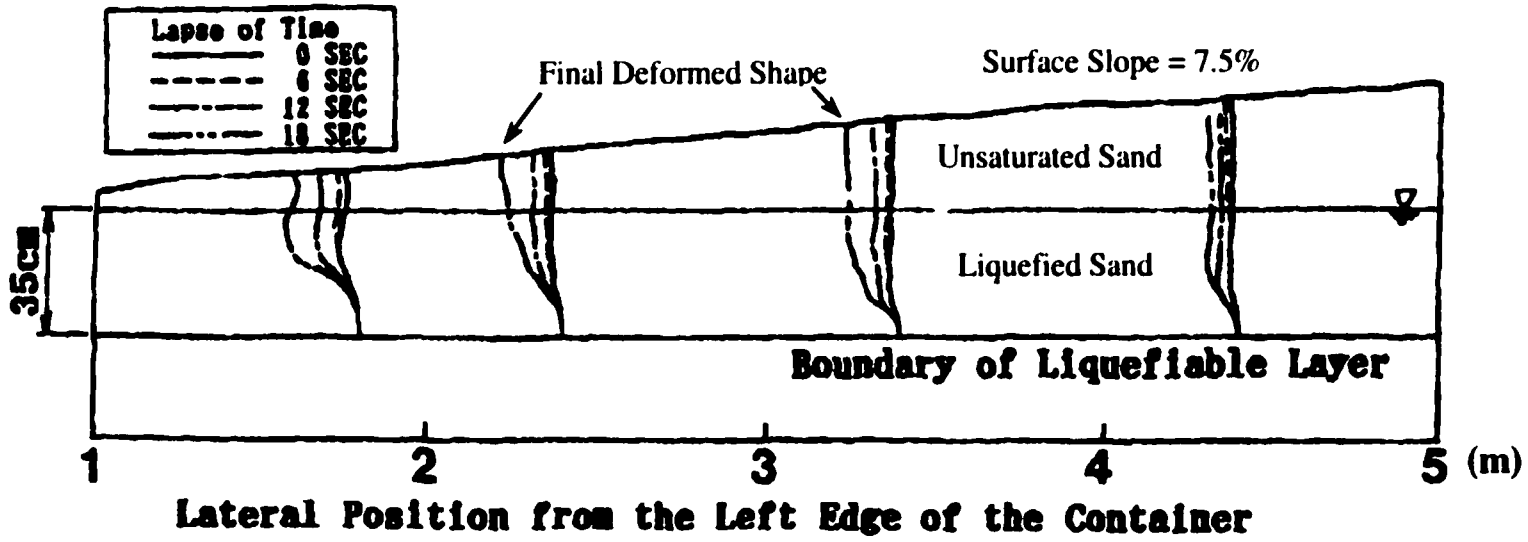


Figure 4.1 An example of time history of lateral displacement in one of the one-g shake-table tests by Sasaki et al (1991)

(modified from Sasaki et al. (1991))

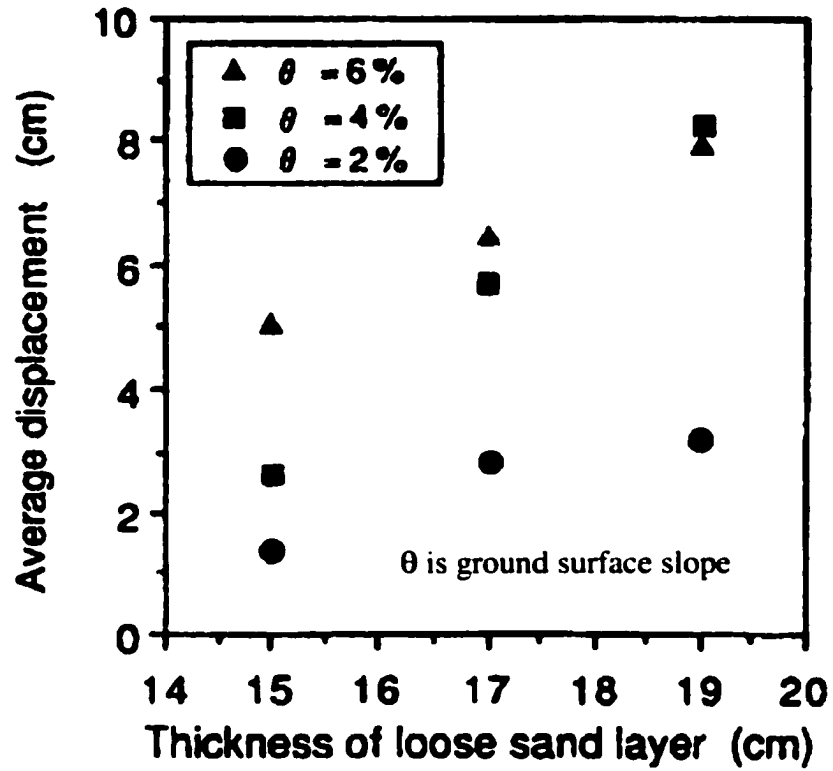
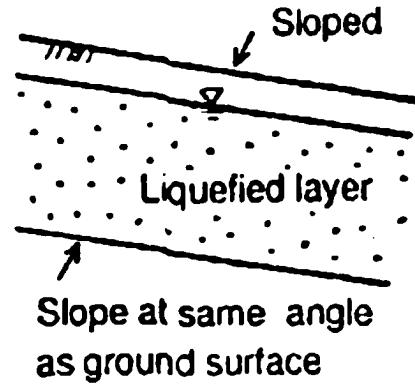
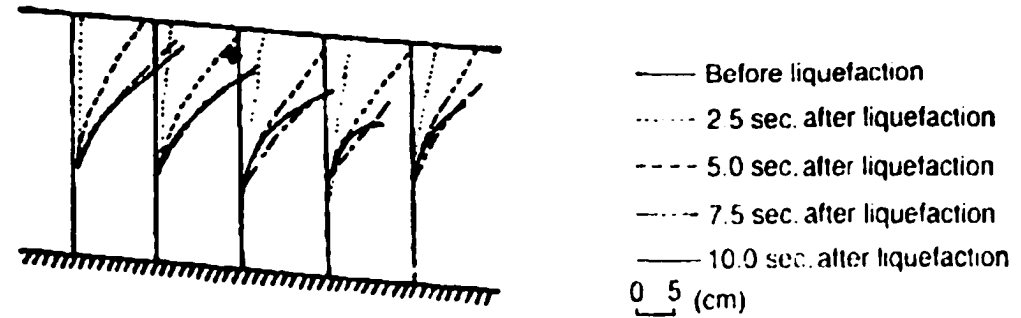


Figure 4.2 Relationship between thickness of loose sand layer and average displacement in one-g shake-table test by Miyajima et al. (1991)

(modified from Miyajima et al. (1991))



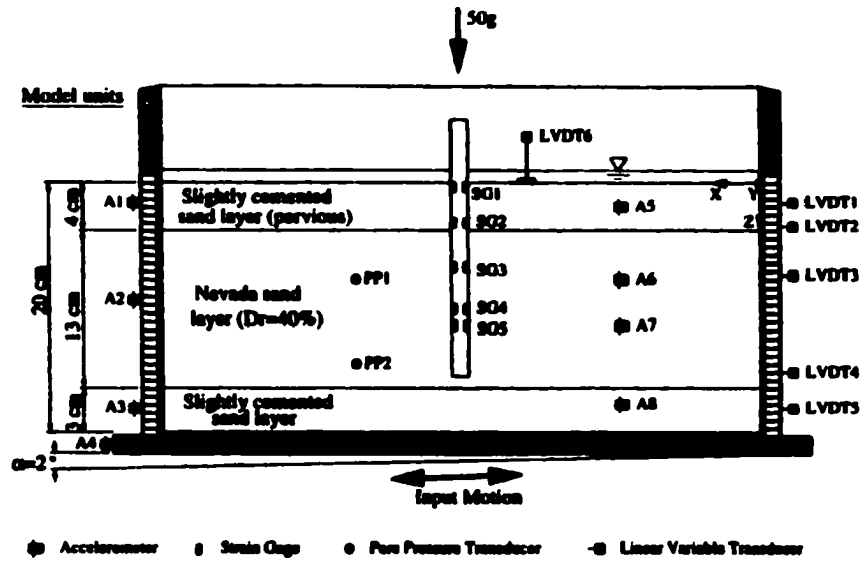
(a) Sketch of a soil model used in the test



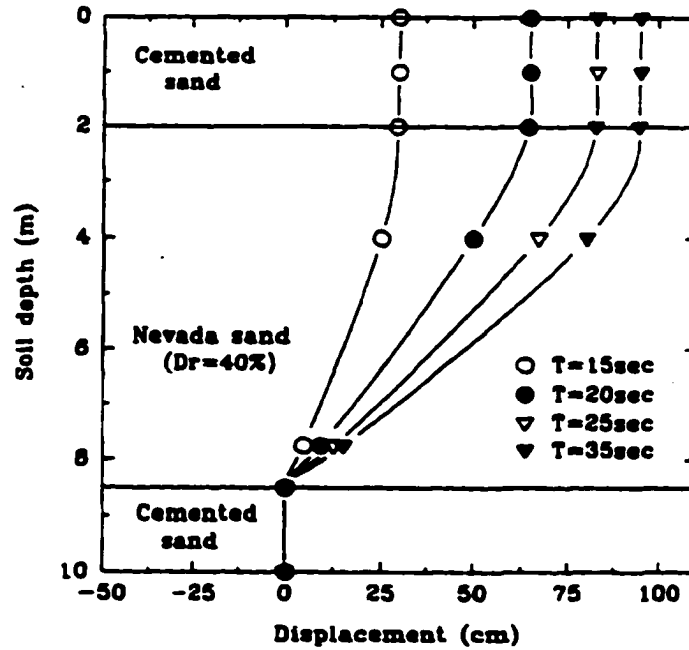
(b) Time history of lateral displacement

Figure 4.3 An example of lateral displacements in one-g shake-table test by Yasuda et al. (1992)

(modified from Yasuda et al. (1992))



(a) Sketch of a model setup and instrumentation location



(b) Soil lateral displacement profiles at different times during shaking

Figure 4.4 An example of the model setup and measured lateral displacements in one of the centrifuge model tests by Abdoun (1997)

(modified from Abdoun (1997))

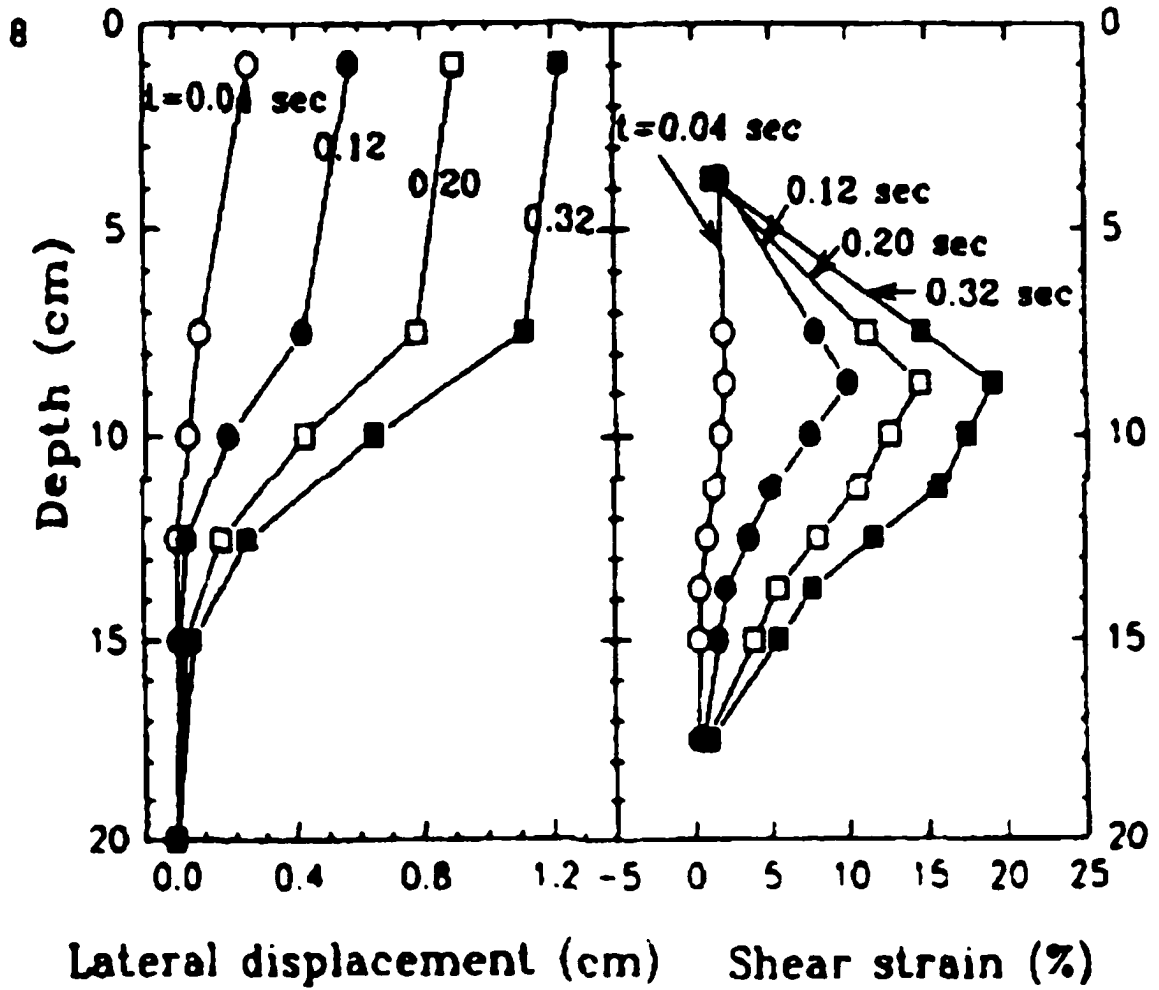
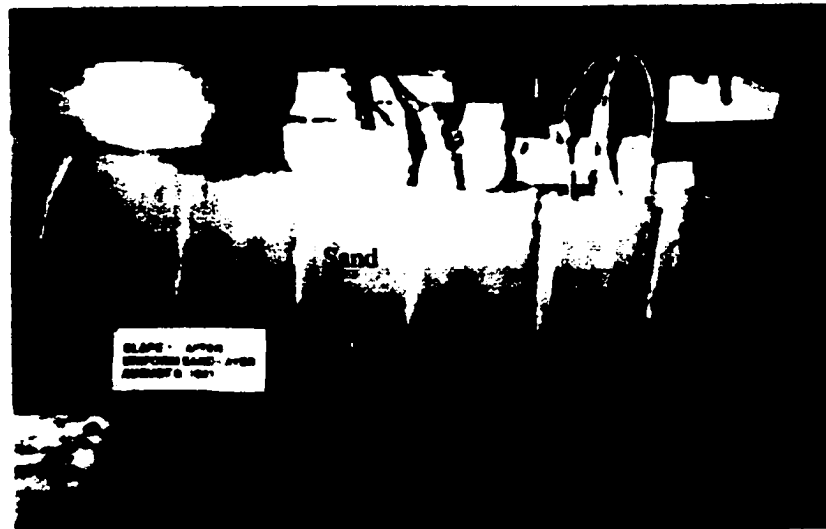
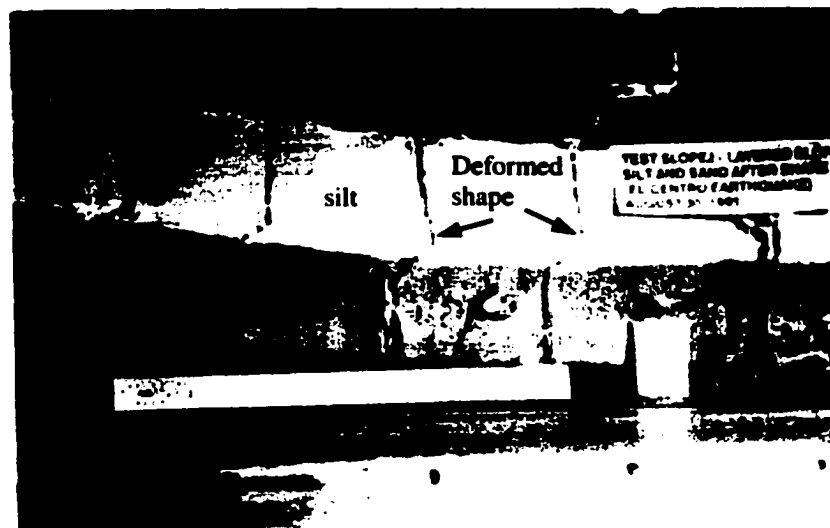


Figure 4.5 An example of the profiles of the measured lateral displacements and shear strains in one of the centrifuge model tests by Taboada and Dobry (1998)

(modified from Taboada and Dobry (1998))



(a) Pattern of lateral displacement in a uniform sand



(b) Pattern of lateral displacement in a two layer system
(a uniform sand layer overlain by a silt layer)

Figure 4.6 Patterns of lateral displacements in centrifuge modeling tests by Fiegel and Kutter (1994b)

(modified from Fiegel and Kutter (1994b))

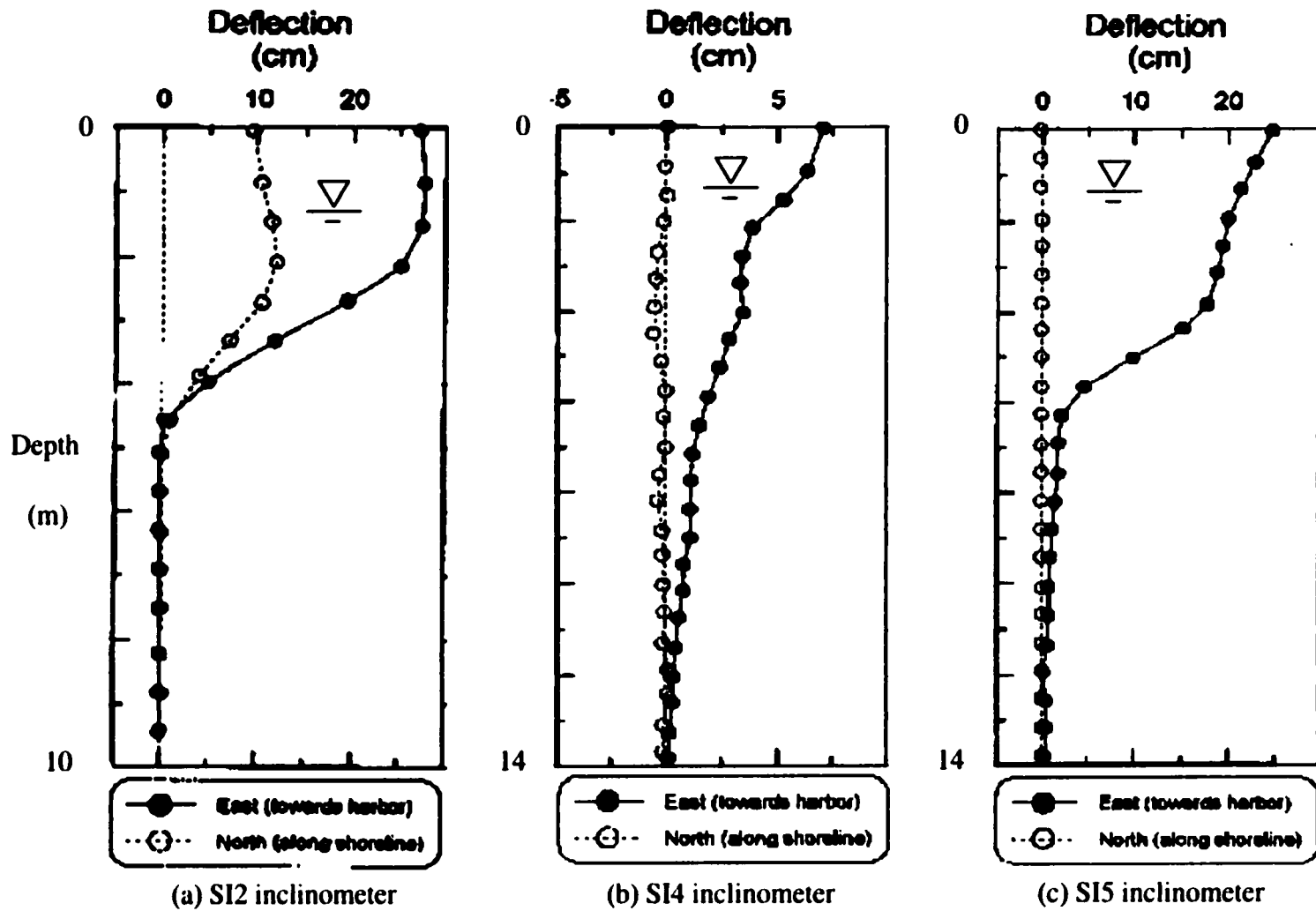


Figure 4.7 Filed measurements of lateral displacements with depth by the inclinometers at one of the Moss Landing case history sites during the 1989 Loma Prieta earthquake (modified from Boulanger et al. (1995))

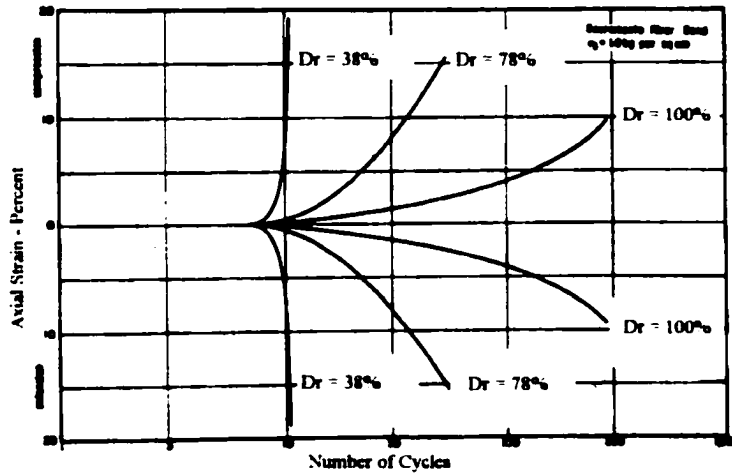


Figure 4.8 Axial strain vs. number of cycles for a sand with different relative density, D_r , in cyclic triaxial tests by Seed and Lee (1966)

(modified from Seed and Lee (1966))

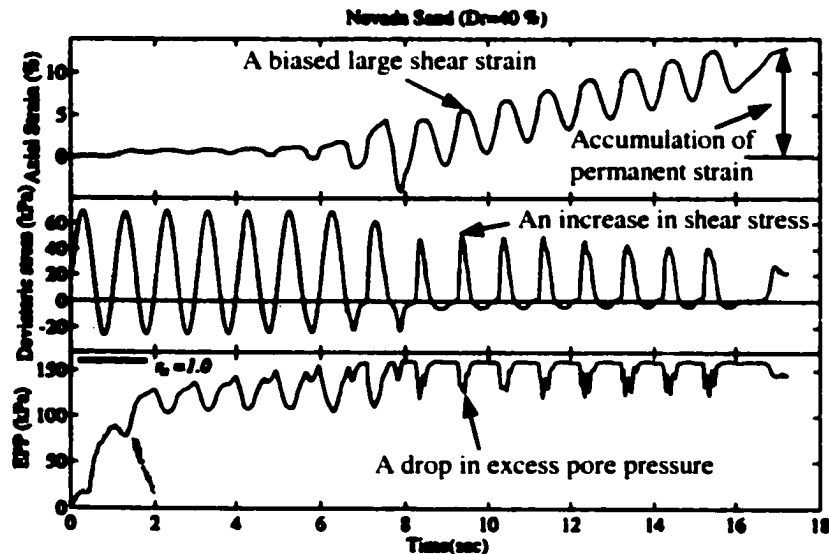


Figure 4.9 Time histories of strain, stress, and excess pore pressure (EPP) for an undrained stress-controlled cyclic triaxial test of Nevada Sand ($D_r = 40\%$) with an imposed static (initial) deviatoric stress tested by Arulmoli et al. (1992)

(modified from Arulmoli et al. (1992))

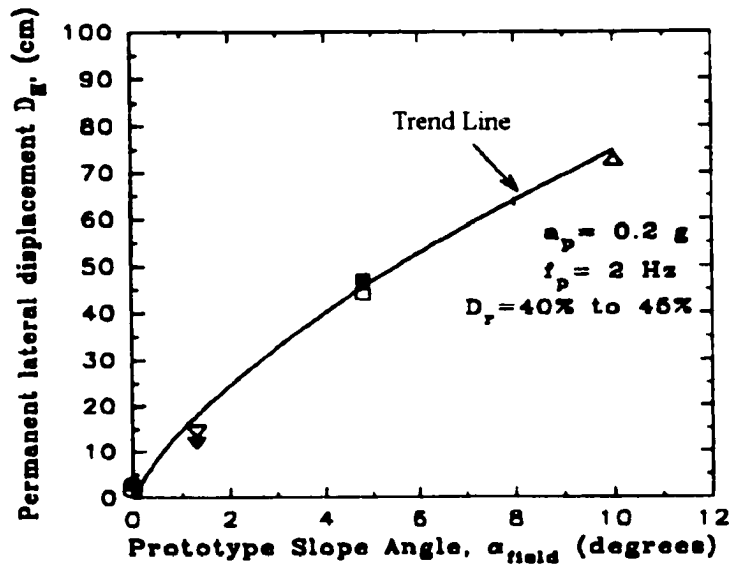


Figure 4.10 Liquefaction-induced permanent lateral displacement vs. prototype slope angle for sloping ground in centrifuge model tests by Taboada and Dobry (1996)

(modified from Taboada and Dobry (1996))

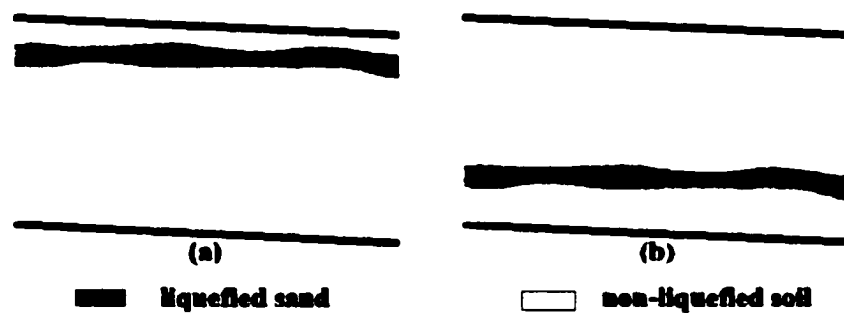


Figure 4.11 Sketches illustrating the potential vertical distribution of a liquefied sand later in a sloping ground

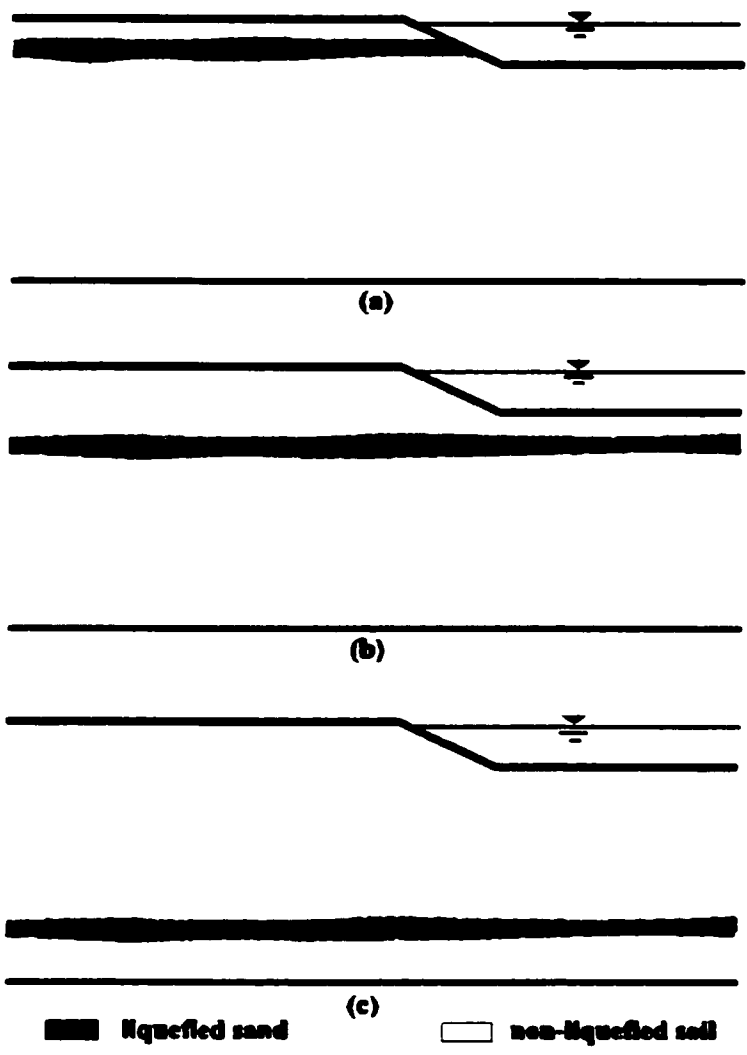


Figure 4.12 Sketches illustrating the potential vertical distribution of a liquefied sand layer in ground with a free face

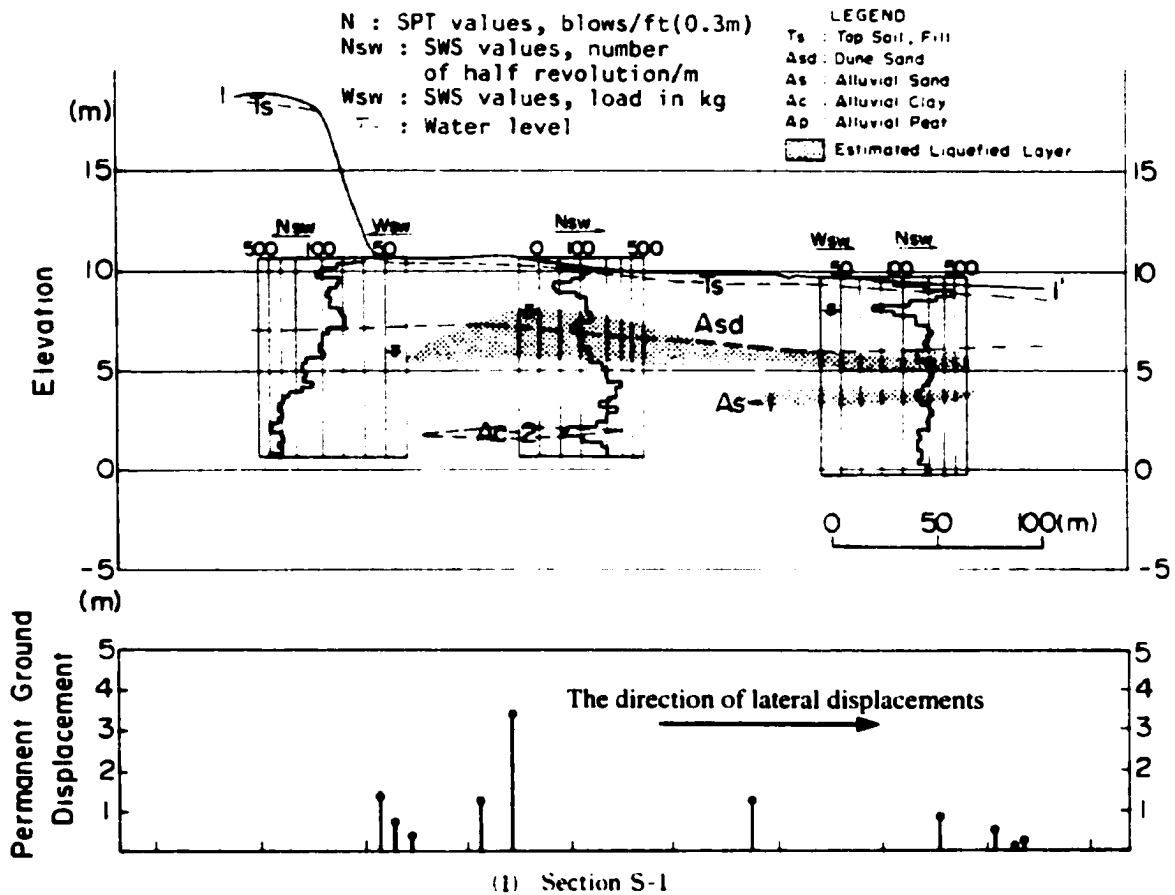


Figure 4.13 An example of non-homogenous soil layers and related liquefaction-induced lateral displacements in the field (Section S-1 in Noshira City under the 1983 Nihonkai-Chubu earthquake)

(modified from Hamada (1992b))

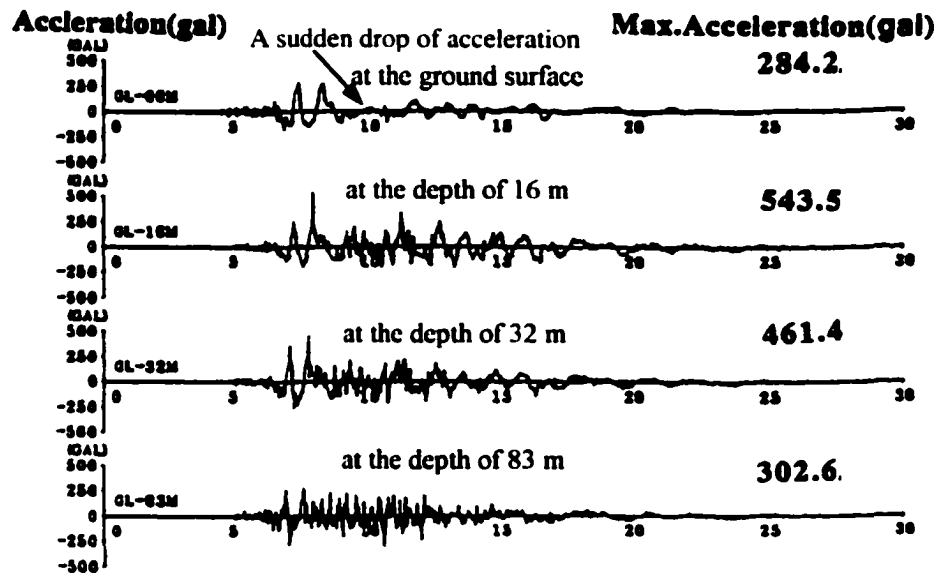


Figure 4.14 Recorded seismic motions in the vertical array of seismometers at Kobe Port Island during the 1995 Hyogoken-Nambu earthquake

(modified from Iwasaki and Tai (1996))

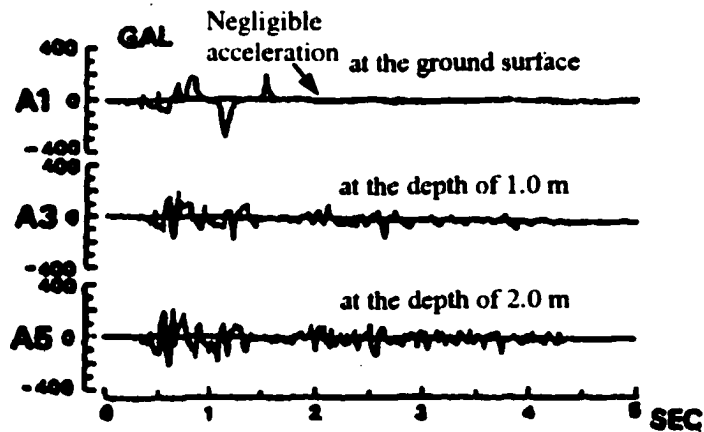


Figure 4.15 Time histories of the acceleration at the different depths in a loose sand in a large shake-table test by Kanatani et al. (1995)

(modified from Kanatani et al. (1995))

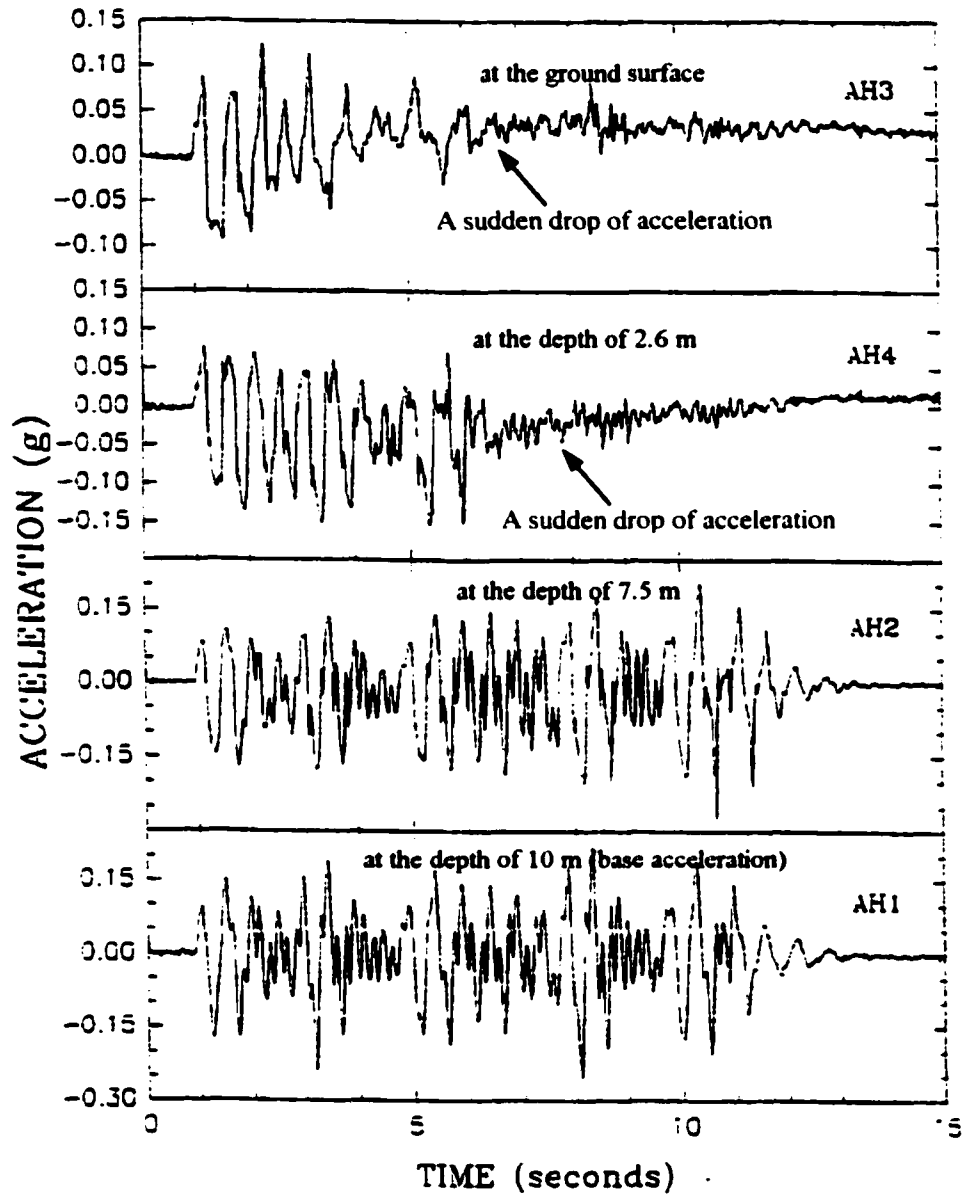


Figure 4.16 Lateral accelerations at the different depths in a sloping ground with the field slope angle of 1.3° in a cyclic centrifuge model test by Taboada (1995)

(modified from Taboada (1995))

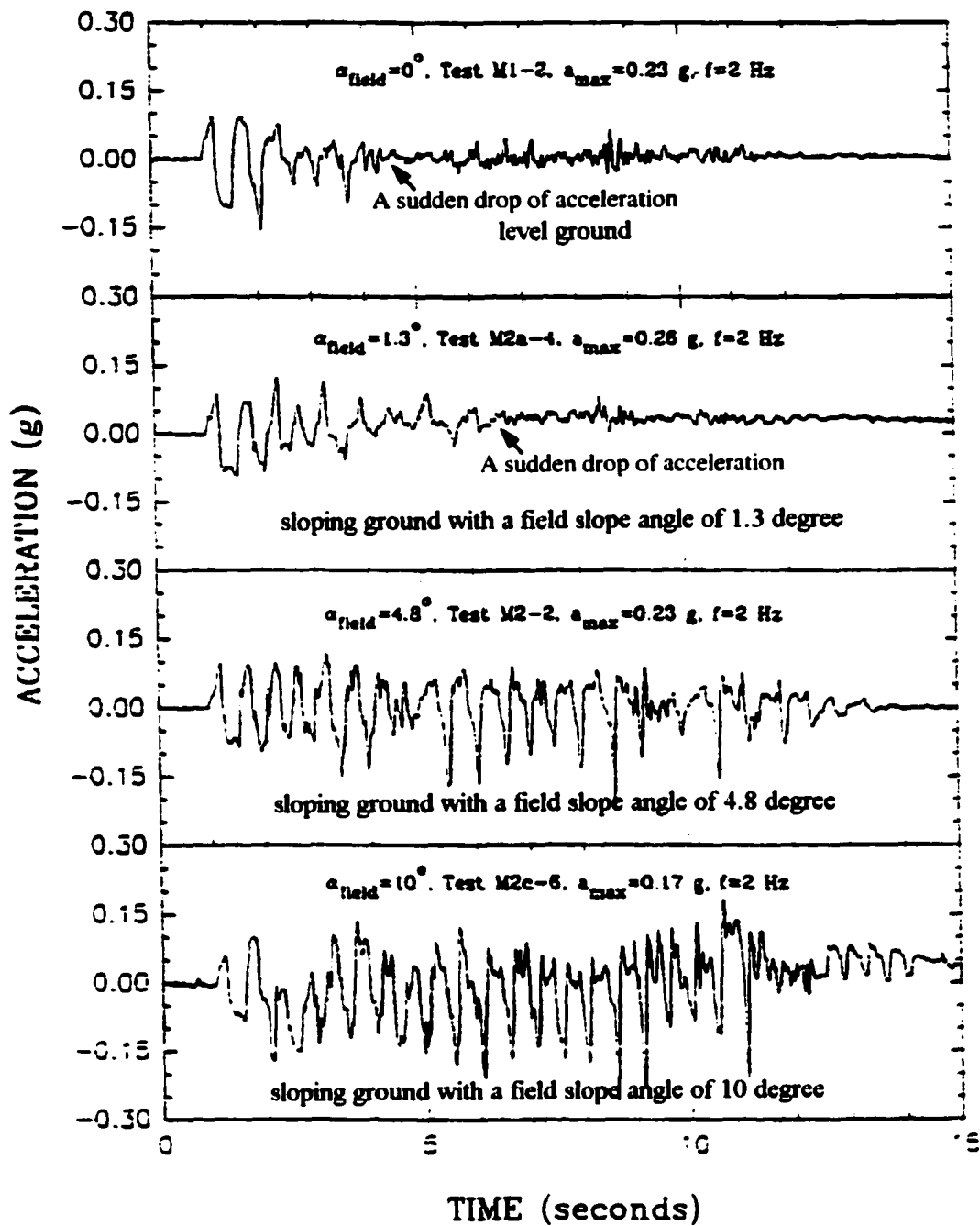


Figure 4.17 Acceleration time histories recorded at the ground surface for level and sloping grounds with the different slope angles in cyclic centrifuge model tests by Taboada (1995)

(modified from Taboada (1995))

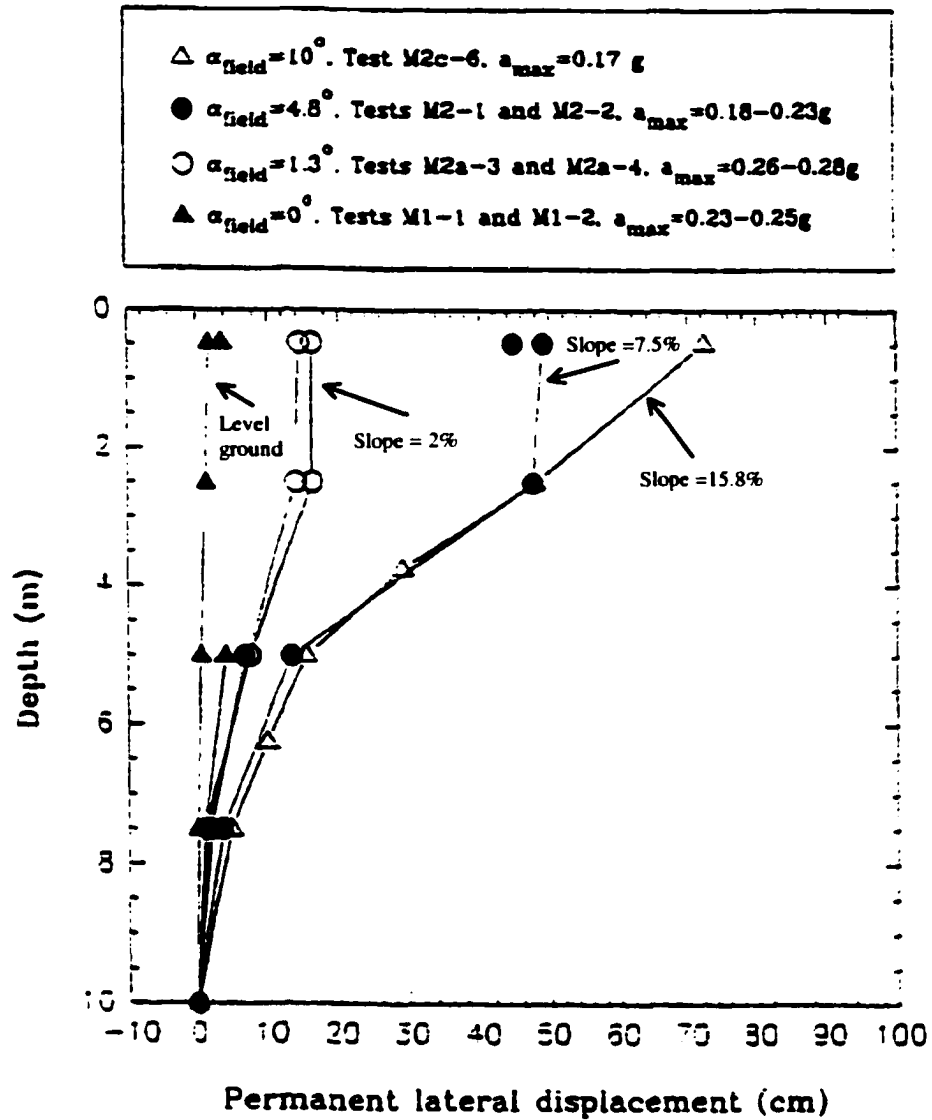


Figure 4.18 Profiles of liquefaction-induced lateral displacements at the end of shaking for sloping grounds with the different slope angles (or slope) in the field, α_{field} , in cyclic centrifuge model tests by Taboada (1995)
 (modified from Taboada (1995))

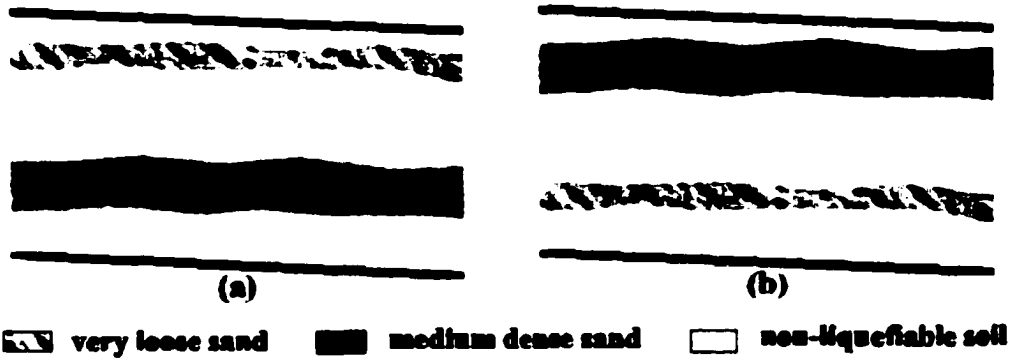


Figure 4.19 Sketches illustrating the potential vertical distribution of two liquefiable layers in a sloping ground

CHAPTER 5 PREVIOUS RESEARCH ON ESTIMATING HORIZONTAL GROUND DISPLACEMENTS ASSOCIATED WITH LIQUEFACTION- INDUCED LATERAL SPREADS

5.1 Introduction

Lateral spreads resulting from soil liquefaction during past earthquakes have caused tremendous damage to engineered structures and lifelines. During the past two decades, many research efforts have been made to estimate liquefaction-induced lateral spreading displacements. Currently, more than a dozen methods have been proposed to predict the magnitude of lateral displacements in lateral spreads. The methods can be grouped into four categories: laboratory scale model simulations, simplified analytical methods, stress-deformation analyses using finite element techniques, and empirical models. The major methods in each of the categories will be briefly reviewed, and the strengths and limitations of each of the methods will be discussed in this chapter.

5.2 Laboratory Scale Model Simulations

5.2.1 Shake-table modeling

In the last decade, Japanese researchers conducted a number of large shake-table tests to model the behavior of liquefaction-induced lateral spreads (Miyajima et al. 1991; Sasaki et al. 1991; Yasuda et al. 1992; Toyota and Towhata 1994). The effects of surface slope, bottom shape, thickness of soil layers, soil density, and other factors on lateral displacements were studied in these tests. The test results improved the understanding of mechanisms and controlling factors of liquefaction-induced lateral displacements. However, because shake-table models are limited in dimensions, laboratory one-g shake-table tests can not realistically simulate field conditions, including complicated soil stratigraphy, soil properties, and stress, drainage, and boundary conditions.

First, soil stratigraphy is complicated, and soil properties vary with depth in the field. So it is not realistic to fully simulate field soil stratigraphy and soil properties in laboratory shake-table models.

The depth to liquefied soils in the field is generally greater than the full height (less than 1.5 m in general) of shake-table models. Thus, the stress conditions in shake-table models are different from those in the field. Toyota and Towhata (1994) recognized that if a soil is contractive in the field, the same soil at the same density in a model under a lower overburden pressure might be dilative. Therefore, the liquefied soil behavior in a shake-table model may differ significantly from the field response.

Also problematic is the fact that shorter drainage paths in a scale model result in more rapid pore pressure dissipation rates than those found in the field (Rauch 1997). Consequently, the liquefied soil in a scale model tends to re-solidify more rapidly, resulting in smaller displacements, when the model is subjected to the same earthquake excitation as a lateral spread in the field.

Capillary rise can also be a significant factor in laboratory scale models when an unsaturated soil layer over a liquefiable soil layer, as is commonly found in the field, is modeled. Capillary action creates negative pore pressures that increase the shear strength of the soil because of larger effective stresses.

Finally, boundary conditions of the soil in a shake-table model may differ greatly from those in the field. For example, rigid box used in a shake-table model may restrict the down-slope lateral displacement at the toe of a slope close to the edge of the box.

5.2.2 Centrifuge modeling

Geotechnical centrifuge equipment has been used to simulate liquefaction-induced lateral spreading of gently sloping ground (Fiegel and Kutter 1994b; Taboada 1995; Elgema et

al. 1996; Abdoun 1997). Centrifuge modeling is another useful tool in investigating the mechanisms and controlling factors involved in liquefaction-induced lateral spreads. Because of its capability in simulating field vertical static stresses in a centrifuge model, centrifuge modeling is also useful in illustrating the pattern of displacements across a vertical section through a liquefied soil. However, centrifuge models of lateral spreading can suffer from the same deficiencies encountered in one-g shake-table models, as discussed in Section 5.2.1. Moreover, centrifuge models of lateral spreading are hampered by two additional, significant problems.

The first drawback with centrifuge models arises from the difficulty in scaling the time rate of pore water seepage (Rauch 1997). For a model accelerated to N g's, seepage and pore pressure dissipation will proceed as if the soil in the prototype had a permeability N times greater than the soil in the centrifuge model (Fiegel and Kutter 1994b). Hence, a model constructed of silt might have the seepage characteristics of clean sand in the field. Simulating the liquefaction and lateral spreading of real soils is thus problematic. An alternative way to solve this problem is to saturate the soil used in a centrifuge model with a fluid of greater viscosity, such as silicone oil or a glycerine-water mix. However, such a fluid may adversely affect the simulation in other ways. For example, the presence of an oily fluid on the constitutive properties of the soil produces unknown effects on intergranular friction in sandy soils, while the effects on fine grained soils like silts and clays are obviously much more complicated (Ko 1994).

Furthermore, Arulanandan and Scott (1993) reported difficulties in accurately determining displacements in centrifuge tests. Very small displacements occurring in the centrifuge model correspond to large movements in a real slope. However, precise displacement measurements in the scale model are much difficult. Arulanandan and Scott consider measured displacements to be inherently less accurate than all other measured data in centrifuge models of liquefaction events.

5.3 Simplified Analytical Methods

5.3.1 Sliding block analysis

Newmark (1965) proposed a practical approach for estimating permanent ground displacements of slopes and embankments due to earthquake shaking based on an analogy to a rigid block resting on a frictional inclined plane under seismic loading. For example, for a given rigid block resting on a frictional inclined plane under seismic loading, if seismic inertial forces acting on the rigid block become large enough that the total (static plus dynamic) driving forces exceed the available resisting forces, the factor of safety calculated by the pseudo-static limit equilibrium analysis will drop below 1.0, at which point the block is no longer in equilibrium. As a result, the block driven by the unbalanced force will move. The calculated seismic acceleration causing the factor of safety equal to 1.0 for the block is defined as yield acceleration. If the earthquake accelerations exceed the yield acceleration at various time intervals, displacements are initiated during those time intervals. The displacements are computed by a simple double integration procedure.

The Newmark (1965) approach is based on several simplified assumptions. These include:

- Displacements occur along a single, well defined slip surface;
- The soil above the slip surface behaves like a rigid block;
- The soil does not undergo strength loss as a result of shaking, and yield acceleration remains constant during sliding;
- No site response analysis is conducted to determine acceleration time history.

The Newmark (1965) approach has been used extensively by engineers and/or modified by a number of researchers. Generally, there are four major types of improvements or modifications to the original Newmark procedure:

- to develop new design charts using the recorded acceleration time histories and/or probability theory (e.g., Franklin and Chang 1977; Lin and Whitman 1986; Yegian et

al. 1991; Jibson 1993);

- to account for the dynamic response of slopes or embankments by applying decoupled (e.g., Madisi and Seed 1978; Bray et al. 1995) or coupled dynamic response analysis (e.g., Lin and Whitman 1983; Kramer and Smith 1997);
- to consider shear strength changes during earthquake shaking (e.g., Houston et al. 1987; Matasovic et al. 1997) or soil shear rate effects (e.g., Lomos and Coelho 1991; Tika-Vassilikos et al. 1993) for non-liquefiable geo-materials;
- to consider shear strength reduction of liquefiable soils due to liquefaction or excess pore pressure build-up during earthquakes (e.g., Sarma 1975; Castro 1987; Baziar 1991; Dobry and Baziar 1992; Byrnes et al. 1992; Jing et al. 1996).

However, despite the improvements or modifications mentioned above, the Newmark approach still has the following limitations, especially when it is applied to estimate displacements in a liquefaction-induced lateral spread:

- The Newmark approach is only suited to a rigid-body movement of soil. However, liquefied soils in a liquefaction-induced lateral spread are associated with large shear deformation and do not behave as a rigid body.
- A well-defined failure plane must be assumed in the Newmark approach. However, the results from one-g shake-table and centrifuge model tests and the observations from previous case histories appear to support the contention that liquefaction-induced lateral spreads are caused by the distributed shear strains throughout whole liquefied layers rather than by the concentrated shear strains along a well-developed shear plane, as discussed in Section 4.2.
- Shear strengths along the assumed shear plane, which are required for the Newmark analysis, are very difficult to determine. First, it is very difficult to obtain representative “undisturbed” saturated granular soil samples for laboratory testing. Second, it is unclear whether the type of shear strength to be used along the slip plane should be the peak or residual strength observed in monotonic undrained shear tests, or those observed in cyclic loading followed by monotonic shear. Furthermore, the shear strength in a liquefiable soil changes dramatically with the development of excess pore pressure, the occurrence of liquefaction, and subsequent deformations

during earthquake shaking. Finally, the dilative response of liquefied soils at large strains may also play a significant role in regaining shear strength at large cyclic shear strains, as discussed in Section 4.3.2.

- A single value for the calculated displacement is obtained for a lateral spread in the Newmark approach. Neither lateral nor vertical distribution of the displacement can be predicted using this approach. However, case histories (e.g., Hamada et al. 1986; Ishihara et al. 1996) have shown that lateral spread displacement markedly increased with the proximity of a free face and decayed logarithmically with increasing distance to the free face, as mentioned in Section 4.5.1.

Despite the above limitations, the Newmark approach has been widely used to estimate dynamic deformations of embankment dams or liquefaction-induced lateral displacements by practical engineers (Chugh 2000). It is believed that this approach will be continuously applied in geotechnical practice due to its following advantages:

- The approach is relatively simple and widely used by the geotechnical engineers.
- Both inertial and static forces can be taken into account in estimating lateral ground displacements.
- Real field recorded time histories of seismic motions can be used in this approach.

5.3.2 Towhata's minimum potential energy approach

Towhata et al. (1991, 1992, 1996, and 1999) developed a mathematical theory for the prediction of lateral ground displacements induced by soil liquefaction. Through the use of the knowledge obtained from shake-table tests, together with the principle of the minimum potential energy at force equilibrium, the theory of maximum possible displacement was developed. Towhata's model predicts maximum possible movements in a lateral spread, corresponding to the ultimate displacements that will occur if the foundation soil remains liquefied for a sufficient length of time. That is, lateral spreading is assumed to continue until a minimum energy state is achieved. In laboratory shake-table tests, the ultimate displacements are produced by shaking the models until down-slope displacements stop while the underlying soil remains liquefied. In the field,

Towhata's model corresponds to a long duration seismic event that results in the maximum possible movement of a lateral spread. Notably, Towhata's model assumes a flow failure under static loads and neglects inertial effects during dynamic loading.

The four key assumptions in Towhata's model, which are based on observations from shake-table model tests, are:

- The distribution of lateral displacements in a vertical cross section of a liquefied soil deposit can be represented by a sinusoidal equation – zero at the bottom and the maximum at the top of the liquefied layer.
- The volume of the liquefied soil is unchanged during deformation.
- The liquefied soil behaves as a liquid governed by the hydraulic gradient. Its shear stiffness and strength are generally set to zero.
- The surficial non-liquefied soil layer behaves like an elastic solid and is modeled as an elastic, 2-D beam that resists lateral movement of the liquefied, subsurface layer.

The advantages of the Towhata model can be summarized as the following:

- The material parameters required in the model are only the unit weights of the liquefied layer and top non-liquefied layer, and the Young's modulus of the top non-liquefied layer.
- The effect of the top non-liquefied layer can be quantified.
- Ground geometry, even though it is relatively simple, and other simplified boundaries can be taken into account.
- Both the lateral and vertical distributions of the displacements can be given.
- The closed-form solutions are available and relatively simple.

However, Towhata's analytical model appears to have four fundamental weaknesses:

- The model is capable of predicting only the maximum or ultimate displacements and generally overestimates lateral displacements in a liquefaction-induced lateral spread in most cases.
- The liquefied soil does not simply behave as a pure liquid with zero shear strength as assumed in the Towhata approach. The characteristics and behavior of liquefied soils

during and after earthquake shaking are much more complicated and have not been fully understood yet.

- Towhata's model relies on a parameter representing the elastic stiffness of the non-liquefied, surface soil layer. This parameter is poorly defined, not well understood, and difficult or impossible to measure (Rauch 1997).
- Only relatively simple geometry can be considered. Most importantly, steep free faces commonly associated with lateral spreads are almost impossible to simulate in the model.

5.3.3 Shamoto's residual shear strain charts

Shamoto et al. (1998) developed three charts to estimate the liquefaction-induced residual shear strain potential for soils with a fines content of 0, 10, and 20% respectively for level ground. Based on these charts, the residual shear strain potential can be estimated if the cyclic stress ratio, adjusted SPT N-value, and fines content of a soil are known. Shamoto et al. (1998) suggested calculating the maximum liquefaction-induced horizontal ground surface displacement in level ground near a waterfront (e.g., in the soils behind a quay wall) by integrating the residual shear strain potential over depth.

The Shamoto et al. (1998) method is simple and may be used to estimate the maximum liquefaction-induced horizontal ground surface displacement in level ground near a waterfront. However, it has several limitations as described below.

- Only the potential, maximum horizontal ground displacement near a waterfront can be estimated. In the field, this maximum displacement may or may not occur depending on the boundary conditions near a waterfront.
- Local slide failure may occur near a waterfront where large static shear stresses exist. The local slide failure may cause large deformations of the soils near a waterfront. However, the Shamoto et al. (1998) method cannot take the local slide failure into account in estimating the potential, maximum horizontal ground displacement.
- The lateral displacement at a location away from a waterfront cannot be directly estimated by the method.

- This method cannot be used to estimate liquefaction-induced lateral displacements for sloping ground.

5.4 Stress-deformation Analysis

5.4.1 The strain potential approach

Seed et al. (1975) developed a procedure for estimating the earthquake-induced slope deformations that occurred in the Upper and Lower San Fernando dams during the 1971 San Fernando earthquake. In this procedure, the static stresses in the soils before the earthquake were computed using a conventional stress-deformation finite-element analysis, and the cyclic shear stresses were calculated using a dynamic linear or equivalent linear finite-element analysis. Based on the computed static and cyclic stress conditions, cyclic laboratory tests were then conducted to predict the strain potential for each element in the finite-element analyses. Horizontal displacements were estimated to be the product of the average strain potential along a vertical section through the slope and the height of that section.

The method implicitly assumes that the strains that develop in the field will be the same as those that develop in a similarly loaded laboratory test specimen and that the maximum shear stress acts in the horizontal direction in all elements. Analyses based on the strain potential approach are clearly approximate.

5.4.2 The stiffness or strength reduction approach

Hamada et al. (1987) modeled a lateral spread in Noshiro, Japan, using a two dimensional finite element mesh representing a plan view of a slide area. The major assumptions in their analysis are:

- The unliquefied, surficial soil layer was modeled as an elastic plate using plane stress elements.

- The underlying liquefied layer was assumed to be liquid with zero shear strength.

Displacements were then computed under a given ground slope and boundary conditions using a static finite element analysis. Despite the very simple nature of this analysis, the computed displacements were in good agreement with the field observations at the Noshiro slide. However, this procedure is highly dependent on the assumed elastic properties of the surficial soil.

Yasuda et al. (1991, 1992) proposed a simplified procedure for prediction of permanent liquefaction-induced ground displacements. In this procedure, they assumed that the permanent ground displacement would occur in liquefied, softened ground due to the static shear stress present before liquefaction. Two static finite element analyses were performed in their procedure. In the first, static stresses were computed using elastic parameters for the soil prior to an earthquake. Then, in the second analysis, the static stresses were held constant while the stiffness of the soil was reduced to simulate softening due to liquefaction. The difference in the displacements computed in the two analyses was then taken to represent the liquefaction-induced movements. The key to the analysis is determining an appropriate stiffness reduction to represent the liquefied soil.

5.4.3 The nonlinear analysis approach

Prevost (1981) and Finn (1990) developed dynamic, 2-D, coupled models to couple shear strength loss during cyclic loading with pore pressure generation. In a nonlinear dynamic finite element procedure (TARA-3FL) proposed by Finn (1990), the pre-earthquake stress-strain state is calculated for each element. During the dynamic part of the analysis, as liquefaction is triggered in elements that are liquefiable, the undrained shear strength of the liquefied elements is allowed to drop to its residual value. Once liquefied, the residual strength of these elements is unable to sustain the pre-earthquake and dynamic shear stresses. The finite element mesh is allowed to progressively deform until equilibrium is restored. Therefore, these finite element models are appropriate only for failures involving flow at a residual shear strength. Finn (1991) reported that the computed deformations were highly dependent on the residual strength specified,

although determining a reliable estimate of the residual strength is difficult.

A somewhat less sophisticated finite element model has been used by Gu et al. (1993, 1994) to calculate the post-earthquake deformations at the Lower San Fernando Dam and Wildlife case history site. The initial effective stresses were determined through incremental finite element analysis simulating the field conditions. The post-earthquake deformation analysis was also conducted using an incremental finite element analysis under fully undrained conditions which considered stress redistribution. In their analyses, the hyperbolic strain softening relationship was introduced to simulate the post-peak behavior of liquefied materials. Excess pore pressures, independently estimated by other approaches, were inputted to specific soil elements. Liquefaction of soil elements then caused an imbalance in shear loads, and the resulting deformations that ended in an equilibrium condition were computed using an iterative procedure.

As introduced by Elgamal et al. (1998, 1999), a new soil constitutive model was developed by Parra (1996), based on the original framework of plasticity theory for frictional cohesionless soils presented by Prevost (1985). The model simulates the characteristics of soil response observed in centrifuge experiments, shake-table tests, and cyclic laboratory sample tests. The observed characteristics include the biased cycle-by-cycle accumulation of cyclic shear strains due to the presence of a locked-in driving shear stress, a strong restraining effect on the magnitude of cyclic and accumulated permanent shear strains due to soil dilation at a large cyclic shear strain, and so on. As commented on by Elgamal et al. (1999), this model primarily focuses on medium, medium-dense, and dense sand (or silt) because loose cohesionless soils may display a dominant contractive response with little dilative tendency and an increased level of accumulated shear deformations.

5.4.4 Summary of stress-deformation analysis approaches

For problems involving the deformation of a soil mass, stress-deformation finite element methods are often well suited for modeling the relevant mechanics and boundary

conditions (Rauch 1997). However, when these methods are applied in estimating liquefaction-induced lateral displacements during earthquakes, engineers and researchers face the following three major challenges.

- First, a very sophisticated constitutive model would be required to meticulously simulate all aspects of a liquefaction-induced lateral spread. A rigorous finite element model would be needed to model seismic excitation, soil softening as a result of the accumulation of excess pore pressures, rapid loss of shear strength as the soil liquefies, large distortion of the liquefied deposit, redistribution of pore water, possible progressive failure, soil dilation at a large cyclic shear strain, and reconsolidation as excess pore pressures are drained. The resulting finite element formulation would require fully-coupled, effective stress, and highly non-linear soil models and would also need to consider both inertial loads and large strains. Much of this modeling challenge is a consequence of the transformations from solid soil to liquid and back to solid, which processes are beyond the scope of conventional solid mechanics.
- The general inadequacy of rigorous numerical models for liquefaction-induced deformations has been recently demonstrated (Manzari et al. 1994). As part of the VELACS project (Verification of Liquefaction Analysis by Centrifuge Studies) (Arulanandan and Scott 1993), numerical predictions were compared with the behavior of carefully constructed centrifuge models. While the onset of liquefaction could be accurately calculated, predictions of the ensuing ground deformations were much less reliable even though the soil conditions in the scale models were well known. Moreover, all of the available numerical procedures were deficient in simulating the behavior of dilative soils.
- Last, but not least, it is very difficult to provide significant details of soil profiles and sufficient accuracy of soil property determinations for rigorous numerical analysis even for large, high-risk projects. For example, the residual strength of a liquefied soil is a key parameter required for almost all the available numerical analyses in estimating post-liquefaction deformations. However, the determination of the residual strength is very difficult and less accurate. Although taking frozen samples to ensure undisturbed samples for the determination of the residual strength in

laboratory tests is the best available technique, this technique is very expensive and is limited to large, high-risk projects. Furthermore, for many soils with substantial fines content, the freezing technique cannot be used. Similar restrictions hold for other specified soil parameters in a given specific numerical model.

5.5 Empirical Models

5.5.1 Hamada's empirical model

Based on pre- and post-earthquake aerial photographs, Hamada et al. (1986) published horizontal ground displacement vector maps for many areas damaged by lateral spreads in Niigata and Noshira, Japan during the 1964 Niigata and 1983 Nihonkai-Chubu earthquakes respectively. In combination with the information from the 1971 San Fernando earthquake, Hamada et al. conducted a simple regression analysis. The parameters chosen as relevant were the thickness of liquefied layers and the steeper slope angle of either the bottom of the liquefied layer or ground surface. The result of the regression is given by:

$$[5.1] \quad D = 0.75 \cdot \sqrt{H} \cdot \sqrt[3]{\theta}$$

where D is the horizontal displacement (m) and H is the thickness (m) of liquefied soil. When more than one soil layer liquefies, H is measured as the distance from the top-most to the bottom-most liquefied soil, including all intermediate soil layers. θ is the slope (%) of either the ground surface or the base of the liquefied soil, whichever is greater. When a free face is present, the surface slope is measured to the toe of a free face.

Equation [5.1] provides a best-fit line for the data compiled by Hamada and his co-workers. However, the database was heavily biased towards the lateral spreads in Noshiro and thus represented a narrow range of seismic and site conditions. The accuracy of the fitted equation outside these confines is unknown, and, consequently, the

usefulness of Hamada's empirical model is limited.

5.5.2 Youd and Perkins' LSI model

Youd and Perkins (1987) evaluated cases of liquefaction-induced lateral spreads that occurred in a very specific geologic setting. Their study was limited to the lateral spread of gently sloping, geologically recent, fluvial deposits of shallow, continuous, saturated, cohesionless, liquefiable soils that had estimated standard penetration resistances ranging from 2 to 10 blows per foot. By applying these restrictions to the cases included in their study, they limited the range of site conditions, thus effectively reducing the variation of topographical and soil factors in their model.

Based on case studies from historical earthquakes in the western United States and Alaska, Youd and Perkins (1987) developed a simple regression equation:

$$[5.2] \quad \log LSI = -3.49 - 1.86 \log R + 0.98M_w$$

where the LSI (the Liquefaction Severity Index) is defined as the general maximum magnitude of ground displacement in inches and assigned an arbitrary upper limit of 100, corresponding to a displacement of 2.5 m, which was considered sufficient to indicate severe failures. R is the horizontal distance (km) to the seismic energy source and M_w is the moment magnitude of an earthquake.

Equation [5.2] reflects the seismic attenuation characteristics of western North America and may not be valid for other regions of the world. The LSI model is primarily based on earthquake factors and is intended to provide a conservative upper bound for predicting horizontal ground displacement for sites that have moderate to high liquefaction susceptibility. Ground displacements that are significantly different from the LSI may occur at sites where site topographical and soil conditions differ significantly from those used in developing the LSI since site-specific factors are not considered in the LSI model.

5.5.3 Bartlett and Youd's MLR model

Bartlett (1991) and Bartlett and Youd (1995) have developed a more sophisticated empirical model for estimating lateral displacement in a liquefaction-induced lateral spread. They studied case history sites for the past seven major earthquakes in the United States and Japan and established a database comprised of 448 sets of data including seismological, topographical, geological, and geotechnical parameters, and 19 observations from Ambraseys (1988). Based on the compiled database, Bartlett and Youd then conducted modified stepwise multiple linear regression (MLR) analyses to identify the factors that most strongly influenced lateral ground displacements and to develop relevant empirical equations. They found that there are two ground geometry conditions which should be handled separately in lateral spreading: one is level ground with a free face and another is sloping ground without a free face. The final MLR equations given by Bartlett and Youd (1995), which are slightly modified from those in Bartlett (1991), are:

for level ground with a free face,

$$[5.3] \quad \log D = -16.366 + 1.178M_w - 0.927 \log R - 0.013R + 0.657 \log W + \\ 0.348 \log T_{15} + 4.527 \log(100 - F_{15}) - 0.922D50_{15}$$

for sloping ground without a free face,

$$[5.4] \quad \log D = -15.787 + 1.178M_w - 0.927 \log R - 0.013R + 0.429 \log S + \\ 0.348 \log T_{15} + 4.527 \log(100 - F_{15}) - 0.922D50_{15}$$

where D is the estimated lateral ground displacements in meters, M_w is the moment magnitude of the earthquake, and R is the nearest horizontal distance (km) to the seismic energy source or fault rupture. T_{15} is the thickness (m) of saturated, cohesionless soils (excluding soils deeper than 20 m or with a clay content greater than 15%) with $N_{1.60}$ equal to or less than 15, where $N_{1.60}$ is the standardized SPT blowcount. F_{15} is the average fines content (the % finer than 0.075 mm) in T_{15} , and $D50_{15}$ is the average mean

grain size D_{50} (mm) in T_{15} . W is the free face ratio (%), defined as the ratio of the toe-to-crest height of the free face and the horizontal distance to the free face toe. S is the gradient of the ground surface (%) defined as the change in elevation over horizontal distance for long, uniform slopes. When the surface topography is not uniform, a special definition of S is used to account for small, local benches (ridges, banks, etc.), as illustrated by Bartlett and Youd (1995).

The Bartlett and Youd MLR equations are a definite improvement over past attempts to estimate liquefaction-induced lateral displacements empirically since they took into account major seismological, topographical, geological, and geotechnical factors. The equations are very simple and straightforward to use. Lateral displacements can be directly estimated from SPT results in addition to seismological and topographical information without the requirement of liquefaction potential analysis. Nevertheless, Bartlett and Youd's model still have some limitations:

- About two thirds (299 out of 448) of the total measurements in their database were from the sites in Niigata City for the 1964 Niigata, Japan earthquake. The soil profiles in Niigata City are unique and relatively simple. The soils in the top 20 m or more are generally uniform clean sands with a shallow ground water table (about 1.0 m). During the earthquake, about 10.0 m or more of thick top saturated sand was liquefied over widespread areas, causing large liquefaction-induced lateral displacements. In addition, the measured horizontal ground displacements in Niigata City were generated from the analyses of pre- and post-earthquake aerial photographs and had an accuracy of about ± 0.72 m (Hamada et al. 1986). As a result, the unique geological setting in Niigata City, in combination with their heavy dependence on the data from Niigata City, makes Bartlett and Youd's model less reliable when the model is applied to a given site where both the soil profile and soil properties are much different from those in Niigata City.
- Bartlett and Youd's database has only 68 observations with measured displacements of smaller than 1.0 m among the total of 448 observations. This means that Bartlett and Youd's model was mainly based on the data with measured displacements greater than 1.0 m. As a result, the displacements predicted by the model are generally twice

or more the measured values for the cases in which the measured displacements are less than 1.0 m in the case history sites studied by Bartlett and Youd. Nevertheless, practical geotechnical engineers have more interest in displacements less than 1.0m or 2.0m because lateral displacements of more than 2.0 m are considered too damaging and cannot be accepted by engineers.

- The SPT position was not same as the position where the field lateral displacement was measured for the majority of the observations in Bartlett and Youd's database. The distance from the nearest SPT position to the location where relevant lateral displacement was measured is about 80.0 m as an average and is more than 100 m (up to 670 m) for 105 observations in their database. Therefore, for cases in which the local soil profile and soil properties at the SPT location are much different from those at the location where relevant lateral displacement was measured, the interpretation of the data concerning soil profile and soil properties would be inappropriate.
- Using average values of soil parameters in the layers with $N_{1,60}$ equal to, or less than 15 through one borehole may mask the obvious geological difference between the different sandy layers in one borehole and cause the final values of F_{15} , $D50_{15}$ for different site conditions to be very close and therefore inappropriately reduce the importance of F_{15} and $D50_{15}$ in the final MLR model.
- Soil properties are characterized only by the SPT, which has poor reliability and repeatability with respect to its testing results when compared with the CPT.

5.5.4 The modified Bartlett and Youd's MLR model

Youd et al. (1999) made several modifications to Bartlett and Youd's (1995) MLR model. These modifications are:

- The MLR equations were corrected for 72 miscalculated displacements from the 1983 Nihonkai-Chubu, Japan earthquake in Bartlett and Youd's (1995) database achieved by dividing the magnitude of each of the miscalculated displacements by a factor of 1.9. With this correction made, the case history data were re-analyzed using the MLR procedure.
- Several sites where boundary effects significantly interfered with free lateral-spread

movement were removed from the data set (8 displacement vectors were removed).

- Additional case history data (82 displacement vectors) were added from three recent earthquakes.
- The functional form of the mean-grain-size term in the MLR equations was modified from $(D50_{15})$ to $\log(D50_{15})$ to improve the performance of the model for coarse grained soil ($D50_{15} > 1.0$ mm). Then the form was additionally adjusted to the form $\log(D50_{15} + 0.1)$ to prevent predicted displacements from becoming large when very small mean grain sizes are entered into the equation.
- The maximum value of fines content entered into the equation was capped at 55 percent.
- The form of the equation was changed from $\log(R)$ to $\log(R^*)$, where $R^* = R + 10^{(0.89M_w - 5.64)}$ to prevent the prediction of very large displacements when R becomes small.

The modified equations after a series of re-analyses on the basis of the above-mentioned modifications are:

for level ground with a free face,

$$[5.5] \quad \log D = -18.084 + 1.581M_w - 1.518 \log R^* - 0.011R + 0.551 \log W + 0.547 \log T_{15} + 3.976 \log(100 - F_{15}) - 0.923 \log(D50_{15} + 0.1)$$

for sloping ground without a free face,

$$[5.6] \quad \log D = -17.614 + 1.581M_w - 1.518 \log R^* - 0.011R + 0.343 \log S + 0.547 \log T_{15} + 3.976 \log(100 - F_{15}) - 0.923 \log(D50_{15} + 0.1)$$

where the symbols are same as those defined in Bartlett and Youd's (1995) equations.

The modified Bartlett and Youd's model corrected errors in the work of Bartlett and Youd (1995), added more case history data to the database, and incorporated changes to the functional form of the model to add robustness to the new MLR model. Most of the added data sets to the database have ground displacements in the 0.25 m to 1.0 m range,

thus overcoming the limitation of the shortage of measured displacements less than 1.0 m in the previous database. Although most of the limitations with Bartlett and Youd's (1995) model still exist in the modified one, the modified model is one of the best available empirical approaches to estimate liquefaction-induced lateral displacements at this stage.

5.5.5 Rauch and Martin's EPOLLS model

Based on case history data for 71 lateral spreads that occurred during 15 past earthquakes, Rauch and Martin (2000) developed a new empirical method, called the EPOLLS model, to predict the average horizontal surface displacement on a potential lateral spread. Although the EPOLLS model was also developed from a multiple linear regression analysis, as was Bartlett and Youd's MLR model, the EPOLLS model is different from the MLR model in the following ways:

- A single average value for each of all the selected parameters in the EPOLLS model was used in Rauch and Martin's database for a lateral spread, that is, only one set of data is collected for one lateral spread. However, a number of sets of data at different locations in a lateral spread were used in Bartlett and Youd's database.
- The EPOLLS model was designed to predict an average horizontal displacement at a site, that is, the average magnitude of all measurable displacements on a lateral spread, while the MLR model predicts different lateral displacements at different locations on a single lateral spread.
- The length of the sliding area in a lateral spread is a key parameter in the EPOLLS model, but not considered in the MLR model.

The EPOLLS model is comprised of three components for predicting lateral displacements: regional, site, and geotechnical components, as shown below. Depending on the availability of the parameters in a given potential lateral spread site, each component can be used separately with increased reliability from regional component to geotechnical component.

Regional component,

$$[5.7] \quad \text{Avg_Horz} = (D_R - 2.21)^2 + 0.149$$

$$[5.8] \quad D_R = (613M_w - 13.9R_f - 2420A_{\max} - 11.4T_d) / 1000$$

Site component,

$$[5.9] \quad \text{Avg_Horz} = (D_R + D_S - 2.44)^2 + 0.111$$

$$[5.10] \quad D_S = (0.523L_{\text{slide}} + 42.3S_{\text{top}} + 31.3H_{\text{face}}) / 1000$$

Geotechnical component,

$$[5.11] \quad \text{Avg_Horz} = (D_R + D_S + D_G - 2.49)^2 + 0.124$$

$$[5.12] \quad D_G = (50.6Z_{\text{FSmin}} - 86.1Z_{\text{liq}}) / 1000$$

where M_w is the moment magnitude of an earthquake, R_f is the distance to a fault rupture (in km), A_{\max} is the peak horizontal acceleration (g) at the ground surface at a site, and T_d is the duration (sec) of strong earthquake motions at the site. L_{slide} is the maximum length (m) measured horizontally from the head to the toe of a lateral spread, S_{top} is the average slope (%) across the surface of a lateral spread, and H_{face} is the height (in m) of a free face. Z_{FSmin} is the depth (in m) to the minimum factor of safety measured in potentially liquefiable soil, and Z_{liq} is the depth (in m) to the top of a liquefied sublayer. Avg_Horz is the estimated average horizontal displacement (in m) in a lateral spread.

Being fairly simple to be applied, Rauch and Martin's EPOLLS model is an alternative tool for predicting average surface horizontal movements on a potential lateral spread. The model has the distinct advantage of allowing engineers to characterize the likely ground movements to a degree commensurate with how well the site conditions are known. However, the following limitations appear with this model:

- For the regional component, the relationship between peak horizontal acceleration A_{\max} and average lateral displacement Avg_Horz does not appear logically reasonable because Avg_Horz decreases with increasing A_{\max} if other parameters remain constant in the EPOLLS model. A similar trend also exists between the duration of strong shaking T_d and Avg_Horz in the EPOLLS model. Logically, if two sites have

the same distance (same R_f) to the fault rupture for a same earthquake (same M_w), a larger lateral displacement is expected at the site that experiences a larger A_{max} and T_d , but the reverse situation is not true: a smaller lateral displacement as predicted by the regional component occurs.

- In the EPOLLS model, there is no parameter characterizing important soil properties such as soil density (or penetration resistance or residual shear strength, etc.) because the depth to the minimum factor of safety Z_{FSmin} and the depth to the top of the liquefied soil Z_{liq} only characterize the soil profile or vertical distribution of the liquefied layers but not the extent of soil liquefaction. For example, if two sites have the same Z_{FSmin} and Z_{liq} but different soil properties, say different soil densities, it is reasonable to envisage that the lateral displacement at the site with much loose sand would be much larger than that at the site with denser soil. However, this important soil parameter is not present in the EPOLLS model.
- It is difficult to determine the duration of strong motions before a potential earthquake and the length of a potential lateral spread for prediction purposes.
- Case histories have shown that lateral displacements decrease with increasing distances to a free face for level ground with a free face. So using average values to characterize lateral displacements for ground with a free face may cause displacements to be overestimated at locations far away from the free face and displacements to be underestimated in the vicinity of the free face.
- Liquefaction potential analysis is needed before using the EPOLLS model.

5.6 Discussion and Conclusions

Several groups of methods have been proposed to estimate liquefaction-induced ground lateral displacements, including laboratory modeling approaches, numerical and analytical analyses, and field-data-based methods.

Laboratory-scale models built on conventional shake-tables and geotechnical centrifuges have been used to investigate lateral spreading under controlled conditions. While useful

in exploring the mechanics of liquefaction-induced failures, laboratory-scale models are unsatisfactory in providing fully realistic models of lateral spreading and are seldom directly used to estimate liquefaction-induced lateral displacements in geotechnical design.

The modified Newmark's (1965) sliding block analytical approaches have been widely used to estimate dynamic deformations of embankment dams or liquefaction-induced lateral displacements by the practical engineers. The major limitation with these approaches is the assumption that the soils in a lateral spread move laterally as a rigid block along a well-defined failure plane. However, field observations in combination with laboratory-scale tests did not support this assumption. Furthermore, shear strengths along the assumed shear plane, which are required for the Newmark analysis, are very difficult to determine.

The analytical model of Towhata et al. (1999) shows promise for providing useful predictions of the maximum or ultimate displacements. However, because liquefied soils are assumed to behave as a liquid with zero shear strength in this model, the model generally overestimates lateral displacements in a liquefaction-induced lateral spread.

The residual shear strain charts proposed by Shamoto et al. (1998) were developed for estimating liquefaction-induced residual shear strain potential for soils in level ground only. The residual shear strains do not relate to static shear stresses or field ground geometry. These charts cannot be directly used to estimate lateral displacements in a lateral spread even though these charts may be applied to give a possible estimation of the maximum lateral displacement at the waterfront for level ground with a free face.

Several models for stress-deformation analysis using finite element techniques have been used to calculate displacements in a lateral spread. Reliability of the predictions using these models mainly depends on: (1) a rigorous and relevant constitutive model and (2) appropriate input data for the analysis. However, first, the expense and difficulty associated with obtaining and testing high quality samples of loose sandy soils and the

need for accurately and repetitively measuring many uncommon material constants for stress-deformation analyses using a rigorous constitutive model significantly limit the applications of numerical methods. Second, the general inadequacy of the available rigorous numerical models for estimating liquefaction-induced deformations has been recently demonstrated (Manzari et al. 1994).

Due to the complicated nature of liquefaction-induced lateral spreads, several available field-data-based empirical models (Hamada et al. 1986; Youd and Perkins 1987; Bartlett and Youd 1995; Youd et al. 1999; Rauch and Martin 2000) have shown advantages for estimating post-liquefaction deformations because of their simplicity and the fact that they are based on field observations. It is difficult to choose one empirical model over another since they all seem to give similar results within a factor of two or three. Generally, both Hamada's model and Youd and Perkins' model characterize only partial factors that control the magnitude of lateral spreading displacements and therefore are useful only to specific geological regions and earthquakes. Rauch and Martin's SPT-based model is a useful tool for predicting average horizontal movements on a potential lateral spread. The SPT-based model of Youd et al (1999) may be the best of the available empirical models to estimate lateral displacements in a liquefaction-induced lateral spread at this stage even though it still has some limitations as noted.

These field-data-based models entirely rely on empirical evidence and do not incorporate the extensive knowledge gained from laboratory studies of soil liquefaction. No CPT-based method to estimate liquefaction-induced lateral displacements is currently available even though the CPT has greater repeatability and reliability and provides a continuous profile compared with other field tests. Therefore, it is suggested that simple semi-empirical approaches be developed for estimating liquefaction-induced lateral displacements using SPT or CPT data on the basis of laboratory testing results and case history data.

CHAPTER 6 ESTIMATION OF THE LATERAL DISPLACEMENT INDEX (POTENTIAL) FROM SPT OR CPT DATA

6.1 Introduction

The mechanisms governing liquefaction-induced lateral spreads have been reviewed and discussed in Chapter 4. The available results from one-g shake table and centrifuge tests and observations from case histories generally support the idea that lateral displacements are associated with distributed residual shear strains throughout liquefied soil layers rather than concentrated strains along a potential failure surface for liquefaction-induced lateral spreads. As a result, the distributed residual shear strains in liquefied layers and the thickness of liquefied layers have important influence on the magnitude of liquefaction-induced lateral displacements.

As discussed in Chapter 4, the magnitude of residual shear strains is primarily a function of two parameters: 1) the maximum shear strains under the static and seismic loading conditions without biased static shear stresses, and 2) the biased (driving) in-situ static shear stresses. The biased in-situ static shear stresses are mainly controlled by the geometric parameters characterizing ground geometry (e.g., ground slope, free face height, and the distance to a free face). Therefore, the three major components influencing the magnitude of liquefaction-induced lateral displacements are the maximum shear strains in liquefied layers, the thickness of liquefied layers, and the geometric parameters at a site (see Figure 6.1).

In this chapter, procedures are developed to estimate the maximum shear strains in liquefied layers under static and seismic loading conditions without biased static shear stresses. A new parameter, defined as the lateral displacement index (potential), is then introduced. The index incorporates two of the three major components determining the magnitude of liquefaction-induced lateral displacements: the thickness of liquefied layers

and the maximum shear strains in liquefied layers. This index will be used as a major parameter in developing several SPT- and CPT-based approaches for estimating liquefaction-induced lateral displacements in the next three chapters of this thesis.

6.2 Estimation of the Maximum Shear Strains from SPT or CPT Data

6.2.1 The maximum shear strains of clean sands as determined by laboratory testing

Cyclic shear strains may be induced by cyclic shear stresses for saturated sandy soils under undrained loading conditions. The maximum amplitude of cyclic shear strains that are induced during undrained cyclic loading for a saturated sandy soil without biased static shear stresses in the direction of cyclic loading is referred to as the maximum shear strain (γ_{\max}) in this research. Figure 6.2 shows cyclic shear stress-strain curves and the relevant maximum shear strain for an undrained cyclic simple shear test of a clean sand without biased static shear stresses in the direction of cyclic loading.

Nagase and Ishihara (1988) conducted cyclic simple shear tests on saturated loose, medium-dense and dense samples of clean Fuji River sand under static and seismic loading conditions without biased static shear stresses. Both uni-directional and multi-directional loading conditions were simulated by employing irregular time histories of the motions that were observed during the major earthquakes in Japan between 1964 and 1983. Based mainly on these laboratory tests, Ishihara and Yoshimine (1992) developed a family of curves that provide a relationship between the maximum amplitude of shear strain (γ_{\max}) and the factor of safety against liquefaction (FS) for different relative densities (D_r) for clean sands (Figure 6.3).

Modification of Ishihara and Yoshimine's (1992) relationship is required to account for dilative response of the soil that may restrict the development of shear strains. Evidence of soil dilative response at large shear strains was observed in undrained cyclic laboratory

tests, one-g shake table studies, centrifuge experiments, and in-situ seismic responses, as discussed in Section 4.3.2. De Alba et al. (1976) also found from large-scale simple shear tests that the specimens tended to dilate as shear strain increased for medium and dense sands. Seed (1979) postulated that only a limited amount of shear strain could be developed for sand at any given relative density, regardless of the number of stress cycles applied, and that further increases in strain could be difficult to achieve unless the full undrained resistance of the soil was exceeded. He proposed a curve (Figure 6.4) to present the relationship between the limiting shear strain and relative density for clean sands. With additional supporting data from Tokimatsu and Yoshimi (1984), who conducted laboratory tests using undisturbed frozen sand samples, Seed et al. (1985) further stated that the values of the limiting shear strains in Figure 6.4 may well be of the correct order of magnitude.

In this study, the relationship between γ_{\max} and FS developed by Ishihara and Yoshimine (1992) were modified by limiting the maximum shear strains for different relative densities of clean sands as proposed by Seed (1979). Figure 6.5 shows the relationship between the maximum amplitude of shear strain (γ_{\max}) and the factor of safety against liquefaction (FS) for different relative densities (D_r) for clean sands. The mathematic expressions for the curves in Figure 6.5 are listed in Equation [6.1]:

$$[6.1a] \quad \text{if } D_r = 90\%, \quad \gamma_{\max} = 3.26 \cdot (FS)^{-1.80} \quad \text{for } 0.7 \leq FS \leq 2.0$$

$$[6.1b] \quad \text{if } D_r = 90\%, \quad \gamma_{\max} = 6.2 \quad \text{for } FS \leq 0.7$$

$$[6.1c] \quad \text{if } D_r = 80\%, \quad \gamma_{\max} = 3.22 \cdot (FS)^{-2.08} \quad \text{for } 0.56 \leq FS \leq 2.0$$

$$[6.1d] \quad \text{if } D_r = 80\%, \quad \gamma_{\max} = 10 \quad \text{for } FS \leq 0.56$$

$$[6.1e] \quad \text{if } D_r = 70\%, \quad \gamma_{\max} = 3.20 \cdot (FS)^{-2.89} \quad \text{for } 0.59 \leq FS \leq 2.0$$

$$[6.1f] \quad \text{if } D_r = 70\%, \quad \gamma_{\max} = 14.5 \quad \text{for } FS \leq 0.59$$

$$[6.1g] \quad \text{if } D_r = 60\%, \quad \gamma_{\max} = 3.58 \cdot (FS)^{-4.42} \quad \text{for } 0.66 \leq FS \leq 2.0$$

$$[6.1h] \quad \text{if } D_r = 60\%, \quad \gamma_{\max} = 22.7 \quad \text{for } FS \leq 0.66$$

$$[6.1i] \quad \text{if } D_r = 50\%, \quad \gamma_{\max} = 4.22 \cdot (FS)^{-6.39} \quad \text{for } 0.72 \leq FS \leq 2.0$$

- [6.1j] if $D_r = 50\%$, $\gamma_{\max} = 34.1$ for $FS \leq 0.72$
- [6.1a] if $D_r = 40\%$, $\gamma_{\max} = 3.31 \cdot (FS)^{-7.97}$ for $1.0 \leq FS \leq 2.0$
- [6.1k] if $D_r = 40\%$, $\gamma_{\max} = 250 \cdot (1.0 - FS) + 3.5$ for $0.81 \leq FS \leq 1.0$
- [6.1l] if $D_r = 40\%$, $\gamma_{\max} = 51.2$ for $FS \leq 0.81$

6.2.2 Estimation of the maximum shear strains using SPT or CPT data for clean sands

Both the factor of safety against liquefaction (FS) and relative densities (D_r) are needed for estimating the maximum shear strains of in-situ clean sands for a given earthquake using the curves in Figures 6.5. The factor of safety can be evaluated from liquefaction potential analysis using the NCEER SPT- or CPT-based methods with SPT or CPT data. Relative density of a clean sand may be estimated from SPT or CPT results using the available correlations. In this study, the correlation proposed by Tatsuoka et al. (1990) was applied to estimate the relative density of clean sands using:

$$[6.2] \quad D_r = -85 + 76 \log(q_{c1N})$$

where D_r is the relative density of a clean sand as a percentage, and q_{c1N} is the normalized CPT tip resistance corrected for effective overburden stresses corresponding to 100 kPa.

Several correlations (e.g., Meyerhof 1957; Seed 1979; Skempton 1986; Kulhawy and Mayne 1991) are available to estimate relative densities of clean sands from SPT blow counts. Tokimatsu and Yoshimi (1983) found that the relative densities estimated using Meyerhof's (1957) correlation with SPT N values that were measured using equipment with a free fall of the hammer (or a rod energy ratio of about 78%) were in good agreement with the relative densities measured in the laboratory for the undisturbed in-situ clean sand samples obtained using the in-situ freezing technique. Ishihara and Yoshimine (1992) also used Meyerhof's (1957) correlation to estimate relative densities of clean sands from SPT results. However, Ishihara and Yoshimine did not specify the

SPT rod energy ratio in their paper. Fortunately, Ishihara et al. (1993) stated that the SPT N-values in Japan are currently obtained mostly by means of a free fall of the hammer, the trip monkey, which has a rod energy ratio of about 78% of the theoretical free-fall energy of the hammer. Therefore, it is reasonable to assume that Ishihara and Yoshimine (1992) implicitly used a rod energy ratio of about 78% as a standard in applying Meyerhof's correlation in their paper. In this study, a modified version of Meyerhof's (1957) correlation with SPT N values corresponding to a rod energy ratio of 78% was used, given by:

$$[6.3] \quad D_r = 16 \cdot \sqrt{(N_1)_{78}} = 14 \cdot \sqrt{(N_1)_{60}}$$

where D_r is relative density of a clean sand as a percentage, $(N_1)_{60}$ is the normalized SPT N value corrected for the rod energy ratio (with a reference energy ratio of 60%), overburden effective stress (with a reference effective stress of 100 kPa), rod length, borehole diameter, and sampling method, as discussed in Youd et al. (2001); and $(N_1)_{78}$ is equal to $(N_1)_{60}/1.3$.

Generally, the calculated relative density using Equation [6.3] is reasonably consistent with the relative densities calculated using some other available correlations (Seed 1979; Skempton 1986; Kulhawy and Mayne 1991) for a given SPT N value.

6.2.3 Estimation of the maximum shear strains using SPT or CPT data for silty sands or sandy silts

The curves in Figure 6.3 proposed by Ishihara and Yoshimine (1992) were developed based on laboratory test results on clean sands. If these curves are used to estimate the maximum shear strains of silty sands or sandy silts using SPT or CPT results, some modifications for the effects of grain characteristics or fines content on the values of the SPT or CPT data and their interpretations must be made.

In this research, the equivalent clean sand normalized SPT N value, $(N_1)_{60cs}$, or the

equivalent clean sand normalized CPT penetration resistance, $(q_{c1N})_{cs}$, was used to account for the effect of grain characteristics or fines content on SPT N values or CPT soundings. The parameter, $(N_1)_{60cs}$ or $(q_{c1N})_{cs}$, can then be treated as the SPT N value or CPT cone tip resistance for a clean sand and be used directly to estimate the maximum shear strains. The relationships between maximum shear strains (γ_{max}) and the factor of safety against liquefaction (FS) for different relative densities (D_r) (or $(N_1)_{60cs}$ and $(q_{c1N})_{cs}$) are shown in Figures 6.5 and were used in this study.

With the known data of the SPT N values or CPT soundings, the parameters for a given earthquake, and other input parameters (e.g., ground water table, unit weight), the $(N_1)_{60cs}$ or $(q_{c1N})_{cs}$ and FS for sandy and silty soils can be estimated from the liquefaction potential analysis using the NCEER SPT- or CPT-based method. The maximum shear strain can then be calculated based on the curves in Figure 6.5 and Equation [6.3] or [6.2] for every reading in the SPT or CPT results.

There is no curve in Figures 6.3 and 6.4 for the soils with a D_r less than 40%. As a result, there is no curve for a relative density less than 40% (or an $(N_1)_{60cs}$ less than 8 or for a $(q_{c1N})_{cs}$ less than 45) in Figure 6.5. In this study, soils with a relative density less than 40% (or $(N_1)_{60cs}$ less than 8 or $(q_{c1N})_{cs}$ less than 45) were assumed to have the same potential maximum shear strains as soils with a relative density of 40% (or an $(N_1)_{60cs}$ equal to 8 or a $(q_{c1N})_{cs}$ equal to 45). The assumption was accepted for the following reasons:

- There is no basis for extrapolating the data beyond the values posted in Figure 6.5;
- Generally, natural sandy soils with an $(N_1)_{60cs}$ less than 8 or a $(q_{c1N})_{cs}$ less than 45 are less common in the field.

Nevertheless, caution should be taken when a substantial amount of soil with an $(N_1)_{60cs}$ less than 8 or a $(q_{c1N})_{cs}$ less than 45 is detected during liquefaction potential analysis. For such cases, more extensive investigation should be taken to evaluate the flow failure susceptibility of the soil, especially when the static shear stresses in the ground are relatively high. The deformations caused by flow failures can be much larger than

lateral spreads and are beyond the scope of this research.

6.3 Estimation of the Lateral Displacement Index of Sandy Soils using SPT or CPT Data

The profile of the calculated maximum shear strain (γ_{\max}) according to depth for a given site where SPT or CPT data are available can be obtained with applying the relevant calculated FS and $(N_1)_{60cs}$ or $(q_{c1N})_{cs}$ to the curves in Figure 6.5. Integrating the calculated γ_{\max} values with depth will produce a value that is defined as the lateral displacement index (LDI) in this study. The LDI can be calculated using:

$$[6.3] \quad \text{LDI} = \int_0^{z_{\max}} \gamma_{\max} dz$$

where Z_{\max} is the maximum depth of liquefied layers at a given CPT or SPT location, and z is depth.

The lateral displacement index incorporates two of the three components dominating the magnitude of liquefaction-induced lateral displacements: namely, the thickness of liquefied layers and the maximum shear strains in liquefied layers, as illustrated in Figure 6.6. Because the thickness of liquefied layers and the maximum shear strains in liquefied layers characterize soil profile, soil properties, and the characteristics of an earthquake (see Figure 6.6), LDI also embodies the effects of the characteristics of both soils and an earthquake on liquefaction-induced lateral displacements. Thus, for certain ground geometry, LDI is a good indicator of the potential of liquefaction-induced lateral displacements.

Figure 6.7 illustrates the major procedures to calculate LDI using SPT data using a working example. Figures 6.8a and 6.8b show SPT N values and fines contents (FC), which can be obtained from the SPT and grain size analysis of relevant soil samples

respectively. Based mainly on SPT N values and fines contents, the equivalent clean sand normalized SPT N value – $(N_1)_{60cs}$ – can be calculated using the NCEER SPT-based method, Figure 6.7c. Then the factor of safety against liquefaction (FS), Figure 6.7d, can be estimated using the NCEER SPT-based method with the $(N_1)_{60cs}$ and major earthquake parameters. With the known $(N_1)_{60cs}$ and FS, the maximum shear strains (γ_{max}), as shown in Figure 6.7e, can be estimated from relationships in Figure 6.5 and Equation [6.3]. Finally, the lateral displacement index (LDI) can be calculated by integrating the γ_{max} with depth (see Figure 6.7f).

The major procedures to calculate the LDI using CPT data are similar to those described above using SPT data. Figures 6.8a and 6.8b show the CPT tip resistance (q_c) and sleeve friction ratio (R_f), which can be calculated directly from CPT soundings. Based mainly on q_c and R_f , the equivalent clean sand normalized tip resistance – $(q_{c1N})_{cs}$ – can be calculated using the NCEER CPT-based method, Figure 6.8c. The factor of safety against liquefaction (FS), Figure 6.8d, can be estimated using the NCEER CPT-based method with $(q_{c1N})_{cs}$ and major earthquake parameters. The potential maximum shear strains (γ_{max}), as shown in Figure 6.8e, can then be estimated from relationships in Figure 6.5 and Equation [6.2]. Finally, the lateral displacement index (LDI) (see Figure 6.8f) can be calculated by integrating the γ_{max} with depth. The major procedures to calculate the LDI using SPT data are similar to those described above using CPT data.

6.4 Effects of Other Major Factors on Calculated Lateral Displacement Index

6.4.1 Maximum surface acceleration

A number of factors may influence the accuracy of calculated lateral displacement index. The maximum surface acceleration is one of the major factors. The maximum surface acceleration at a site is one important parameter used in evaluating liquefaction potential of sandy soils. However, its determination is difficult without recorded accelerographs for a given earthquake because it may vary with soil stratigraphy, soil properties,

earthquake properties, the relative location of the site to the epicenter and even ground geometry. Its significant effects on estimated ground settlements have been discussed in Section 3.4.1. Similar effects on calculated lateral displacement index may be expected. Therefore, for important projects, a site specific response analysis is required to determine maximum surface accelerations.

6.4.2 Transitional zone or thin sandy soil layers

The effects of a transitional zone between a soft clayey layer and a stiffer sandy soil layer or a thin sandy soil layer sandwiched by two thick soft layers on CPT sounding and estimated factor of safety against liquefaction have been discussed in Section 3.4.3. Using a working example, Figure 6.9 illustrates the effect of transitional zones on the calculated factor of safety (FS) and its corrections. Based on the I_c profile shown in Figure 6.9c, there are three major transitional zones (circled by dashed-lines in Figures 6.9a and 6.9c) at about 7 m, 8 m, and 13 m depths. These transitional zones result in three very thin layers at which the calculated factors of safety are below 1.0, as shown in Figure 6.9d. However, generally, the calculated factors of safety for both the soft clayey layer and the stiff sandy soil layer that are associated with each of the transitional zones are greater than 1.0. This suggests that the calculated factors of safety for the transitional zones do not reflect the “true” values of FS but the effects of transitional zones on FS. Therefore, such miscalculated FS should be corrected based on engineering judgement. Figure 6.9e is a profile of FS after the correction has been exercised for the working example. In this research, such a simple correction (if applicable) for the effect of a transitional zone on FS has been followed in estimating FS using CPT data.

The effect of thin sandy soil sandwiched between two soft clayey soil layers on cone tip resistance and the resulting factor of safety is more complicated than that of transitional zones. Further research is required to quantify the effect and no correction procedure is recommended at this stage.

6.4.3 Correction factor K_c in the NCEER CPT-based method

Robertson and Wride (1998) (i.e. the NCEER CPT-based method) recommended that the correction factor K_c is set to be equal to one when the CPT data plot in the zone defined by $1.64 < I_c < 2.36$ and $F < 0.5\%$. The purpose of this recommendation was to avoid confusing very loose clean sands with denser sands containing fines because both very loose clean sands and denser sands containing fines may fit in the same zone. As a result, if a soil has CPT data that fit in this zone is a denser sand containing fines, the calculated $(q_{c(IN)})_{cs}$ for the soil with this recommendation may be reduced by up to 50% of the “real” value calculated without the recommendation. This recommendation is on the conservative side in evaluating liquefaction potential of sandy soils. However, on the other hand, this recommendation may result in over-estimating of the lateral displacement index for sites with denser sands containing fines. Therefore, soil sampling is recommended to further clarify soil properties for the specific sites where a large amount of the soils have CPT data that fit in the zone defined by $1.64 < I_c < 2.36$ and $F < 0.5\%$.

6.4.4 A cutoff line of I_c equal to 2.6 in the NCEER CPT-based method

A cutoff line of I_c equal to 2.6 is set in the Robertson and Wride (1998) to distinguish the sandy and silty soils with clayey soils which are believed non-liquefiable in general. Gilstrap (1998) studied the case histories by using Robertson and Wride’s method and compared the I_c calculated using the CPT soundings with the index test results of the samples that were taken from the boreholes close to the CPT locations at the case history sites. He found that more than 95% of the samples that had the associated CPT soundings with calculated I_c greater than 2.6 were classified as clayey soils based on the index test results. He then concluded that the I_c cutoff line of 2.6 is generally reliable for identifying clayey soils. However, he also noticed that 20% to 50% of the samples that had the associated CPT soundings with calculated I_c ranging from 2.4 to 2.6 were also classified as clayey soils as well based on the index test results. This implies that the cutoff line of I_c equal to 2.6 may appear to be slightly conservative for some clayey soils. Therefore, soil sampling is recommended to further clarify soil properties for sites at

which a large amount of soils have a calculated I_c greater than 2.4.

6.5 Discussion and conclusions

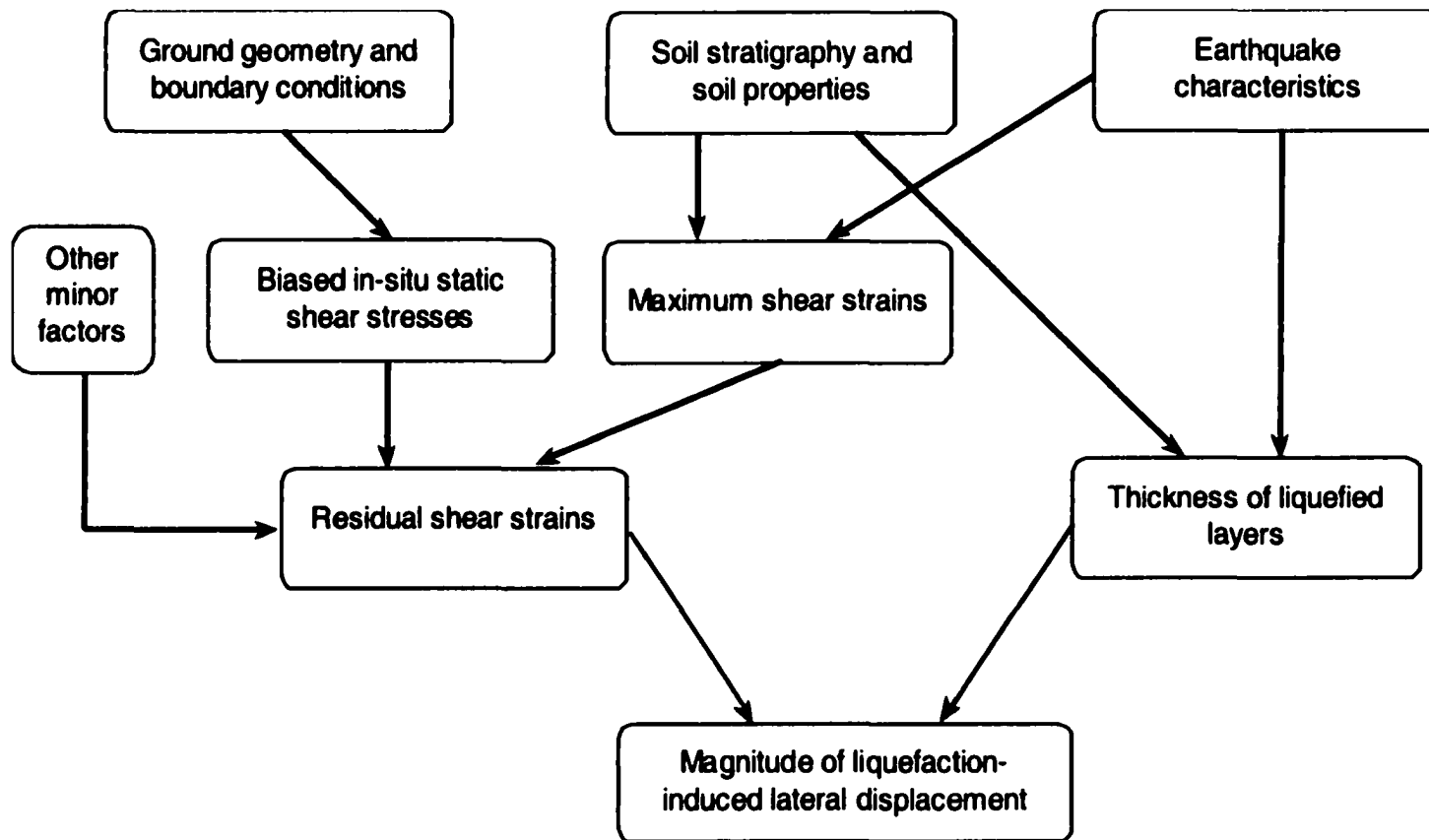
In this chapter, based mainly on laboratory test results, procedures were developed to estimate the maximum shear strains of sandy or silty soils using in-situ SPT or CPT results for a given earthquake. A new parameter, defined as the lateral displacement index (potential), was then introduced. It is calculated by integrating the maximum shear strains with depth. This parameter can be calculated using either SPT or CPT data. The procedures for calculating this parameter are simple with only a few additional calculations following SPT- or CPT-based liquefaction potential analysis.

The lateral displacement index incorporates two of the three components dominating the magnitude of liquefaction-induced lateral displacements namely: the thickness of liquefied layers and the maximum shear strains in liquefied layers. This index also captures the effects of the characteristics of both soils and an earthquake on liquefaction-induced lateral spreads. The index appears to be a good indicator of the potential of lateral displacements for a given ground condition during a given earthquake.

There is no curve in Figures 6.3 and 6.4 for the soils with a D_r less than 40%. As a result, there is no curve for a soil with a relative density (D_r) less than 40% in Figure 6.5. In this study, because of a lack of laboratory test data, soils with a relative density less than 40% (or $(N_1)_{60cs}$ less than 8 or $(q_{c1N})_{cs}$ less than 45) were assumed to have the same potential maximum shear strains as soils with an $(N_1)_{60cs}$ equal to 8 or a $(q_{c1N})_{cs}$ equal to 45. Therefore, caution should be taken when a substantial amount of soil with an $(N_1)_{60cs}$ less than 8 or a $(q_{c1N})_{cs}$ less than 45 is detected during liquefaction potential analysis. For such cases, more extensive investigation should be undertaken to evaluate the flow failure susceptibility of the soil, especially when the static shear stresses in the ground are relatively high. The deformations caused by flow failures can be much larger than lateral spreads and are beyond the scope of this research.

A number of factors may influence the accuracy of calculated lateral displacement index. For important projects, a site specific response analysis is required to determine the maximum surface acceleration for the studied site. The effect of a transitional zone between a sandy soil and a clayey soil may be corrected based on engineering judgement. Soil sampling is recommended to clarify soil properties for specific sites where a large amount of soils have CPT data that fit in the zone defined by $1.64 < I_c < 2.36$ and $F < 0.5\%$ or in the zone of I_c greater than 2.4 when the NCEER CPT-based method is used to estimate liquefaction potential and to estimate lateral displacement index.

It is expected that the magnitude of liquefaction-induced lateral displacements may be estimated using the lateral displacement index and the geometric parameters characterizing ground geometry (or biased static shear stresses) – the third of the three components dominating the magnitude of liquefaction-induced lateral displacements. In next three chapters, empirical correlations among the magnitude of lateral displacements, the lateral displacement index, and the geometric parameters will be established based on the available case histories during past major earthquakes.



-143-

Figure 6.1 A flowchart illustrating the components dominating magnitude of lateral displacements in a liquefaction-induced lateral spread

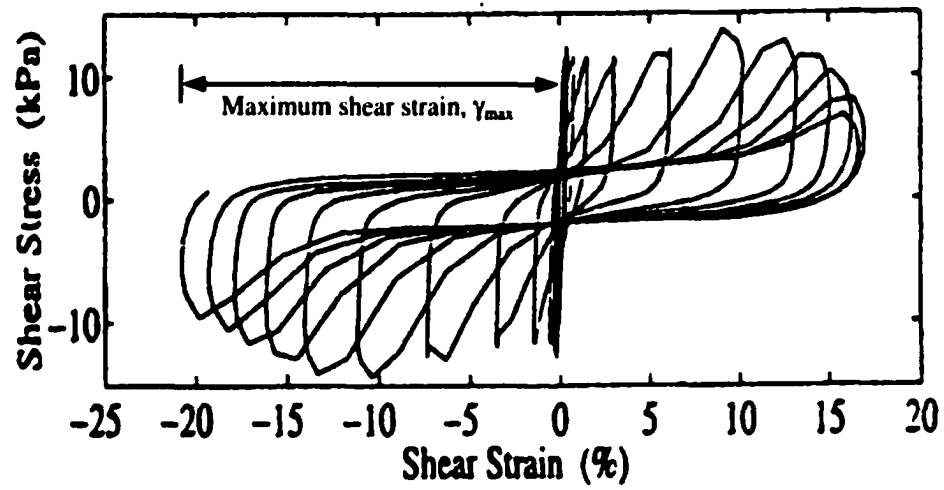


Figure 6.2 Cyclic shear stress-strain curves and the maximum shear strain from an undrained cyclic simple shear test for a clean sand without biased static shear stresses

(modified from Arulmoli et al. (1992))

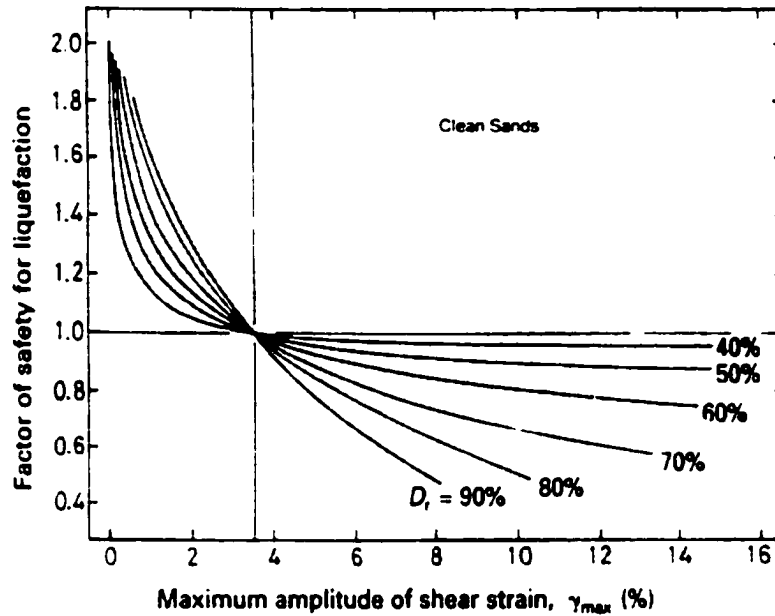


Figure 6.3 Relationships between factor of safety and maximum shear strain for clean sands from laboratory tests (modified from Ishihara and Yoshimine (1992))

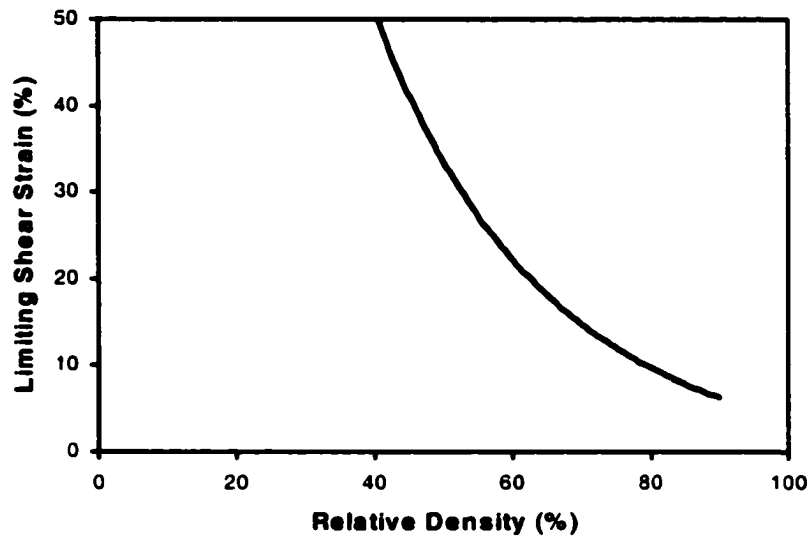


Figure 6.4 Limiting shear strains in laboratory cyclic simple shear tests (modified from Seed (1979))

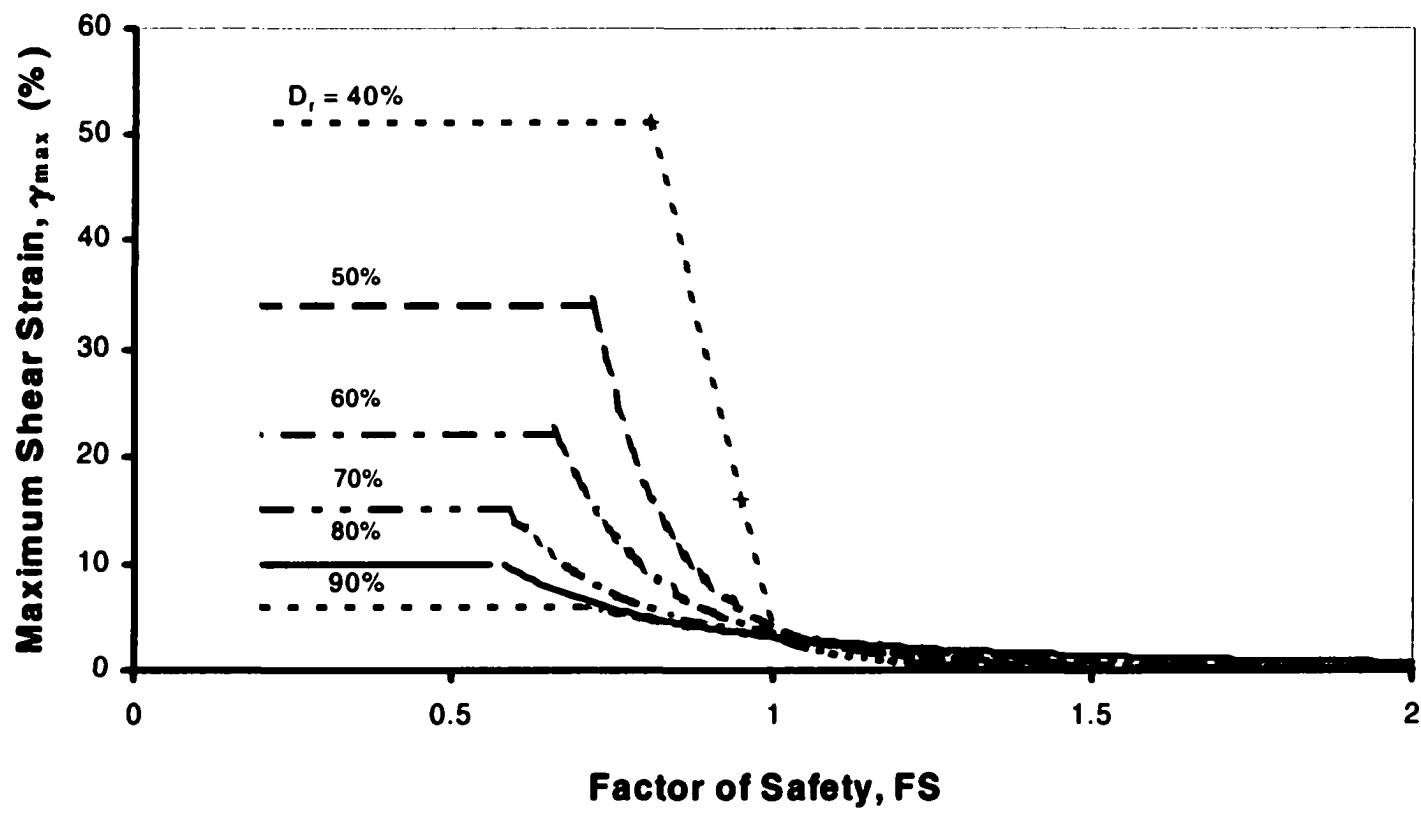


Figure 6.5 Relationships between maximum shear strain and factor of safety for different relative densities (D_r) for clean sands
(based on data from Ishiraha and Yoshimine (1992) and Seed (1979))

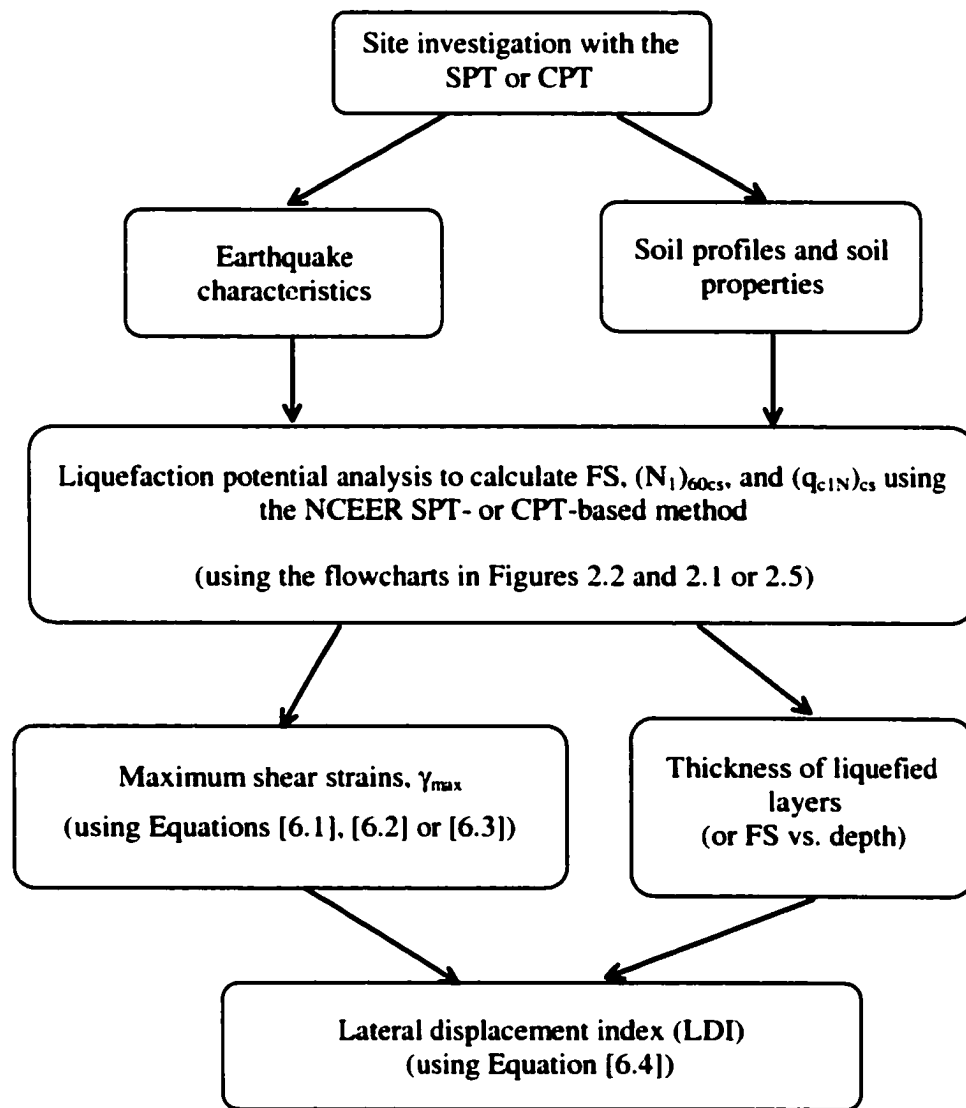


Figure 6.6 A flowchart illustrating the major procedures in calculating lateral displacement index (LDI)

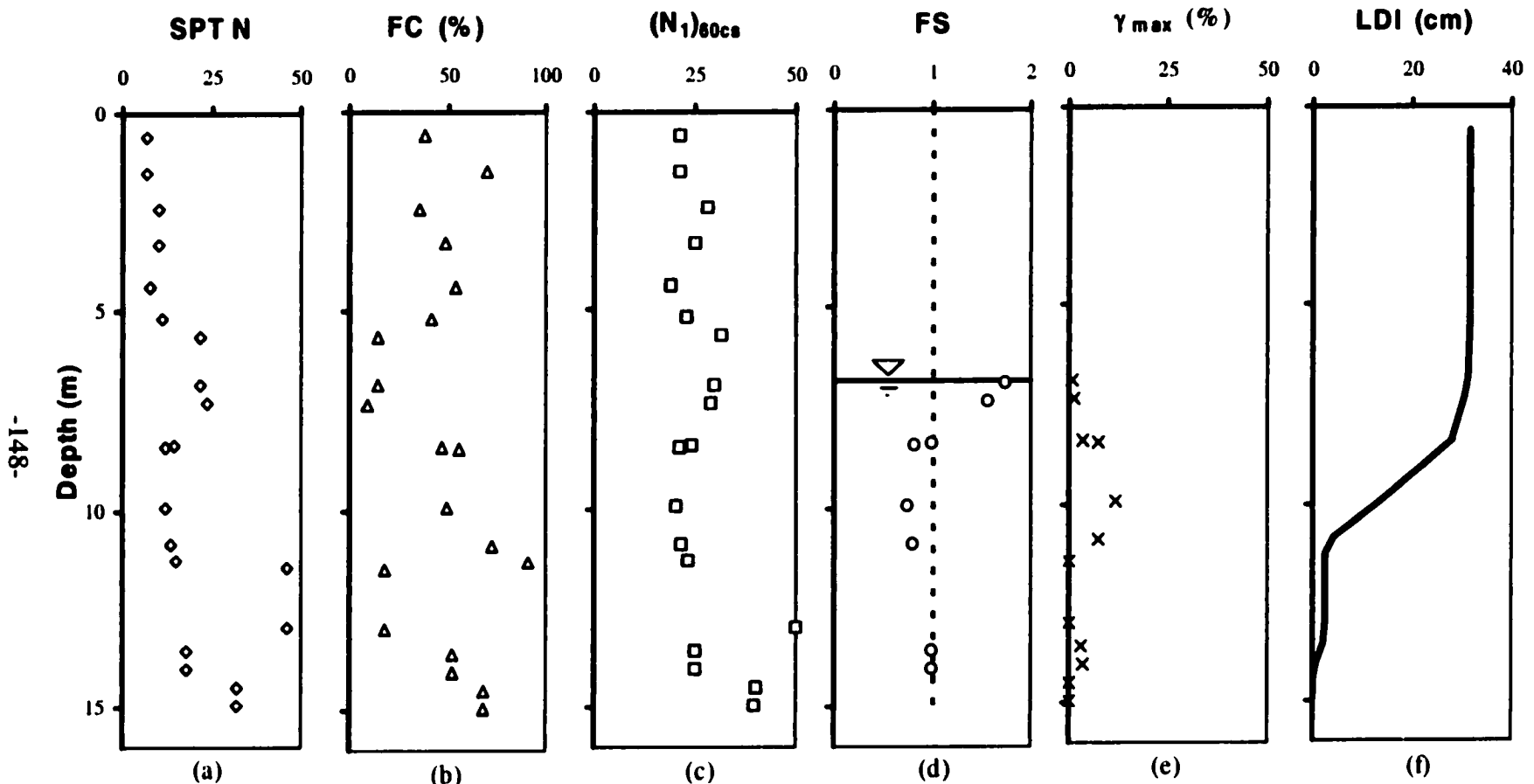


Figure 6.7 Example plots illustrating major procedures in calculating lateral displacement index (LDI) using the SPT-based approach with SPT data

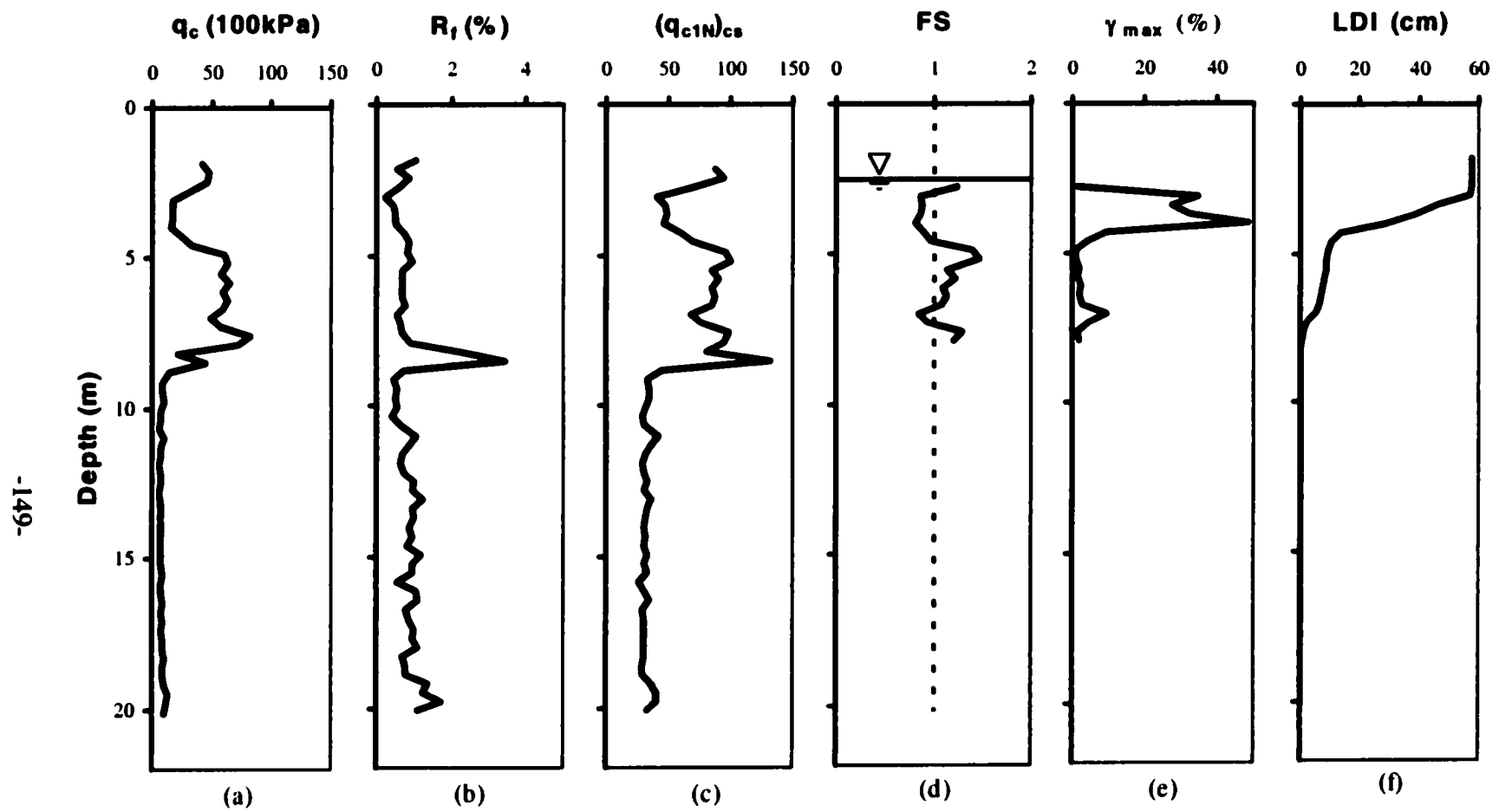


Figure 6.8 Example plots illustrating major procedures in calculating lateral displacement index (LDI) using the CPT-based approach with CPT data

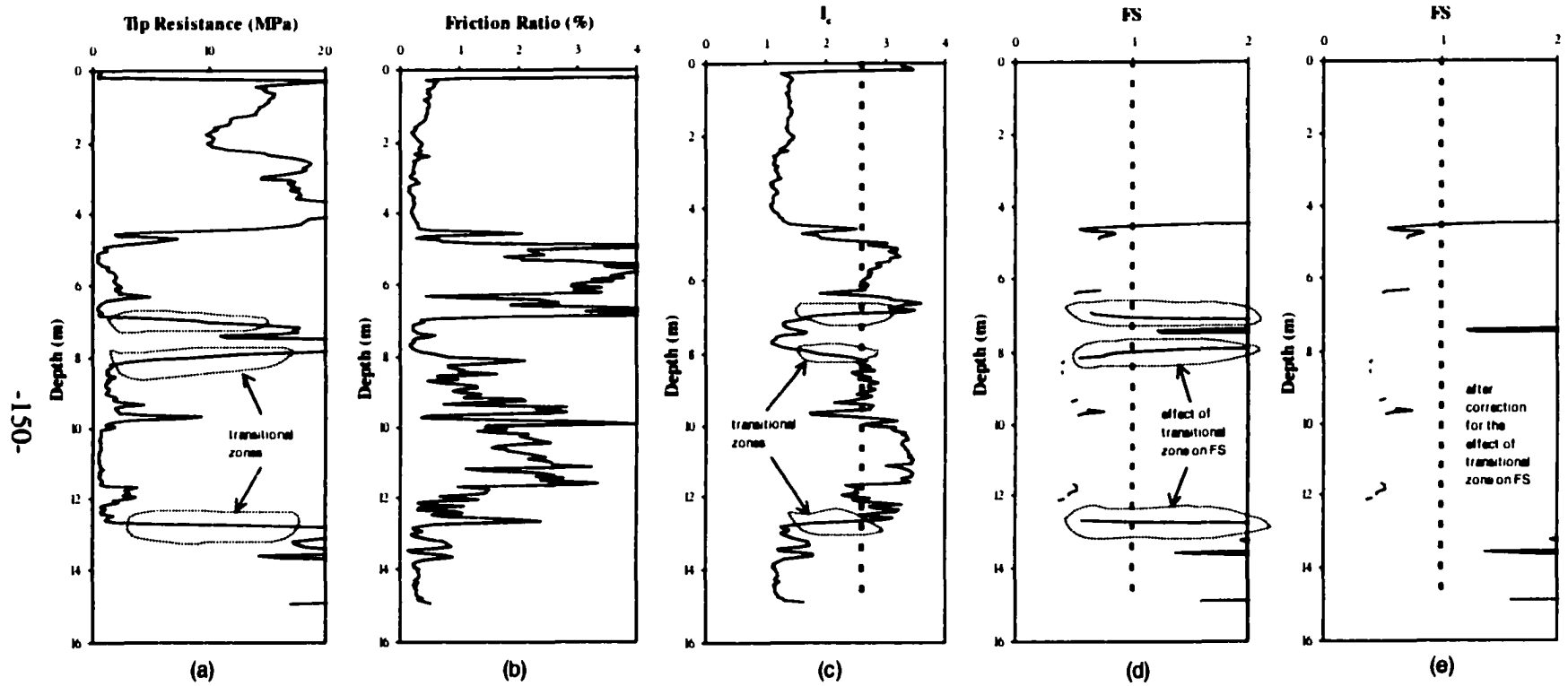


Figure 6.9 Effect of a transitional zone between a clayey soil layer and a sandy soil layer on the factor of safety against liquefaction and its correction

CHAPTER 7 ESTIMATION OF LIQUEFACTION-INDUCED LATERAL DISPLACEMENTS FOR GENTLY SLOPING GROUND WITHOUT A FREE FACE USING SPT OR CPT DATA

7.1 Introduction

A number of liquefaction-induced lateral spreads have occurred during past major earthquakes throughout the world. Most of the lateral spreads, especially those that occurred in Japan and the USA, have been extensively investigated. These well-documented case histories provide valuable data for developing practical approaches to estimate liquefaction-induced lateral displacements. In this chapter and Chapters 8 and 9, several semi-empirical approaches are developed to estimate the magnitude of liquefaction-induced lateral displacements based on the study of available case histories.

The three major components influencing the magnitude of liquefaction-induced lateral displacements are biased static shear stresses, the thickness of liquefied layers, and the maximum shear strains in liquefied layers, as discussed in Chapters 4 and 6. Biased static shear stresses are mainly controlled by the geometric parameters characterizing ground geometry (e.g., ground slope, free face height, and the distance to a free face). The thickness of liquefied layers and the maximum shear strains in liquefied layers have been incorporated into one parameter – the lateral displacement index (LDI), as introduced in Chapter 6. Therefore, it appears that the magnitude of liquefaction-induced lateral displacements is mainly controlled by the geometric parameters and LDI.

Bartlett (1991) observed that there are generally two distinct types of lateral spreads: 1) a lateral spread towards a free face, and 2) a lateral spread down a gentle slope where a free face is not present. Therefore, the two types of lateral spreads are studied separately in this thesis. This chapter only focuses on the estimation of liquefaction-induced ground lateral displacements for gently sloping ground without a free face.

A simple approach to estimate the magnitude of liquefaction-induced lateral displacements using SPT or CPT data for gently sloping ground without a free face is presented in this chapter. First, an empirical correlation among measured lateral displacement (LD), LDI, and ground slope for gently sloping ground is established on the basis of case history studies, as illustrated in Figure 7.1. An approach is then introduced to estimate liquefaction-induced lateral displacements using SPT or CPT data (characterizing soil profile and soil properties), earthquake magnitude and peak surface acceleration (characterizing on earthquake properties), and a ground slope (characterizing ground geometry for sloping ground) for gently sloping ground without a free face. The application and performance of the proposed approach are also discussed in this chapter.

7.2 Geometric Parameters for Gently Sloping Ground

7.2.1 Lateral displacement patterns in gently sloping ground

Both the results of one-g shake-table and centrifuge model tests and observations from the available case histories during past major earthquakes indicate that ground slope for gently sloping ground is one of major parameters controlling the magnitude of liquefaction-induced lateral displacements, as discussed in Section 4.5. Generally, the magnitude of lateral displacements increases with increasing ground slope.

However, lateral displacements in a lateral spread are not uniform even for sloping ground with a uniform slope. Sasaki et al. (1992) observed that the lateral displacement reached its maximum at the top of a slope, while it was at a minimum at the toe of a slope in their shake table tests of a uniform sand model with a uniform surface slope. In addition to lateral displacements, subsidence and cracking (extension) occurred near the top, but heaving and compression were evident near the toe. These displacement patterns were also observed in case histories of lateral spreads (e.g., Hamada et al. 1986; Youd and Kiehl 1996). The above-mentioned observations appear to support the assumption

that the distance to the toe of a slope is another parameter influencing lateral displacements in sloping ground.

The interactions of ground movements in a lateral spread play an important role in the lateral displacement patterns for a sloping ground with several distinct slopes. Because the lateral displacement for a steeper slope tend to be larger than that for a flatter one for similar soil and loading conditions, lateral displacements in the ground with different ground slopes may be complicated due to the interactions of ground movements. For example, for given soil and loading conditions, the lateral displacement at the lower end of a flatter slope that is immediately followed by a steeper slope may be larger than that at the same location in the same slope but without the presence of the steeper slope. Similar displacement patterns can be envisaged at the upper end of a flatter slope that immediately follows a steeper slope. For this case, the lateral displacement at the upper end of the flatter slope may be larger than that at the same locations in the same slope but without the presence of the steeper slope. Such displacement patterns have been observed in practice as Figure 7.2 shows the displacement patterns in a lateral spread that occurred in Noshiro City, Japan during the 1983 Nihonkai-Chubu earthquake. In an extreme case, the ground with a flatter slope opposing the direction of an adjacent steeper slope may move in the down-slope direction of the steeper slope, i.e. a direction against its own down-slope direction. The above observations support the hypothesis that the closest distance to the crest or the toe of a steeper slope is an additional parameter influencing the displacements in a flatter slope adjacent to the steeper slope.

Lateral variations in soil conditions in the ground may add more complexity to the displacement patterns in a lateral spread. Lateral displacement is expected to be larger in a location with a larger lateral displacement index (LDI) even for ground with a uniform slope. As a result, the interactions of ground movements in a lateral spread may be much more complicated for a sloping ground with several distinct slopes and various lateral soil conditions. The complicated interactions may veil the actual importance of ground slope in a lateral spread, which has made some researchers (e.g., Doi and Hamada 1992) think that there is no clear correlation between the magnitude of lateral displacements and the

ground slope at a given location for sloping ground.

7.2.2 Selection of a major geometric parameter for gently sloping ground

Several other geometric parameters, in addition to ground slope, may affect the magnitude of lateral displacements in a lateral spread, as discussed in Section 7.2.1. However, the effect of each of these geometric parameters on lateral displacement may be different for the different portions on sloping ground. Figure 7.3 is a sketch illustrating the major geometric parameters controlling lateral displacements in each of several zones in sloping ground with several distinct slopes. Lateral displacements are expected to be influenced by several geometric parameters in zones 2, 4, 5, 7 and 8 in Figure 7.3 because of the interactions of lateral movements in these zones. On the other hand, the lateral displacement may be mainly controlled by its own ground slope for each of zones 1, 3, and 6 in Figure 7.3 due to the less significant effects of other geometric parameters on the lateral displacements in these zones. As a result, the only major geometric parameter for each of zones 1, 3, and 6 may be its own ground slope.

The study in this chapter mainly focuses on the zones where ground slope is the only major geometric parameter that controls lateral displacement of gently sloping ground without a free face. These zones include the upper part of a long slope in a lateral spread (e.g., zone 1), the upper part of a steeper long slope adjacent to flatter slopes (e.g., zone 3), and the middle part of a flatter long slope connecting to an upper steeper slope (e.g., zone 6), as shown in Figure 7.3. Therefore, ground slope is the only geometric parameter that is used in developing a SPT- or CPT-based approach to estimate liquefaction-induced lateral displacements for gently sloping ground without a free face in this research.

Minor local variations in topography appear to have little influence on general ground movements in a lateral spread, as observed by Youd and Kiehl (1996). Therefore, ground slope, S , used in this research is defined as the average gradient (as a percentage) over relatively long (say 20 m or more) ground with a similar general gradient. Figure 7.4

illustrates the definition of ground slope (S) on gently sloping ground.

7.3 Case Histories

7.3.1 Collection of case histories

Many liquefaction-induced lateral spreads that have occurred during past major earthquakes throughout the world have been extensively investigated. These well-documented case histories provide valuable data for developing practical approaches to estimate liquefaction-induced lateral displacements. In this thesis, case histories from thirteen past major earthquakes were investigated.

The following data for each of the available case histories have been collected and applied in developing SPT- or CPT-based approaches in this thesis:

- Measured lateral displacements in a liquefaction-induced lateral spread;
- Results of the SPT or CPT tested at the locations that were close to the locations where the relevant lateral displacements were measured;
- Geometric parameters (e.g., ground slope, free face height, distance to a free face) characterizing ground geometry of a studied site;
- Earthquake-related parameters (e.g., earthquake magnitude, peak surface acceleration) characterizing earthquake characteristics;
- Other parameters, such as the location of the ground water table, unit weight of soils.

The case histories data were mainly collected from the available reports and published papers that are referred to in this thesis. Partial data, especially for the case sites in Niigata City during the 1964 Niigata earthquake, were obtained from the database that was compiled by Bartlett (1991) and then published by Dr. T. Leslie Youd of Brigham Young University on his homepage (<http://www.et.byu.edu/ce/faculty/youd/>) for researchers to download.

Case histories have been divided into three categories in this thesis: 1) gently sloping ground without a free face, 2) nearly level ground with a free face, and 3) gently sloping ground with a free face. Brief introductions to the case histories in each of the three categories are given in this section and Sections 8.3 and 9.3 respectively.

Six case histories associated with six different earthquakes for gently sloping ground without a free face were studied in this chapter. A summary of the major parameters for the case histories studied in this chapter is provided in Table 7.1. Of the six case histories, SPT data were available for five of the cases. Only two cases feature CPT measurements.

7.3.2 Case sites in San Francisco during the 1906 San Francisco, California, Earthquake

The 1906 San Francisco earthquake, with an epicenter near San Francisco, occurred on April 18 at 5:12 a.m. Pacific Standard Time. A moment magnitude of 7.9 was derived and used by Kanamori (1978) and Bartlett (1991), and the value was adopted in this study.

Liquefaction-induced ground failures that occurred during the 1906 San Francisco earthquake caused significant damage in San Francisco and elsewhere in northern California and were indirectly responsible for extensive fire damage in San Francisco as a result of the severing of water lines, which greatly hampered efforts to control the conflagration (Youd and Hoose 1976). Several researchers (Youd and Hoose 1976, 1987; O'Rourke et al. 1992a; Pease and O'Rourke 1998) studied the liquefaction-induced lateral spreads during the earthquake, and focusing mainly on the zones where severe lateral spreads occurred, namely the Mission Creek area and the South of Market area.

Soil borings with penetration tests were performed before 1964 for the Mission Creek and South of Market areas, as reported by Youd and Hoose (1976, 1978). These borings provide useful information about the soil stratigraphy and the depth of the water table.

However, the penetration tests were conducted using non-standard SPT equipment. Because the blow counts were not consistent with those obtained by means of the standard penetration test, O'Rourke et al. (1992a) suggested avoiding using the test data in the simplified liquefaction potential analysis.

Additional investigations were performed by Pease and O'Rourke (1993) at three locations in the Mission District and at one location in the South of Market area. A combination of conventional boring and sampling procedures, standard penetration tests (SPT), and electric cone penetration (CPT) were used in the investigations. A total of 4 SPTs and 17 CPTs were conducted.

A typical soil profile in the areas where liquefaction-induced lateral spreads occurred during the earthquake consisted of about a 2 m topsoil layer and a 0 to 8 m thick artificial sand fill layer underlain by a natural sand or clay layer and recent bay mud with a maximum thickness of approximately 20 m. The submerged loose sand fills were primarily poorly graded dune sands with negligible silt or clay; they were typically 2 to 4 m thick and were identified as liquefiable soil (Pease and O'Rourke 1998). The topography in the areas was relatively gentle with ground slopes ranging from 1.0% to 2.3%.

In this study, seventeen CPT soundings (Pease and O'Rourke 1993) were used because of their excellent quality for evaluating liquefaction potential. A total of eight points (4 for the Mission Creek area and 4 for the South of Market area) of lateral displacement measurements were collected from Pease and O'Rourke (1998) for these sites. The locations of these measurements were fairly close to the CPT locations, generally within 150 m to the CPT locations.

Based on an empirical correlation proposed by Joyner and Boore (1988), a maximum surface acceleration of 0.6 g was estimated by Bartlett (1991) and was adopted in this study for these two case sites.

7.3.3 The case site in the Furu-Sumida Creek area, Tokyo during the 1923 Kanto, Japan, Earthquake

The Kanto earthquake, with an epicenter in the Sagami Bay and a magnitude of 7.9, occurred on September 1, 1923 at 11:58 a.m. (Hamada et al. 1992a). Several liquefaction-induced lateral spreads were investigated by Hamada et al. (1992a), but only one case site, the Furu-Sumida Creek area, Tokyo, provided enough information to determine the ground geometry, soil conditions, and the magnitude of lateral displacements, and therefore was studied in this research.

Two SPTs were conducted at locations close to the ground cracking zone where the ground surface slope was estimated to be about 1.6% before the earthquake (Hamada et al. 1992a). A typical soil profile in the crack zone consisted of about a 10 m thick layer of fine sand with about 10% fines content and an overlain soft silt layer to an unknown depth. The fine sand layer was estimated to be liquefied during the earthquake with an estimated peak ground acceleration of 0.25 g at the site (Hamada et al. 1992a). Judgement was required to estimate the lateral displacement that occurred at this site because of the lack of detailed measurements.

7.3.4 Case sites in Fukui Plain during the 1948 Fukui, Japan, Earthquake

The Fukui earthquake, with an epicenter below the eastern part of the Fukui Plain in Japan and an estimated moment magnitude of 7.0, occurred at 16:13 on June 28, 1948 (Hamada et al. 1992b). Extensive liquefaction-induced lateral spreads were observed in several areas in the Fukui Plain, and a number of measurements of the lateral displacements were made using pre- and post- earthquake aerial photos, as reported by Hamada et al. (1992b). Unfortunately, only four SPTs in these sites were available for evaluating liquefaction potential, significantly limiting the data that could be used in this research.

Four measurements of lateral displacements at Morita-cho, Fukui Plain were collected for

this study. The locations of these measurements were relatively close to the locations of the SPT, and the ground slopes ranged from 0.4% to 3.4% at the sites. The subsurface soils consisted of alternate layers of clay, silt, silty sand, sand, and sandy gravel, making soil conditions very complex, as commented on by Hamada et al. (1992b). The peak surface acceleration was estimated at about 0.25 g for the site (Rauch 1997). Although the measurements of the lateral displacements for this site were based on aerial photos, the accuracy of the measurements was very poor, and only with a tolerance of about ± 1.92 m, as reported by Hamada et al. (1992b).

7.3.5 Case sites in Niigata City during the 1964 Niigata, Japan, Earthquake

The Niigata earthquake, with an epicenter in the Japan Sea and a magnitude of 7.5, occurred on June 16, 1964 at 1:01 p.m., Japan (Hamada et al. 1986; Hamada 1992a). In Niigata City, which was about 50 km from the epicenter, buildings, bridges, oil storage tanks, lifeline facilities, were extensively damaged. Sand boils and ground fissures that resulted from soil liquefaction were observed in extensive areas throughout Niigata City. It was reported that liquefaction occurred mostly in reclaimed former channels of the Shinano and Tsusen Rivers in Niigata City (Hamada et al. 1986). Liquefaction-induced lateral spreads were observed in both ground with a free face and ground with a very gentle slope. The case sites with a gentle surface slope and without a free face are investigated in this chapter.

Soil profiles in the lateral spread zones with gentle surface slopes in Niigata City were relatively simple. Generally, the soils down to about 20 m from the surface are relatively clean, fine or medium sands. The estimated thickness of the liquefied layers ranged from 3 m to 15 m (average 9.7 m) for the sites with gentle ground slopes.

Based on Hamada et al. (1986) and other unpublished ground failure maps and borehole logs, Bartlett (1991) compiled a comprehensive database for case sites in Niigata City. The database consisted of the measured lateral displacements, relevant ground surface slopes, and SPT results. Even though Hamada (1992a) published a great deal of data

about the case sites in Niigata City, it is difficult to obtain more accurate data, especially the data for ground slopes and SPT results, from the available reports and papers for these sites than from those collected by Bartlett (1991). Therefore, partial data from Bartlett's database were used in this study for the case sites in Niigata City. The distance from the closest location of several SPTs to the location of lateral displacement measurement was more than 100 m for some case sites in Niigata City in Bartlett's database. To avoid potentially incorrect interpretations of ground conditions for these sites, the data for these sites were not used in this study. A total of 103 lateral displacement measurements from the sites in Niigata City were collected, and the results of 27 SPTs associated with the lateral displacement measurements were used in this study.

The ground slopes for the case sites in Niigata City were relatively long and uniform, and within a narrow range (from 0.2% to 0.9%). The measured lateral displacements varied from 0.8 m to 4.6 m for the data used for this study. The lateral displacements were measured using pre- and post-earthquake aerial photographs, and the accuracy of the measurements was estimated to be ± 0.72 m in Niigata City (Hamada 1992a). In addition, a peak surface acceleration of 0.19 g was reported by Kawasumi (1968) and Bartlett (1991), and the value was used for all the sites in Niigata City in this research.

7.3.6 The Juvenile Hall case history during the 1971 San Fernando, California, Earthquake

The San Fernando earthquake, with an epicenter of about 13 km north-northeast of San Fernando, occurred on February 9, 1971 at 6:01 a.m. Pacific Standard Time and registered a magnitude of 6.4 on the Richter scale (O'Rourke et al. 1992b). Substantial damage was caused by liquefaction-induced lateral spreads in the area of the Upper Van Norman Reservoir during this earthquake. The San Fernando Valley Juvenile Hall was one of the major sites associated with liquefaction-induced lateral spreads in gently sloping ground and was studied in this research.

The Juvenile Hall case site was about 12 km from the epicenter of the 1971 San Fernando

earthquake, but just several kilometers away from the main trace of surface faulting on the upthrust block in the earthquake. The lateral spread in the area of the Juvenile Hall was associated with the movement of a large amount of soil (about 1350 m long and 350 m wide) down a slope with an average gradient of about 1.2% (Bartlett 1991).

The soils within the top 10 to 15 m at the site were mainly alluvium deposits. The soil profile at the site consisted of several laterally and vertically variable units. The significant variations in sediment units were believed to be due to the complicated depositional history of the site, as explained by Bennett (1989). The top unit, Unit A, was a silty sand and above the ground water table. The sublayer beneath Unit A, Unit B1, was a poorly sorted, loose sandy silt and silty sand. The fines content varied from 50% to 80%, with an average of 65%, and the clay content was about 10% for the soils in this unit. This unit was identified as the layer of sediment that liquefied during the 1971 earthquake (Bennett 1989). The sublayer Unit B2 was sandy silt with an average clay content of 19% and was probably not susceptible to liquefaction due to large clay friction, as noted by Bennett. Unit C, dense silty sand with high liquefaction resistance, and Unit D, stiff sandy silt with an average clay content of 21%, were identified by Bennett as unliquefied deposits.

Bennett (1989) performed site investigations of the site with eleven CPTs and six SPTs. However, the penetration tests were mainly conducted along one section transverse to the lateral spread. The results of the available five CPTs and five SPTs were used in this study.

Because of the uniform measured lateral displacement of 1.68 m and a ground slope of 1.2% at the main part of the section where most of the penetration tests were conducted, only one set of data were used for this site in this research. The lateral displacement measurements close to the boundaries of the lateral spread in this site were not collected in this research in consideration of the effects of boundaries or margins.

7.3.7 Case sites in Noshiro City during the 1983 Nihonkai-Chubu, Japan, Earthquake

The Nihonkai-Chubu earthquake, with a magnitude of 7.7, occurred in the Japan Sea about 90 km west of Aomori Prefecture on May 26, 1983 at 12:00 a.m., causing severe damage to the coastal areas of the Tohoku region (Hamada et al. 1986; Hamada 1992b). In the city of Noshiro, in particular, which was located about 100 km from the epicenter, severe damage to houses, buildings, and buried tanks and pipes was caused by liquefaction-induced lateral spreads.

Hamada et al. (1986) and Hamada (1992b) conducted extensive investigations of the liquefaction-induced lateral spreads that occurred in Noshiro City during the Nihonkai-Chubu earthquake. A total of 27 sections with soil profiles, SPT results, and measured values of lateral displacements were presented in their report. The lateral displacements were measured using pre- and post-earthquake aerial photographs. The accuracy of the measurement of lateral displacements was estimated as ± 17 cm, which is much better than that for the case sites in Niigata City and Fukui Plain. A total of 32 SPTs were reported by Hamada et al. (1986), and the data of 21 SPTs were used in this study.

Most of the urban area in Noshiro City was built on sand dunes along the Japan Sea coast and the alluvial plane of the Yoneshiro River (Hamada et al. 1986). Large lateral displacements of up to 5.0 m occurred in the sand dune areas with various gentle slopes. In contrast, relatively small lateral displacements, less than 0.5 m, occurred in the area, mostly on the alluvial plain. Generally, the subsurface soils in areas where large displacements occurred consisted of top sandy fill, dune sand, alluvial sand, and alluvial clay (Hamada 1992b). The dune sand and alluvial sand were estimated to have partially liquefied, with the thickness of liquefied layers varying from 1.0 to 7.0 m. The two sands were relatively clean with less than 5% fines content (Bartlett 1991).

The ground slopes in the liquefied areas varied from less than 1% to up to 7.5%. Due to the interactions of the lateral movements in a lateral spread for sloping ground with

various ground slopes, as discussed in Section 7.2, it was difficult to select the locations where lateral displacements were mainly associated with their own ground slopes. Using the criteria described in Section 7.2, a total of 23 measurements of lateral displacements were collected from 14 soil sections for the case sites in Noshiro City in this research. The peak surface acceleration in Noshiro City was estimated to be about 0.25 g (Hamada et al. 1986), and the value was adopted in this study.

7.4 Estimating Equivalent CPT Data from SPT Data

Currently, the cone penetration test (CPT) has become very popular for site characterization because of its greater repeatability and reliability and its continuous profile of measurements as compared with other in-situ tests. The CPT has also been increasingly used in predicting liquefaction potential in geotechnical practice because of its advantages. However, a CPT-based method to estimate liquefaction-induced lateral displacements has not been developed yet.

One of the objectives of this research is to develop approaches to estimate the lateral displacements in a lateral spread using CPT data. In developing these approaches, case history data with CPT results are required. Unfortunately, CPT data were available only at the sites for two case histories for gently sloping ground without a free face, for one history for nearly level ground with a free face, and for two case histories for gently sloping ground with a free face. The data from these limited case histories are not sufficient to develop the CPT-based approaches. In this research, a compromise was adopted to obtain equivalent CPT data from available SPT N-values for case histories where there were no in-situ CPT data. A detailed introduction to this procedure is presented in the following sections.

7.4.1 The soil behavior type index and fines content

Soil behaviour charts have been developed to estimate soil type from CPT data (e.g.,

Olsen and Malone 1988; Robertson 1990). As a result, grain characteristics such as apparent fines content of sandy soils can be estimated directly from CPT data using any of these soil behaviour charts, such as that by Robertson (1990). Based on Robertson's (1990) soil behaviour chart, the boundaries of soil behaviour type are given in terms of soil behaviour type index (I_c) by Robertson and Wride (1997), as listed in Table 7.2. I_c is a function of normalized CPT tip resistance and friction ratio, as defined in Robertson and Wride (1998).

Robertson and Wride (1997) suggested a simplified relationship between the soil behaviour type index (I_c) and apparent fines content (FC) as Equation 7.1.

$$\begin{aligned}
 [7.1a] \quad & FC (\%) = 0 && \text{if } I_c < 1.26 \\
 [7.1b] \quad & FC (\%) = 1.75I_c^{3.25} - 3.7 && \text{if } 1.26 \leq I_c \leq 3.5 \\
 [7.1c] \quad & FC (\%) = 100 && \text{if } I_c > 3.5
 \end{aligned}$$

Even though the apparent FC may be different from the actual fines content in soils, as stated by Robertson and Wride (1997), because the apparent FC is also affected by the degree of plasticity of the fines and other factors, the apparent FC may be approximately treated as actual fines content for soils with low plasticity fines. If the calculated FC using Equation [7.1] under a given I_c is treated as actual fines content, it is found that the calculated fines content is not quite consistent with the soil type in Table 7.2. For example, the calculated fines content using [7.1] for I_c equal to 2.6 is 35%. However, the relevant soil type for I_c equal to 2.6 in Table 7.2 is sandy silt to clayey silt that may generally have fines content of up to 50% or more. Furthermore, the calculated FC for I_c equal to 2.95 is only 55%, but the relevant soil type for I_c equal to 2.95 is silty clay that may have fines content of up to 100%. Therefore, it appears that Equation [7.1] tends to give a lower value of calculated FC than the actual fines content.

Gilstrap (1998) compared the calculated FC using Equation [7.1] with the actual fines content measured in the field for nine case history sites and found that Equation [7.1] generally under-predicts fines content values for soils with more than 20% fines content.

Similar studies were conducted for the case sites of Heber Road (57 sets of data) and River Park (52 sets of data), California in this research on the basis of CPT data and relevant grain size data reported by Bennett et al. (1981). In combination with the 125 sets of data from nine case history sites studied by Gilstrap (1998), a total of 234 sets of data were collected. These data are plotted in Figure 7.5 as well as the curve for Equation [7.1] and a fitted curve for the data for comparison. The fitted curve can be expressed as Equation [7.2]:

$$[7.2] \quad I_c = -6.146E-08(FC)^4 + 1.564E-05(FC)^3 - 1.411E-03(FC)^2 + 6.232E-02(FC) + 1.387$$

The calculated fines content using [7.2] is now becoming much more consistent with the soil type in Table 7.2. For instance, the calculated fines content using [7.2] for I_c equal to 2.6 is 56.7% for sandy silt to clayey silt. And the calculated FC for I_c equal to 2.95 is now 92% for silty clay. In this research, Equation [7.2] is used to approximately express the relationship between I_c and fines content (FC).

7.4.2 Converting SPT data to equivalent CPT data

Several studies (e.g., Robertson et al. 1983; Kulhawy and Mayne 1990) have been performed to relate the SPT N value to CPT cone resistance q_c . Robertson et al. (1983) presented a relationship between SPT N value and CPT cone resistance q_c , as shown in Figure 7.6, on the basis of the data collected from 18 sites. Although Kulhawy and Mayne (1991) provided additional data to the data in Figure 7.6 and gave a new best-fit curve, Lunne et al. (1997) commented that these additional data did not define the SPT energy ratio, which was probably lower than that for the data by Robertson et al. (1983). So the correlation in Figure 7.6 was recommended by Lunne et al. (1997).

Mean grain size, D_{50} (mm), is required when the correlation in Figure 7.6 is applied. Because D_{50} cannot be estimated directly from CPT data, it is difficult to use this correlation with CPT data. Therefore, Equation [7.3] was developed by Lunne et al.

(1997) to combine the soil type and I_c in Table 7.2 with the CPT-SPT ratios given in Figure 7.6:

$$[7.3] \quad (q_c/P_a)/N_{60} = 8.5 (1.0 - I_c/4.6)$$

where P_a is the atmospheric pressure, q_c is CPT tip resistance with the same unit as P_a , N_{60} is the SPT N value corresponding to an energy ratio of 60%, and I_c is the soil behaviour type index.

In this research, converting SPT data to CPT data is necessary in order to use a large amount of SPT data in case histories because of insufficient CPT data. Equation [7.2] is used to correlate fines content, which is usually measured with SPT, with I_c , which is a key parameter used in the NCEER CPT-based method for liquefaction potential analysis. Equation [7.3] is then used to convert SPT N values to CPT tip resistance, q_c . With known I_c and q_c , the NCEER CPT-based method can be applied to evaluate liquefaction potential for the available case sites.

7.5 Establishment of Correlation among Lateral Displacement, Lateral Displacement Index, and Ground Slope for Gently Sloping Ground without a Free Face

The magnitude of liquefaction-induced lateral displacements is primarily controlled by the lateral displacement index (LDI) and geometric parameters characterizing ground geometry, and ground slope is a major geometric parameter for gently sloping ground, as discussed in Sections 7.1 and 7.2. This implies that a general correlation may exist among LDI, ground slope, and the magnitude of lateral displacement.

Case history data concerning lateral spreads that occurred during past major earthquakes provide a good opportunity to establish this correlation. In this section, following the procedures illustrated in Figure 7.1, the empirical correlation is established on the basis of case history studies.

For simplicity, if the actual lateral displacement is assumed to be linearly proportional to LDI for a given ground slope, the ratio of LD to LDI will then depend solely on ground slope. Based on this concept, the case history data are used to develop an empirical correlation between LD/LDI and ground slope in next two sections.

7.5.1 Correlation between LD/LDI and ground slope using SPT data

A total of five case histories in which SPT data were available were studied for gently sloping ground without a free face. First, the NCEER SPT-based method was applied to evaluate liquefaction potential using SPT data and earthquake parameters for each of the sites for the available five case histories with SPT data (see Table 7.1). The lateral displacement index (LDI) was then calculated for each of the sites based on the procedures described in Section 6.3. An average of the calculated values of LDI was used as a final LDI value if more than one SPT that was conducted at the locations close to the location where the relevant lateral displacement was measured were available. Finally, a total of 132 data sets from the five case histories were obtained, as listed in Table A1 in Appendix A. The data included measured lateral displacement, LDI, and ground slope.

Figure 7.7 is a plot of LD/LDI vs. ground slope with the data of which the values of LDI were calculated using SPT data for the five case histories. A general trend of increasing LD/LDI with increasing ground slope can be seen from Figure 7.7. A fitted trend line for the data is also shown in Figure 7.7. Equation [7.4] is a mathematical expression of the trend line:

$$[7.4] \quad \frac{LD}{LDI} = S + 0.2 \quad (\text{for } 0.2\% < S < 3.5\%)$$

where LD is actual lateral displacement, LDI is the lateral displacement index, and S is ground slope as a percentage.

A dominant portion (95%) of the data in Figure 7.7 was collected from two Japanese case histories – Niigata and Noshiro. The soils that were estimated to be liquefied at the sites for these two case histories were generally clean sands. Because ground slopes at all the sites for Niigata case history were between 0.2% and 0.9% and with an average of about 0.5%, the data for this case history control only the lower part of the trend line in Figure 7.7 for ground slope less than 1%. Therefore, the data for Noshiro case history dominate the trend line in Figure 7.7 for ground slope greater than 1%, especially for ground slope greater than 3.5% in which all the four points in Figure 7.7 are exclusively from Noshiro case history. The data from the other three case histories fit well with the trend line as well as the data for Niigata and Noshiro case histories in Figure 7.7 for ground slopes ranging from about 0.5% to 3.5%. In this study, the recommended range of ground slope is between 0.2% and 3.5% for Equation [7.4].

7.5.2 Correlation between LD/LDI and ground slope using CPT data

To establish the correlation of LD/LDI and ground slope for case history data in which the values of LDI are calculated using CPT data, a similar procedure as for the cases using SPT data in Section 7.5.1 was followed but with using the NCEER CPT-based method and CPT data to evaluate liquefaction potential and then to calculate LDI. A database with a total of 140 data sets from the six case histories associated with six past major earthquakes was established, as listed in Table A1 in Appendix A. The LDI for each of the sites for the San Francisco and Juvenile Hall case histories was directly calculated using in-situ CPT data. The LDI for each of the sites for the other four case histories was calculated using the equivalent CPT data that were converted from the SPT data using the procedures introduced in Section 7.4.

Figure 7.8 is a plot of LD/LDI versus L/H for the data of which the values of LDI were calculated using the available in-situ CPT data for the San Francisco and Juvenile Hall case histories. The curve in Figure 7.8 is a graphical expression of Equation [7.4] that was developed using the NCEER SPT-based method and SPT data. Figure 7.8 shows that the data for the San Francisco case history associated with the 1906 San Francisco

earthquake fairly fit the curve with significant scatter.

However, a point representing the data for the Juvenile Hall case history associated with the 1971 San Fernando earthquake is far removed from the curve in Figure 7.8. It is believed that the main reason for this inconsistency is because the NCEER CPT-based method generally treats the soils with an I_c greater than 2.6 as non-liquefiable soils. An I_c equal to 2.6 corresponds to a calculated fines content of about 57% when Equation [7.2] is used. Nevertheless, the fines contents range from 50% to 80% with an average of 65% for the soils that were estimated by Bennett (1989) to be liquefied for the Juvenile Hall case site. This implies that the majority of the liquefied soils in the Juvenile Hall area may have a calculated I_c greater than 2.6 and thus be evaluated as non-liquefiable soils by the NCEER CPT-based method, which caused a smaller calculated value of LDI and thus a higher value of LD/LDI, as shown in Figure 7.8. As suggested by Robertson and Wride (1997, 1998), samples should be obtained for soils with an I_c greater than 2.6 and evaluated using the other criteria, such as the Chinese criteria (NCEER 1997). Therefore, the point for the Juvenile Hall site may be ignored in qualifying the correlation between LD/LDI and ground slope using CPT data in Figure 7.8.

It is very difficult to develop a general CPT-based correlation between LD/LDI and ground slope using the limited data in Figure 7.8, even though the data from San Francisco case history fairly support the assumption that Equation [7.4] may also be applicable to the cases in which the LDI is calculated using the NCEER CPT-based method and CPT data. To verify this assumption, the data from the other four case histories where no CPT data were available were used. The values of the LDI for these four case histories were calculated using the NCEER CPT-based method and the equivalent CPT data that were converted from the SPT data.

Figure 7.9 is a plot of LD/LDI versus ground slope (S) for the data of which the values of the LDI were calculated using the equivalent CPT data for the four case histories. The curve that is a graphical expression of Equation [7.4] is also shown in Figure 7.9. Generally, the data fit the curve well in Figure 7.9. The good agreement between the data

shown in Figure 7.9 and Equation [7.4] may suggest that the relationship between LD/LDI and ground slope is independent of either using SPT or CPT data and possibly that it solely captures the influence of ground slope on lateral displacements. This is encouraging, however, additional CPT-based data from new case histories are required to further verify this observation.

7.6 An Approach to Estimate Liquefaction-induced Lateral Displacements Using SPT or CPT Data for Gently Sloping Ground without a Free Face

Preliminary studies of the available case histories generally support the assumption that the relationship between LD/LDI and ground slope may be independent of either using SPT or CPT data and may be characterized by Equation [7.4]. Therefore, estimates of liquefaction-induced lateral displacements for gently sloping ground without a free face using SPT or CPT data may be obtained by:

- Assessing liquefaction potential using either the NCEER SPT- or CPT-based methods;
- Calculating the lateral displacement index (LDI);
- Measuring ground slope (S);
- Estimating lateral displacement (LD) using Equation [7.5].

$$[7.5] \quad LD = (S + 0.2) \cdot LDI \quad (\text{for } 0.2\% < S < 3.5\%)$$

Figure 7.10 is a flowchart illustrating the major steps to apply the proposed approach for gently sloping ground without a free face. First, site investigation with the SPT or CPT, which must be penetrated at locations close to the location where estimates of liquefaction-induced lateral displacements are needed, is conducted. The liquefaction potential of the studied site is evaluated using either the NCEER SPT- or CPT-based method with the SPT or CPT data and earthquake parameters that are estimated based on a design earthquake for the site. The LDI for each studied location in the site can then be

calculated based on the procedures introduced in Section 6.3. With the measured value of ground slope (S) for each location in the site, Equation [7.5] can be used to estimate the lateral displacements at the studied locations.

Except for the four cases for the Noshiro case history where ground slopes up to 7.5% were presented, the ground slopes that were used in developing the correlation between LD/LDI and ground slope varied from 0.2% to 3.5% for all the other five case histories. Therefore, the recommended range of ground slope is between 0.2% and 3.5% for Equation [7.5].

The proposed approach was developed using the data from only six case histories associated with six past earthquakes and as such is applicable only for similar earthquakes and ground conditions, as summarized in Table 7.1. The moment magnitudes for the six earthquakes ranged from 6.4 and 7.9, and the peak surface accelerations varied from 0.19 g to 0.6 g. However, the 1971 San Fernando earthquake associated with the Juvenile Hall case history was only one with moment magnitude (6.4) of less than 7.0 among the six earthquakes. In particular, Juvenile Hall case site was only about 12 km from the epicenter and just several kilometers away from the main trace of surface faulting in the earthquake and experienced a peak surface acceleration of about 0.55 g. Therefore, the proposed approach may mainly be applicable to sites associated with an earthquake with an estimated moment magnitude of 7.0 to 8.0. In addition, a dominant portion (95%) of the case history data used in developing the proposed approach was from the sites where soils thought to be liquefied were generally clean sands only.

The proposed approach may be used to estimate lateral displacements in some zones in gently sloping ground without a free face. These zones generally include the upper part of a long slope in a lateral spread (e.g., zone 1 in Figure 7.3), the upper part of a steeper long slope adjacent to flatter slopes (e.g., zone 3), and the middle part of a flatter long slope connecting to an upper steeper slope (e.g., zone 6), as shown in Figure 7.3. This is because the dominating geometric parameter characterizing ground geometry in these

zones is ground slope only, and other geometric parameters have much less effects on the lateral displacements in these zones than ground slope does.

The studies of the Juvenile Hall case history in Section 7.5.2 indicated that the method to calculate LDI using the NCEER CPT-based method and in-situ CPT data may underestimate LDI for soils with a high fines content (greater than about 55%) and low clay content (less than about 15%) because soils with an I_c greater than 2.6 are generally assumed as to be non-liquefiable for the NCEER CPT-based method. As suggested by Robertson and Wride (1997,1998), samples should be obtained for soils with an I_c greater than 2.6, and their liquefaction potential should be evaluated using other criteria, such as the Chinese criteria. As a result, LDI should be calculated based on the results of liquefaction potential analyses for all the soils in a soil profile with an I_c either greater or less than 2.6.

The proposed approach may be used to estimate the magnitude of liquefaction-induced lateral displacements for gently sloping ground without a free face for low to medium-risk projects or to provide preliminary estimates for high-risk projects. However, engineering judgement must be exercised because liquefaction-induced ground lateral spreading is a complicated phenomenon and a number of assumptions and simplifications were involved in developing the proposed approach.

7.7 Performance of the Proposed Approach

7.7.1 Accuracy of the proposed approach

The measured lateral displacements are compared with the calculated lateral displacements using the proposed approach with SPT data for the available five case histories studied in this chapter, as shown in Figure 7.11. 93% (27 out of 29) of the calculated lateral displacement values for the four case histories (Noshiro, Juvenile, Fukui, and Kanto) and 84% (87 out of 103) of the calculated displacement values for

Niigata case history fall in the zone between the 100 percent over-prediction bound-line and 50 percent under-prediction bound-line, as shown in Figure 7.11. The accuracy of the calculated displacements for the Niigata case history may be lower than that for other case histories given: (a) the relatively poor accuracy (± 0.72 m) of the measured displacements and (b) relatively flat ground slopes (0.2 to 0.9%), where local topography variations and/or the presence of buildings may have more significant effects on lateral displacements than those for steeper slopes.

Figure 7.12 compares the measured lateral displacements with calculated values using the proposed approach with in-situ CPT data or the equivalent CPT data that were converted from SPT data for the available six case histories studied in this chapter. 92% (33 out of 36) of the calculated displacement values for the five case histories (Noshiro, Juvenile Hall, Fukui, Kanto, and San Francisco) and 86% (89 out of 103) of the calculated displacement values for the Niigata case history are greater than 50% and less than 200% of the relevant measured values, as indicated in Figure 7.12.

Figures 7.11 and 7.12 show the likely variability of calculated displacements using the proposed approach with SPT or CPT data. Considerable scatter is evident as lateral displacements could be either underestimated or overestimated by up to a factor of two based on the available data.

7.7.2 Comparison with the MLR model of Youd et al. (1999)

Other than the proposed semi-empirical approach in this study, the MLR model of Youd et al. (1999) is probably the best field-test-based empirical model for estimating lateral displacements on a liquefaction-induced lateral spread at present, as discussed in Section 5.5. A logical question is how well estimations from the proposed approach compare with those from the MLR model of Youd et al. (1999).

Because of differences in the model parameters for these two methods, the best way to compare the two models is to estimate lateral displacements at actual sites where all of

the necessary values are known. To avoid compiling a new database of parameters for the MLR model of Youd et al. (1999), only the estimates of lateral displacements for the sites of the Niigata case history were compared in this comparison analysis. This is because both the locations and the relevant measured values of lateral displacements for all the sites associated with the Niigata case history studied in this chapter are identical to those for some sites associated with the Niigata case history investigated by Youd et al. (1999).

A comparison of lateral displacements measured at sites for the Niigata case history and calculated by both the proposed approach in this study and the MLR model of Youd et al. (1999) for gently sloping ground without a free face is shown in Figure 7.13. Figure 7.13 indicates that the calculated values for lateral displacements obtained by both the proposed approach and the MLR model of Youd et al. (1999) are generally between 50% to 200% of the relevant measured values for the Niigata case history. This preliminary comparison based on limited data from the Niigata case history appear to indicate that the accuracy of the proposed approach is similar to or slightly lower than that of the MLR model of Youd et al. (1999) for estimating lateral displacements for this case history. Further evaluations using data from new case histories are definitely required to compare and evaluate the performance of both the proposed method and the MLR model before any solid conclusions can be made.

Figure 7.14 shows a comparison of lateral displacements calculated by the proposed approach in this study and by the MLR model of Youd et al. (1999) for different ground slopes for the Niigata case history. This comparison generally indicates that the proposed approach predicted slightly larger values of lateral displacements than the MLR model of Youd et al. (1999) for the studied cases in which ground slopes ranged from 0.2% to 0.9%.

Compared with the MLR model of Youd et al. (1999), the proposed method has two advantages, as discussed in next section.

7.8 Discussion

Compared with the other available empirical methods (including the MLR model of Youd et al. (1999)), the proposed method has two distinct advantages. The first is that the distribution of lateral displacement with depth below the ground surface can be estimated from the proposed method. The variation of lateral displacements with depth at a given location can be reasonably assumed to be similar to the variation of the lateral displacement index with depth, as illustrated in Figures 6.8f and 6.9f. This profile may be valuable for the design of underground structures (e.g., pipelines) and foundations (e.g., piles). The second advantage is that soil properties can be better characterized by the proposed approach. For instance, an individual value for each of measured fines contents is used in the proposed method while a single average value of fines contents for all the sandy soils that have a normalized SPT N value of less than 15 is assigned to an SPT profile in the MLR model of Youd et al. (1999).

Engineered structures (e.g., quay walls, retaining walls, piles, tanks, or pipelines) may alter the patterns and magnitude of lateral displacements in a liquefaction-induced lateral spread. The proposed approach was developed using the data from case history sites where engineered structures had little or no effect on lateral spreads. It is expected that the proposed approach may over-estimate lateral displacements at sites where engineered structures pose significant restrictions to the lateral movements of the ground.

Caution should be exercised when a substantial zone of soils with a low $(N_1)_{60cs}$ or $(q_{c(IN)})_{cs}$ is encountered during liquefaction potential analysis. For such cases, more extensive investigation should be made and other approaches should be taken to evaluate the potential for flow failure of the soil, especially when the static shear stresses in the ground are relatively high. Deformations caused by flow failures can be much larger than those by lateral spreads, and their estimation is beyond the scope of this research.

The proposed approach characterizes the effects of soil profile and properties, earthquake

characteristics, and ground geometry on liquefaction-induced lateral displacements. Other factors that may also influence lateral displacements, such as the redistribution and drainage of excess pore pressures in the ground, are not quantified in the current approach and would need to be evaluated on a case-by-case basis.

As discussed in Section 7.2.1, the interactions of the ground movements in a lateral spread for a sloping ground with several distinct slopes play an important role in controlling the displacement patterns in a lateral spread. Lateral displacements in some zones of a lateral spread are influenced not only by their own surface slopes but also by the adjoining slopes and the distance to these adjacent slopes. These zones are illustrated in zones 2, 4, 5, 7, and 8 in Figure 7.3. The lateral displacements in these zones cannot be directly calculated by the proposed approach but may be inferred based on judgement and the calculated lateral displacements in other zones where lateral displacements can be directly estimated from the above-mentioned approach.

The proposed approach has two limitations similar to two of the limitations that were discussed in Section 5.5.3 for the Bartlett and Youd's MLR model. First, the majority of case history data (see Table 7.1) that were used to develop the proposed approach were collected from two Japanese case histories (Niigata and Noshiro). Second, there were only 13 observations with measured displacements equal to or smaller than 1.0 m among the total of 140 observations in the database for gently sloping ground without a free face in this study.

7.9 Conclusions

An approach to estimate liquefaction-induced lateral displacements using either SPT or CPT data for gently sloping ground without a free face has been developed based on available results from laboratory tests and data from case histories. The proposed approach captures the mechanisms of liquefaction-induced lateral spreads and characterizes the major factors influencing lateral displacements. The proposed approach

can be used to obtain estimates of both the magnitude and distribution of liquefaction-induced lateral displacements for gently sloping ground without a free face for low to medium-risk projects or to provide preliminary estimates for high-risk projects. The proposed method can be easily applied with only a few additional calculations following the NCEER SPT- or CPT-based liquefaction-potential analysis.

Given the complexity of liquefaction-induced lateral spreads, considerable variations in magnitude and distribution of lateral displacements are expected. Generally, the calculated lateral displacements from the six available case histories studied in this chapter showed variations between 50% and 200% of measured values. Preliminary studies of the Niigata case history indicated that the accuracy of the proposed approach was similar to or slightly less than that of the MLR model of Youd et al. (1999) for estimating lateral displacements for the Niigata case history. Further evaluations using data from new case histories are definitely required to compare and evaluate the performance of both the proposed method and the MLR model before any solid conclusions can be made. Furthermore, it is expected that the proposed approach may over-estimate lateral displacements at sites where engineered structures pose significant restrictions to ground movements.

The proposed approach was developed using the data from only six case histories associated with six past earthquakes and as such is applicable only for similar earthquakes and ground conditions. The recommended range for ground slope is between 0.2% and 3.5% for the proposed approach. Additional data from new case histories are required to better quantify liquefaction-induced lateral spreads, to evaluate and update the proposed approach, and to expand the existing range for ground slope.

Table 7.1 Summary of the major parameters for case histories for gently sloping ground without a free face

Case History	Noshiro (1983)	Juvenile Hall (1971)	Niigata (1964)	Fukui (1948)	Kanto (1923)	San Francisco (1906)
References	Hamada et al. (1986), Hamada (1992b), and Bartlett (1991)	Bennett (1989), and O'Rourke et al. (1992b)	Bartlett (1991), Bartlett and Youd (1995), Hamada (1992a), Hamada et al. (1986)	Hamada et al. (1992b), and Rauch (1997)	Hamada et al. (1992a), and Rauch (1997)	Pease and O'Rourke (1993, 1998), O'Rourke et al. (1992), and Youd and Hoose (1976, 1987)
Number of LD measurements	23	1	103	4	1	8
Measured Lateral Displacement, LD (cm)	65 – 298	168	80 – 460	100 – 350	250	60 – 210
Liquefied Soils	Mainly clean dune sand and alluvial sand	Alluvium with fines content of 50% to 80%	Mainly clean, fine or medium sands	Silt, silty sand, sand, and sandy gravel	Fine sand with about 10% fines	Relatively clean dune sand
Thickness of Liquefied Soils (m)	1.0 – 7.0	0.9 – 3.0	3.0 – 15.0	1.7 – 5.7	8.0 – 8.8	1.3 – 8.5
Lateral Displacement Index, LDI (cm)	17 – 164	60 (SPT) 18 (CPT)	37 – 538	19 – 250	184 – 232	33 – 173
Ground Slope (%)	0.2 – 7.5	2.6	0.2 – 0.9	0.4 – 3.4	1.6	1.0 – 2.3
Moment Magnitude of the Earthquake, M_w	7.7	6.4	7.5	7.0	7.9	7.9
Peak Surface Acceleration, a_{max} (g)	0.25	0.55	0.19	0.25	0.25	0.6
Number of SPT or CPT	21 (SPT)	5 (SPT) 5 (CPT)	27 (SPT)	3 (SPT)	2 (SPT)	17 (CPT)

Table 7.2 Boundaries of Soil Behaviour Type

(modified from Robertson and Wride (1997))

Soil Behaviour Type Index, I_c	Soil Behaviour Type (Robertson 1990)
$I_c < 1.31$	Gravelly sand to dense sand
$1.31 < I_c < 2.05$	Sands: clean sand to silty sand
$2.05 < I_c < 2.60$	Sand Mixtures: silty sand to sandy silt
$2.6 < I_c < 2.95$	Silt Mixtures: clayey to silty clay
$2.95 < I_c < 3.60$	Clays: silty clay to clay
$I_c > 3.60$	Organic soils: peats

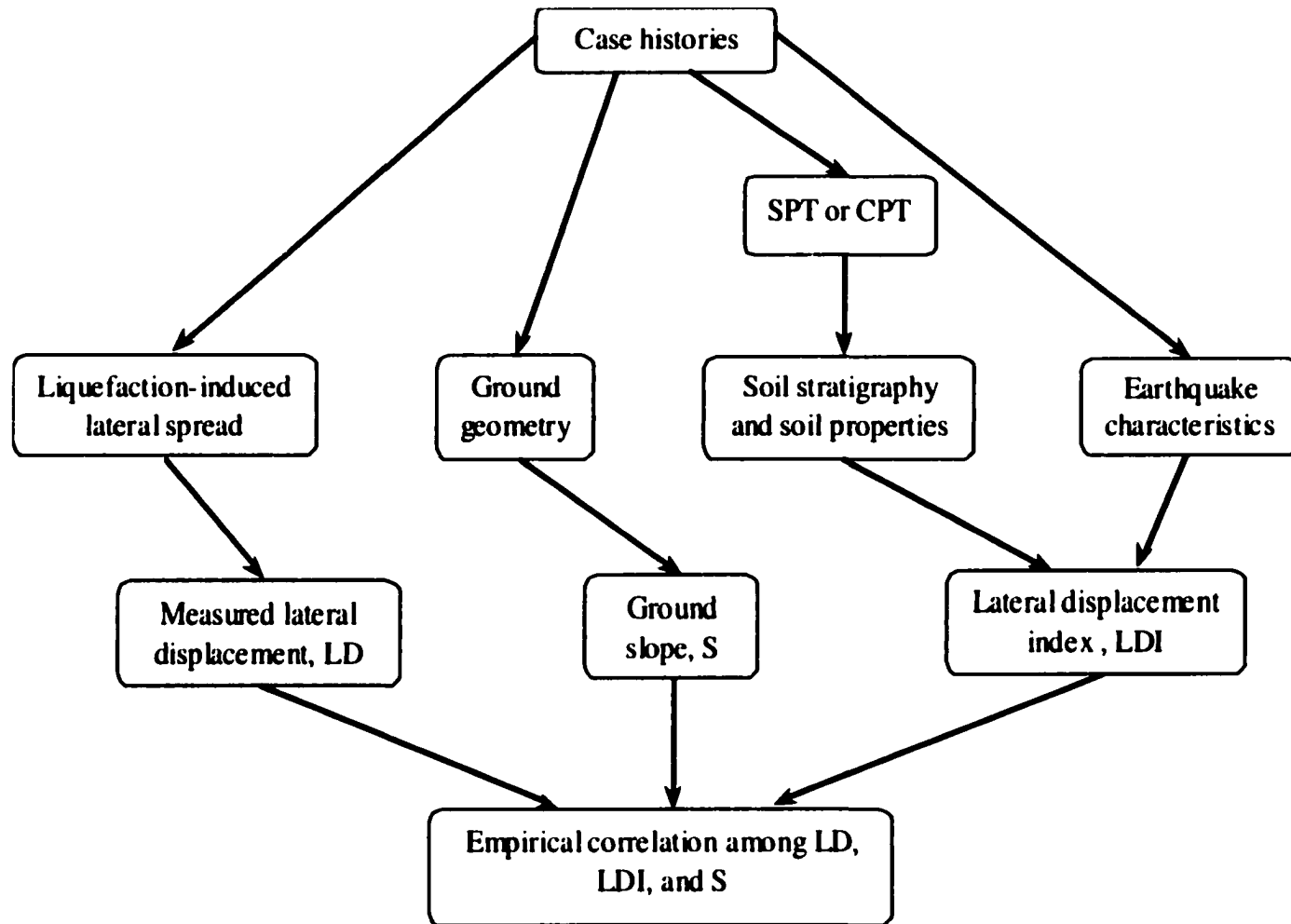


Figure 7.1 Conceptual flow chart for developing an empirical correlation between LD, LDI, and S for gently sloping ground without a free face

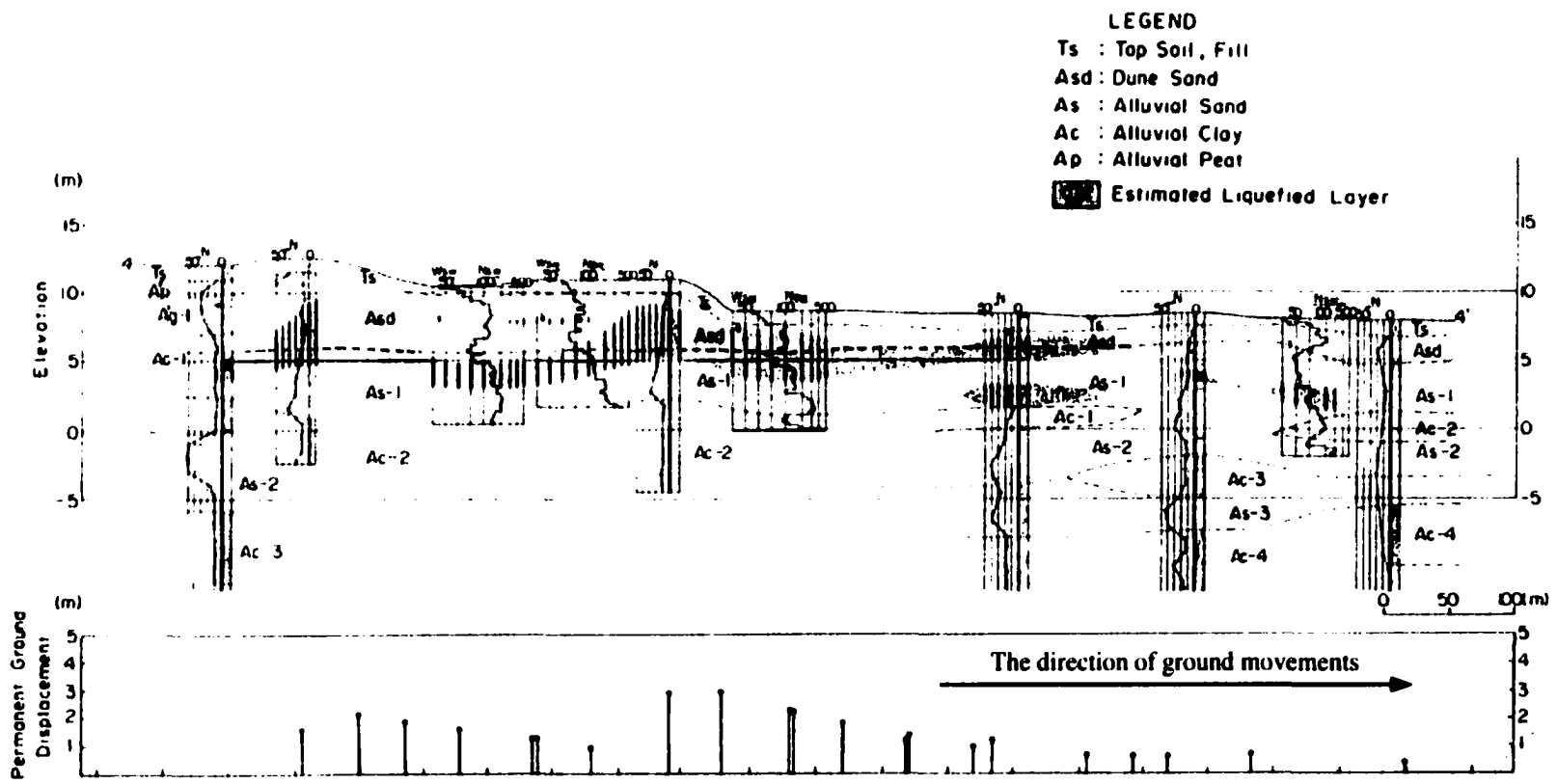


Figure 7.2 Lateral displacement patterns observed in a gently sloping ground with various slopes in a case site under the 1983 Nihonkai-Chubu earthquake
 (modified from Hamada et al. (1986))

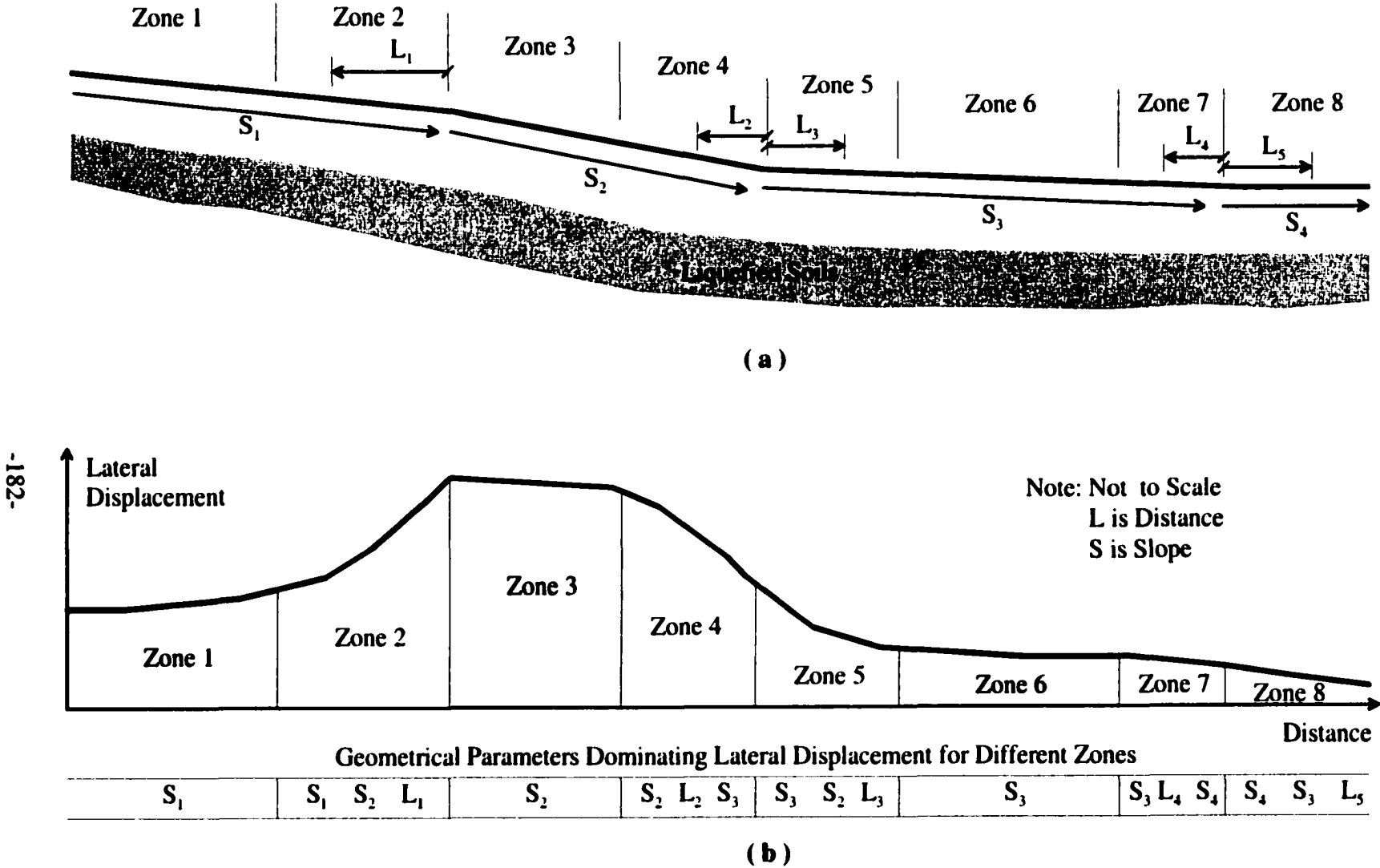


Figure 7.3 A sketch illustrating (a) geometric parameters and (b) lateral displacement patterns in a gently sloping ground

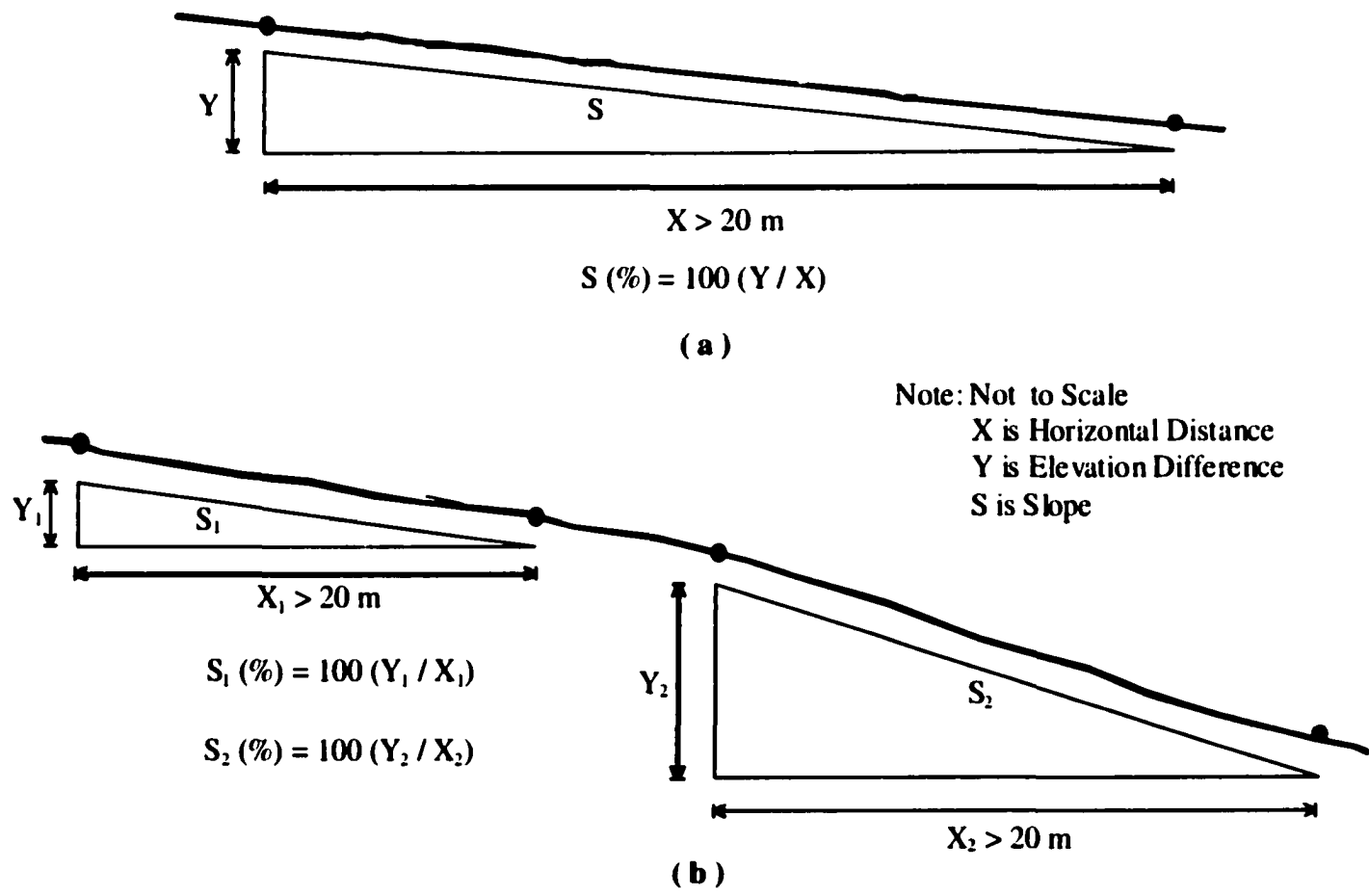


Figure 7.4 Definition of ground slope, S, in gentle slope ground: (a) single slope (b) multiple slopes

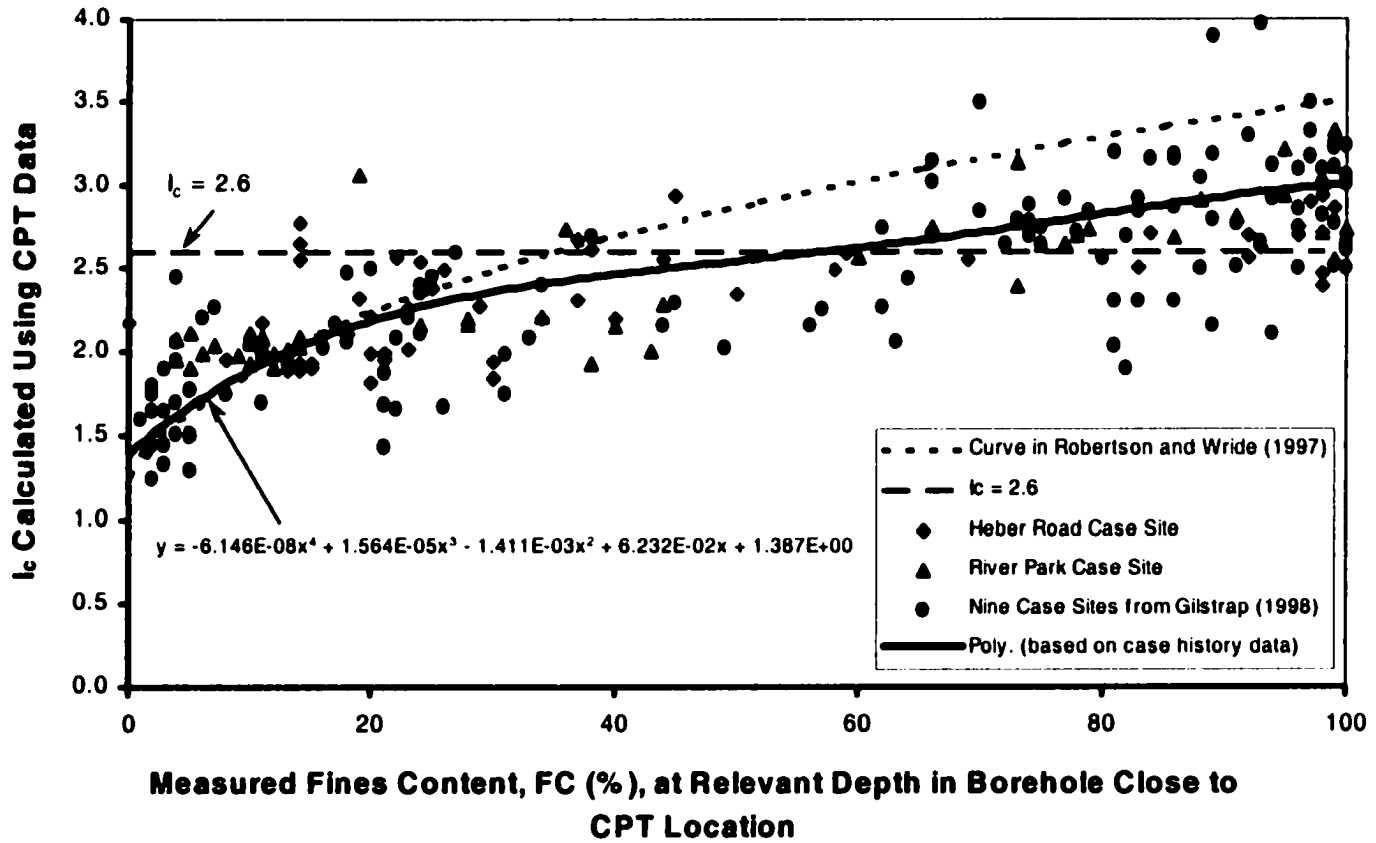


Figure 7.5 Relationship between the soil behaviour type index (I_c) calculated from CPT and fines content (FC)

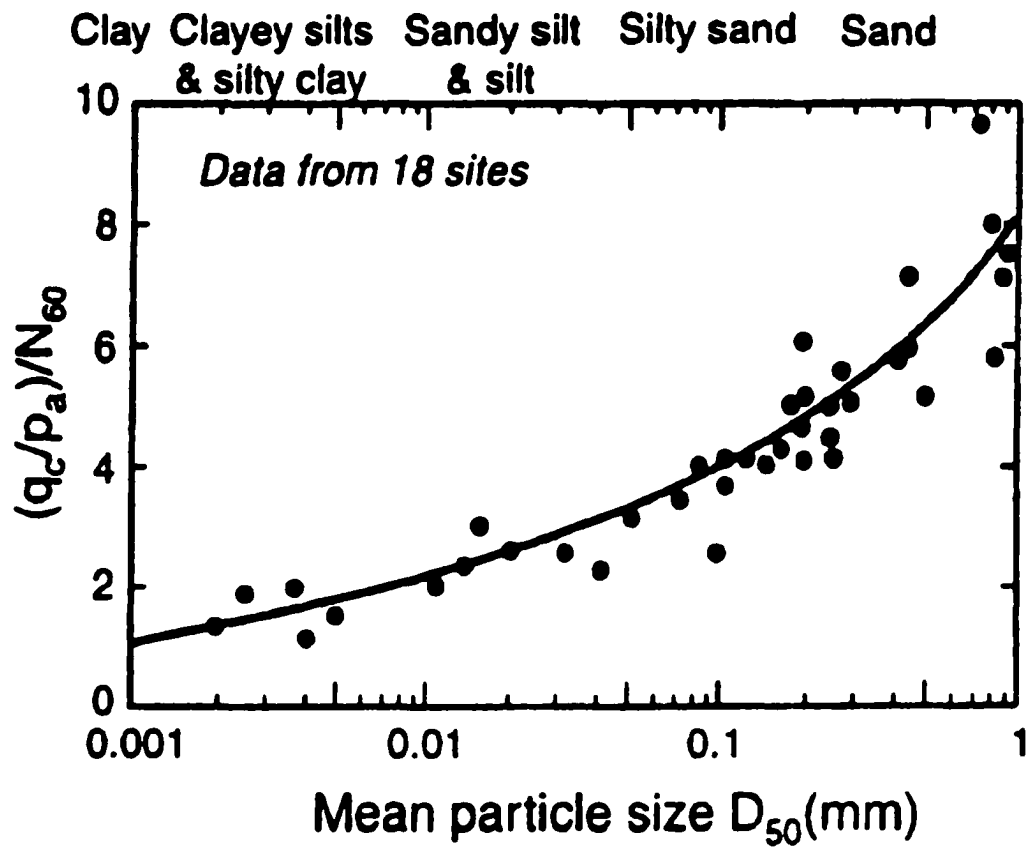


Figure 7.6 CPT - SPT correlations with mean grain size

(modified from Robertson et al. (1983))

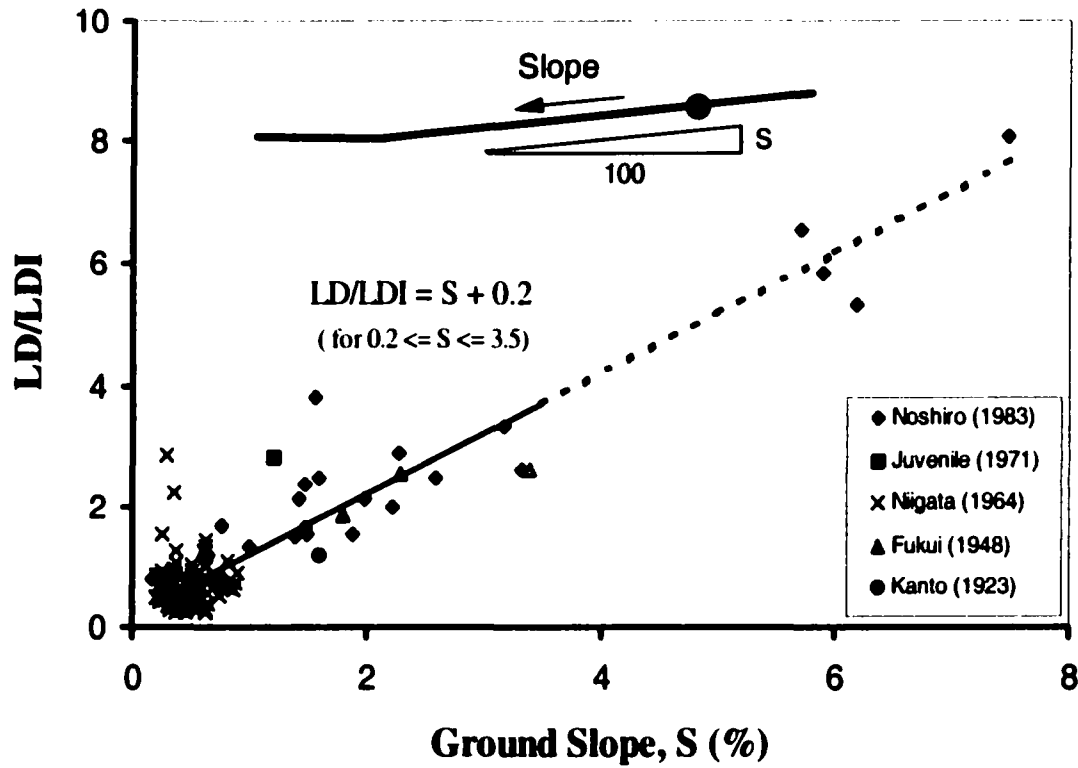


Figure 7.7 Relationship between the ratio of measured lateral displacement (LD) to lateral displacement index (LDI) and ground slope for the data of which the values of LDI were calculated using SPT data for five case histories for gently sloping ground without a free face

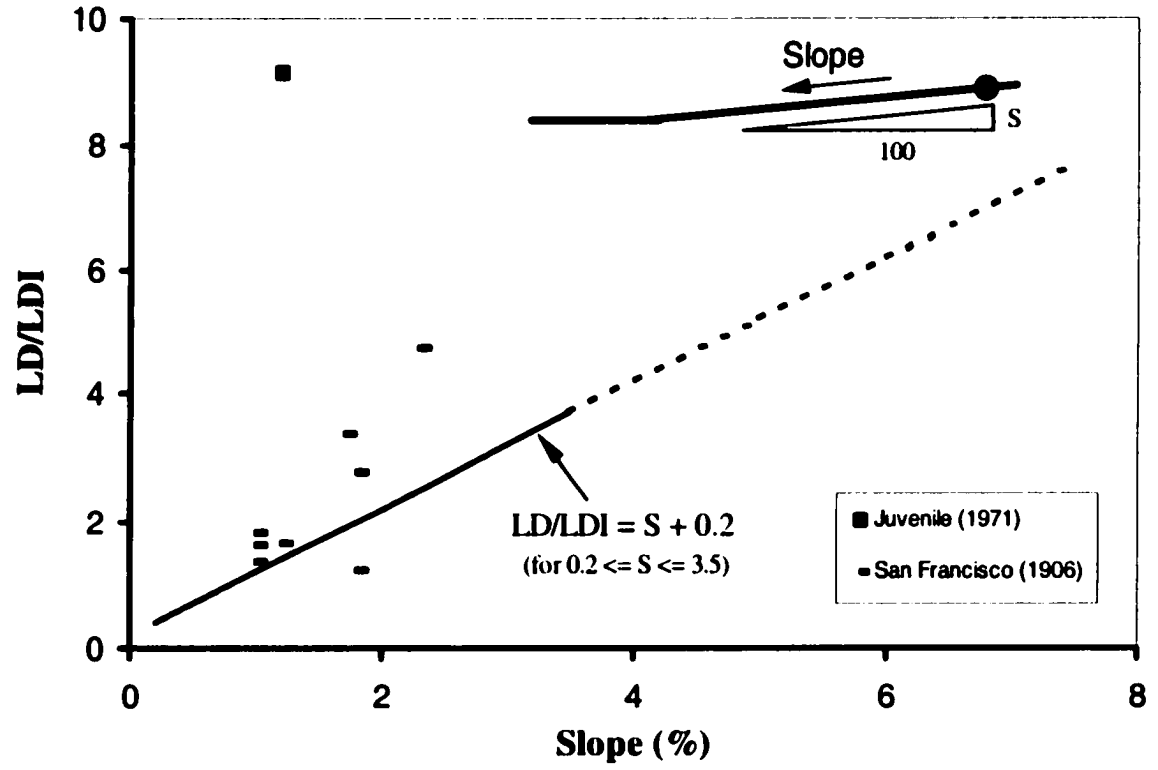


Figure 7.8 Relationship between the ratio of measured lateral displacement (LD) and lateral displacement index (LDI) and ground slope for the data of which the values of LDI were calculated using in-situ CPT data for two case histories for gently sloping ground without a free face

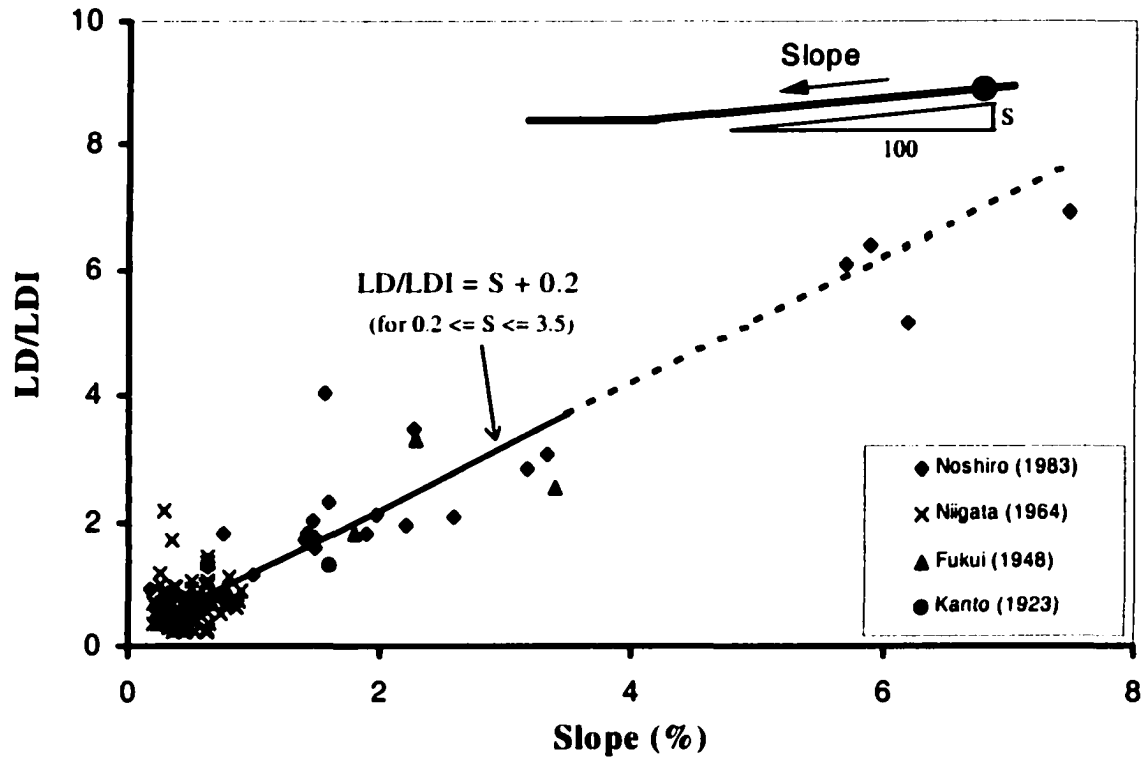


Figure 7.9 Relationship between the ratio of measured lateral displacement (LD) and lateral displacement index (LDI) and ground slope for the data of which the values of LDI were calculated using the equivalent CPT data that were converted from SPT data for four case histories for gently sloping ground without a free face

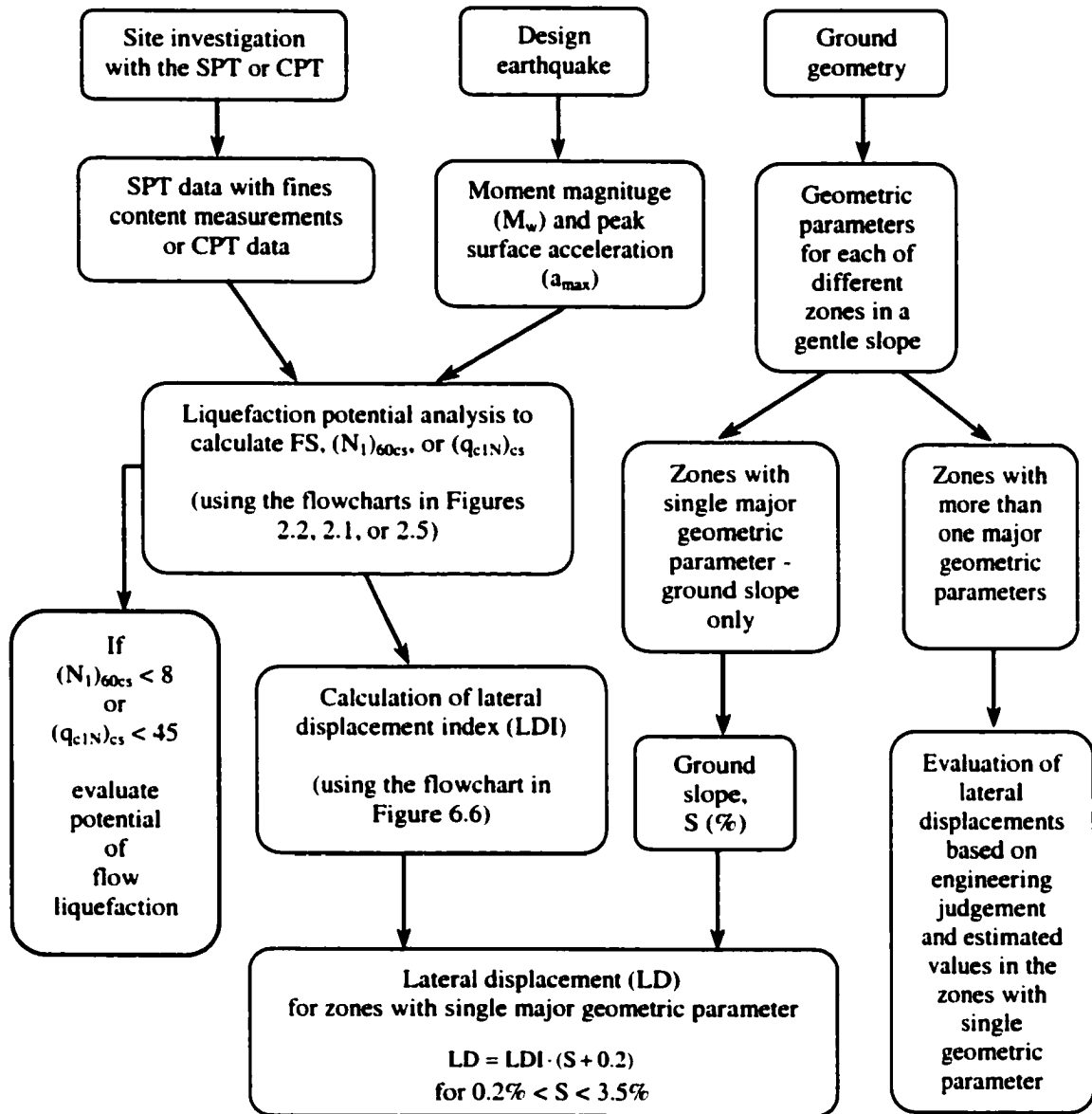


Figure 7.10 A flow chart illustrating the application of the proposed approach to estimate lateral displacements in a liquefaction-induced lateral spread for gently sloping ground without a free face using SPT or CPT data

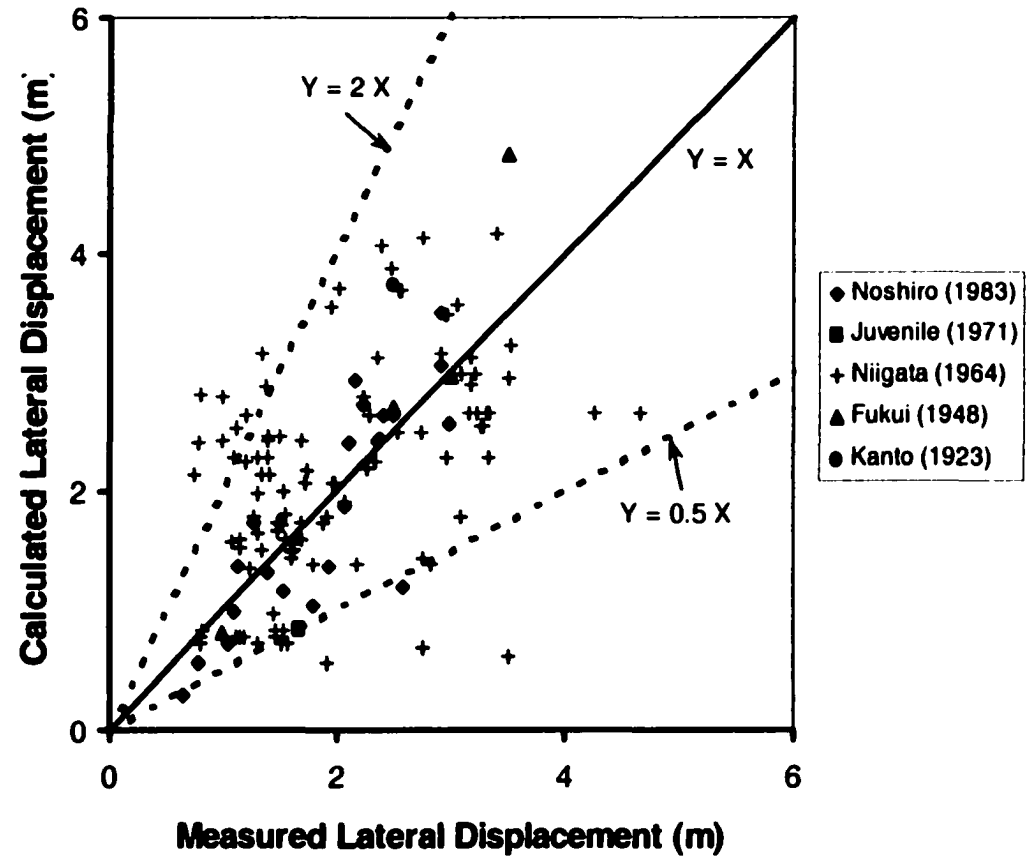


Figure 7.11 Comparison of the values of lateral displacements measured at sites for the five case histories and calculated using the proposed approach with SPT data for gently sloping ground without a free face

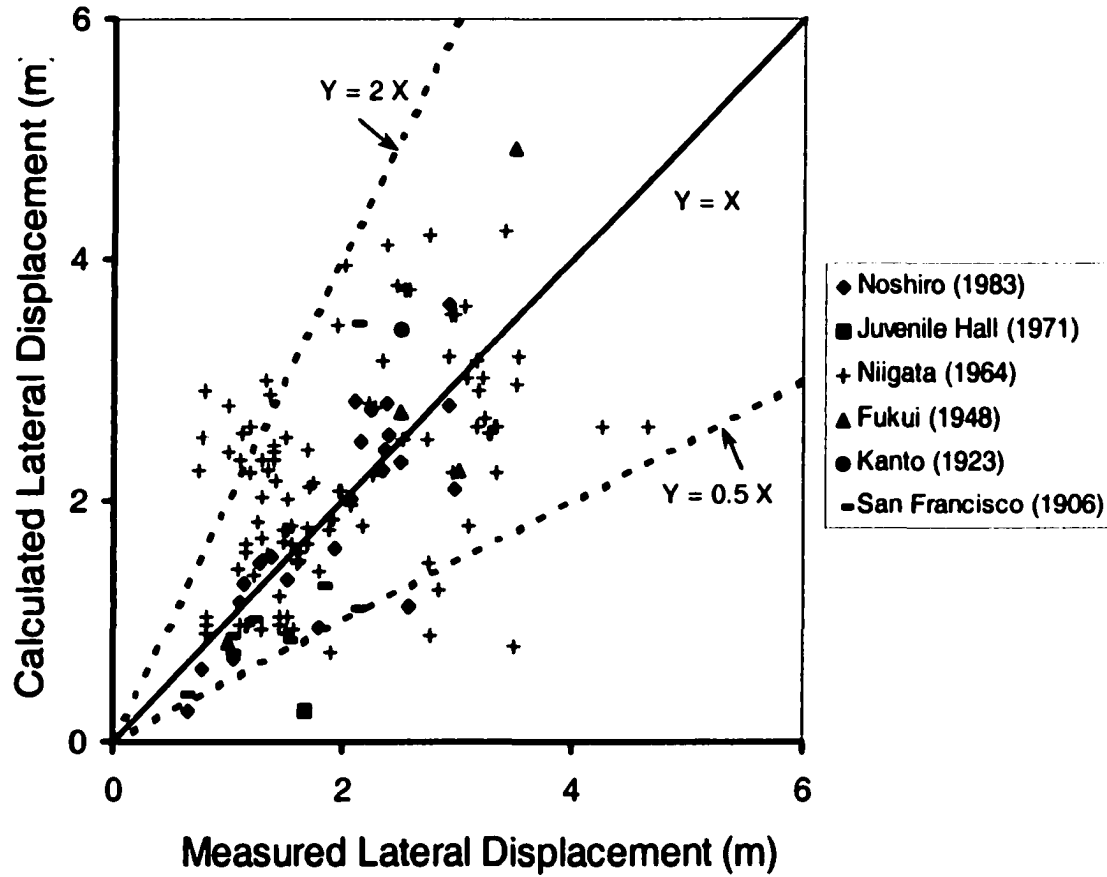


Figure 7.12 Comparison of the values of lateral displacements measured at sites for six case histories and calculated by the proposed approach using in-situ or equivalent CPT data for gently sloping ground without a free face

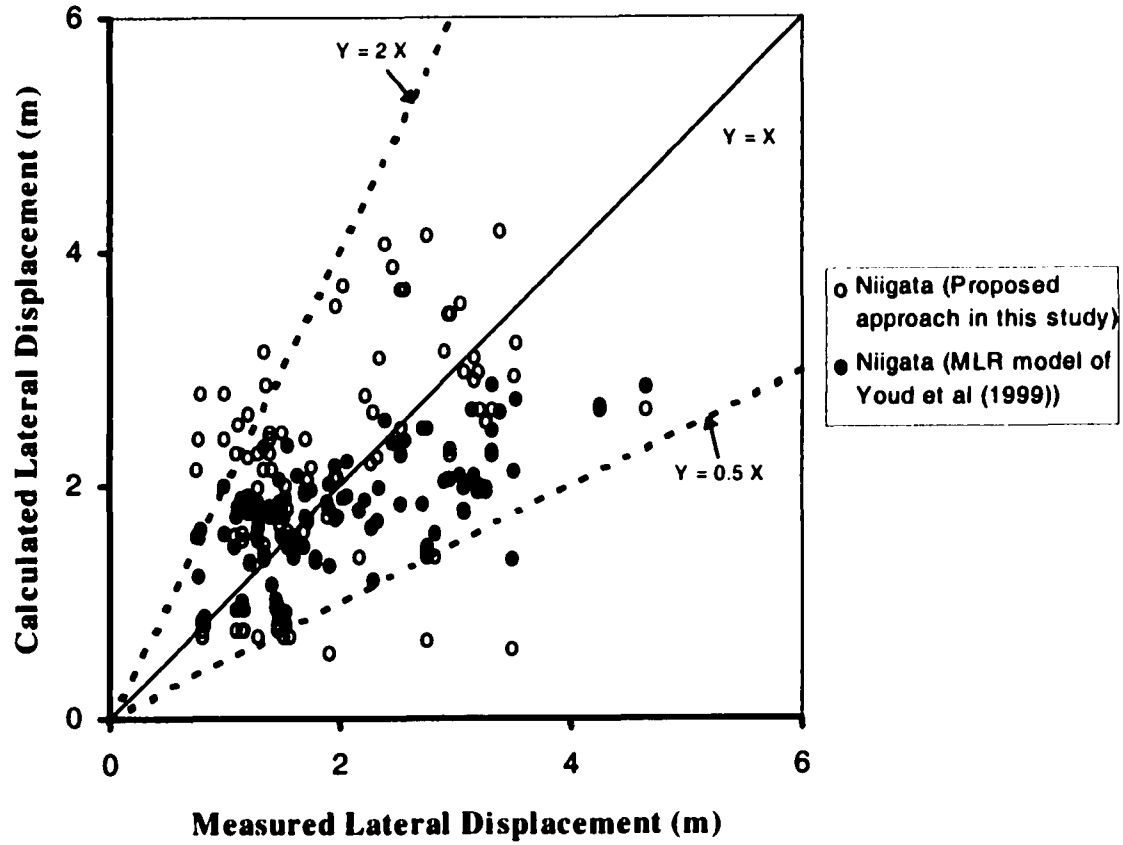


Figure 7.13 Comparison of lateral displacements measured at sites for the Niigata case history and calculated by the proposed approach and by the MLR model of Youd et al. (1999) for gently sloping ground without a free face

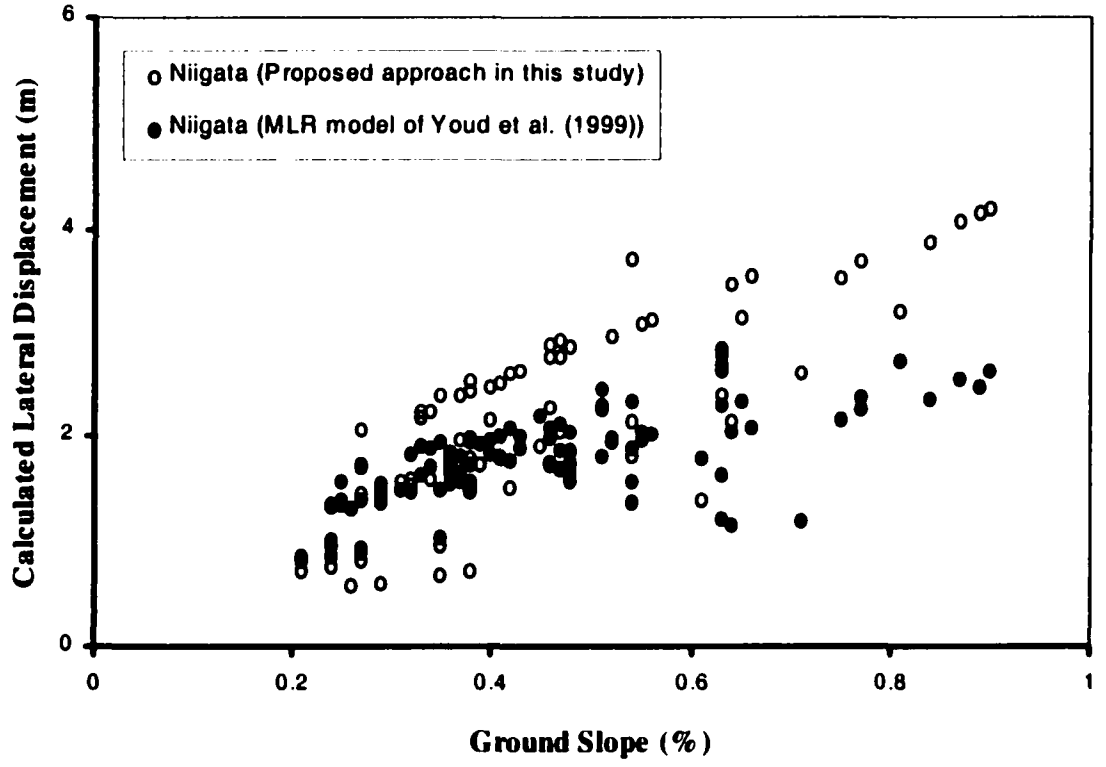


Figure 7.14 Comparison of lateral displacements calculated by the proposed approach and by the MLR model of Youd et al. (1999) for different ground slope for the Niigata case history for gently sloping ground without a free face

CHAPTER 8 ESTIMATION OF LIQUEFACTION-INDUCED LATERAL DISPLACEMENTS FOR LEVEL GROUND WITH A FREE FACE USING SPT OR CPT DATA

8.1 Introduction

Generally, liquefaction-induced lateral spreads occur on ground with two distinct types of ground geometry: 1) gently sloping ground without a free face; 2) level or gently sloping ground with a free face. An approach to estimate lateral displacements in a liquefaction-induced lateral spread using SPT or CPT data for gently sloping ground without a free face has been developed in Chapter 7. In this chapter, based on procedures similar to those in Chapter 7, an approach is developed for estimating lateral displacements in a liquefaction-induced lateral spread using SPT or CPT data for nearly level ground with a free face. Lateral spreads in gently sloping ground with a free face will be investigated in next chapter.

Perfectly level ground rarely exists in the field. Therefore, the ground with a slope of less than 0.15% is defined as a “level” ground in this study.

8.2 Geometric Parameters for Level Ground with A Free Face

8.2.1 Lateral displacement patterns in level ground with a free face

Bartlett (1991) observed from case history studies that lateral spread displacement markedly increased with the proximity of a free face and decayed logarithmically with

increasing distance from the free face for ground with a free face. He also observed that lateral spread displacement increased with increasing the height of a free face. Similar trends were observed in the Kobe Port areas during the 1995 Hyogoken-Nambu earthquake (Ishihara et al. 1996).

Figure 8.1 is a sketch illustrating general lateral displacement patterns and major geometric parameters for three zones on level ground with a free face. As well as the height of a free face and the distance to a free face, other geometric parameters may also influence ground lateral displacements, especially in the zones close to a free face. For example, lateral displacements in the zones close to a free face (e.g., Zones 2 and 3 in Figure 8.1) may also be influenced by the slope of the free face.

Lateral variations in soil conditions in the ground may add more complexity to lateral displacement patterns in a lateral spread. Lateral displacement tends to be larger in a location with a larger lateral displacement index (LDI).

Furthermore, both the patterns and magnitude of lateral displacements may be altered dramatically if engineered structures, such as retaining walls, bridge piers, quay walls, and so on, within or supporting the ground are present. Generally, these structures may restrain lateral movement of the ground.

8.2.2 Selection of a major geometric parameter for level ground with a free face

As shown in Figure 8.1, several different geometric parameters may influence lateral displacements in some zones for level ground with a free face. In this chapter, studies are focused only on the zones where lateral displacements are primarily associated with two geometric parameters – free face height (H) and the distance to a free face (L) – such as Zone 1 in Figure 8.1.

Generally, lateral displacements increase with decreasing L and increasing H . Bartlett and Youd (1995) and Youd et al. (1999) used the H/L ratio to characterize ground

geometry for ground with a free face in developing their empirical models to estimate lateral displacements on the basis of case history data. They found that the H/L ratio had a good correlation with the magnitude of lateral displacements in the zone where H/L was equal to or less than 20% for ground with a free face. For simplicity, similar to Bartlett and Youd' approach, the L/H ratio is used to characterize ground geometry in the zone where L/H is equal to or greater than 5 for level ground with a free face in this study.

The definition of free face height and distance to a free face is illustrated in Figure 8.2. H is the elevation difference between the surface of level ground and the toe of a free face. L is the horizontal distance from the toe of a free face.

8.3 Case Histories

The collection of case history data from past major earthquakes has been introduced in Section 7.3.1. In this chapter, six case histories associated with six different past earthquakes for nearly level ground with a free face are studied. A summary of the major parameters for these case histories is provided in Table 8.1. Of the six case histories, SPT data were available for five of the cases, and CPT soundings were available only for the Moss Landing case history. A brief introduction to each of the case histories is given below.

8.3.1 Portage Creek #1 and Twenty Mile River case sites, Alaska during the 1964 Alaska, Earthquake

The March 27, 1964 Alaska earthquake was one of the most powerful earthquakes in the last century (Bartlett and Youd 1992). A moment magnitude of 9.2 was assigned to the earthquake (Hansen et al. 1966; Kanamori 1978). The epicenter was located in the northern end of Prince William Sound about 130km east-southeast of Anchorage (McCulloch and Bonilla 1970).

Liquefaction-induced lateral spreads caused extensive damage to highway and railroad bridges within a 130 km radius of the zone of energy release during the earthquake (Bartlett and Youd 1992). McCulloch and Bonilla (1970) investigated the effects of the 1964 Alaska earthquake on the Alaska railroad, focusing mainly on the damage caused by lateral spreads. Bartlett and Youd (1992) made further detailed studies on some of the lateral spreads that caused damage to railroad and highway bridges on several rivers. The two case sites that had a ground surface with a slope of less than 0.15%, Portage Creek #1 and Twenty Mile River, were studied in this chapter.

Common features for these two sites were that 1) large cracks were observed within the abutment embankments of the bridges due to lateral spreads; 2) only one measurement of lateral displacements for each case site was conducted at a location close to a free face. The soil profile for Portage Creek #1 consisted of a silty, sandy, gravelly fill (upper 2.5 m), a sandy silt (from 2.5 m to 8 m), dense silty sand and sandy gravel (from 8 m to 21 m). The soils at the Twenty Mile River site consisted of layers of gravel, silty gravel, and sand and the grain size became finer and less gravelly with depth. Detailed descriptions of these sites were given in McCulloch and Bonilla (1970) and Bartlett and Youd (1992).

8.3.2 Case sites in Niigata City during the 1964 Niigata, Japan, Earthquake

The 1964 Niigata earthquake was briefly introduced in Section 7.3.5. Liquefaction-induced lateral spreads were observed in both ground with a free face and ground with a very gentle slope in Niigata City during this earthquake. The case sites with gentle surface slopes (with absence of a free face) were investigated in Chapter 7. The case sites with a free face and a ground slope of less than 0.15% will be studied in this chapter.

Generally, the soils down to about 20 m from the surface were relatively clean, fine or medium sands in Niigata City. The estimated thicknesses of the liquefied layers ranged from 0.6 m to 18.1 m (average 11.0 m) for the sites with a free face and a ground slope of less than 0.15%.

Bartlett (1991) compiled a comprehensive database for the case sites in Niigata City, as discussed in Section 7.3.5. Partial data from Bartlett's database were adopted for this study. The distance from the closest location of the SPTs to the location of the lateral displacement measurement was more than 100 m for some case sites in Bartlett's database for the Niigata case history. To avoid potentially incorrect interpretations of ground conditions for these sites, the data for these sites were not adopted in this study. Finally, a total of 69 sets of data from Niigata City were collected, and a total of 29 SPTs associated with the lateral displacement measurements were used for the study in this chapter.

Bartlett (1991) found that ground displacements near the bridge abutments in Niigata City during the 1964 Niigata earthquake appeared to have been impeded by the structures. For example, the displacement vectors near the north abutment of the Echigo railroad in Niigata City suddenly decreased from approximately 8 m to 3 m. Therefore, in order to minimize the variability of lateral displacement due to bridge interference, Bartlett did not compile displacement vectors found within 50 m of the bridges.

The measured lateral displacements varied from 0.4 m at a location about 200 m away from the river bank (as a free face) of the Shinano River to a maximum of up to 10.0 m at a location close the river bank for the data used in this study. The lateral displacements were measured using pre- and post-earthquake aerial photographs, and the accuracy of the measurements was estimated to be ± 0.72 m for the Niigata case history (Hamada 1992a). The free face heights for the case sites in Niigata City were between 4.9 m and 5.2 m. In addition, a peak surface acceleration of 0.19 g was reported by Kawasumi (1968) and Bartlett (1991), and the value was used for all the sites in Niigata City in this research.

Most of the revetments along the Shinano River, which were built of steel sheet piles and wooden piles, collapsed during the earthquake (Hamada 1992a). Therefore, it is believed that these revetments did little to restrict the lateral movements of the soils behind them. This may be one of reasons that extensive lateral spreads with large lateral displacements

occurred along the river bank of Shinano River in Niigata City during the earthquake.

8.3.3 The Jensen Filtration Plant case site, San Fernando during the 1971 San Fernando, California, Earthquake

A brief introduction to the 1971 San Fernando earthquake has been given in Section 7.3.6. Substantial damage was caused by liquefaction-induced lateral spreads in the area of the Upper Van Norman Reservoir during this earthquake (O'Rourke et al. 1992b). The Jensen Filtration Plant was one of major sites associated with the liquefaction-induced lateral spreads in the ground with a free face in the area and is studied in this chapter.

O'Rourke et al. (1992b) conducted detailed investigations of the Jensen Filtration Plant case site and compiled available site investigation reports. They reported six detailed cross-sections with shown SPT N values for the site. The results of a total of 27 SPTs were collected from their report for this site, and they were used in this study.

The soil profiles at the site consisted of three types of deposits: top artificial sand fill, alluvium, and weathered to intact sandstone of the Saugus Formation. The thickness of the artificial sand fill varied from zero on the west side of the site to 17 m on the east and was about 10 m to 15 m in the areas where lateral displacements occurred during the earthquake. The sand fill was generally above the ground water table. The thickness of the alluvium layer beneath the sand fill ranged from about 1.0 m to 10.0 m. A partial layer of the alluvium was liquefied during the earthquake as estimated from liquefaction potential analysis. The fines content in the alluvium layer typically varied from 32% to 62%, with an average of 47%. The average fines content of 47% was assigned to the alluvium in this study because of the lack of detailed measured fines content data with the SPT.

The site was not level and has two distinct plateaus with elevation difference of about 4 m to 6 m on the south part of the site. The free face heights in this site were relatively high and varied from about 10 m on the south part of the site to 17 m on the north part.

Lateral displacements were measured using pre- and post-earthquake aerial photos, and the accuracy of the measured horizontal displacements was about ± 0.47 m (O'Rourke et al. 1992b). Lateral displacements up to 3.0 m were observed at locations close to the free face. The lateral movements of the ground were observed as far as 400 m from the free face. The 16 lateral displacement measurements in the middle part of the lateral spread at the site were collected in this study.

8.3.4 Case sites in Moss Landing, California during the 1989 Loma Prieta, California, Earthquake

The Loma Prieta earthquake, with an epicenter near Loma Prieta Mountain in the Santa Cruz Mountains, California, occurred on October 17, 1989 at 5:04 p.m. Pacific Standard Time (O'Rourke and Pease 1992) and registered a moment magnitude of 7.0 (Boulanger et al. 1995). Liquefaction-induced deformations during this earthquake caused a lot of damage over an extensive area ranging from very near the epicenter to more than 100 km away. Extensive liquefaction-induced lateral spreads were observed in some areas of Moss Landing located on Monterey Bay about 21 km from the epicenter of the earthquake. Case sites in Moss Landing were investigated in this study.

Boulanger et al. (1995, 1997) and Mejia (1998) conducted investigations of the liquefaction-induced lateral spreads that occurred in Moss Landing during the 1989 Loma Prieta earthquake. Field investigation methods included SPT, CPT, and shear-wave velocity measurements. A total of 13 CPT soundings from these investigations were used in this study.

The soil profiles varied from site to site at Moss Landing due to their various depositional histories. Generally, the top layer of the soil, varying from 4.0 m to 10.0 m in thickness, was fairly clean dune or beach sand deposits. The soils under the sand deposits were interlayered sand, silty sand, gravelly sand, silty clay, and clay. Liquefaction in the Moss Landing area during the Loma Prieta earthquake appeared to have occurred primarily in

recent deposits at depths less than about 12 m (Boulanger et al. 1997).

Although lateral displacements of up to 1.5 m were observed in some sites at Moss Landing, the majority of lateral displacement measurements were less than half a meter. The major feature for the Moss Landing case history was that the lateral displacements at the three sites in Moss Landing were measured by three slope inclinometers that were installed at the sites prior to the 1989 Loma Prieta earthquake (Boulanger et al. 1997). However, all the three inclinometers were installed at the top edge of a steep riverbank (as a free face), i.e. very close to a free face. Furthermore, the measured lateral displacements in these three sites were relatively small and ranged from 8 cm to 28 cm.

A total of 10 lateral displacement measurements were collected at the sites for Moss Landing in this research. The free face heights for these sites ranged from 2.0 to 6.0 m. The peak surface acceleration at Moss Landing during the earthquake was estimated at about 0.25 g by Boulanger et al. (1995), and this value was used in this study.

8.3.5 Case sites in Dagupan City, Philippines during the 1990 Luzon, Philippines, Earthquake

An earthquake with a moment magnitude of 7.6 occurred in the town of Rizai on Luzon Island in the Philippines at 4:26 local time on July 16, 1990 (Wakamatsu et al. 1992). Low-lying areas in Central Luzon suffered greatly from liquefaction-related effects. Most liquefaction-induced lateral spreads were concentrated in Dagupan City, and they were studied in this chapter.

The city of Dagupan was located on the southern shores of the Lingayen Gulf, about 90 km from the epicenter of the 1990 Luzon earthquake. Large liquefaction-induced lateral displacements of up to 6.0 m were observed at sites along the riverbanks in Dagupan City. Wakamatsu et al. (1992) as well as Ishihara et al. (1993) and Tokimatsu et al. (1994) conducted detailed investigations with the available SPT results from the sites.

The soil profiles in most parts of the studied sites consisted of man-made sandy fills and/or alluvial deposits of sandy soil that overlie a clay layer at a depth below 10 - 15 m. The ground water table was very shallow, being about 0.5 to 1.0 m below the ground surface during the earthquake. The estimated thickness of the liquefied layers in the sites was about 5 to 8 m.

A total of eight lateral displacement measurements associated with three SPTs were collected for this case history. The free face heights varied from 4.0 m to 11.5 m for the sites. The peak surface acceleration for the sites during the earthquake was estimated at about 0.20 g by Ishihara et al. (1993), and this value was used in this study.

8.3.6 Case sites around the Kobe Port during the 1995 Hyogoken-Nanbu (Kobe), Japan, Earthquake

At 5:46 a.m. (local time) on January 17, 1995, the Hyogoken-Nanbu (Kobe) earthquake, with an epicenter at the northern part of Awaji island, occurred in Japan (Kimura 1996). The moment magnitude of the earthquake was estimated at 6.9 by Ejiri et al. (1996). The earthquake caused severe and widespread liquefaction of the soils in reclaimed lands as well as two manmade islands (Port and Rokko Islands) in the areas around the Kobe Port. As a result, large liquefaction-induced ground displacements occurred and caused severe damage to quays, bridges, foundations of buildings, and buried lifeline facilities.

Hamada et al. (1995) conducted a survey of the liquefaction-induced ground displacements in the reclaimed areas, including two artificial islands, around the Kobe Port, by using pre- and post-earthquake aerial photographs. In addition, they also investigated the soil conditions in the liquefied areas by collecting the extensive existing borehole data with SPT results. In this study, lateral displacement measurements and soil conditions for the sites around the Kobe Port were mainly based on Hamada et al.'s (1995) report.

A number of lateral displacement measurements were conducted by Hamada et al. (1995)

using pre- and post-earthquake aerial photographs. The accuracy of the measurements was about ± 0.33 m horizontally. Up to 5.0 m of lateral displacements were observed on the ground close to the quay walls. A total of 72 lateral displacement measurements that were typical for the studied sections and the relevant results of 18 SPTs were collected from their report and used in this study.

The deposits in the reclaimed areas were essentially fill overlying soft Holocene marine clay, which, in turn, rested on a series of Pleistocene deposits: alternate layers of dense sand and stiff clays. The thickness of the fill in the areas varied from 5 m to 25 m, being about 15 m on average. The fill was mainly sand and gravel, with some clay containing boulders. It is believed that partial or whole fill layers were liquefied during the earthquake. The thickness of the liquefied layers ranged from about 10 m to 16 m, as estimated by using the SPT data in this study. The ground water table was about 2.0 to 4.0 m from the ground surface at the sites.

A unique feature for these studied sites was that the ground along the shore line (as a free face) in the reclaimed areas was fully supported by caisson type quay walls that usually had a typical cross-section of about 15 m in height and 10 m in width. During the earthquake, the majority of the quay walls moved laterally as well as tilted towards the sea. However, none of them were turned over, and all of them still provided firm lateral support to the soil behind them after the earthquake.

The distance from the Kobe Port to the epicenter of the earthquake was about 17 km. The recorded peak ground acceleration at the Kobe Port during the earthquake was 0.54 g in the horizontal direction (Inagaki et al. 1996), and this value was used in this study.

8.4 Establishment of the Correlation between LD, LDI, and L/H Using SPT or CPT Data

The three major components controlling the magnitude of liquefaction-induced lateral

displacements are the maximum shear strains in liquefied layers, the thickness of liquefied layers, and the geometric parameters at a studied site, as discussed in Sections 4.2 and 6.1. The thickness of liquefied layers and the maximum shear strains in liquefied layers have been incorporated into one parameter – the lateral displacement index (LDI), as introduced in Section 6.3. The two major geometric parameters for level ground with a free face are free face height (H) and the distance to a free face (L), and the ratio L/H has been adopted as an integrated geometric parameter for level ground with a free face in this study, as discussed in Section 8.2. Therefore, it appears that the LDI and L/H are two key parameters controlling the magnitude of liquefaction-induced lateral displacements (LD). This means that a general correlation may exist between LD, LDI, and L/H. Case history data concerning lateral spreads that occurred during past major earthquakes provide a good opportunity to establish this correlation. In this study, following the procedures illustrated in Figure 8.3, the correlation is established on the basis of case history data.

8.4.1 Development of the correlation between LD, LDI, and L/H using SPT data

SPT data were available for five of the six case histories studied in this chapter. Different from the other four case histories with available SPT data, ground lateral displacements for the Kobe Port case history were significantly influenced by quay walls. Therefore, the data from the Kobe Port case history were not used in developing the correlation between LD, LDI, and L/H.

For each of the four case histories with SPT data, the NCEER SPT-based method was first applied to evaluate the liquefaction potential. The LDI was then calculated for each of the cases. An average value of the calculated LDIs was used as the final LDI value that is associated with the relevant lateral displacement measurement if more than one SPT profile was available at the locations close to the position where the relevant lateral displacement was measured. Finally, a database with a total of 95 data sets from the four case histories was established, as listed in Table A2 in Appendix A.

For simplicity, if the actual lateral displacement is assumed to be linearly proportional to LDI for a given L/H, the ratio of LD to LDI will then depend solely on L/H. Based on this concept, the case history data were used to develop an empirical correlation between LD/LDI and L/H.

Figure 8.4 is a plot of LD/LDI vs. L/H for the data of which the values of LDI were calculated using SPT data for the available four case histories. The data in Figure 8.4 are predominantly from the 1964 Niigata case history; however, the results from the other three case histories generally follow the same trend. Although there is considerable scatter, Figure 8.4 shows a definite trend of decreasing LD/LDI with increasing L/H for L/H greater than 5. A general trend line for all the data in Figure 8.4 is given by:

$$[8.1] \quad \frac{LD}{LDI} = 5 \cdot \left(\frac{L}{H} \right)^{-0.7} \quad (\text{for } 5 < L/H < 40)$$

where LD is the actual lateral displacement, LDI is the lateral displacement index, H is free face height, and L is the horizontal distance to the toe of a free face. This relationship is applicable only for the range of earthquake properties and ground conditions listed in Table 8.1.

8.4.2 Development of the correlation between LDI, LD, and L/H using CPT data

Even though Equation [8.1] was developed using the NCEER SPT-based method and SPT data, logically, the equation may be in-situ-test independent if Equation [8.1] correctly characterizes the relationship between LD/LDI and the geometric parameters – L and H – for level ground with a free face. In the development of Equation [8.1], only LDI was calculated using the NCEER SPT-based method and SPT data. The LDI is a value calculated by integrating the calculated γ_{\max} with depth for a given location and a given earthquake. The γ_{\max} is a parameter characterizing the shear strain potential of a given soil during a given earthquake. Therefore, both γ_{\max} and LDI depend on soil profile and properties, and the characteristics of an earthquake only. The NCEER SPT-based

method and SPT data are used only to estimate the values of the γ_{\max} and LDI and are not essential for the calculation of the γ_{\max} and LDI. Other methods (e.g., the NCEER CPT-based method) for the liquefaction potential analysis of sandy soils may also be used to calculate the γ_{\max} and LDI using the relevant data (e.g., CPT data), provided that the calculated values of the γ_{\max} and LDI using all the methods are equivalent.

In order to evaluate this concept and to examine whether Equation [8.1] is still applicable to the case in which the LDI is calculated using the NCEER CPT-based method and CPT data, a database with a total of 105 sets of the data for the available five case histories was established, as listed in Table A2 in Appendix A. The LDI for each of the sites for the Moss Landing case history was directly calculated using in-situ CPT data. The LDI for each of the sites for the other four case histories (not including Kobe Port case history) was calculated using the equivalent CPT data that were converted from the SPT data using the procedures discussed in Section 7.4.

Figure 8.5 is a plot of LD/LDI versus L/H for the data from the Moss Landing case history. The values of the LDI in Figure 8.5 were calculated using the NCEER CPT-based method and in-situ CPT data. The curve in Figure 8.5 is a graphical expression of Equation [8.1] that was developed using the NCEER SPT-based method and SPT data. Figure 8.5 indicates that the data for the Moss Landing case history fit the curve well for L/H greater than 5.

Figure 8.6 is a plot of LD/LDI versus L/H for the four case histories in which only SPT data were available. The values of the LDI in Figure 8.6 were calculated using the NCEER CPT-based method and the equivalent CPT data that were converted from the SPT data. The curve that is a graphical expression of Equation [8.1] is also shown in Figure 8.6. Generally, the data also fit the curve well in Figure 8.6 for L/H greater than 5.

In summary, Figures 8.5 and 8.6 generally support the idea that Equation [8.1] is still applicable to characterize the correlation between LD/LDI and L/H for the case in which

the LDI is calculated using the NCEER CPT-based method and CPT data.

8.5 An Approach to Estimate Liquefaction-induced Lateral Displacements for Level Ground with a Free Face Using SPT or CPT Data

Preliminary studies of the available case histories generally support the assumption that the relationship between LD/LDI and L/H may be independent of either using SPT or CPT data and may be characterized by Equation [8.1]. Therefore, estimates of liquefaction-induced lateral displacements for nearly level ground with a free face using SPT or CPT data may be obtained by:

- Evaluating liquefaction potential using either the NCEER SPT- or CPT-based method;
- Calculating the lateral displacement index (LDI);
- Measuring free face height (H) and the distance to a free face (L);
- Estimating lateral displacement (LD) using Equation [8.2].

$$[8.2] \quad LD = 5 \cdot \left(\frac{L}{H} \right)^{-0.7} \cdot LDI \quad (\text{for } 5 < L/H < 40)$$

Figure 8.7 is a flowchart illustrating the major steps to apply the proposed approach for level ground with a free face. First, site investigation with the SPT or CPT, which must be tested at locations close to the position where the estimate of liquefaction-induced lateral displacements is needed, is conducted. The liquefaction potential of the studied site is evaluated using either the NCEER SPT- or CPT-based method with SPT or CPT data and earthquake parameters that are estimated based on a design earthquake at the site. The LDI for each studied location at the site can then be calculated. With the measured value of L and H, Equation [8.2] can be used to estimate lateral displacements at the studied locations.

The ratios of L to H for the proposed approach are not recommended beyond the range of

5 to 40. During the development of the correlation between LD/LDI and L/H based on the available five case histories, it was found that measured lateral displacements (LD) varied significantly for a given calculated lateral displacement index (LDI) when the L/H was less than 5. One major reason for this observation is that another geometric parameter, the slope of a free face, in addition to L and H, may influence the lateral displacements in the zone close to a free face, as discussed in Section 8.2. The possibility of local slump failure or flow failure also increases in the zone close to a free face with a steep slope due to the presence of high static shear stresses. Furthermore, as discussed in Section 2.3.3, the presence of relatively high static shear stresses in a soil within a zone close a steep free face may either increase or decrease the cyclic resistance of the soil depending upon its initial state (Vaid and Sivathayalan 2000). However, the simplified methods (including the NCEER SPT- or CPT-based method used in this research) for liquefaction potential analysis were developed for level or gently sloping ground and are not applicable to the ground with relatively high static shear stresses such as the zone close to a steep slope (or a steep free face). On the other hand, the ratios of L to H for all the case sites studied in this research are less than 40.

The proposed approach was developed using the data from only five case histories associated with five past major earthquakes and as such is applicable only for similar ground and earthquake conditions, as summarized in Table 8.1. The moment magnitudes for the five earthquakes ranged from 6.4 and 9.2, and the peak surface accelerations varied from 0.19 g to 0.55 g. Nevertheless, the 1971 San Fernando earthquake associated with the Jensen Filtration Plant case history was the only one with a moment magnitude (6.4) of less than 7.0. Therefore, the proposed approach may mainly be applicable to sites associated with an earthquake with an estimated moment magnitude of 7.0 or over. In addition, sixty-six percent of the case history data used in developing the proposed approach were from the Niigata case history in which soils thought to be liquefied were generally clean sands only.

The proposed approach may be used to estimate liquefaction-induced lateral displacements for nearly level ground with a free face for low to medium-risk projects or

to provide preliminary estimates for high-risk projects. However, engineering judgement must be exercised because liquefaction-induced ground lateral spreading is a complicated engineering phenomenon and a number of assumptions and simplifications were involved in developing the proposed approach.

8.6 Performance of the Proposed Approach

8.6.1 Accuracy of the proposed approach

The measured lateral displacements are compared with the calculated lateral displacements using the proposed approach with SPT data for L/H ranging from 5 to 40 for the available five case histories associated with the five different earthquakes studied in this chapter, as shown in Figure 8.8. All the points for the four case histories (Noshiro, Juvenile, Fukui, and Kanto) and 90% of the points for the Niigata case history in Figure 8.8 fall in the zone between the 50 percent under-prediction bound-line and 100 percent over-prediction bound line, as shown in Figure 8.8. Given the relatively poor accuracy (± 0.72 m) of the measured displacements for the Niigata case history, it is reasonable to expect that the accuracy of the calculated displacements for the Niigata case history is lower than that for other case histories.

Figure 8.9 compares the measured lateral displacements with the values calculated by the proposed approach using in-situ CPT data or the equivalent CPT data that were converted from SPT data for L/H ranging from 5 to 40 for the available six case histories associated with the six different earthquakes studied in this chapter. All the calculated displacement values for the five case histories (Noshiro, Juvenile Hall, Fukui, Kanto, and San Francisco) and 90% of the calculated displacement values for the Niigata case history are between 50% and 200% of the relevant measured values, as indicated in Figure 8.9.

Figures 8.8 and 8.9 show the likely variability of calculated displacements using the proposed approach with SPT or CPT data. Considerable scatter is evident as lateral

displacements could be either underestimated or overestimated by up to a factor of two based on the available data.

8.6.2 Comparison with the profile of field lateral displacements measured by inclinometers

The Moss Landing case history is the only case history where the profiles of field liquefaction-induced lateral displacements were measured by pre-installed inclinometers for level ground with a free face, as introduced in Section 8.3.4. The proposed approach in this chapter can be used to estimate both the magnitude and distribution with depth of lateral displacements in a liquefaction-induced lateral spread. This raises the question of how well the estimated magnitude and distribution with depth of lateral displacements at the three sites in Moss Landing match the actual measurements by the inclinometers. Unfortunately, these three case sites are not ideal for this kind of comparisons because of the following two major reasons.

- All the three inclinometers were installed at the top edge of a steep riverbank (as a free face) and the ratios (L/H) of the distance to a free face and free face height are less than 3. However, the recommended range for L/H is from 5 to 40 in the proposed approach. Hence, these records are outside the recommended range.
- The simplified procedure (including the NCEER CPT- or SPT-based method used in this research) for estimating liquefaction potential were developed based on the field performance data for level and gentle slopes where static shear stresses are relatively low. The presence of static shear stresses at a given confining stress may either increase or decrease the cyclic resistance of sand depending upon its initial state (Vaid and Sivathayalan 2000). A correction factor, K_α , was developed by Seed (1983) to extrapolate the simplified procedure to higher static shear stress conditions (such as steep slopes) than those embodied in the case history data set from which the simplified procedure was derived (Youd et al. 2001). However, the participants of NCEER (1997) and then Youd et al. (2001) concluded that a general recommendation for use of K_α is not advisable at present and the correction factor should not be used

by nonspecialists in geotechnical earthquake engineering or in routine engineering practice. As a result, the NCEER CPT- or SPT-based method should not be directly applied to the three sites at Moss Landing because of the presence of high static shear stresses.

For illustration purposes only, the calculated lateral displacement with depth that were estimated by the proposed approach using CPT data from CPT UC-4 that was close to the inclinometer SI-2 installed at one location in Moss Landing is shown in Figure 8.10 and compared with the measured lateral displacement profile. As expected, the estimated values are not consistent with the measured ones. Similar comparisons for the other two locations of Moss Landing were also conducted. The detailed results for all the three locations are listed in Appendix B of this thesis.

In addition to the two major reasons mentioned above, several other factors may also contribute to this disagreement. As discussed in Section 6.4, several factors may affect the calculation of the lateral displacement index when the NCEER CPT-based method is used, including the effects of thin sandy soil layers, correction factor K_c or/and a cutoff line of I_c equal to 2.6. For example, the soil layer in the depth range of between 5 m and 6 m shown in Figure 8.10 was estimated to be liquefied during the earthquake and it contributed to about one third of the estimated value of the lateral displacement index. However, from Figure 8.10c, one can see that this soil layer had I_c values very close to 2.6. In this condition, soil sampling is recommended to clarify the soil properties and to evaluate its liquefaction potential. As discussed in Section 4.6, the three-dimensional distribution of liquefied layers may also have an effect on the magnitude and distribution of liquefaction-induced lateral displacements. For instance, a deep liquefied soil layer may contribute less to the total lateral displacement than that for a shallow liquefied soil layer with the same value of calculated lateral displacement index because of the different effects of lateral confinement. More than half of the total estimated value of the lateral displacement index was contributed by the soil layer in the depth range of between 12 m and 13 m in Figure 8.10, but no measured lateral displacement occurred at this depth. Nevertheless, the effect of the three-dimensional distribution of liquefied layers

was not quantified at the current research. More studies are required in this field. If the zone of liquefaction at the depth range of 12 m to 13 m is removed from the profile shown in Figure 8.10h, the predicted profile is similar to that of the measured.

8.6.3 Comparison with the MLR model of Youd et al. (1999)

Similar to the procedures in Section 7.7.2, the proposed approach in this study is compared with the MLR model of Youd et al. (1999). To avoid compiling a new database of parameters for the MLR model of Youd et al. (1999), the estimates of lateral displacements obtained by the two methods were compared only for two (Alaska and Niigata) of the six case histories studied in this chapter.

A comparison of lateral displacements measured at sites for L/H ranging from 5 to 40 for the two case histories and calculated by both the proposed approach in this study and the MLR model of Youd et al. (1999) for level ground with a free face is shown in Figure 8.11. Figure 8.11 indicates that the calculated values for lateral displacements obtained by both the proposed approach and the MLR model of Youd et al. (1999) are generally between 50% and 200% of the relevant measured values for the Niigata and Alaska case histories. This preliminary comparison appears to indicate that the accuracy of the proposed approach may be similar to that of the MLR model of Youd et al. (1999) for estimating lateral displacements for the studied two case histories. Further evaluations using data from new case histories are definitely required to compare and evaluate the performance of both the proposed method and the MLR model before any solid conclusions can be made.

Figure 8.12 compares the lateral displacements calculated by using the proposed approach in this study and by using the MLR model of Youd et al. (1999) for L/H ranging from 5 to 40 for the Niigata and Alaska case histories. This comparison generally supports the observation that the estimates of lateral displacements obtained by both the methods are consistent for the two case histories and that the proposed approach predicts slightly larger values of lateral displacements than the MLR model of Youd et al.

(1999) when the values of L/H are between 5 and 10.

As discussed in Section 7.7.2, compared with the MLR model of Youd et al. (1999), the proposed method has two advantages. The first is that in addition to the variation of lateral displacement with distance from the free face, the distribution of lateral displacement with depth below the ground surface can also be estimated from the proposed method. The second advantage is that soil properties can be better characterized by the proposed approach than by the MLR model of Youd et al. (1999).

8.7 Lateral Spreads Restricted by Engineered Structures

In developing the proposed approach in this study, data from case history sites in the Kobe Port area during the 1995 Hyogoken-Nambu (Kobe) earthquake were not used. The main reason was that ground lateral displacements at the sites in the Kobe Port area were believed to be greatly restricted by caisson-type quay walls which supported the ground behind them and still provided support for the ground even after the earthquake. As a result, the actual lateral displacements in the ground were generally less than the expected values for the same ground conditions but without the quay walls.

Figure 8.13 is a plot of LD/LDI vs. L/H for the data for the Kobe Port case history. A trend of decreasing LD/LDI with increasing L/H can be seen from Figure 8.13 even though significant scatter of the data is evident. Nevertheless, the trend line for the data from the Kobe earthquake in Figure 8.13 is quite different from another trend line that is shown in the upper part of Figure 8.13. The latter of the two trend lines was developed in Section 8.4 using the data from the case history sites where engineered structures had little or no effect on the lateral displacements of the ground. Therefore, it is believed that the restriction of ground lateral movements by the gravity quay walls at the sites in the Kobe Port area may be one of major factors that contributed to the difference between these two trend lines in Figure 8.13. Fundamentally, due to the presence of the continuous rigid quay walls as a free face, the actual static shear stresses in the soils behind the walls may be significantly less than those for the ground with a same height of a free face but

without the walls. As a result, the equivalent free face height to that of the ground without the walls would be lower than the actual free face height for the Kobe Port case history. Other factors would also contribute to the difference in two trendlines in Figure 8.13. For example, the thickness of the estimated liquefied layers was about 10 m to 16 m thick. As discussed in Section 4.8.2, for a thick liquefied layer, the liquefaction of a lower sublayer may partially or fully isolate a upper sublayer from further seismic acceleration and therefore may limit resultant liquefaction-induced lateral displacements. Figure 4.14 has shown that a sudden drop of acceleration at the ground surface was recorded at Kobe Part Island during the 1995 Hyogoken-Nambu earthquake.

Other engineered structures (e.g., piles, pipelines, or piers) may also restrict ground lateral displacements and change lateral displacement patterns in a liquefaction-induced lateral spread. Bartlett (1991) also noted that ground displacements near the bridge abutments appeared to have been impeded by the piers and bridges for the areas along the Shinano River in Niigata City during the 1964 Niigata earthquake. For example, the displacement vectors near the north abutment of the Echigo railroad in Niigata City suddenly decreased from approximately 8 m at the location 50 m away from the bridge to 3 m in the vicinity of the bridge.

Soil improvements to limit or prevent liquefaction may significantly reduce liquefaction potential and, in turn, also reduce potential lateral displacements in the improved areas. Furthermore, lateral displacement magnitude and patterns in the non-improved areas that are adjacent to improved areas may be influenced as well by such soil improvements.

8.8 Discussion

As discussed in Section 7.8, compared with the other available empirical methods, the proposed method has two distinct advantages. The first is that in addition to the variation of lateral displacement with distance from the free face, the distribution of lateral displacement with depth below the ground surface can also be obtained from the

proposed method. This profile may be valuable for the design of underground structures (e.g., pipelines) and foundations (e.g., piles). The second advantage is that soil properties can be better characterized by the proposed approach.

As discussed in Section 8.7, engineered structures (e.g., quay walls, retaining walls, piles, tanks, or pipelines) may alter lateral displacements in a liquefaction-induced lateral spread. The proposed approach was developed using the data from case histories in which engineered structures had little or no effect on lateral spreads. It is expected that the proposed approach may over-estimate lateral displacements at sites where engineered structures pose significant restrictions to ground movements.

Caution should be exercised when a substantial zone of soils with a low $(N_1)_{60cs}$ or $(q_{c1N})_{cs}$ is encountered during liquefaction potential analysis. For such cases, more extensive investigation should be made and other approaches should be taken to evaluate the potential for flow failure of the soil, especially when the static shear stresses in the ground are relatively high. Deformations caused by flow failures can be much larger than those by lateral spreads, and their estimation is beyond the scope of this research.

The proposed approach characterizes the effects of soil profile and properties, earthquake characteristics, and ground geometry on liquefaction-induced lateral displacements. Other factors (such as the redistribution and drainage of excess pore pressures in the ground, acceleration isolation due to liquefaction of underlying soils, and three-dimensional distribution of liquefied layers) may also influence lateral displacements, as discussed in Sections 4.6, 4.7 and 4.8. These factors were not quantified in the current approach and would need to be evaluated on a case-by-case basis.

8.9 Conclusions

An approach to estimate liquefaction-induced lateral displacements using either SPT or CPT data for nearly level ground with a free face has been developed based on available

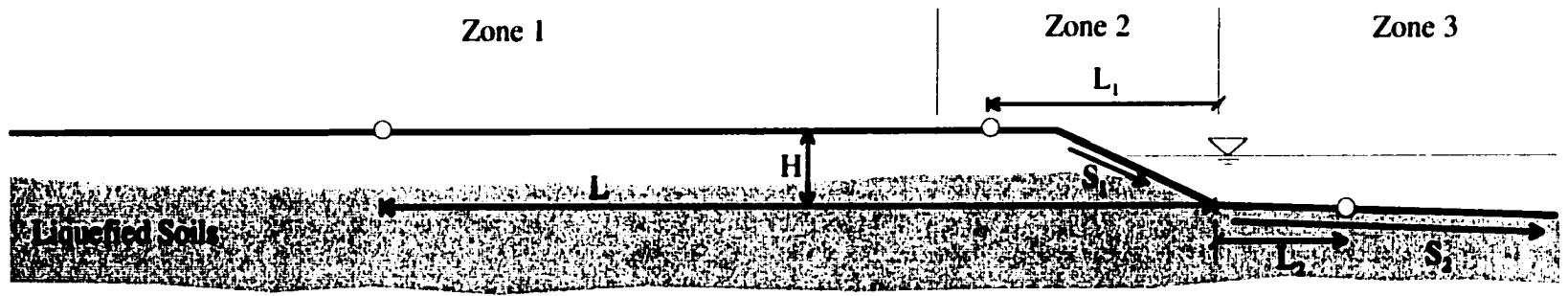
results from laboratory tests and data from case histories. The proposed approach captures the mechanisms of liquefaction-induced lateral spreads and characterizes the major factors influencing lateral displacements. The proposed approach can be used to obtain estimates of both the magnitude and distribution of liquefaction-induced lateral displacements for level ground with a free face for low to medium-risk projects or to provide preliminary estimates for high-risk projects. The proposed method can be easily applied with only a few additional calculations following the NCEER SPT- or CPT-based liquefaction-potential analysis.

Given the complexity of liquefaction-induced lateral spreads, considerable variations in magnitude and distribution of lateral displacements are expected. Generally, the calculated lateral displacements from the five available case histories studied in this chapter showed variations between 50% and 200% of measured values. The preliminary comparison based on data from two of the five case histories indicated that the accuracy of the proposed approach was similar to that of the MLR model of Youd et al. (1999) for estimating lateral displacements for the two studied case histories. However, further evaluations using data from new case histories are definitely required to compare and evaluate the performance of both the proposed method and the MLR model before any solid conclusions can be made. In addition, it is expected that the proposed approach may over-estimate lateral displacements at sites where engineered structures pose restrictions to ground movements.

The proposed approach was developed using the data from only five case histories associated with five past major earthquakes, especially about two thirds of the data were from the Niigata case history and as such is applicable only for similar earthquakes and ground conditions. The recommended range for the ratio of L to H is between 5 and 40 for the proposed approach. Additional data from new case histories are required to better quantify liquefaction-induced lateral spreads, to evaluate and update the proposed approach, and to expand the existing range for the ratio of L to H.

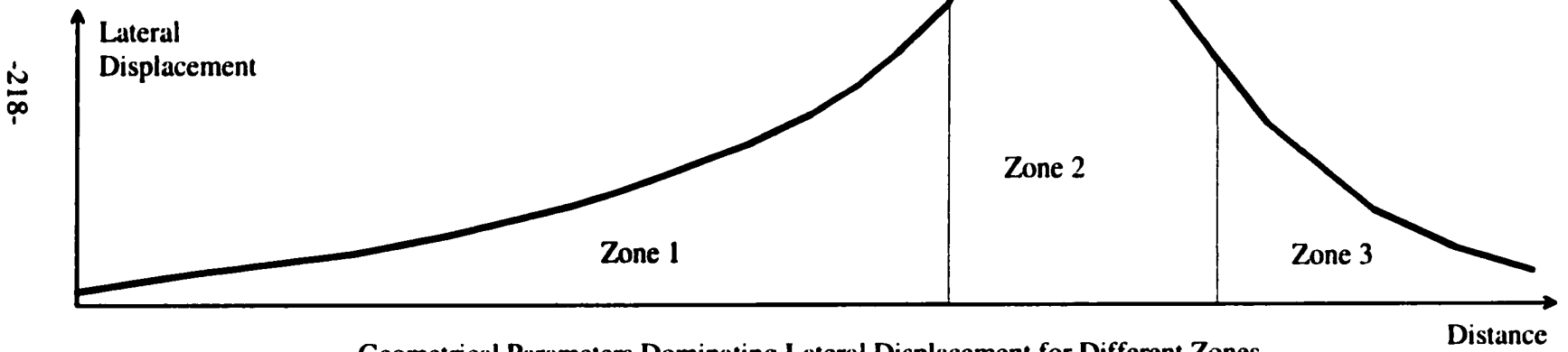
Table 8.1 Summary of the major parameters for case histories for nearly level ground with a free face

Case History	Kobe Port (1995)	Dagupan (1990)	Moss Landing (1989)	Jensen Plant (1971)	Niigata (1964)	Alaska (1964)
References	Hamada et al. (1995), Inagaki et al. (1996), Kimura (1996), and Ejiri et al. (1996)	Ishihara et al. (1993), Wakamatsu et al. (1992), Tokimatsu et al. (1994)	Boulanger et al. (1995, 1997), Mejia (1998), O'Rourke and Pease (1992)	O'Rourke et al. (1992)	Bartlett (1991), Bartlett and Youd (1995), Hamada (1992), Hamada et al. (1986)	Bartlett (1991), Bartlett and Youd (1995), McCulloch and Bonilla (1970)
Number of LD measurements	72	8	10	16	69	2
Measured lateral displacement, LD (cm)	34 – 500	50 – 600	8 – 140	2 – 300	41 – 1015	157 – 191
Liquefied soils	Sand fill with gravel and various fines content up to 30%	Fine clean sand and silty sand	Clean sand and silty sand	Alluvium with fines content of 32% to 62%	Mainly clean, fine or medium sands	Sand and gravel, silty sand, sandy silt.
Thickness of liquefied soils (m)	10 – 16	5.1 – 8.6	0.8 – 5.2	0.0 – 7.7	0.6 – 18.1	4.0 – 9.4
Lateral displacement index, LDI (cm)	250 – 665	79 – 220	17 – 114	5 – 120	246 – 637	69 – 173
Free face height, H (m)	12 – 20	4 – 11.5	1.9 – 5.8	10.4 – 17.2	4.9 – 5.2	2.4, 4.9
L/H	0 – 24.6	0.9 – 27.3	2.6 – 23.5	1.3 – 30.5	1.8 – 36.2	2.0, 6.2
Moment magnitude of the earthquake, M_w	6.9	7.6	7.0	6.4	7.5	9.2
Peak surface acceleration, a_{max} (g)	0.54	0.2	0.25	0.55	0.19	0.31
Number of SPT or CPT	18 (SPT)	3 (SPT)	13 (CPT)	27 (SPT)	47 (SPT)	4 (SPT)



(a)

Note: Not to Scale
 L is Distance
 S is Slope
 H is Height

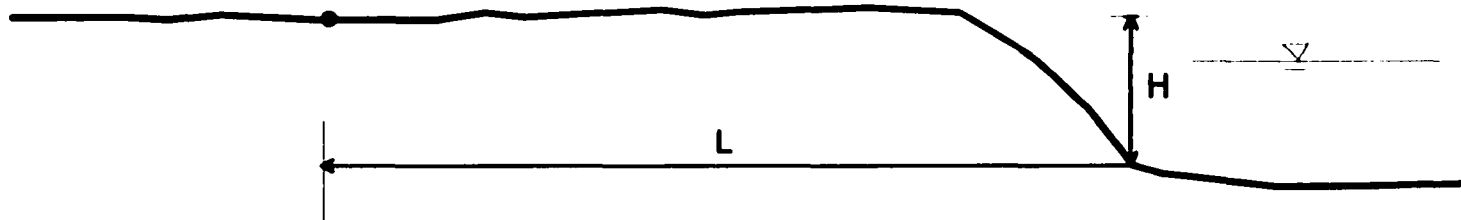


Geometrical Parameters Dominating Lateral Displacement for Different Zones

L	H		S_1	L_1	H	S_2	S_1	S_2	L_2	H
---	---	--	-------	-------	---	-------	-------	-------	-------	---

(b)

Figure 8.1 A sketch illustrating (a) geometric parameters and (b) lateral displacement patterns on level ground with a free face



Note: Not to Scale
L is Horizontal Distance
H is Elevation Difference

Figure 8.2 Definition of free face height (H) and the distance to a free face (L) for level ground with a free face

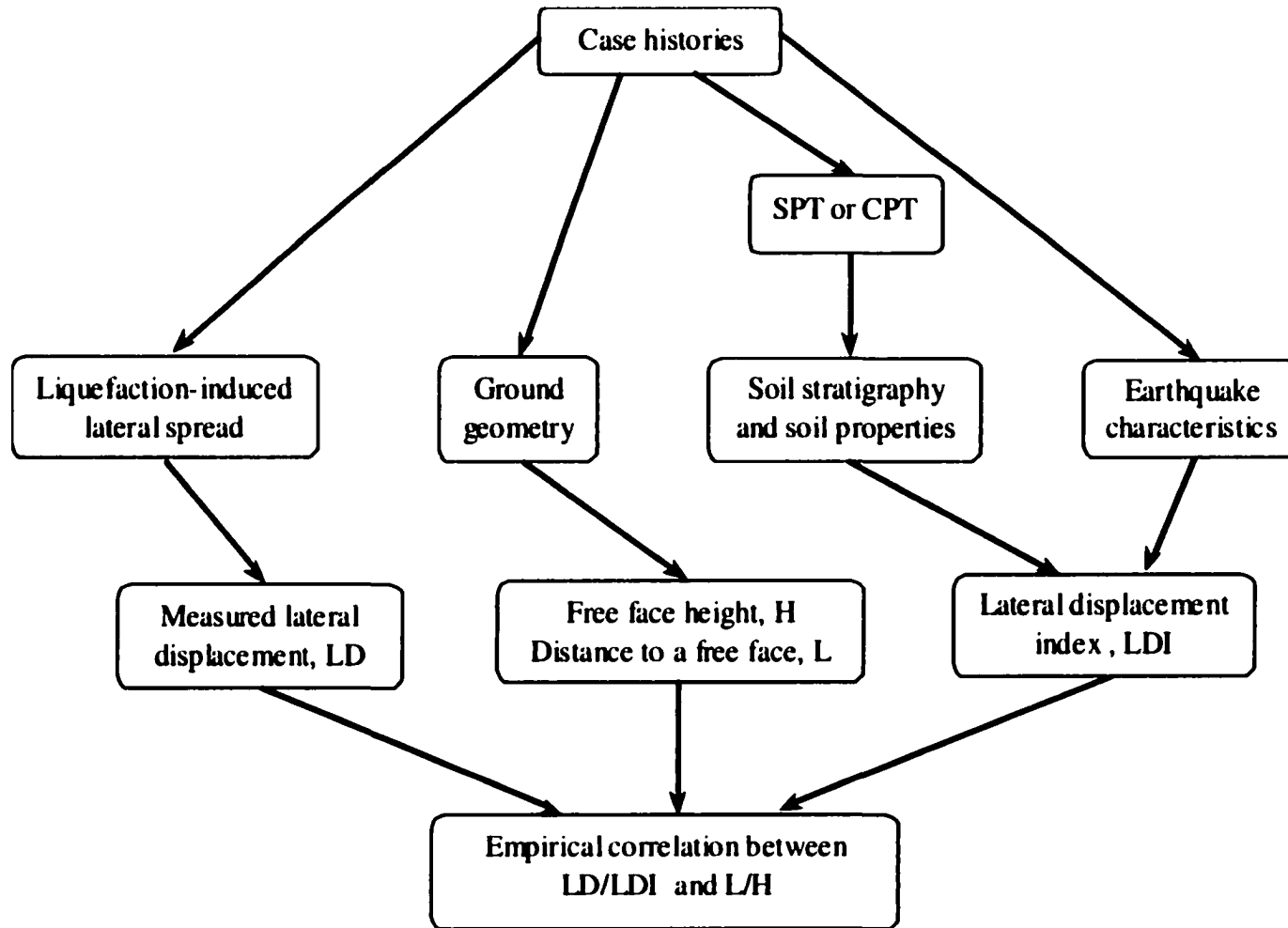


Figure 8.3 Conceptual flow chart for developing an empirical correlation between LD/LDI and L/H for level ground with a free face

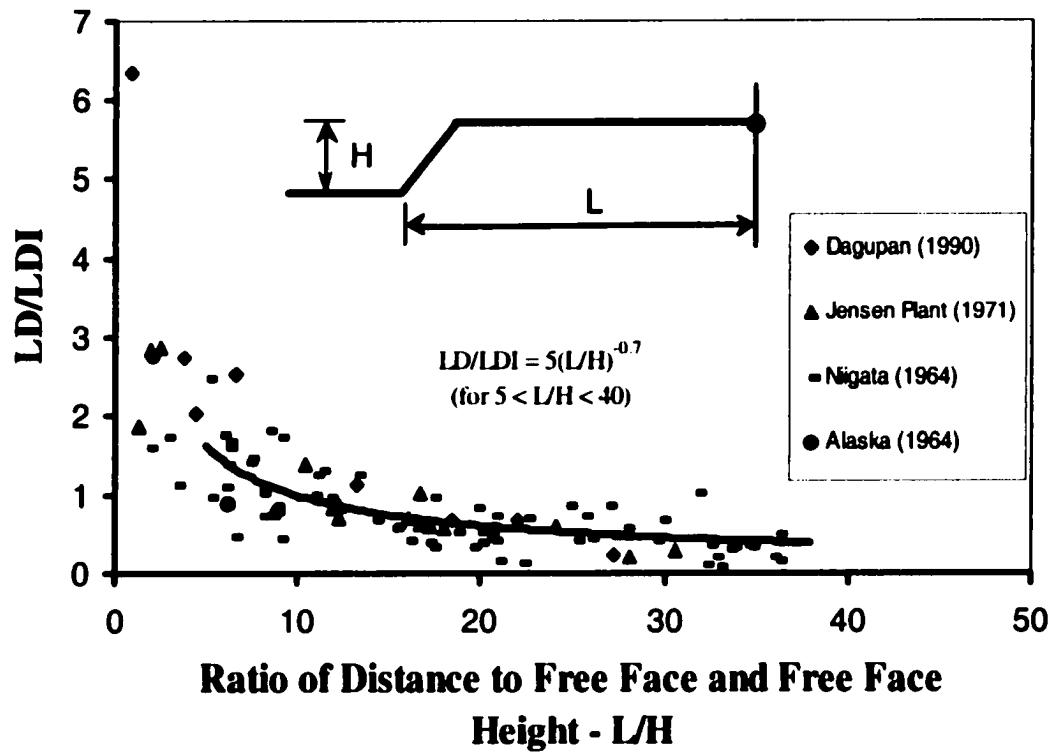


Figure 8.4 Relationship between LD/LDI and L/H for the data of which the values of LDI were calculated using SPT data for the available four case histories for level ground with a free face

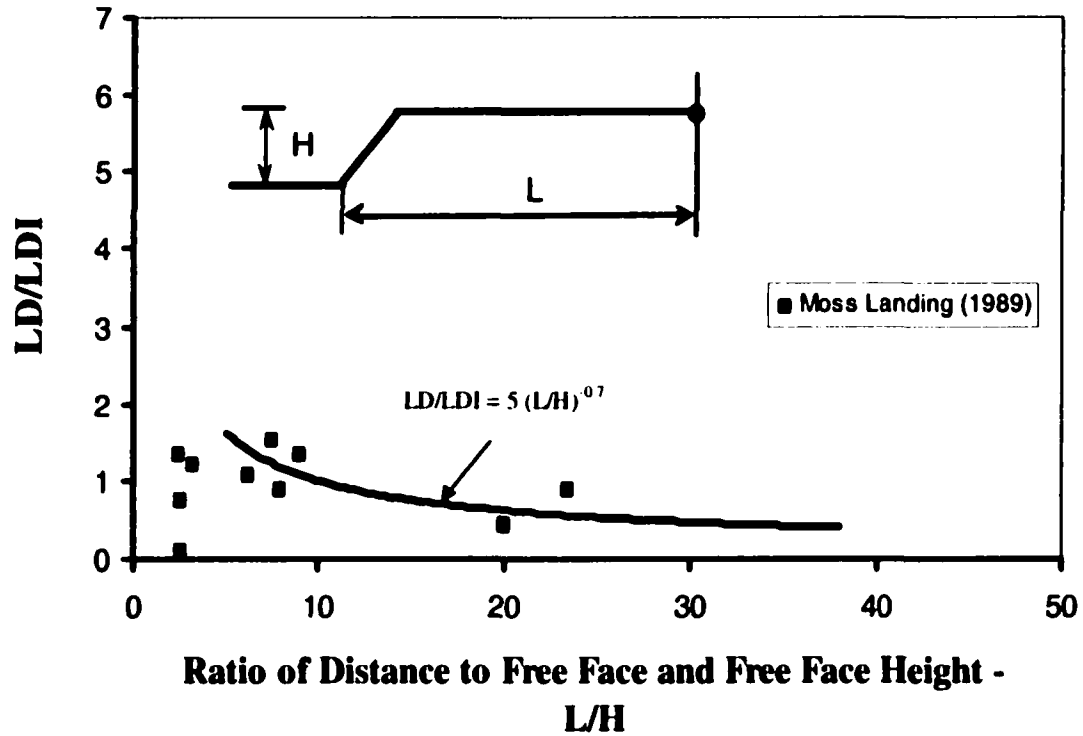


Figure 8.5 Relationship between LD/LDI and L/H for the data of which the values of LDI were calculated using in-situ CPT data for the Moss Landing case history for level ground with a free face

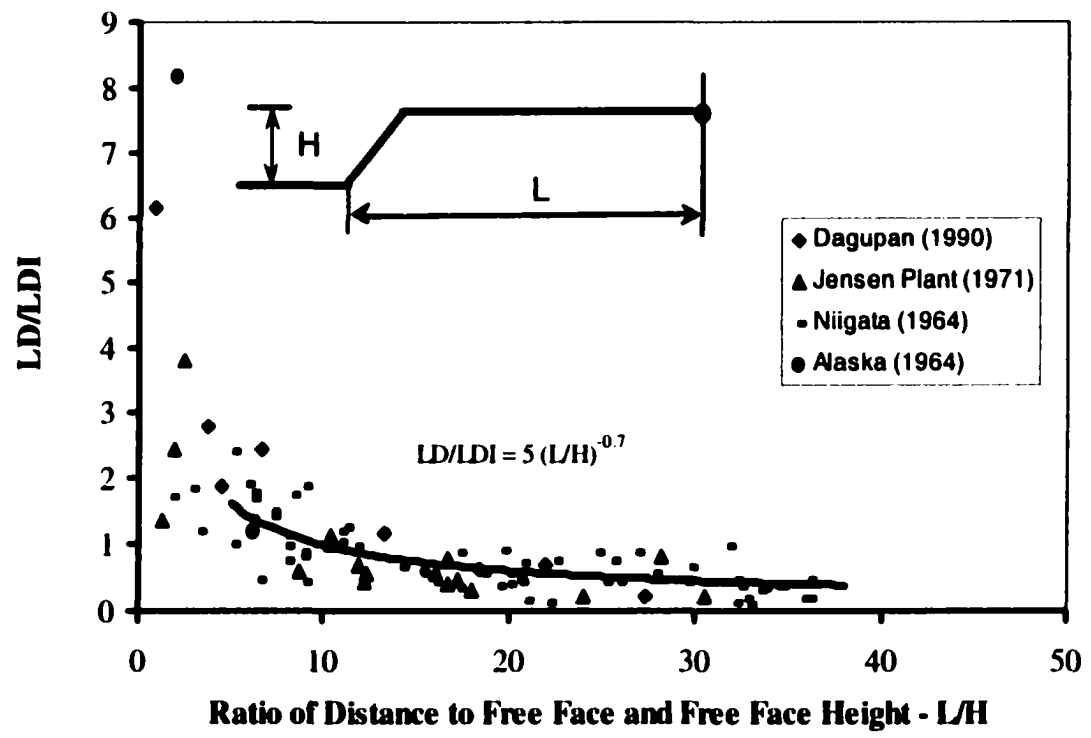


Figure 8.6 Relationship between LD/LDI and L/H for the data of which the values of LDI were calculated using the equivalent CPT data that were converted from SPT data for the four case histories where only SPT data were available for level ground with a free face

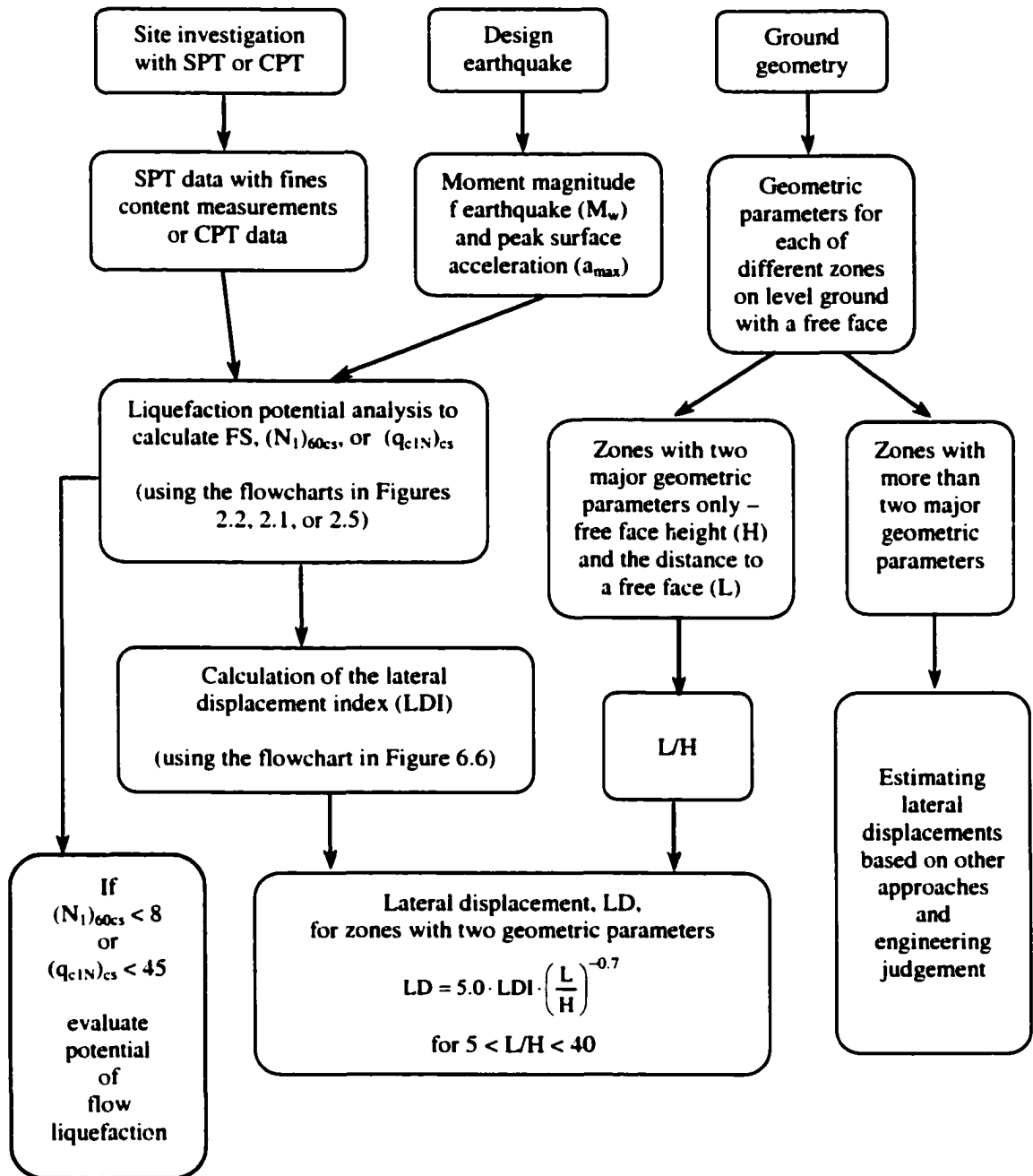


Figure 8.7 A flowchart illustrating major steps in the application of the proposed approach to estimate lateral displacements in a liquefaction-induced lateral spread for level ground with a free face using SPT or CPT data

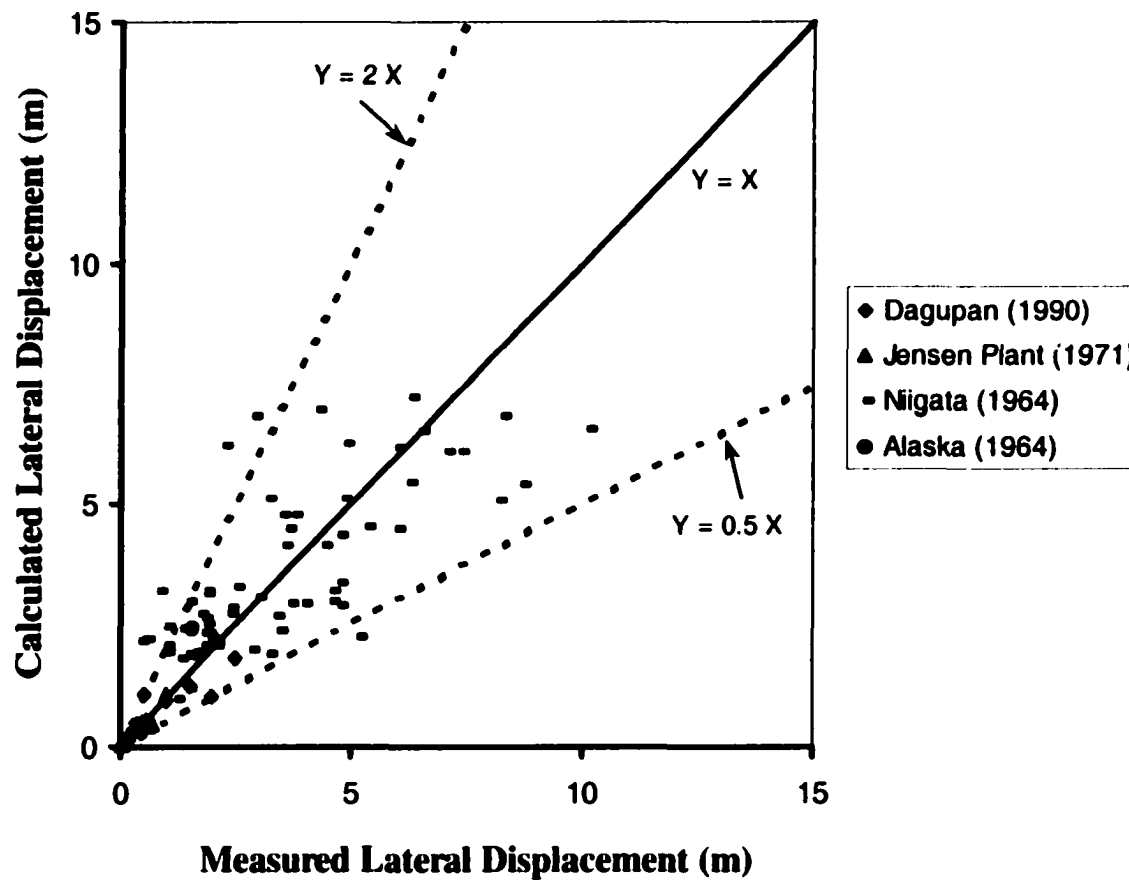


Figure 8.8 Comparison of lateral displacements measured at sites for the four case histories and calculated by the proposed approach using SPT data for level ground with a free face

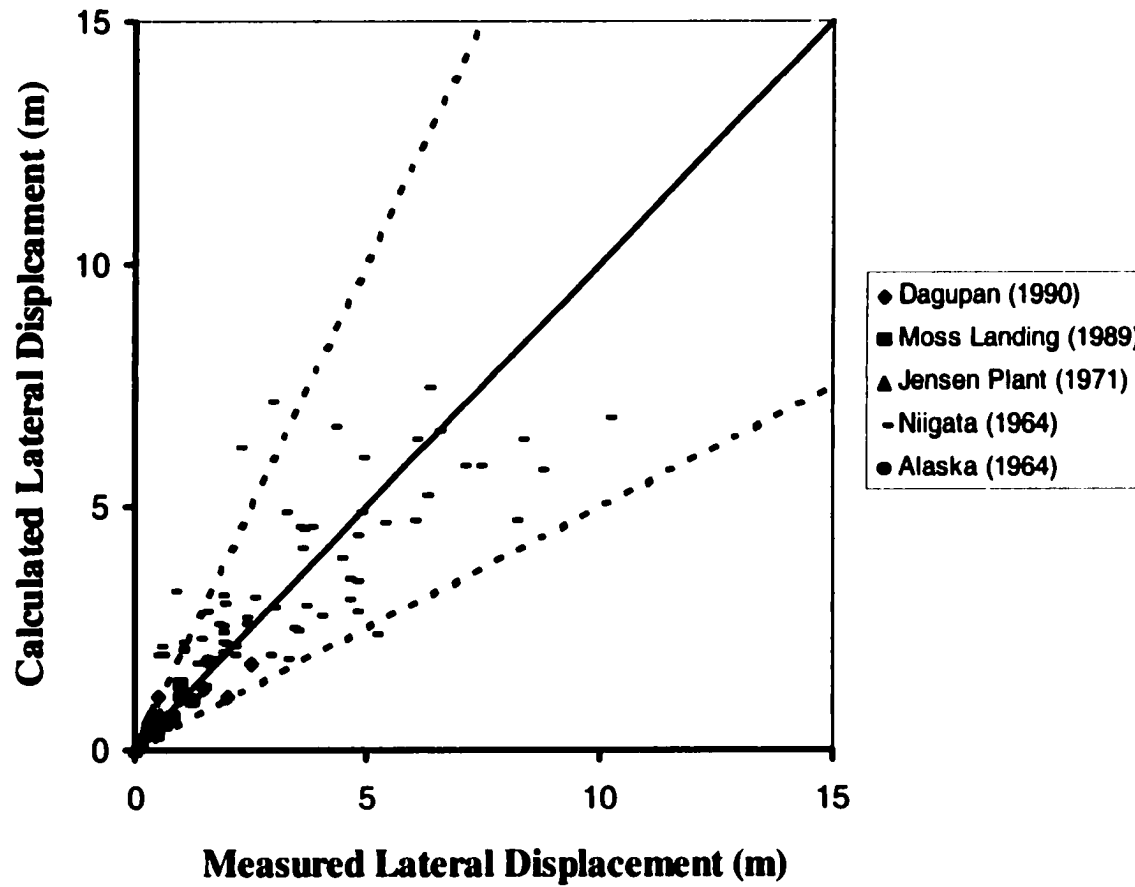


Figure 8.9 Comparison of lateral displacements measured at sites for the five case histories and calculated by the proposed approach using in-situ or equivalent CPT data for level ground with a free face

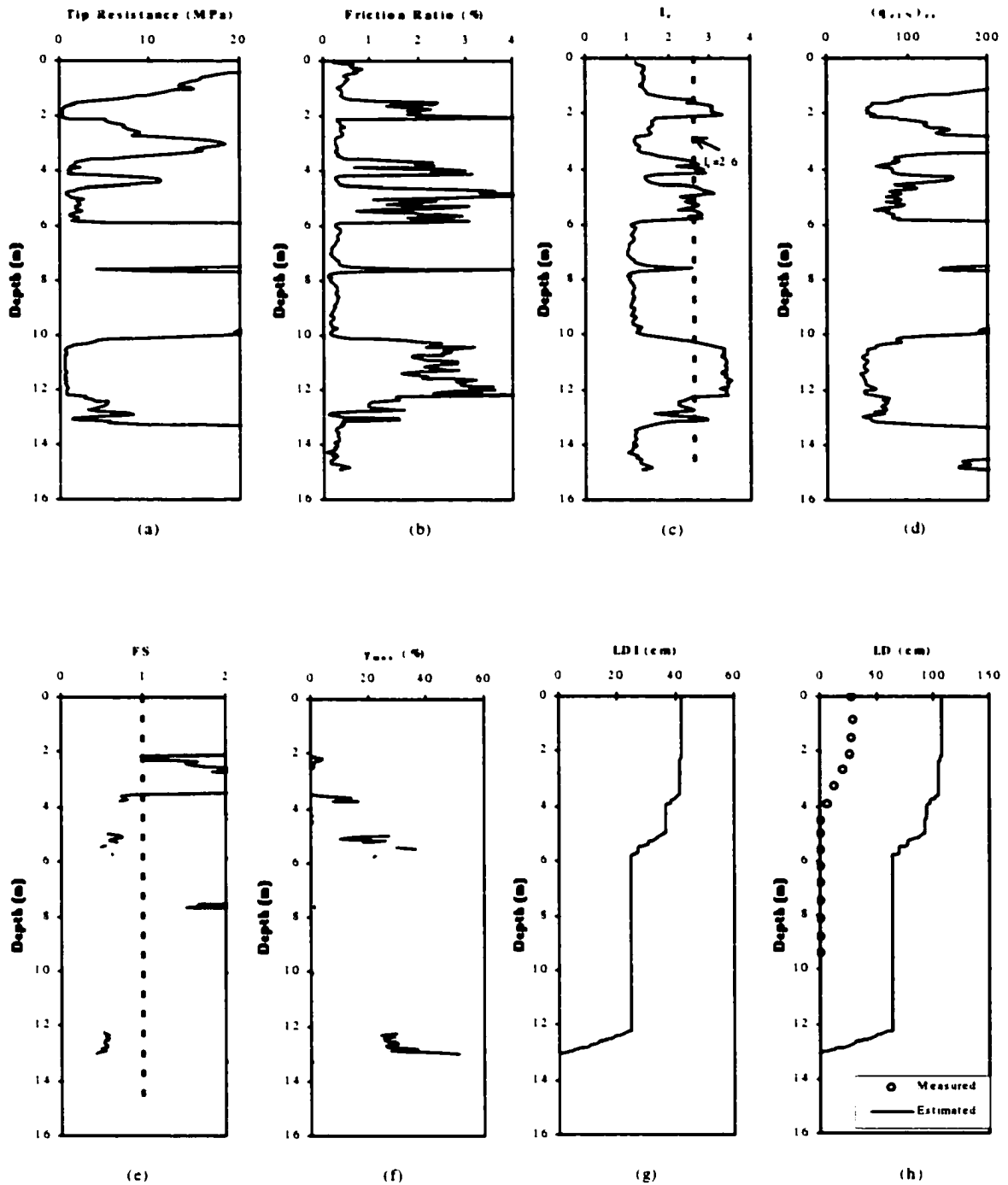


Figure 8.10 An example to illustrate the estimated (using the data from CPT UC-4) and measured profile (from inclinometer SI-2) of lateral displacements (towards the river) with depth for one site at Moss Landing

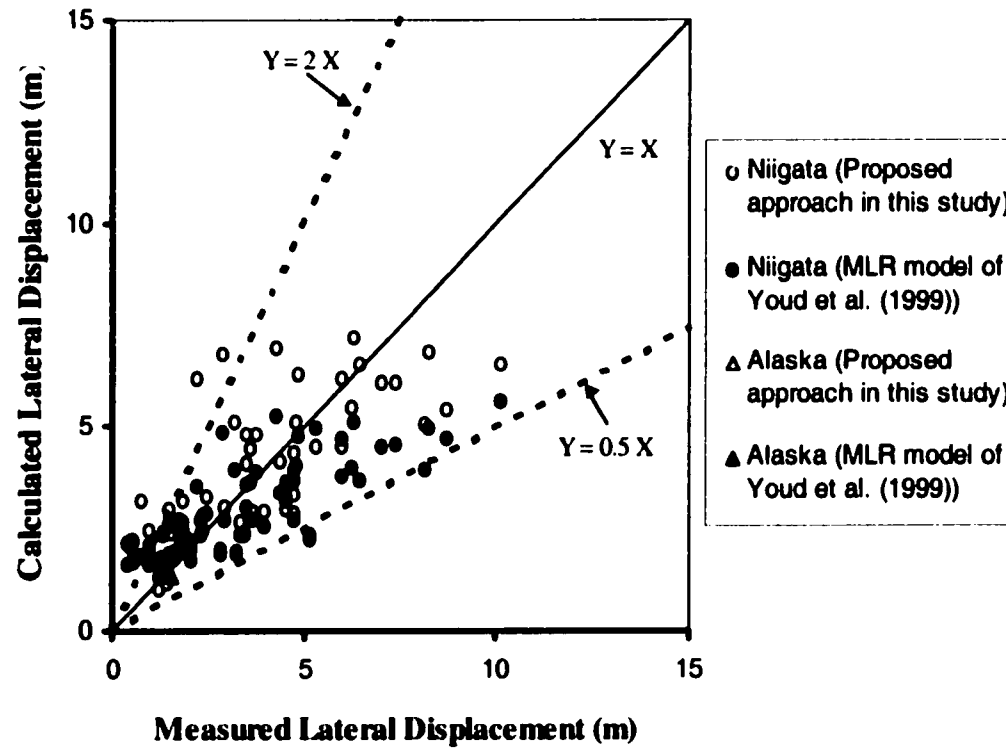


Figure 8.11 Comparison of lateral displacements measured at sites for two case histories and calculated by the proposed approach and by the MLR model of Youd et al. (1999) for level ground with a free face

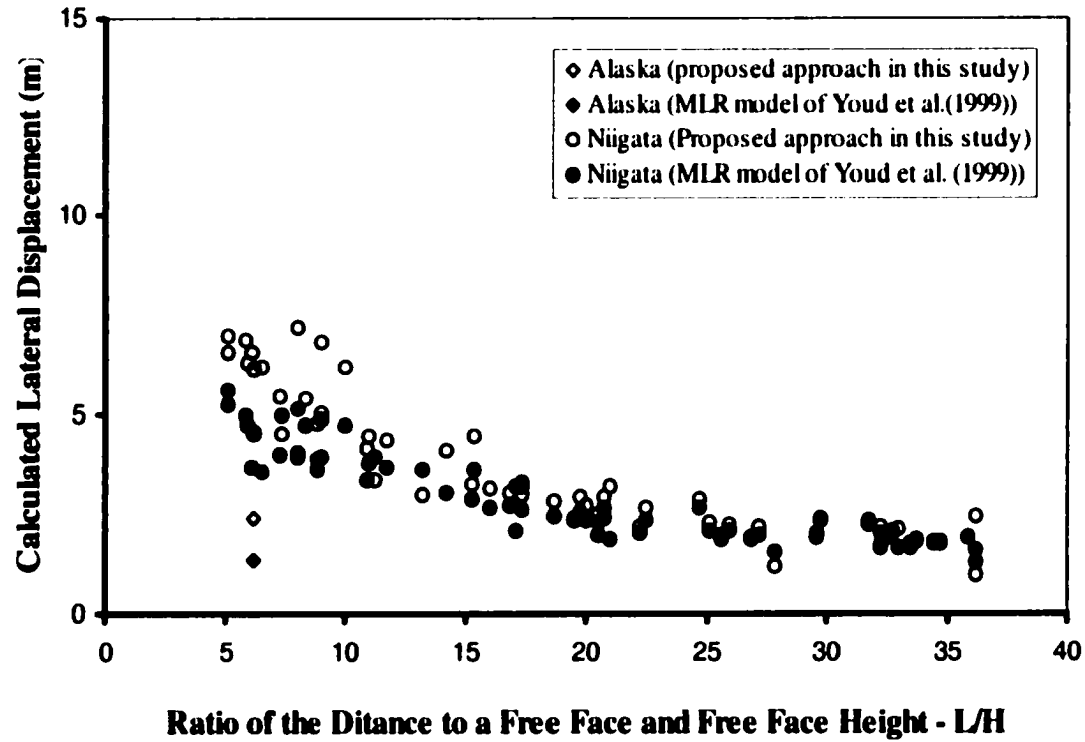


Figure 8.12 Comparison of lateral displacements calculated by the proposed approach and by the MLR model of Youd et al. (1999) for different L/H ratios for two case histories for level ground with a free face

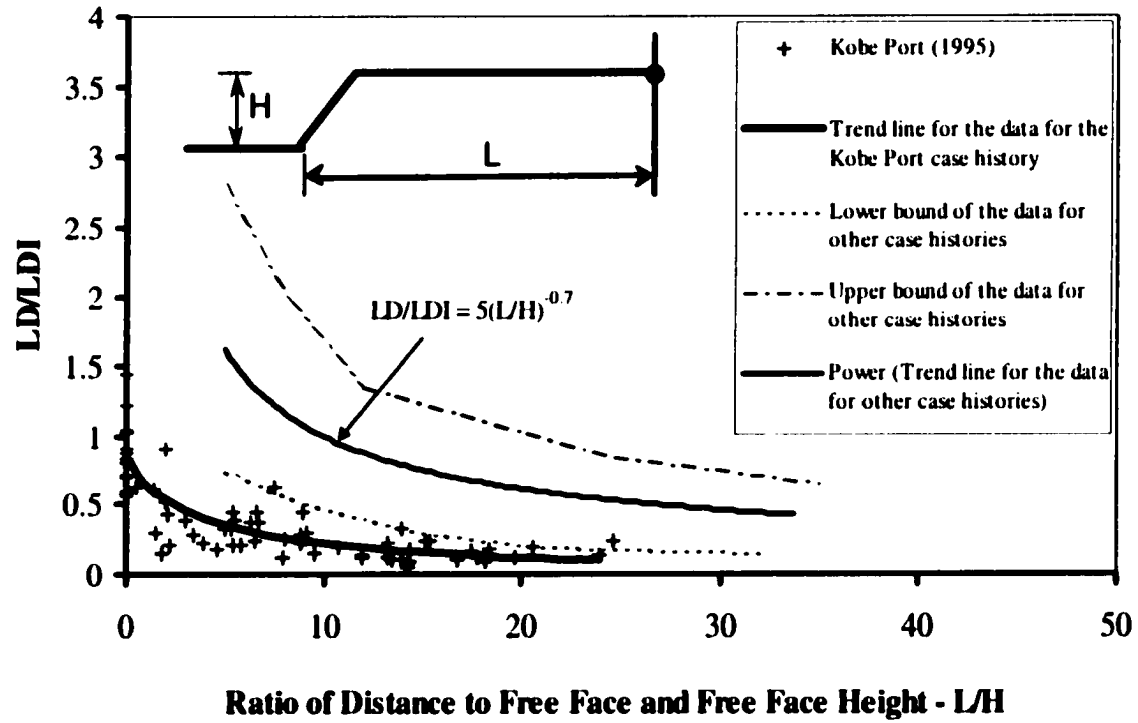


Figure 8.13 Relationship between ratio of measured lateral displacement (LD) to the lateral displacement index (LDI) and L/H for the Kobe Port case history where quay walls restricted the lateral displacements of the ground

CHAPTER 9 ESTIMATION OF LIQUEFACTION-INDUCED LATERAL DISPLACEMENTS FOR GENTLY SLOPING GROUND WITH A FREE FACE USING SPT OR CPT DATA

9.1 Introduction

An approach to estimate lateral ground displacements associated with liquefaction-induced lateral spreads using SPT or CPT data was developed in Chapter 7 for gently sloping ground without a free face and in Chapter 8 for nearly level ground with a free face respectively. However, lateral spreads can also occur in gently sloping ground with a free face. In this chapter, based mainly on case history studies, an approach is developed to estimate liquefaction-induced lateral displacements for gently sloping ground with a free face using SPT or CPT data.

9.2 Geometric Parameters for Gently Sloping Ground with A Free Face

For gently sloping ground with a free face, lateral spreads are expected to be influenced by both the gently sloping ground and the free face. Lateral displacement patterns and geometric parameters controlling lateral displacements in a lateral spread have been discussed in Section 7.2 and illustrated in Figure 7.3 for gently sloping ground without a free face and discussed in Section 8.2 and illustrated in Figure 8.1 for level ground with a free face. Generally, lateral displacement patterns are complicated for either gently sloping ground without a free face or level ground with a free face. As well as ground slope for gently sloping ground without a free face, and free face height and distance to a free face for level ground with a free face, other geometric parameters may also influence lateral displacements in some zones in a lateral spread. Therefore, lateral displacement patterns could be very complicated, and three or more major geometric parameters exist for gently sloping ground with a free face.

However, in some zones with simple ground geometry (e.g., zone 1 in Figure 9.1), the effects of ground geometry on lateral displacements may be characterized by three major geometric parameters only: ground slope (S), free face height (H), and the distance to a free face (L). In this chapter, research focuses on the zones in ground with a simple ground geometry (e.g., zone 1 in Figure 9.1).

A positive ground slope (e.g., Figure 9.1a) is assigned to the ground sloping toward a free face (e.g., a channel) and a negative ground slope (e.g., Figure 9.1b) is assigned to the ground sloping away from a free face. The definitions for S, H, and L are same as those in Chapters 7 and 8, as illustrated in Figures 7.4 and 8.2.

9.3 Case Histories

An introduction to the collection of case history data associated with available past major earthquakes was presented in Section 7.3.1. In this chapter, four case histories associated with four different past major earthquakes for gently sloping ground with a free face are studied. A summary of the major parameters for these case histories is provided in Table 9.1. Of the four case histories, SPT data were available for all the cases, and CPT soundings were available for the Heber Road and Wildlife case histories only. A brief introduction to each of the case histories is given below.

9.3.1 Case sites in Niigata City during the 1964 Niigata, Japan, Earthquake

The 1964 Niigata earthquake was briefly introduced in Section 7.3.5. Liquefaction-induced lateral spreads were observed in both ground with a free face and ground with a very gentle slope in Niigata City during this earthquake. The case sites for gently sloping ground without a free face and for level ground with a free face have been investigated in Chapters 7.3.5 and 8.3.2 respectively. In this section, the case sites for gently sloping ground with a free face in Niigata City are studied.

Generally, the soils down to about 20 m from the surface are relatively clean, fine or medium sands in Niigata City. The estimated thickness of the liquefied layers ranged from 2 m to 12 m for the sites where the ground had a very gentle slope of -0.3% to +0.4% and a free face of 3.4 m to 5.2 m in height. A total of 32 data sets from Bartlett's (1991) database for the case sites in Niigata City were collected, and a total of 15 SPTs associated with the lateral displacement measurements were used for the study in this chapter. The measured lateral displacements, using pre- and post-earthquake aerial photographs, varied between 0.6 m and 6.2 m for the data used in this study. The accuracy of the measurements of lateral displacements for the Niigata case history was estimated to be ± 0.72 m horizontally (Hamada 1992a). In addition, a peak surface acceleration of 0.19 g was reported by Kawasumi (1968) and Bartlett (1991), and the value was used for all the sites in Niigata City in this research.

9.3.2 The Heber Road case history during the 1979 Imperial Valley, California, Earthquake

The 1979 Imperial Valley earthquake, with a moment magnitude of 6.5, occurred on October 15 at 23:16 GMT (Dobry et al. 1992). The epicenter was located 3 km south of the United States/Mexico border. Liquefaction-induced lateral spreads that resulted from the earthquake were observed at several sites in the Imperial Valley region (Youd and Wieczorek 1982). A well-known large lateral spread that occurred at the Heber Road site during the earthquake is studied in this research.

The Heber Road site was located 1.6 km northeast of the beginning of the Imperial Fault surface rupture. A lateral spread about 160 m wide and 100 m long shifted the Heber Road and a parallel canal toward a 2 m deep depression with a maximum lateral displacement of 4.2 m. The average ground slope in the lateral spreading area was about 1.5%.

Bennett et al. (1981) conducted field investigations with 16 mechanical CPTs and 7 SPTs at the site. Norton (1983) also performed 10 electric cone penetration tests at the Heber

Road site. The soil profile for the site consisted of a top 1.0 to 1.5 m thick layer of sandy fill, an approximately 4.0 m thick layer of fluvial sediment with three distinct laterally varied sub-units beneath the fill, and at least two cycles of channel sands alternating with lacustrine clay (Youd and Bennett 1983). The partial fluvial sediment, especially the loose channel sand with 14% to 37% fines in the central part of the fluvial sediment in the lateral spreading area, was liquefied during the earthquake.

A total of 17 lateral displacement measurements from the central part of the lateral spread were collected based on Youd and Bartlett's survey results. A total of 8 electric CPTs conducted by Norton (1983) and 6 SPTs performed by Bennett et al. (1981) were used in this study. Various values ranging from 0.46 to 0.8 for the peak surface acceleration at the Heber Road site were estimated and used by different researchers (Norton 1983; Youd and Bennett 1983; Castro 1987; Bartlett 1991; Rauch 1997; and Gilstrap 1998). A peak surface acceleration of 0.6 g used by Gilstrap (1998) was assigned to the Heber Road site during the earthquake in this study.

9.3.3 The Wildlife case history during the 1987 Superstition Hills, California, Earthquake

On November 24, 1987, at 5:15 PST, the Superstition Hills earthquake with a moment magnitude of 6.5 occurred in the Imperial Valley, California (Dobry et al. 1992). The unique features associated with this earthquake were that it was the first time in history that in-situ excess pore pressures which built up to 100 percent of the initial effective overburden pressures were recorded in the field by pre-installed piezometers and that a liquefaction-induced lateral displacement was measured by a pre-installed inclinometer at the Wildlife site in the Imperial Valley during the earthquake. The Wildlife site was about 31 km from the epicenter of the 1987 Superstition Hills earthquake. A peak surface acceleration of 0.21 g was recorded by a strong motion seismometer at the site.

Detailed site investigations with the CPT and SPT were conducted by several researchers to characterize the stratigraphy at the Wildlife site (Bennett et al. 1984). The typical soil

profile at the Wildlife site consisted of three distinct units in the upper 12 m as defined by Bennett et al. (1984): an approximately 3 m thick layer of silt, a 4 m thick layer of silty sand or sandy silt with 17% to 50% fines, and a 5 m thick layer of clayey silt or silty clay. The silty sand or sandy silt layer was identified as the liquefiable layer by the primary investigators (Bennett et al. 1984).

In addition to one lateral displacement measured by an inclinometer at the Wildlife site, as reported by Holzer et al. (1989), Youd and Bartlett (1988) conducted a survey at the site and reported additional lateral displacement measurements. A total of five lateral displacements, with values ranging from 0.11 m to 0.23 m, were collected for this site, and the results of 4 CPTs and 3 SPTs associated with the measurements were used in this study. The ground slope at the site was about -0.5% . The height of the free face was 2.4 m.

9.3.4 Case sites in Shiribeshi River area, Japan during the 1993 Hokkaido-nansei-oki, Japan, Earthquake

The 1993 Hokkaido-nansei-oki earthquake occurred on July 12, 1993 at 10:17 p.m. beneath the Sea of Japan off the Oshima Peninsula in Hokkaido, registering a magnitude of 7.8 on the JMA Scale (Isoyama 1994). Liquefaction-induced lateral spreads caused by the earthquake were observed in several areas along the river valley of the Siribeshi-toshibetsu River in Kitahiyama Town, which is located on the coast of the Sea of Japan.

Isoyama (1994) conducted investigations of lateral spreads in the areas along the river valley of the Siribeshi-toshibetsu River. The investigations included the collection and interpretation of aerial photos taken before and after the earthquake and information associated with soil conditions in the five areas. Because detailed soil profiles with SPT data were available only in one of the five areas, Area D, lateral spreads in Area D were studied in this research.

The strata in Area D consisted mainly of 1 to 2 m thick clayey topsoil, about 6 m of thick

silty sand with about 10% fines, and clayey soils. The silty sand layer was estimated to have liquefied completely during the earthquake (Isoyama 1994).

A total of six lateral displacement measurements with values of 1 m to 3 m and the data from 4 SPTs were used for the area in this study. The ground slopes at the sites were between 0.7% and 0.8%. The heights of free faces ranged from 1.9 to 2.5 m.

9.4 Evaluation of Superimposition Approach

An approach to estimate lateral ground displacements associated with liquefaction-induced lateral spreads using SPT or CPT data has been developed in Chapter 7 for gently sloping ground without a free face and in Chapter 8 for level ground with a free face. Gently sloping ground with a free face incorporates two ground conditions: gently sloping ground without a free face and level ground with a free face. This raises the question of whether liquefaction-induced lateral displacements for gently sloping ground with a free face can be estimated simply by superimposing the two components of the estimated lateral displacements: one for gently sloping ground without a free face and the other for level ground with a free face. The performance of this superimposition approach will be evaluated using the data from available case histories in this section.

Following the procedures described in Section 6.3, the lateral displacement index (LDI) for each of the sites for the Niigata and Hokkaido case histories was calculated using the SPT-based procedures and SPT results. Because the two proposed approaches developed in Chapters 7 and 8 can be used with either SPT or CPT data, the LDI for the Heber Road and Wildlife case histories was calculated using both the available SPT and CPT data. The data for the calculated LDI, together with measured lateral displacement, ground slope (S), free face height (H), the distance to a free face (L), and other relevant parameters used in this study, are listed in Table A3 in Appendix A.

The first component of lateral displacement (LD_{slope}) for gently sloping ground without a

free face can be estimated by the proposed approach that was developed in Chapter 7, as shown in Equation [9.1].

$$[9.1a] \quad LD_{\text{slope}} = (S + 0.2) \cdot LDI \quad (\text{for } 0.2\% < S < 3.5\%)$$

$$[9.1b] \quad LD_{\text{slope}} = -(-S + 0.2) \cdot LDI \quad (\text{for } -0.2\% > S > -3.5\%)$$

The second component of lateral displacement (LD_{freeface}) for level ground with a free face can be estimated by the proposed approach that was developed in Chapter 8, as shown in Equation [9.2].

$$[9.2] \quad LD_{\text{freeface}} = 5.0 \cdot \left(\frac{L}{H} \right)^{-0.7} \cdot LDI \quad (\text{for } 5 < L/H < 40)$$

Therefore, based on the superimposition assumption, the calculated lateral displacement (LD) for gently sloping ground with a free face is the sum of the two components: LD_{slope} and LD_{freeface} .

To evaluate the performance of this superimposition approach, the calculated lateral displacements were compared with the measured values for the four available case histories, as shown in Figure 9.2. Figure 9.2 indicates that the superimposition approach does not work well. In general, the calculated lateral displacements are larger than the measured values for ground with a positive slope but smaller than the measured values for ground with a negative slope for the four case histories. This implies that the superimposition approach over-estimates lateral displacements for ground with a positive slope and under-estimates lateral displacements for ground with a negative slope. Therefore, a new approach is required to estimate lateral displacements for gently sloping ground with a free face.

9.5 A Preliminary Approach to Estimate Lateral Displacements for Gently Sloping Ground with A Free Face Using SPT or CPT Data

To study the effect of ground slope on lateral displacements for gently sloping ground with a free face, a procedure similar to that in Section 8.4.1 for level ground with a free face was followed. The data for the four available case histories, as listed in Table A3 in Appendix A, were used to illustrate the relationship between LD/LDI and L/H for gently sloping ground with a free face, as shown in Figure 9.3. A trend line that characterizes the general relationship between LD/LDI and L/H and the relevant lower and upper bounds for level ground with a free face, which were developed in Chapter 8, are also shown in Figure 9.3.

The data for three of the four case histories (Hokkaido, 1993; Wildlife, 1987; and Heber Road, 1979) as illustrated in Figure 9.3 indicate that the points for ground with a positive slope generally fall in the zone above the trend line while the points for ground with a negative slope are in the zone below the trend line even though some of the points fall in a zone between the upper and lower bounds for “level” ground with a free face. This suggests that ground slope does in fact play some role in controlling the magnitude of lateral displacements for gently sloping ground with a free face.

For the data from the Niigata case history in Figure 9.3, the situation is more complicated than that for the other three case histories. The partial data for ground with a positive slope fall in the zone below the trend line, while the partial data for ground with a negative slope fall in the zone above the trend line. This observed trend seems to be inconsistent with that observed from the other three case histories. Several possible reasons may cause this inconsistency. First, the ground slopes for this case history were very gentle, ranging from -0.3% to 0.4% only and close to “level” ground that were defined as ground with a slope ranging from -0.15% to +0.15% in this study. In such cases, local topography variations and/or the presence of buildings may have significant effects on the magnitude of lateral displacements and may veil the importance of the very gentle slopes. Second, the relatively poor accuracy (± 0.72 m) of the measured

displacements at site in Niigata City may be another reason.

As a preliminary approach, the effect of a ground slope on LD/LDI may be estimated from Figure 9.3 by measuring the difference between the actual value of LD/LDI and the relevant value from the trend line in Figure 9.3 for a given value of L/H. Figure 9.4 shows the relationship between ground slope and its relevant difference in LD/LDI for each of the points in Figure 9.3. A general trend of increasing difference in LD/LDI with increasing ground slope can be fairly seen in Figure 9.4 even though the data in Figure 9.4 show significant scattering. A trend line, as shown in Figure 9.4, can be used to approximately represent the general relationship between ground slope and its relevant difference in LD/LDI. Equation [9.3] is a mathematical expression of the trend line in Figure 9.4.

$$[9.3] \quad \Delta\left(\frac{LD}{LDI}\right) = 0.5 \cdot S \quad (\text{for } -0.5\% \leq S \leq 1.5\%)$$

where S is ground slope in percent, and $\Delta\left(\frac{LD}{LDI}\right)$ is the effect of ground slope on the value of LD/LDI.

Based on Equations [9.3] and [8.1], the preliminary empirical relationship between LD/LDI, S , and L/H can be established for gently sloping ground with a free face, as shown in Equation [9.4].

$$[9.4] \quad \left(\frac{LD}{LDI}\right) = 5.0 \cdot \left(\frac{L}{H}\right)^{-0.7} + 0.5 \cdot S$$

$$\text{for } 5 < L/H < 40 \text{ and } -0.5\% \leq S \leq 1.5\%$$

Equation [9.4] represents a preliminary correlation between LD/LDI, S , and L/H for the limited available case history data and may be used with caution to estimate liquefaction-

induced lateral displacements for gently sloping ground with a free face. The major procedures for this preliminary approach are as follows:

- Evaluate liquefaction potential using either the NCEER SPT- or CPT-based method;
- Calculate the lateral displacement index (LDI);
- Measure ground slope (S), free face height (H), and the distance to a free face (L);
- Estimate lateral displacements (LD) using Equation [9.5].

$$[9.5] \quad LD = LDI \cdot (0.5 \cdot S + 5.0 \cdot (L/H)^{-0.7})$$

$$\text{for } 5 < L/H < 40 \text{ and } -0.5\% \leq S \leq 1.5\%$$

Figure 9.5 is a flowchart illustrating the major steps to apply the preliminary approach for gently sloping ground with a free face. The recommended ranges of parameters for the preliminary approach are 5 to 40 for the L/H ratio and -0.5 to 1.5% for ground slope for gently sloping ground with a free face. The preliminary approach was developed using the limited data with a limited range of ground slope from the available four case histories associated with four different past earthquakes and as such is applicable only for similar earthquakes and ground conditions, as summarized in Table 9.1.

The preliminary approach may be used to estimate liquefaction-induced lateral displacements for gently sloping ground with a free face for low to medium-risk projects or to provide preliminary estimates for high-risk projects. However, caution must be exercised in using this preliminary approach with being aware of the significant scattering in Figure 9.4. Engineering judgement must be exercised because liquefaction-induced ground lateral spreading is a complicated engineering phenomenon and a number of assumptions and simplifications were involved in developing the preliminary approach.

9.6 Performance of the Preliminary Approach

The measured lateral displacements are compared with the calculated lateral displacements using the preliminary approach for the available four case histories in Figure 9.6. 90% of the calculated displacement values are between 50% and 200% of the relevant measured values for the four case histories, as indicated in Figure 9.6. Figure 9.6 shows the likely variability of calculated displacements using the preliminary approach with SPT or CPT data. Considerable scatter is evident as lateral displacements could be either underestimated or overestimated by up to a factor of two based on the available data.

Other than the preliminary semi-empirical approach in this study, the MLR model of Youd et al. (1999) is probably the best field-test-based empirical model for estimating lateral displacements on a liquefaction-induced lateral spread at present, as discussed in Section 5.5. However, there is no equation for estimating lateral displacements for gently sloping ground with a free face for the MLR model. The users of the MLR model must decide whether free-face or ground-slope conditions predominate lateral displacements at their studied sites when the MLR model is used and then use either the equation for free-face case (Equation [5.5]) or the equation for ground-slope case (Equation [5.6]) (Bartlett and Youd 1995) to estimate the lateral displacements. Therefore, quantitative comparison with the MLR model of Youd et al. (1999) was not conducted in this research.

9.7 Discussion

As discussed in Section 8.7, engineered structures (e.g., quay walls, retaining walls, piles, tanks, or pipelines) may alter lateral displacements in a liquefaction-induced lateral spread. The preliminary approach was developed using the data from case histories in which engineered structures had little or no effect on lateral spreads. It is expected that the preliminary approach may over-estimate lateral displacements at sites where

engineered structures pose great restrictions to the lateral movements of the ground.

Caution should be exercised when a substantial zone of soils with a low $(N_1)_{60cs}$ or $(q_{cIN})_{cs}$ is encountered during liquefaction potential analysis. For such cases, more extensive investigation should be made and other approaches should be taken to evaluate the potential for flow failure of the soil, especially when the static shear stresses in the ground are relatively high. Deformations caused by flow failures can be much larger than those by lateral spreads, and their estimation is beyond the scope of this research.

The preliminary approach characterizes the effects of soil profile and properties, earthquake characteristics, and ground geometry on liquefaction-induced lateral displacements. As discussed in Chapter 4, other factors that may also influence lateral displacements, such as the redistribution and drainage of excess pore pressures in the ground, are not quantified in the current approach and would need to be evaluated on a case-by-case basis.

9.8 Conclusions

A preliminary approach to estimate liquefaction-induced lateral displacements using either SPT or CPT data for gently sloping ground with a free face has been developed based on limited case history data. The preliminary approach captures the mechanisms of liquefaction-induced lateral spreads and characterizes the major factors influencing lateral displacements. The preliminary approach may be used to estimate both the magnitude and distribution of liquefaction-induced lateral displacements for the recommended ranges of the geometrical parameters for gently sloping ground with a free face for low to medium-risk projects or to provide preliminary estimates for high-risk projects. The preliminary method can be easily applied with only a few additional calculations following the NCEER SPT- or CPT-based liquefaction-potential analysis.

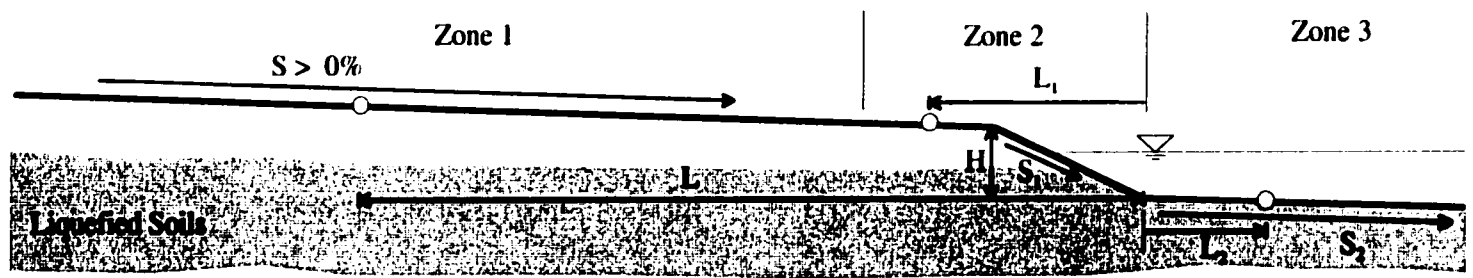
Given the complexity of liquefaction-induced lateral spreads, considerable variations in magnitude and distribution of lateral displacements are expected. Generally, the calculated lateral displacements from the four available case histories studied in this chapter showed variations between 50% and 200% of measured values.

The preliminary approach was developed using the very limited data from only four case histories associated with four past earthquakes and as such is applicable only for similar earthquakes and ground conditions. Additional data are required to better quantify liquefaction-induced lateral spreads and to evaluate the preliminary approach.

The preliminary approach was developed based on data with limited ranges. The ratio of L to H ranged between 5 and 40, and ground slope varied within the range of -0.5% to 1.5% only. Therefore, it is not recommended that the preliminary approach be applied to cases in which the values for the three major geometric parameters are beyond their relevant ranges. More data from new case histories are needed to update the preliminary approach and to expand the existing ranges for the geometric parameters.

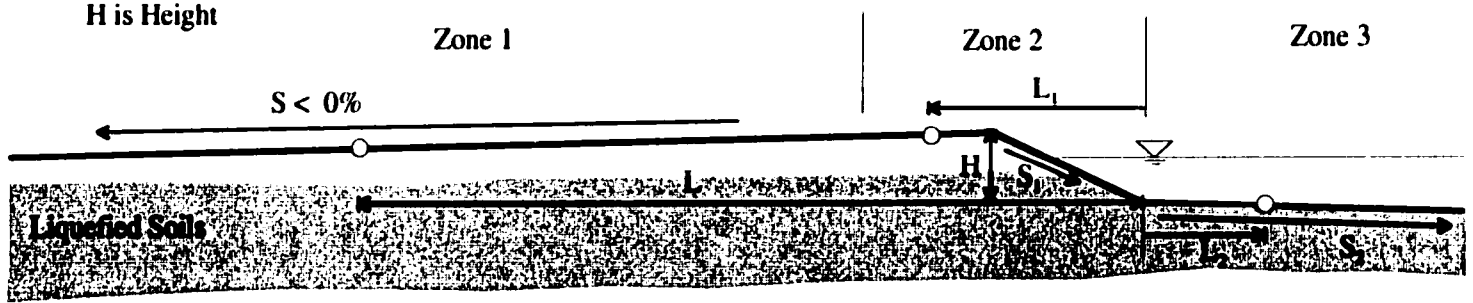
Table 9.1 Summary of the major parameters for the available case histories for gently sloping ground with a free face

Case History	Hokkaido (1993)	Wildlife (1987)	Heber Road (1979)	Niigata (1964)
References	Isoyama (1994)	Bennett et al. (1984), Dobry et al. (1992), Holzer et al. (1989), and Youd and Bartlett (1988)	Bennett et al. (1981), Dobry et al. (1992), Norton (1983), and Youd and Bennett (1983)	Bartlett (1991), Bartlett and Youd (1995), Hamada (1992), Hamada et al. (1986)
Number of LD measurements	6	5	17	32
Measured lateral displacement, LD (cm)	96 – 286	11 – 23	30 – 424	67 – 617
Liquefied soils	Silty sand with about 10% fines	Silty sand or sandy silt with 17% to 50% fines	Channel sand with 14% to 37% fines	Mainly clean, fine or medium sands
Thickness of liquefied soils (m)	4.5 – 5.5	0 – 2.7	0 – 5.3	0.6 – 18.1
Lateral displacement index, LDI (cm)	130 – 210	24 – 35	82 – 192	78 – 402
Ground slope (%)	0.7, 0.8	-0.47	1.5	-0.34 to 0.48
Free face height, H (m)	1.9 – 2.5	2.4	1.6	3.4 – 5.2
L/H	17 – 36	2.4 – 10.2	7.6 – 25	4.9 – 37.3
Moment magnitude of the earthquake, M_w	7.7	6.5	6.5	7.5
Peak surface acceleration, a_{max} (g)	0.25	0.21	0.6	0.19
Number of SPT or CPT	4 (SPT)	3 (SPT) 4 (CPT)	6 (SPT) 8 (CPT)	15 (SPT)



Note: Not to Scale
 L is Distance
 S is Slope
 H is Height

(a)



(b)

Geometric Parameters Dominating Lateral Displacement for Different Zones

L	H	S	S	S ₁	L ₁	H	S ₁	S ₂	L ₂	H
---	---	---	---	----------------	----------------	---	----------------	----------------	----------------	---

(c)

Figure 9.1 A sketch illustrating geometric parameters in different zones for gently sloping ground with a free face

(a) a positive ground slope (b) a negative ground slope (c) geometric parameters

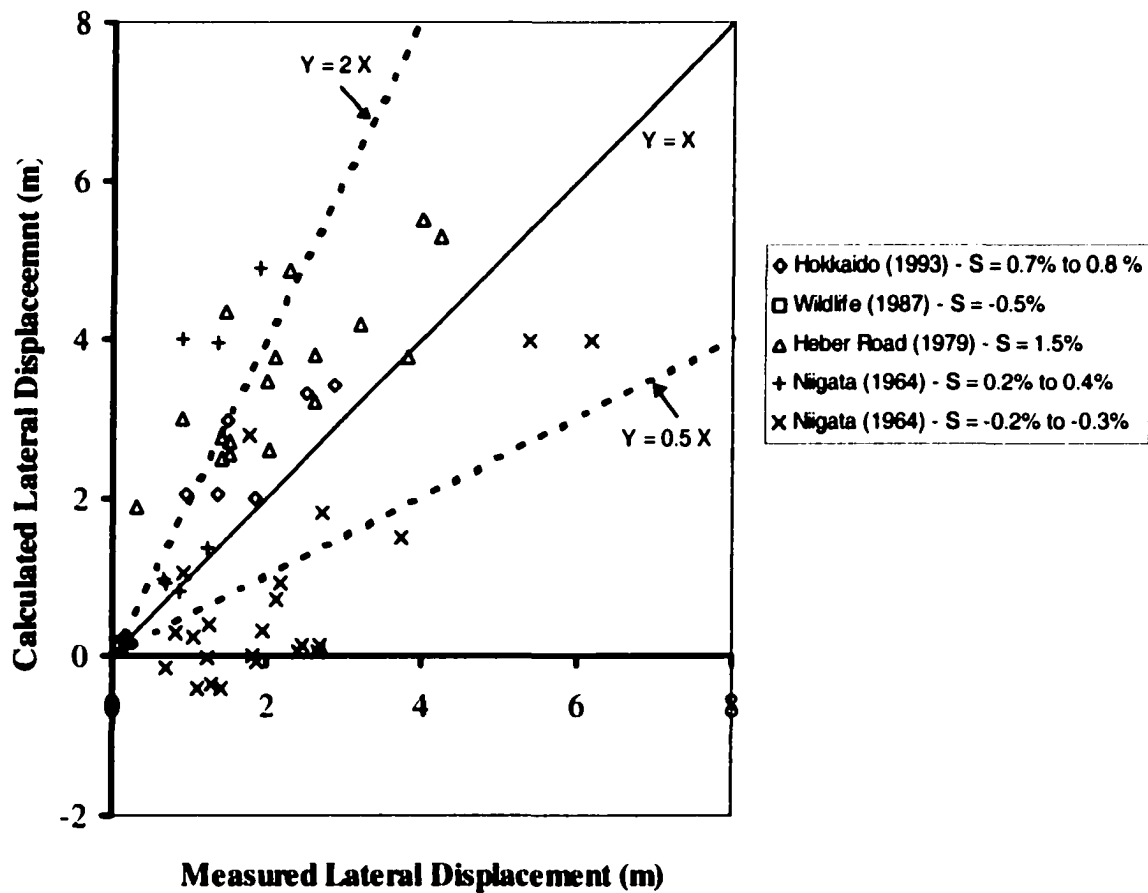


Figure 9.2 Comparison of lateral displacements measured at case history sites and calculated using the superimposition approach for gently sloping ground with a free face

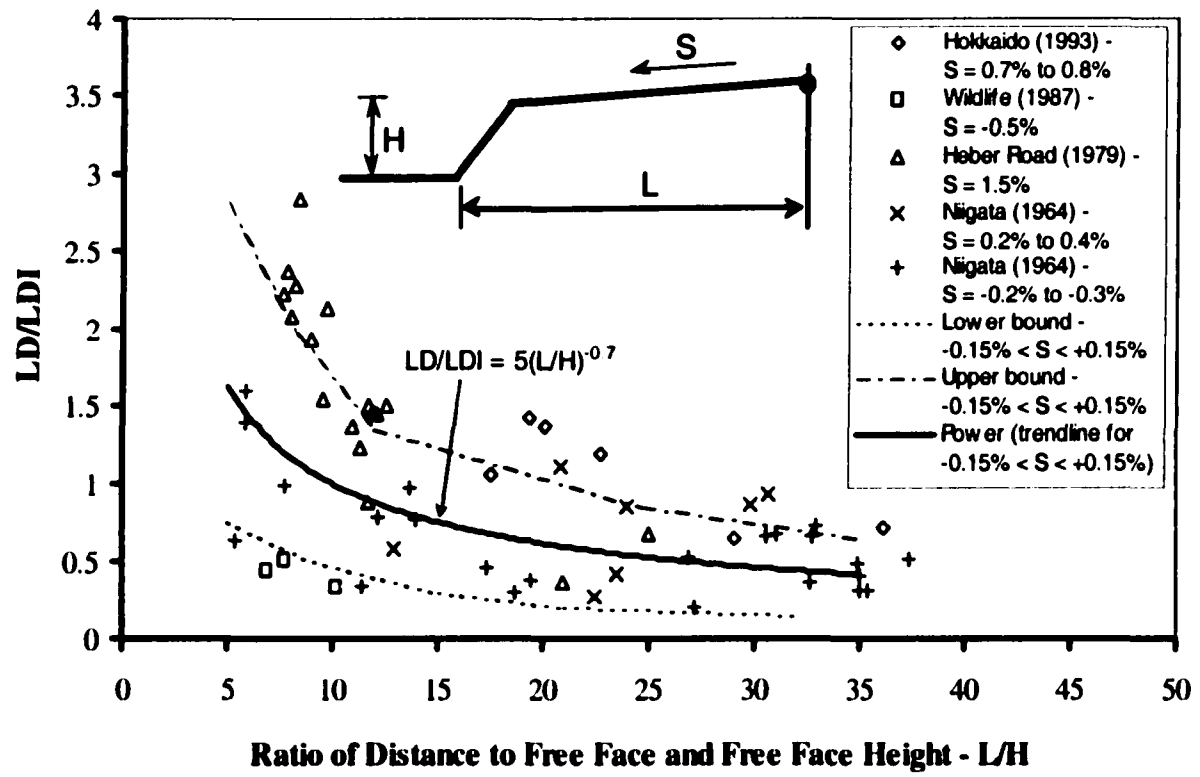


Figure 9.3 Relationship between the ratio of measured lateral displacement (LD) to the lateral displacement index (LDI) and L/H for the available four case histories for gently sloping ground with a free face

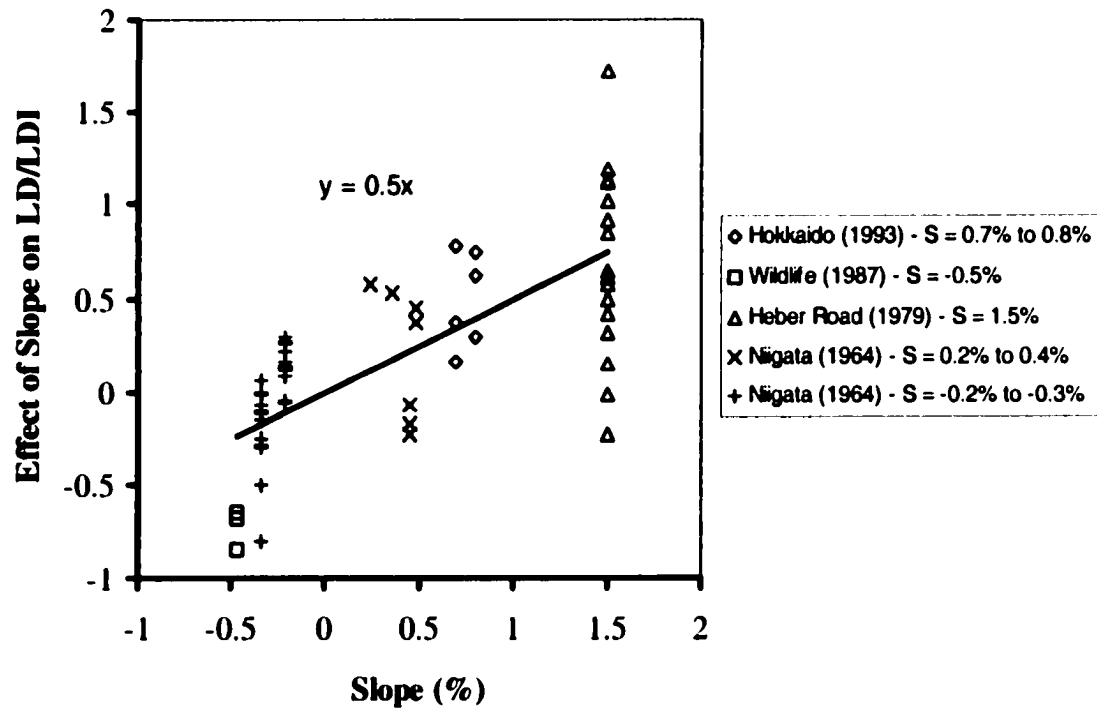


Figure 9.4 Relationship between ground slope and its effect on LD/LDI for the available four case histories for gently sloping ground with a free face

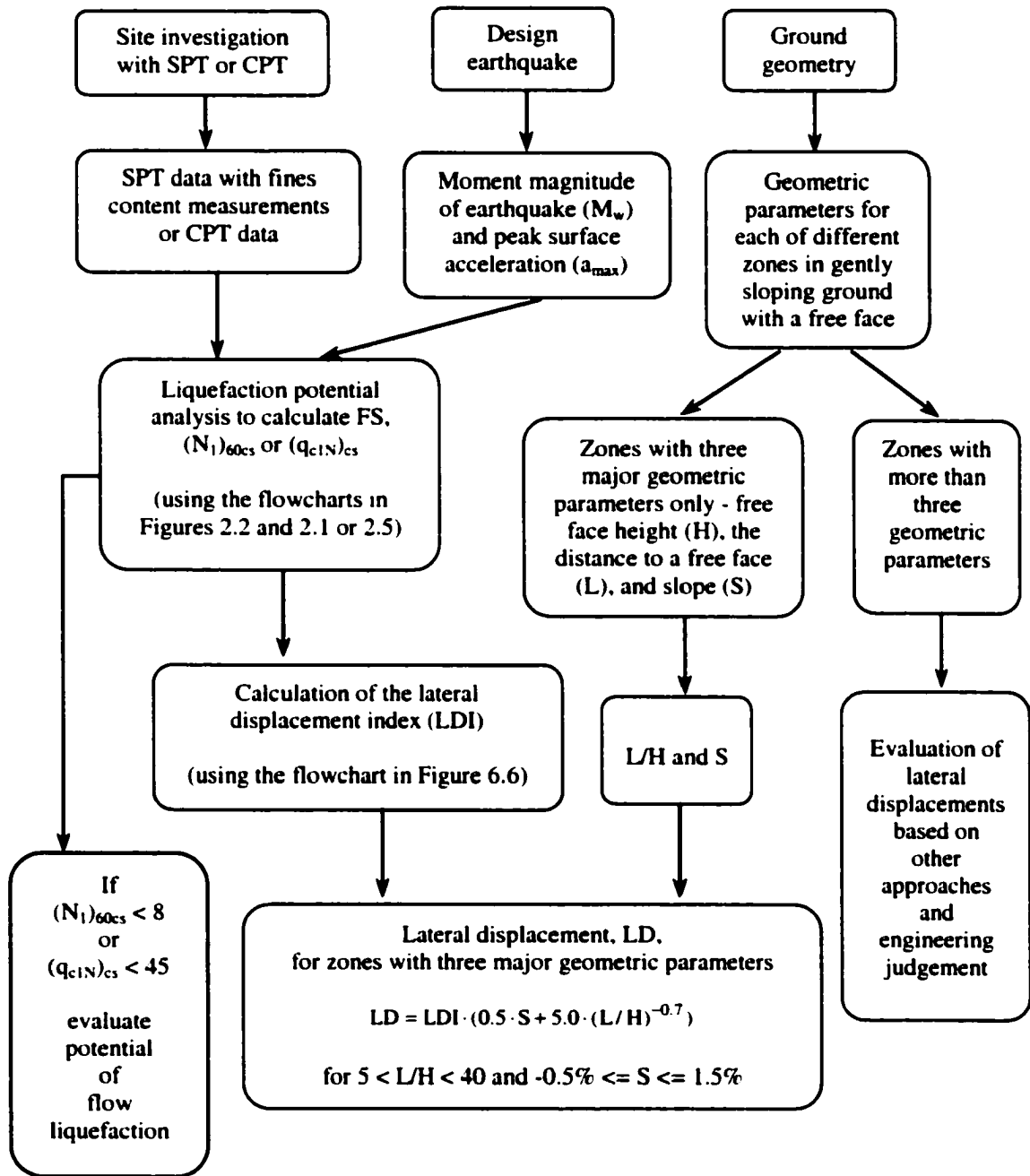


Figure 9.5 A flow chart illustrating the application of the preliminary approach to estimate lateral displacements in a liquefaction-induced lateral spread using SPT or CPT data for gently sloping ground with a free face

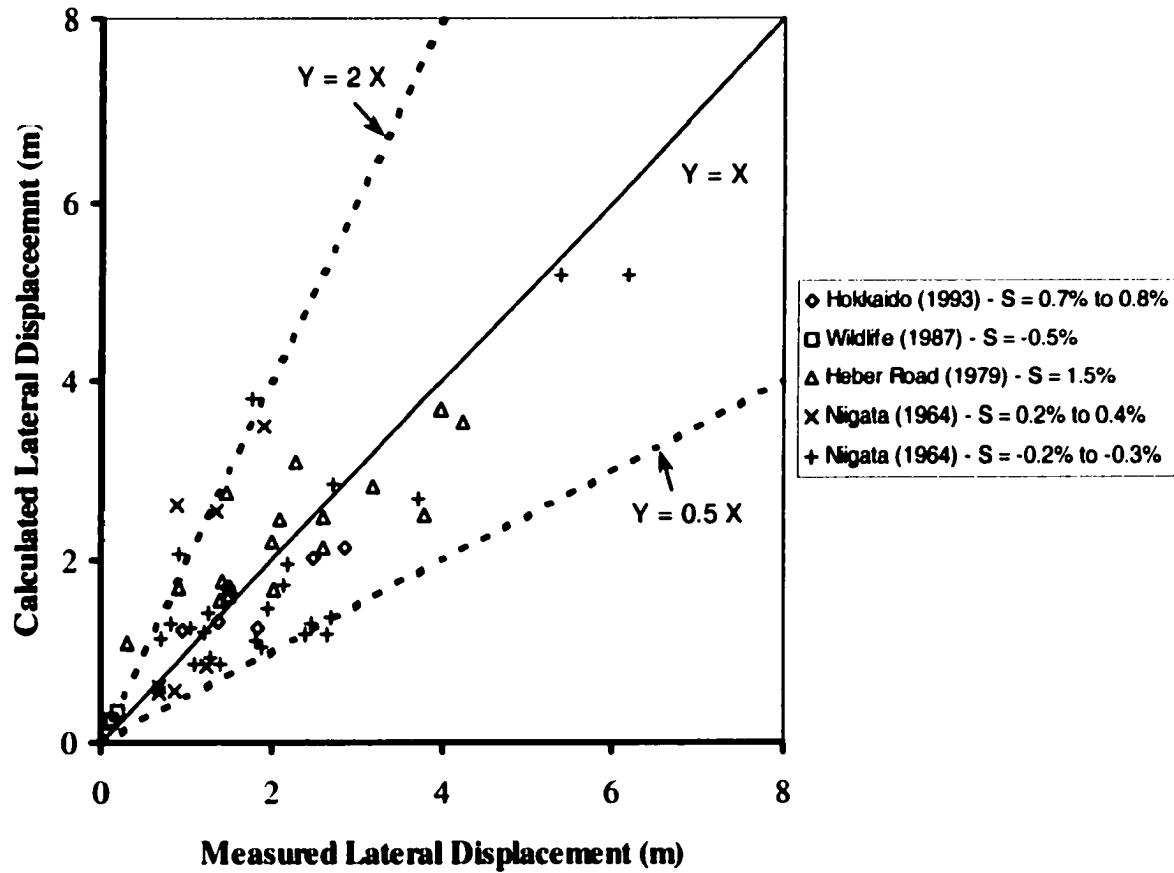


Figure 9.6 Comparison of lateral displacements measured at the available four case history sites and calculated using the preliminary approach for gently sloping ground with a free face

CHAPTER 10 GENERAL DISCUSSION AND CONCLUSIONS

10.1 Soil Liquefaction

Although earthquakes are among the most severe natural disasters, they cannot be prevented from occurring and will remain one of the world's major natural hazards. Earthquake shaking may cause a loss of strength or stiffness in a saturated sandy soil in the ground. The process leading to such loss of strength or stiffness is called soil liquefaction, and its consequences can be enormous, with significant financial and environmental implications and risks to human safety. During past major earthquakes, enormous damage to engineered structures and lifelines has been caused by liquefaction-induced ground failures

Soil liquefaction is a complex phenomenon that can be affected by a variety of factors that control either the liquefaction resistance of soils or the cyclic stresses induced by a given earthquake. A number of factors influence the liquefaction resistance of soils including soil density, soil composition and grain characteristics, in-situ stress conditions, soil structure and age, and previous strain history. The cyclic stresses induced by a given earthquake are mainly controlled by the magnitude of a given earthquake, the peak surface acceleration, and in-situ stress conditions in soils.

A number of approaches to evaluate the liquefaction potential of sandy soils have been developed over the years. In general, the most common approach used by engineers is the cyclic stress approach (e.g., Seed and Idriss 1971). Results of several field tests have been used in the cyclic stress approach to evaluate the liquefaction resistance of sandy soils. The standard penetration test (SPT) has been the most commonly used in-situ test for characterizing the liquefaction resistance of sandy soils due to its simplicity. Because of its greater repeatability and reliability and the continuous nature of its profile as

compared with other field tests, the CPT has been increasingly used in evaluating liquefaction potential for sandy soils in geotechnical practice. In this thesis, the NCEER SPT- or CPT- based methods, as summarized by Youd et al. (2001), were used to evaluate the liquefaction resistance of saturated sandy soils.

Soil liquefaction can result in both engineered structure failures and ground failures. Engineered structure failures include bearing capacity failures of buildings, the buoyant rise of buried structures, failures of retaining walls, and other structural failures caused by ground failures. Generally, liquefaction-induced ground failures include flow slides, lateral spreads, ground oscillation, ground settlements, and sand boils. The research in this thesis focused on liquefaction-induced ground settlements and lateral spreads only.

10.2 Estimation of Liquefaction-induced Ground Settlements

10.2.1 Overview

Liquefaction-induced ground settlements are essentially vertical deformations of surficial soil layers caused by the densification and compaction of loose granular soils following earthquake loading. They may occur in both level and sloping ground during an earthquake. During past major earthquakes, significant damage to engineered structures and lifelines has been caused by liquefaction-induced ground settlements.

Several methods have been proposed to estimate liquefaction-induced lateral ground displacements, including numerical models, laboratory testing approaches, and field-test-based methods. Challenges associated with sampling loose sandy soils limit the applications of numerical and laboratory testing approaches in routine practice. Field-test-based methods are likely best suited to provide simple, reliable, and direct methods to estimate liquefaction-induced ground deformations for low- to medium-risk projects and to provide preliminary estimates for high-risk projects.

To date, only an SPT-based method (Tokimatsu and Seed 1987) has been used to calculate liquefaction-induced ground settlements. A method to estimate liquefaction-induced ground settlements based on the CPT has not yet been developed even though the CPT has several advantages compared with other field tests and has been increasingly used in predicting liquefaction potential in geotechnical practice. Therefore, a simple CPT-based approach to estimate liquefaction-induced ground settlements was needed in the practice of geotechnical engineering.

10.2.2 The proposed CPT-based approach

A CPT-based approach to estimate liquefaction-induced ground settlements for sites with level ground was presented in Chapter 3. The approach combined the NCEER CPT-based method to estimate liquefaction resistance with laboratory test results on clean sand to evaluate liquefaction-induced volumetric strains for sandy and silty soils. For sites with level ground, far from any free face (e.g., river banks, seawalls), the volumetric strain of a soil is reasonably assumed to be equal or close to the vertical strain of the soil. A value obtained by integrating a vertical strain for each soil layer in a soil profile with depth is an appropriate approximation of liquefaction-induced ground settlement. Equation [10.1] is used to estimate the magnitude of liquefaction-induced ground settlements in the proposed CPT-based approach:

$$[10.1] \quad S_L = \sum_{i=1}^n \varepsilon_{v_i} \Delta z_i$$

where S_L is the calculated liquefaction-induced ground settlement at the CPT location; ε_{v_i} is the post-liquefaction volumetric strain for the soil sub-layer i ; Δz_i is the thickness of the sub-layer i ; and n is the number of soil sub-layers.

The proposed method was used to estimate liquefaction-induced ground settlements at both the Marina District and Treasure Island sites during the Loma Prieta, California, earthquake of October 17, 1989. Reasonable agreement between settlements calculated

using the proposed CPT-based method and measured at the two case history sites provided encouragement that the proposed methodology captures the dominant factors influencing liquefaction-induced ground settlements. Although further evaluations using future case history data are required, the proposed method appears to provide a satisfactory estimate of liquefaction-induced ground settlements, should be useful for low to medium risk projects and also provide preliminary estimations for higher risk projects.

A number of factors may influence the accuracy of calculated settlements in estimating liquefaction-induced ground settlements. The maximum surface acceleration at a studied site is one of the major factors. Its determination is difficult without measured values at a studied site, and rough estimates using available simple correlations often create much uncertainty concerning the estimated liquefaction-induced ground settlements. For important projects, a site specific response analysis is required to determine the maximum surface acceleration.

Fines content or mean grain size of sandy soils may affect liquefaction-induced ground settlements. However, their effects on the calculated settlements may be partially included in the proposed CPT-based approach. More studies are required to investigate these effects, and no further correction is recommended at this stage.

The effects of a transitional zone between a sandy soil and a clayey soil or the effects of thin sandy soil sandwiched between two soft clayey soil layers on cone tip resistance are evident. They may also influence the estimation of liquefaction-induced ground settlements when using CPT data. However, these effects on the calculated settlements may also be partially incorporated with the proposed CPT-based approach. More studies are required as well to quantify the effects.

Both vertical and horizontal distribution of liquefied layers at a site may play a role in ground surface settlements. Ignoring the effect of the three-dimensional distribution of liquefied layers on ground surface settlements may result in over-estimating liquefaction-induced ground settlements for some sites. Unfortunately, no reliable measure is

available to quantify this effect at this stage. Therefore, engineering judgement is needed to consider the effect in order to avoid an overly conservative design.

The NCEER CPT-based method may be conservative in evaluating liquefaction potential and estimating liquefaction-induced ground settlements for some sites where a large amount of the soils are fitted in the zone defined by $1.64 < I_c < 2.36$ and $F < 0.5$. Therefore, soil sampling with some index tests is strongly recommended to further clarify soil properties for the sites.

10.3 The Mechanisms and Controlling Factors of Liquefaction-induced Lateral Spreads

Liquefaction-induced lateral spreads are a pervasive type of liquefaction-induced ground failures for gentle slopes or on level (or gently inclined) ground with a free face (e.g., river banks, sea walls, road cuts). During past major earthquakes, enormous damage to engineered structures and lifelines has been caused by liquefaction-induced ground lateral spreads. Much research has been conducted to investigate the mechanisms and controlling factors of lateral spreads mainly by means of laboratory cyclic triaxial or simple shear tests, one g shake table tests, and dynamic geotechnical centrifuge model tests. The review of the available testing results of these tests and the studies of case histories associated with past earthquakes generally suggested the following conclusions and observations:

- Test results from one g shake table and centrifuge model tests and observations from case histories generally support the hypothesis that lateral displacements in a liquefaction-induced lateral spread result from distributed residual shear strains throughout liquefied layers. Three major components controlling the magnitude of liquefaction-induced lateral displacements are the maximum shear strains in liquefied layers, the thickness of liquefied layers, and geometric parameters characterizing

ground geometry (e.g., ground slope, free face height, and the distance to a free face) at a studied site.

- Soil properties (e.g., soil density, soil composition, grain characteristics, as well as structure and age), earthquake characteristics (e.g., earthquake magnitude, the distance to seismic energy or fault rupture, peak horizontal ground acceleration, the duration of strong motion), and ground geometry are three of the most important factors influencing liquefaction-induced ground lateral spreads.
- Several other factors may influence liquefaction-induced lateral displacements as well. The restraint on shear strain due to soil dilative response at large strain may lead to a strong restraining effect on the magnitude of cyclic and accumulated residual shear strains of soils in a lateral spread. Seismic acceleration of a soil layer in level ground or gentle slopes (less than 5%) may be reduced due to the liquefaction of the underlying loose soil layers. This reduction of acceleration may limit resultant lateral displacements in a liquefaction-induced lateral spread. Both boundaries and the three-dimensional distribution of liquefied layers may have an effect on lateral displacements in lateral spreads. The effect will be on a case-by-case basis. Redistribution (including the development of a water film beneath a low permeability layer) and drainage of excess pore pressures in liquefied layers during earthquakes may also play some role in a lateral spread. However, it is very difficult to quantify their effects.

Liquefaction-induced lateral spreading under seismic loading is a complicated phenomenon. Its mechanisms and controlling factors have not been fully understood currently and more studies are needed.

10.4 Previous Research on Estimating Liquefaction-induced Lateral Displacements

Several groups of methods have been proposed to estimate liquefaction-induced ground

lateral displacements, including laboratory modeling approaches, numerical and analytical analyses, and field-data-based methods.

Laboratory-scale models built on conventional shake-tables and geotechnical centrifuges are useful in exploring the mechanics of liquefaction-induced failures. However, laboratory-scale models are unsatisfactory in providing fully realistic models of lateral spreading and are seldom directly used to estimate liquefaction-induced lateral displacements in geotechnical design.

Several simplified analytical methods have been used to estimate liquefaction-induced ground deformations. The major limitation for the modified Newmark's (1965) sliding block analytical approaches is the assumption that the soils in a lateral spread move laterally as a rigid block along a well-defined failure plane. However, field observations in combination with laboratory-scale tests did not support this assumption. The analytical model of Towhata et al. (1999) shows promise for providing useful predictions of the maximum or ultimate displacements. However, because liquefied soils are assumed to behave as a liquid with zero shear strength in this model, the model generally overestimates lateral displacements in a liquefaction-induced lateral spread. The residual shear strain charts proposed by Shamoto et al. (1998) did not relate to static shear stresses or field ground geometry. These charts cannot be directly used to estimate lateral displacements in a lateral spread even though these charts may be applied to give a possible estimation of the maximum lateral displacement at the waterfront for level ground with a free face.

Several models for stress-deformation analysis using finite element techniques have been used to calculate displacements in a lateral spread. Reliability of the predictions using these models mainly depends on two major aspects: (1) a rigorous and relevant constitutive model and (2) appropriate input data for the analysis. However, first, the expense and difficulty associated with obtaining and testing high quality samples of loose sandy soils and the need for accurately and repetitively measuring many uncommon material constants for stress-deformation analyses using a rigorous constitutive model

significantly limit the applications of numerical methods. Second, the general inadequacy of the available rigorous numerical models for estimating liquefaction-induced deformations has been recently demonstrated (Manzari et al. 1994).

Due to the complicated nature of liquefaction-induced lateral spreads, several available field-data-based empirical models (Hamada et al. 1986; Youd and Perkins 1987; Bartlett and Youd 1995; Youd et al. 1999; Rauch and Martin 2000) have shown advantages for estimating post-liquefaction deformations because of their simplicity and the fact that they are based on field observations. It is difficult to choose one empirical model over another since they all seem to give results correct to within a factor of two or three. Generally, both Hamada's model and Youd and Perkins' model characterize only partial factors that control the magnitude of lateral spreading displacements and therefore are useful only to specific geological regions and earthquakes. Rauch and Martin's SPT-based model is a useful tool for predicting average horizontal movements on a potential lateral spread. It is believed that Bartlett and Youd's SPT-based model is more satisfying since it takes into account all the major factors that control lateral displacements. The SPT-based model of Youd et al (1999) may be the best of the available empirical models to estimate lateral displacements in a liquefaction-induced lateral spread at this stage even though it still has some limitations.

These field-data-based models are empirical and do not incorporate the extensive knowledge gained from laboratory studies of soil liquefaction. No CPT-based method to estimate liquefaction-induced lateral displacements is currently available even though the CPT has greater repeatability and reliability and provides a continuous profile compared with other field tests. Therefore, it was suggested that simple semi-empirical approaches be developed for estimating liquefaction-induced lateral displacements using SPT or CPT data on the basis of laboratory testing results and case history data.

10.5 Estimation of Liquefaction-induced Lateral Displacements Using SPT or CPT Data

10.5.1 The proposed approaches for estimating liquefaction-induced lateral displacements using SPT or CPT data

Based mainly on laboratory test results, the SPT/CPT-based procedures were developed to estimate the maximum shear strains of sandy or silty soils during undrained seismic loading in Chapter 6. A new parameter, defined as the lateral displacement index (LDI), was then introduced. This parameter is a value calculated by integrating the maximum shear strains with depth based on either SPT- or CPT-based procedures.

The lateral displacement index incorporates two of the three components dominating the magnitude of liquefaction-induced lateral displacements: the thickness of liquefied layers and the maximum shear strains in liquefied layers. This index also embodies the effects of both soil properties and earthquake characteristics on liquefaction-induced lateral spreads. Therefore, the index is a good indicator of the lateral displacement potential for a given ground geometry.

The three major components influencing the magnitude of liquefaction-induced lateral displacements are the thickness of liquefied layers, the maximum shear strains in liquefied layers, and geometric parameters characterizing ground geometry. The thickness of liquefied layers and the maximum shear strains in liquefied layers have been incorporated into one parameter – the lateral displacement index (LDI). Therefore, the magnitude of liquefaction-induced lateral displacements is primarily controlled by the lateral displacement index (LDI) and the major geometric parameters characterizing ground geometry. This implies that a general correlation may exist between the LDI, the magnitude of lateral displacement (LD), and the major geometric parameters.

Lateral spreads occur either on gentle slopes ranging from 0.3 to 5 percent or on level (or gently inclined) ground with a free face (e.g., river banks, sea walls, road cuts). In this

research, ground geometry associated with lateral spreads was divided into three categories: gently sloping ground without a free face, level ground with a free face, and gently sloping ground with a free face. Ground slope (S) was used as a major geometric parameter characterizing ground geometry for gently sloping ground without a free face in this research. Both the distance to a free face (L) and free face height (H) were adopted as the major geometric parameters to characterize ground geometry for level ground with a free face. Ground slope, L, and H were used for gently sloping ground with a free face.

Case history data concerning lateral spreads that occurred during past major earthquakes provide a good opportunity to establish the correlation between the LDI, the magnitude of lateral displacement (LD), and the major geometric parameters. In this research, a total of sixteen case histories associated with thirteen past major earthquakes were studied. The data from six, six, and four of all the case histories were used to develop the correlations for gently sloping ground without a free face, level ground with a free face, and gently sloping ground with a free face respectively.

Based on the established correlations between LD, LDI, and major geometric parameters, three approaches were proposed to estimate the magnitude of liquefaction-induced lateral displacements for gently sloping ground without a free face, level ground with a free face, and gently sloping ground with a free face respectively. The following equations are used to estimate the magnitude of lateral displacements in the proposed approaches:

for gently sloping ground without a free face,

$$[10.2a] \quad LD = (S + 0.2) \cdot LDI \quad (\text{for } 0.2\% < S < 3.5\%)$$

for level ground with a free face,

$$[10.2b] \quad LD = 5 \cdot \left(\frac{L}{H} \right)^{-0.7} \cdot LDI \quad (\text{for } 5 < L/H < 40)$$

for gently sloping ground with a free face,

$$\begin{aligned} [10.2c] \quad LD &= LDI \cdot (0.5 \cdot S + 5.0 \cdot (L/H)^{-0.7}) \\ &\text{(for } 5 < L/H < 40 \text{ and } -0.5\% \leq S \leq 1.5\%) \end{aligned}$$

where S is ground slope in percentage, L is the distance to a free face in meters, H is free face height in meters, LDI is the lateral displacement index in centimeters, and LD is lateral displacement in centimeters

10.5.2 Performance of the proposed approaches

Given the complexity of liquefaction-induced lateral spreads, considerable variations in magnitude and distribution of lateral displacements are expected. Generally, about 90% of the calculated lateral displacements using the proposed approaches showed variations between 50% and 200% of measured values for the available case histories studied in this research. Therefore, the proposed approaches could underestimate or overestimate liquefaction-induced lateral displacements by up to a factor of two.

Preliminary comparisons of calculated and measured lateral displacements for two case histories indicated that the accuracy of the proposed approaches was generally similar to that of the MLR model of Youd et al. (1999) for estimating lateral displacements for gently sloping ground without a free face or level ground with a free face for the studied cases. Further evaluations are required using data from new case histories before a general conclusion can be made.

10.5.3 Advantages of the proposed approaches

Compared with available field-data-based empirical methods (including the MLR model of Youd et al. (1999)), the proposed approaches have the following advantages.

The first distinct advantage is that the distribution of lateral displacement with depth below the ground surface can be obtained from the proposed approaches. The variation of lateral displacements with depth at a given location can be reasonably assumed to be similar to the variation of the lateral displacement index with depth. This profile may be valuable for the design of underground structures (e.g., pipelines) and foundations (e.g., piles).

Soil properties and soil profiles can be better characterized by the proposed approach. For instance, an individual value for each of measured fines contents is used in the proposed method while a single average value of fines contents for all the sandy soils that have a normalized SPT N value of less than 15 is assigned to an SPT profile in the MLR model of Youd et al. (1999). In addition, earthquake characteristics can be better characterized by the proposed approach because of using site specific peak surface acceleration.

The proposed approaches combine available results from laboratory tests with data from case histories associated with past major earthquakes, capture the mechanisms of liquefaction-induced lateral spreads, and characterize the major factors influencing lateral displacements. Either SPT or CPT data can be used in the proposed approaches to estimate lateral displacements. The proposed approaches can be applied to obtain estimates of both the magnitude and distribution of liquefaction-induced lateral displacements for gently sloping ground without a free face, level ground with a free face, and gently sloping ground with a free face. The proposed approaches are quite simple and can be applied with only a few additional calculations following the NCEER SPT- or CPT-based liquefaction-potential analysis.

10.5.4 Limitations of the proposed approaches

As discussed in Section 10.5.2, the calculated lateral displacements using the proposed approaches generally showed variations between 50% and 200% of measured values for the available case histories studied in this research. Therefore, the proposed approaches

could underestimate or overestimate liquefaction-induced lateral displacements by up to a factor of two.

The proposed approach mainly characterizes the effects of soil profile and properties, earthquake characteristics, and ground geometry on liquefaction-induced lateral displacements. Other factors that may also influence lateral displacements as discussed in Chapter 4, such as the redistribution and drainage of excess pore pressures in the ground, are not quantified in the current approach and would need to be evaluated on a case-by-case basis.

The proposed approaches were developed using the limited data from the available case histories. As a result, the proposed approaches are applicable only for similar earthquakes and ground conditions, as summarized in Tables 7.1, 8.1 and 9.1. The case history data used for developing the proposed approaches, especially the approach for gently sloping ground without a free face, were dominantly from two Japanese case histories associated with the 1964 Niigata and 1983 Nihonkai-Chubu earthquakes, where the liquefied soils were mainly clean sand only. The values for the geometric parameters used in developing each of the proposed approaches were within limited ranges, as specified in Equations [10.2a], [10.2b], and [10.2c]. Therefore, it is not recommended that the approaches be applied when the values of the geometric parameters go beyond the specified ranges.

In-situ CPT data were available only for five of the sixteen case histories studied in this thesis. In developing the proposed approaches using CPT data, the equivalent CPT data that were converted from SPT data were used to assist in establishing the correlations between LD, LDI, and the major geometric parameters. This procedure might add some uncertainties to the proposed approaches for using CPT data. Therefore, additional case history data, especially with CPT data, are required to evaluate the proposed approaches.

Lateral displacements in some zones of a lateral spread are affected not only by the selected major geometric parameters that were used in the proposed approaches but also

by other geometric parameters that were not considered in the proposed approaches. These zones have been specified in Sections 7.2.2 and 8.2.2. The lateral displacements in these zones cannot be directly calculated using the proposed approaches.

10.5.5 Application of the proposed approaches

The applications of the proposed approaches have been discussed in detail in Sections 7.6, 8.5, and 9.5 and illustrated in the flowcharts in Figures 7.10, 8.7, and 9.5 for the three categories of ground geometry. A general summary is given below.

The proposed approaches may be used to estimate liquefaction-induced lateral displacements in level or gently sloping ground with or without a free face for low to medium-risk projects or to preliminarily evaluate liquefaction-induced lateral displacements in the ground for high-risk projects. However, caution and engineering judgement must be exercised because liquefaction-induced ground lateral spreading is a complicated phenomenon and a number of assumptions and simplifications were involved in developing the proposed approaches.

As discussed in Section 10.5.4, the proposed approaches are applicable only for similar earthquakes and ground conditions, as summarized in Tables 7.1, 8.1 and 9.1. Furthermore, it is not recommended that the proposed approaches be applied when the values of the geometric parameters are beyond the ranges specified in Equations [10.2a], [10.2b], and [10.2c].

Lateral displacements in some zones of a lateral spread are affected not only by the geometric parameters that were used in the proposed approaches but also by other geometric parameters that were not considered in the proposed approaches. These zones have been specified in Sections 7.2.2 and 8.2.2. The lateral displacements in these zones cannot be directly calculated using the proposed approaches.

It should be emphasized that engineered structures (e.g., quay walls, retaining walls, piles, tanks, or pipe lines) in the ground may restrict lateral movements of the ground and change the lateral displacement patterns in a liquefaction-induced lateral spread. The proposed approaches were developed using data for the case history sites in which engineered structures have little or no effect on lateral spreading of the ground. Therefore, it is expected that the proposed approaches may over-estimate lateral displacements at sites where engineered structures pose significant restrictions to ground movements.

Caution should be exercised when a substantial zone of soils with a low $(N_1)_{60cs}$ or $(q_{c1N})_{cs}$ is encountered during liquefaction potential analysis. For such cases, more extensive investigation should be made and other approaches should be taken to evaluate the potential for flow failure of the soil, especially when the static shear stresses in the ground are relatively high. Deformations caused by flow failures can be much larger than those by lateral spreads, and their estimation is beyond the scope of this research.

The studies of the Juvenile Hall case history indicated that the method for calculating LDI using the NCEER CPT-based method and in-situ CPT data may under-estimate LDI for soils with a high fines content (greater than about 55%) and low clay content (less than about 15%) because soils with an I_c greater than 2.6 are generally assumed as to be non-liquefiable for the NCEER CPT-based method. As suggested by Robertson and Wride (1997,1998), samples should be obtained for soils with an I_c of equal to or greater than 2.6, and their liquefaction potential should be evaluated using other criteria, such as the Chinese criteria. As a result, LDI should be calculated based on the results of liquefaction potential analyses for all the soils in a soil profile with an I_c either greater or less than 2.6.

10.6 Recommendations for Future Work

Further evaluations of the proposed CPT-based approach for estimating liquefaction-

induced ground settlements are required using more data from new case histories. In addition, several other factors such as boundaries and the three-dimensional distribution of liquefied layers may also influence ground settlements but were not considered in the current proposed approach. More research is also needed to investigate quantitatively the effects of these factors on liquefaction-induced ground settlements.

Several factors (including boundaries and three-dimensional distribution of liquefied layers, redistribution and drainage of excess pore pressures in a lateral spread, isolation of acceleration due to liquefaction of underlying soil layers) may also influence liquefaction-induced lateral displacements, as discussed in Chapter 4. However, they were not quantified in the current proposed approaches. More research is needed to investigate quantitatively the effects of these factors on liquefaction-induced lateral displacements and to better quantify lateral displacements.

The proposed approaches for estimating liquefaction-induced lateral displacements were developed using the limited data from limited case histories and as such are applicable only for similar earthquakes and ground conditions. In-situ CPT data were available only for five of all the sixteen case histories studied in this thesis. In developing the proposed approaches for using CPT data, the equivalent CPT data that were converted from SPT data were used to assist in establishing the correlations between LD, LDI, and the major geometric parameters. This procedure has posed some uncertainties to the proposed approaches for using CPT data. Therefore, additional case history data, especially with CPT data, are required to evaluate the proposed approaches.

The proposed approaches for estimating lateral displacements were developed based on data with limited ranges. More data from new case histories are needed to update the proposed approaches and to expand the existing ranges for the geometric parameters.

References

- Abdoun, T.H. 1997. Modeling of seismically induced lateral spreading of multi-layered soil and its effect on pile foundations. Ph.D. thesis, the Rensselaer Polytechnic Institute, May.
- Aki, K. 1988. Local site effects on strong ground motion. *In Proceedings, Earthquake Engineering and Soil Dynamics II - Recent Advances in Ground Motion Evaluation*, ASCE, Geotechnical Special Publication No. 20, pp. 103-155.
- Ambraseys, N.N. 1988. Engineering Seismology. *Earthquake Engineering and Structural Dynamics*, Vol. 17, pp. 1-105.
- Arango, I. 1996. Magnitude scaling factors for soil liquefaction evaluations. *Journal of Geotechnical Engineering*, ASCE, 122(11): 929-936.
- Arulanandan, K., and Scott, R. (Ed.) 1993. Verification of Numerical Procedures for the Analysis of Soil Liquefaction Problems, Vol. 1 and 2, Balkema, Rotterdam.
- Arulmoli, K., Muraleetharan, K.K., Hossain, M.M., and Fruth, L.S. 1992. VELACS-verification of liquefaction analyses by centrifuge studies , laboratory testing program, soil data report. The Earth Technology Corporation, Project No. 90-0562, March.
- Bardet, J.P., and Kapuskar, M. 1991. Site investigation of the Marina District of San Francisco in September 1990. Report to the National Science Foundation, University of Southern California, February, p. 94.
- Bardet, J.P., Kapuskar, M., Martin, G.R., and Proubet, J. 1992. Site-response analyses. The Loma Prieta, California, Earthquake of October 17, 1989 - Marina District, U. S. Geological Survey Professional Paper 1551-F, pp. F85-F114.
- Bartlett, S.F. 1991. Empirical analysis of horizontal ground displacement generated by liquefaction-induced lateral spreads. Ph.D. Thesis, Brigham Young University, August.
- Bartlett, S.F., and Youd, T.L. 1992. Case histories of lateral spreads caused by the 1964 Alaska Earthquake. Case Studies of Liquefaction and Lifelines Performance during Past Earthquakes: Technical Report NCEER-92-0002, Vol.2, National Center for

- Earthquake Engineering Research, State University of New York at Buffalo, N.Y.
- Bartlett, S.F., and Youd, T.L. 1995. Empirical prediction of liquefaction-induced lateral spread. *Journal of Geotechnical Engineering, ASCE*, **121(4)**: 316-328.
- Baziar, M.H. 1991. Engineering evaluation of permanent ground deformations due to seismically-induced liquefaction. Ph.D. thesis, Rensselaer Polytechnic Institute, Troy, New York.
- Begemann, H.K.S.Ph. 1969. The Dutch static penetration test with the adhesion jacket cone. *LGM Mefefelingen*, **12 (4)**: 69-100.
- Bennett, M.J. 1989. Liquefaction analysis of the 1971 ground failure at the San Fernando Valley Juvenile Hall, California. *Bulletin of the Association of Engineering Geologists*, Vol. XXVI, No. 2, pp. 209-226.
- Bennett, M.J. 1990. Ground deformation and liquefaction of soil in the Marina District. Effects of the Loma Prieta Earthquake on the Marina District, San Francisco, California, U.S. Geological Survey Open-File Report 90-253, pp. D1-D36.
- Bennett, M.J. 1998. Sand boils and settlement on Treasure Island after the earthquake. The Loma Prieta, California, Earthquake of October 17, 1989 - Liquefaction, U. S. Geological Survey Professional Paper 1551-B, pp. B121-B128.
- Bennett, M.J., McLaughlin, P.V., Sarmiento, J.S., and Youd, T.L. 1984. Geotechnical investigation of liquefaction sites, Imperial Valley, California. U.S. Geological Survey, Menlo Park, California 94025, Open-File Report 84-252, p.103.
- Bennett, M.J., Youd, T.L., Harp, E.L., and Wieczorek, G.F. 1981. Subsurface investigation of liquefaction, Imperial Valley Earthquake, California, October 15, 1979. U.S. Geological Survey, Menlo Park, California, 94025, Open-File Report 81-502, p.83.
- Berg, P. van den. 1994. Analysis of soil penetration. Delft University Press, the Netherlands, p. 175.
- Boatwright, J., Seekins, L.C., Fumal, T.E., Liu, H.P., and Mueller, C.S. 1992. Ground-motion amplification. The Loma Prieta, California, Earthquake of October 17, 1989 - Marina District, U. S. Geological Survey Professional Paper 1551-F, pp. F35- F49.
- Bonilla, M.G. 1992. Geologic and historical factors affecting earthquake damage. The Loma Prieta, California, Earthquake of October 17, 1989 - Marina District, U. S.

Geological Survey Professional Paper 1551-F.

- Boulanger, R.W., Idriss, I.M., and Mejia, L.H. 1995. Investigation and evaluation of liquefaction related ground displacements at Moss Landing during the 1989 Loma Prieta earthquake. Department of Civil & environmental Engineering, University of California at Davis, report No. UCD/CGM-95/02.
- Boulanger, R.W., Mejia, L.H., and Idriss, I.M. 1997. Liquefaction at Moss Landing during Loma Prieta earthquake. *Journal of Geotechnical and Geoenvironmental Engineering, ASCE*, **123**(5): 453-468.
- Byrne, P.M. 1991. A model for predicting liquefaction induced displacement. *In Proceedings of the Second International Conference on Recent Advances in Geotechnical Earthquake Engineering and Soil Dynamics, March, St. Louis, Missouri, Vol. 2, pp. 1027-1035.*
- Bray, J.D., Augello, A.J., Leonards, G.A., Repetto, P.C., and Byrne, R.J. 1995. Seismic stability procedures for solid-waste landfills. *Journal of Geotechnical Engineering, ASCE*, **121**(2): 139-151.
- Byrne, P.M., Jitno, H., and Salgado, F. 1992. Earthquake induced displacements of soil-structures systems. *In Proceedings of the tenth World Conference on Earthquake Engineering, A.A. Balkema, Rotterdam, the Netherlands, pp. 1407-1412.*
- Campanella, R.G., Davies, M.P., Boyd, T.J., and Everard, J.L. 1994. Geoenvironmental subsurface site characterization using in-situ soil testing methods. *In Proceedings of the 1st International Congress on Environmental Geotechnics, Edmonton, Alberta.*
- Campanella, R.G., and Robertson, P.K. 1988. Current status of the piezocone test. *In Proceedings of the International Symposium on Penetration Testing, ISOPT-1, Orlando, 1, 93-116, Balkema Publication, Rotterdam.*
- Casagrande, A. 1975. Liquefaction and cyclic deformation of sands: a critical review. *The Fifth Panamerican Conference on Soil Mechanics and Foundation Engineering, Buenos Aires, Argentina, pp.81-131.*
- Castro, G. 1987. On the behavior of soils during earthquakes - liquefaction. *Developments in Geotechnical Engineering 42, Soil Dynamics and Liquefaction, ed. A. S. Cakmak, Department of Civil Engineering, Princeton University, pp. 169-204.*
- Chugh, A.K. 2000. An examination of simplified earthquake-induced displacement

- procedures for earth structures: discussion. *Canadian Geotechnical Journal*, **37**: 729-730.
- Clayton, C.R.I., Matthews, M.C., and Simons, N.E. 1995. *Site investigation*. Second Edition, Blackwell Science Ltd.
- De Alba, P., Seed, H.B., and Chan, C.K. 1976. Sand liquefaction in large-scale simple shear tests. *Journal of the Geotechnical Engineering Division, ASCE*, **102**(GT9): 909-927.
- Dobry, R., and Abdoun, T. 1998. Post-triggering response of liquefied sand in the free field and near foundations. *Geotechnical Earthquake Engineering and Soil Dynamics III, Geotechnical Special Publication No.75, ASCE, Vol. 1, Seattle, Washington, August 3-6, pp. 270-293.*
- Dobry, R., and Baziar, M.H. 1992. Modeling of lateral spreads in silty sands by sliding soil blocks. *Stability and Performance of Slopes and Embankments-II, Geotechnical Special Publication No. 31, Berkeley, California, June 29 - July 1, Vol. 1, pp. 625-652.*
- Dobry, R., Baziar, M.H., O'Rourke, T.D., Roth, B.L., and Youd, T.L. 1992. Liquefaction and ground failure in the Imperial Valley, Southern California, during the 1979, 1981 and 1987 earthquakes. *Case Studies of Liquefaction and Lifeline Performance during Past Earthquakes, Vol. 2, Technical Report NCEER-92-0002, February 17, pp. 4-1 - 4-84.*
- Dobry, R., Ladd, R.S., Yokel, F.Y., Chung, R.M., and Powell, D. 1982. Prediction of pore water pressure buildup and liquefaction of sands during earthquakes by the cyclic strain method. *NBS Building Science Series 138, National Bureau of Standards, Gaithersburg, Maryland, 150p.*
- Doi, M., and Hamada, M. 1992. A summary of case studies on liquefaction-induced ground displacements. *In Proceedings of the fourth U.S. - Japan Workshop on Earthquake Resistant Design of Lifeline Facilities and Countermeasures against Soil Liquefaction, Technical Report NCEER-92-0019, M. Hamada and T. D. O'Rourke (eds.), August 12, pp. 115 - 129.*
- Egan, J.A., and Wang, Z.L. 1991. Liquefaction-related ground deformation and effects on facilities at Treasure Island, San Francisco, during the 17 October 1989 Loma

- Prieta Earthquake. *In Proceedings of the Third Japan-U.S. Workshop on Earthquake Resistant Design of Lifeline Facilities and Countermeasures for Soil Liquefaction*, Tech. Report NCEER-91-0001, pp.57-76.
- Ejiri, J., Sawada, S., Goto, Y., and Toki, K. 1996. Peak ground motion characteristics. *Special Issue on Geotechnical Aspects of the January 17 1995 Hyogoken-Nambu Earthquake*, *Soils and Foundations*, January, pp. 7 – 14.
- Elgamal, A., Dobry, R., Parra, E., and Yang, Z. 1998. Soil dilation and shear deformations during liquefaction. *In Proceedings: Fourth International Conference on Case Histories in Geotechnical Engineering*, St. Louis, Missouri, March 9-12, pp. 1238-1259.
- Elgamal, A., Yang, Z., Parra, E., and Dobry, R. 1999. Modeling of liquefaction-induced shear deformation. *In Proceedings of the Second International Conference on Earthquake Geotechnical Engineering*, Lisboa, Portugal, 21-25, June, Vol. 3, pp.895-900.
- Elgamal, A., Zeghal, M., Taboada, V., and Dobry, R. 1996. Analysis of site liquefaction and lateral spreading using centrifuge records. *Soils and Foundations*, **36**(2): 111-121.
- Fear, C.E. 1996. In-situ testing for liquefaction evaluation of sandy soils. Ph.D. Thesis, University of Alberta.
- Fiegel, G.L., and Kutter, B.L. 1994a. Liquefaction mechanism for layered soils. *Journal of Geotechnical Engineering*, ASCE, **120**(4): 737-735.
- Fiegel, G.L., and Kutter, B.L. 1994b. Liquefaction-induced lateral spreading of mildly sloping ground. *Journal of Geotechnical Engineering*, **120**(12): 2236-2243.
- Finn, W.D.L. 1981. Liquefaction potential: developments since 1976. *In Proceeding of the First International Conference on Recent Advances in Geotechnical Earthquake Engineering and Soil Dynamics*, St. Louis, MO, Vol. 1, pp.655-681.
- Finn, W.D.L. 1990. Analysis of post-liquefaction deformations in soil structures. H. Bolton Seed, Memorial Symposium Proceedings, May, Editor J. M. Duncan, Vol. 2, pp. 291-312.
- Finn, W.D.L. 1991. Assessment of liquefaction potential and post-liquefaction behavior of earth structures: developments 1981 – 1991 (state-of-the-art paper). *In*

- Proceedings, 2nd International Conference on Recent Advances in Geotechnical Earthquake Engineering and Soil Dynamics, St. Louis, Missouri, Vol. 3, pp. 1833-1850.
- Finn, W.D.L. 1995. The evolution of geotechnical earthquake engineering practice in North America: 1954-1994. *In* Proceedings: Third International Conference on Recent Advances in Geotechnical Earthquake Engineering and Soil Dynamics, April 2-7, Vol. 2, St. Louis, Missouri, pp.881-908.
- Finn, W.D.L., Lee, K.W., and Martin, G.R. 1977. An effective stress model for liquefaction. *Journal of the Geotechnical Engineering Division, ASCE*, **103**(GT6): 517 – 533.
- Franklin, A.G., and Chang, F.K. 1977. Earthquake resistance of earth and rock-fill dams: permanent displacements of earth embankments by Newmark sliding block analysis. Miscellaneous Paper S-71-17, Report 5, U. S. Army Engineer Waterways Experiment Station, Vicksburg, Miss.
- Gilstrap, S.D. 1998. CPT based liquefaction resistance analyses evaluated using case histories. Master of Science Thesis, Department of Civil Environmental Engineering, Brigham Young University, Technical Report CEG-98-01, July.
- Glaser, S.D. 1994. Estimation of surface displacements due to earthquake excitation of saturated sands. *Earthquake Spectra, Earthquake Engineering Research Institute (EERI)*, Vol. 10, No. 3, August, pp. 489 - 517.
- Gu, W.H., Morgenstern, N.R., and Robertson, P.K. 1993. Progressive failure of the Lower San Fernando Dam. *Journal of Geotechnical Engineering, ASCE*, **119**(2): 333 - 349.
- Gu, W.H., Morgenstern, N.R., and Robertson, P.K. 1994. Post-earthquake deformation analysis of wildlife site. *Journal of Geotechnical Engineering, ASCE*, **120**(2): 274 - 289.
- Hamada, M. 1992a. Large ground deformations and their effects on lifelines: 1964 Niigata earthquake. *Case Studies of Liquefaction and Lifeline Performance During Past Earthquake*, Vol. 1, Technical Report NCEER-92-0001, National Center for Earthquake Engineering Research, Buffalo, NY, pp. 3-1 – 3-123.
- Hamada, M. 1992b. Large ground deformations and their effects on lifelines: 1983

- Nihonkai-Chubu earthquake. Case Studies of Liquefaction and Lifeline Performance During Past Earthquake, Vol. 1, Technical Report NCEER-92-0001, National Center for Earthquake Engineering Research, Buffalo, NY, pp. 4-1 – 4-85.
- Hamada, M., Isoyama, R., and Wakamatsu, K. 1995. The Hyogoken-Nambu (Kobe) Earthquake, Liquefaction, Ground Displacement and Soil Condition in Hanshin Area. Monograph, Association for Development of Earthquake Prediction, School of Science and Engineering, Waseda University and Japan Engineering Consultants, Ltd., 194 p.
- Hamada, M., and O'Rourke, T.D. 1992. Case studies of liquefaction and lifeline performance during past earthquakes. Volume 1, Japanese Case Studies, Technical Report NCEER-92-0001, National Center for Earthquake Engineering Research, Buffalo, NY.
- Hamada, M., Towhata, I., Yasuda, S., and Isoyama, R. 1987. Study of permanent ground displacement induced by seismic liquefaction. *Computers and Geotechnics*, 4(4): 197-220.
- Hamada, M., Wakamatsu, K., and Yasuda, S. 1992a. Liquefaction-induced ground deformation during the 1923 Kanto earthquake. Case Studies of Liquefaction and Lifeline Performance During Past Earthquakes, Vol. 1, Technical Report NCEER-92-0001, National Center for Earthquake Engineering Research, Buffalo, NY.
- Hamada, M., Yasuda, S., Isoyama, R., and Emoto, K. 1986. Study on liquefaction induced permanent ground displacements. Association for the Department of Earthquake Prediction in Japan, Tokyo, Japan, p. 87.
- Hamada, M., Yasuda, S., and Wakamatsu, K. 1992b. Large ground deformations and their effects on lifelines: 1948 Fukui earthquake. Case Studies of Liquefaction and Lifeline Performance During Past Earthquakes, Vol. 1, Technical Report NCEER-92-0001, National Center for Earthquake Engineering Research, Buffalo, NY.
- Hansen, W.R., Eckel, E.B., Schaem, R.E., Lyle, W.G., Chance, G. 1966. The Alaska earthquake, March 27, 1964: field investigations and reconstruction effort. U.S.G.S. Professional Paper 541, Government Printing Office, Washington, D.C., 111 p.
- Harder, L.F., and Boulanger, R. 1997. Application of K_{σ} and K_{α} correction factors. *In* Proceedings of the NCEER Workshop on Evaluation of Liquefaction Resistance of

- Soils, Edited by T. L. Youd and I. M. Idriss, Technical Report NCEER-97-0022, Salt Lake, Utah, December 31, pp. 167-190.
- Harder, L.F., and Seed, H.B. 1986. Determination of penetration resistance for coarse-grained soils using the Becker hammer drill. Report UCB/EERC-86/06, Earthquake Engineering Research Center, University of California, Berkeley, 126 p.
- Holzer, T.L., and O'Rourke, T.D. 1990. Effects of the Loma Prieta earthquake on the Marina District, San Francisco, California. U.S. Geological Survey, Open-file report 90-253.
- Holzer, T.L., Youd, T.L., and Bennett, M.J. 1989. In situ measurement of pore pressure build up during liquefaction. *In Proceedings of the 20th Joint Meeting of the U.S. - Japan Cooperative Program in the National Resources, Panel on Wind and Seismic Effects*, U.S. Department of Commerce.
- Houston, S.L., Houston, W.N., and Padilla, J.M. 1987. Microcomputer-aided evaluation of earthquake-induced permanent slope displacements. *Microcomputers in Civil Engineering*, 2 (3): 207 – 222.
- Hryciw, R.D. 1991. Post Loma Prieta earthquake CPT, DMT and shear wave velocity investigations of liquefaction sites in Santa Cruz and on Treasure Island. Final Report to the U. S. Geological Survey, Award No. 14-08-0001-G1865, December.
- Hryciw, R.D., Rollins, K.M., and Homolka, M. 1991. Soil amplification at Treasure Island during the Loma Prieta earthquake. *In Proceedings: Second International Conference on Recent Advances in Geotechnical Earthquake Engineering and Soil dynamics*, March 11-15, St. Louis, Missouri, pp. 1679-1685.
- Idriss, I.M. 1990. Response of soft soil sites during earthquakes. *In Proceedings H. B. Seed Memorial Symp.*, Vol. 2, BiTech Publishers, Vancouver, BC, May, pp.273-289.
- Inagaki, H., Iai, S., Sugano, T., Yamazaki, H., and Inatomi, T. 1996. Performance of caisson type quay walls at Kobe Port. *Special Issue on Geotechnical Aspects of the January 17 1995 Hyogoken-Nambu Earthquake*, Soils and Foundations, January, pp. 119 – 136.
- Ishihara, K. 1985. Stability of natural deposits during earthquakes. *In Proceedings of the Eleventh International Conference on Soil Mechanics and Foundation Engineering*, San Francisco, 12-16, August, pp. 321-376.

- Ishihara, K. 1996. Soil behaviour in earthquake geotechnics. Oxford Science Publications.
- Ishihara, K., Acacio, A., and Towhata, I. 1993. Liquefaction-induced ground damage in Dagupan in the July 16, 1990 Luzon earthquake. *Soils and Foundations*, **33**(1): 133 - 154.
- Ishihara, K., Yoshida, K., and Kato, M. 1996. Ground deformation characteristics caused by lateral spreading during the 1995 Hanshin-Awaji Earthquake. *In Proceedings of the Sixth Japan-U.S. Workshop on Earthquake Resistant Design of Lifeline Facilities and Countermeasures for Soil Liquefaction*, Tech. Report NCEER-96-0012, pp.221-242.
- Ishihara, K., and Yoshimine, M. 1992. Evaluation of settlements in sand deposits following liquefaction during earthquakes. *Soils and Foundations*, **32**(1): 173-188.
- Isoyama, R. 1994. Liquefaction-induced ground failures and displacements along the Shiribeshi-toshibetsu River caused by the 1993 Hokkaido-nansei-oki earthquake. *In Proceedings from the Fifth U.S.-Japan Workshop on Earthquake Resistant Design of Lifeline Facilities and Countermeasures Against Soil Liquefaction*, September 29 - October 1, Snowbird, Utah, Technical Report NCEER-94-0026.
- Iwasaki, Y., and Tai, M. 1996. Strong motion records at Kobe Port Island. Special Issue on Geotechnical Aspects of the January 17 1995 Hyogoken-Nambu Earthquake, *Soils and Foundations*, January, pp. 29 – 40.
- Iwasaki, T., Tatsuoka, F., Tokida, K., and Yasuda, S. 1978. A practical method for assessing soil liquefaction potential based on case studies at various sites in Japan. *In Proceeding of the Second International Conference of Microzonation*, San Francisco, CA, Vol. 2, pp.885-896.
- Jamiolkowski, M., Ladd, C.C., Germaine, J.T., and Lancellotta, R. 1985. New developments in field and laboratory testing of soils. *In Proceedings of the Eleventh International Conference on Soil Mechanics and Foundation Engineering*, San Francisco, 12-16 August, Vol. 1, pp. 57-153.
- Jamiolkowski, M. and LoPresti, D.C.F. 1992. Discussion on “Correlation between liquefaction resistance and shear wave velocity.” By K. Tokimatsu and A. Uchida, *Soils and Foundations*, **32**(2): 145 – 148.

- Jefferies, M.G. 1999. A critical view of liquefaction. *Physics and Mechanics of Soil Liquefaction*, Balkema, Rotterdam, pp. 221 – 235.
- Jibson, R.W. 1993. Predicting earthquake-induced landslide displacements using Newmark's sliding block analysis. *Transportation Research Record No. 1411*, Transportation Research Board (TRB), Washington, D.C., pp. 9 - 17.
- Jing, L., Wang, S., and Zhang, R. 1996. Study on mechanism of ground lateral deformation induced by liquefaction (in Chinese). *Earthquake Engineering and Engineering Vibration*, **16**(3): 128-136.
- Joyner, W.B., and Boore, D.M. 1988. Measurement, characterization and prediction of strong ground motion. *Earthquake Engineering and Soil Dynamics II, Recent Advances in Ground Motion Evaluation*, ASCE, No. 20, pp. 43 - 102.
- Juang, C.H., Chen, C.J., and Tien, Y.M. 1999a. Appraising CPT-based liquefaction resistance evaluation methods – artificial neural network approach. *Canadian Geotechnical Journal*, **36**(3): 443-454.
- Juang, C.H., Rosowsky, D.V., and Tang, W.H. 1999b. Reliability-based method for assessing liquefaction potential of soils. *Journal of Geotechnical and Geoenvironmental Engineering*, ASCE, **125**(8): 684-689.
- Kanamori, H. 1978. Quantification of earthquake. *Nature*, Vol. 271, pp. 411-414.
- Kanatani, M., Nishi, K., and Touma, J. 1995. Large shake table tests of saturated sand layer and numerical simulations by nonlinear analysis method. *First International Conference on Earthquake Geotechnical Engineering*, Vol. 2, Kenji Ishihara (Editor), A. A. Balkema/Rotterdam/Brookfield, pp. 705-710.
- Kawasumi, H. 1968. Introduction to Niigata Earthquake of 1964. *General Report on the Niigata Earthquake of 1964*, Published by Tokyo Electrical Engineering College Press, 2-2 Nishiki-cho, Kanda, Chiyoda-ku, Tokyo, Japan, pp. 1 - 6.
- Kayen, R.E., and Mitchell, J.K. 1997. Assessment of liquefaction potential during earthquakes by Arias intensity. *Journal of Geotechnical and Geoenvironmental Engineering*, ASCE, **123**(12): 1162 – 1174.
- Kimura, M. 1996. Damage statistics. *Special Issue on Geotechnical Aspects of the January 17 1995 Hyogoken-Nambu Earthquake*, *Soils and Foundations*, January, pp. 1 – 6.

- Ko, H. Y. 1994. Modeling seismic problems in centrifuges. Centrifuge 94, Leung, Lee & Tan (eds), Balkema, Rotterdam, pp. 3 – 12.
- Koga, Y. and Matsuo, O. 1990. Shaking table tests of embankments resting on liquefiable sandy ground. *Soils and Foundations*, **30**(4): 162 – 174.
- Kokusho, T. 1999. Water film in liquefied sand and its effect on lateral spread. *Journal of Geotechnical and Geoenvironmental Engineering*, **125**(10): 817 -826.
- Kramer, S.L. 1996. *Geotechnical Earthquake Engineering*. Prentice-Hall, Inc., 653 p.
- Kramer, S.L., and Smith, M.W. 1997. Modified Newmark model for seismic displacements of compliant slopes. *Journal of Geotechnical and Geoenvironmental Engineering*, **123** (7).
- Krinitzsky, E.L., Chang, F.K., and Nuttli, O.W. 1988. Magnitude-related earthquake ground motions. *Bul. Assoc. of Engrg. Geologists*, **25**(4): 399 – 423.
- Kulhawy, F.H., and Mayne, P.W. 1991. Relative density, SPT and CPT interrelations. *In Proceedings of the First International Symposium on Calibration Chamber Testing, ISCCCT1, Potsdam, New York, 28-29 June*, pp. 197-211.
- Law, K.T. 1990. Geotechnical aspects. The 1989 Loma Prieta (San Francisco Area) Earthquake: Site Visit Report, Internal Report No. 594, National Research Council Canada, May, pp. 9-20.
- Lee, F.H., and Schofield, A.N. 1988. Centrifuge modelling of sand embankments and islands in earthquakes. *Geotechnique*, **38** (1): 45 – 58.
- Lee, K.L., and Albaisa, A. 1974. Earthquake induced settlements in saturated sands. *Journal of Geotechnical Engineering, ASCE*, **100**(GT4): 387-406.
- Lemos, L.J.L., and Coelho, P.A.L.F. 1991. Displacements of slopes under earthquake loading. *In Proceedings of 2nd Conference Recent Advances in Geotechnical Earthquake Engineering and Soil Dynamics, St. Louis, Missouri*.
- Lin, J.S., and Whitman, R.V. 1983. Decoupling approximation to the evaluation of earthquake-induced plastic slip in earth dams. *Earthquake Engineering and Structure Dynamics*, Vol. 11, pp. 667 – 678.
- Lin, J.S., and Whitman, R.V. 1986. Earthquake induced displacements of sliding blocks. *Journal of Geotechnical Engineering*, **112**(1): 44 – 59.
- Liu, H., and Qiao, T. 1984. Liquefaction potential of saturated sand deposits underlying

- foundation of structure. *In Proceedings, 8th World Conference on Earthquake Engineering, San Francisco, Vol. 3, pp. 199 – 206.*
- Lunne, T., Robertson, P.K., and Powell, J.J.M. 1997. *Cone Penetration Testing in Geotechnical Practice. Blackie Academic & Professional, London, UK.*
- Makdisi, F.I., and Seed, H.B. 1978. *Simplified procedure for estimating dam and embankment earthquake-induced deformations. Journal of Geotechnical Engineering, ASCE, Vol. 104, No. GT7, July.*
- Manzari, M.T., Arulanandan, K., and Scott, R.F. 1994. *VELACS project: a summary of achievements. In Proceedings, 5th U. S.-Japan Workshop on Earthquake Resistant Design of Lifeline Facilities and Countermeasures against Soil Liquefaction, Technical Report NCEER-94-0026, T. D. O'Rourke and M. Hamada (eds.), November, pp. 389 – 404.*
- Marchetti, S. 1982. *Detection of liquefiable sand layers by means of quasi-static penetration tests. In Proceedings, 2nd European Symposium on Penetration Testing, Amsterdam, Vol. 2, pp. 458 – 482.*
- Matasovic, N, Kavazanjian, E., and Yan, L. 1997. *Newmark deformation analysis with degrading yield acceleration. In Proceedings of Geosynthetics '97, Long Beach, California.*
- McCulloch, D.S., and Bonilla, M.G. 1970. *Effects of the earthquake of March 27, 1964, on the Alaska railroad, U. S. Geological Survey Professional Paper 545-D, 161p.*
- Mejia, M.J. 1998. *Liquefaction at Moss Landing. The Loma Prieta, California, Earthquake of October 17, 1989 - Liquefaction, U. S. Geological Survey Professional Paper 1551-B, pp. B129-B150.*
- Meyerhof, G.G. 1957. *Discussion on research on determining the density of sands. In Proceedings of 4th International Conference of Soil Mechanics and Foundation Engineering, London, Vol. 3, pp. 110.*
- Miyajima, M., Kitaura, M., and Ando, K. 1991. *Experiments on liquefaction-induced large ground deformation. In Proceedings, Third Japan-U.S. Workshop on Earthquake Resistant Design of Lifeline Facilities and Countermeasures for Soil Liquefaction, San Francisco, CA, T. D. O'Rourke and M. Hamada (eds.), National Center for Earthquake Engineering Research, SUNY-Buffalo, pp. 269-278.*

- Mulilis, J.P., Chan, C.K., and Seed, H.B. 1975. The Effects of Method of Sample Preparation on the Cyclic Stress-Strain Behavior of Sands. Report No. EERC 75-18, Earthquake Engineering Research Center, University of California, Berkeley, California, July.
- Nagase, H., and Ishihara, K. 1988. Liquefaction-induced compaction and settlement of sand during earthquakes. *Soils and Foundations*, **28**(1): 65-76.
- National Research Council (NRC) 1982. Earthquake engineering research - 1982, overview and recommendations. Report by The Committee on Earthquake Engineering, National Research Council, National Academy Press. Washington, DC.
- NCEER 1997. Proceeding of the NCEER Workshop on Evaluation of Liquefaction Resistance of Soils, Edited by Youd, T. L., and Idriss, I. M., Technical Report NCEER-97-0022, Salt Lake City, Utah, Decemeber 31, 1997.
- Newmark, N.M. 1965. Effects of earthquakes on dams and embankments. *Geotechnique*, **15**(2): 139-160.
- Norton, W.E. 1983. In situ determination of liquefaction potential using the PQS probe. Technical Report GL-83-15, Geotechnical Laboratory, U. S. Army Engineer Waterways Experiment Station, Vicksburg, Miss., September, 44p.
- Olsen, R.S., and Malone, P.G. 1988. Soil classification and site characterization using the cone penetrometer test. International Symposium on Cone Penetration Testing, CPT'95, Linkoping, Sweden, Vol. 2, pp. 887-893.
- Olsen, R.S., and Mitchell, J.K. 1995. CPT stress normalization and prediction of soil classification. *In* Proceedings of the International Symposium on cone Penetrometer Testing – CPT'95, Linkoping, Sweden, October.
- O'Rourke, T.D., Beaujon, P.A., and Scawthorn, C.R. 1992a. Large ground deformations and their effects on lifeline facilities: 1906 San Francisco earthquake. Case Studies of Liquefaction and Lifeline Performance During Past Earthquakes, Vol. 2, Technical Report NCEER-92-0002, National Center for Earthquake Engineering Research, Buffalo, NY.
- O'Rourke, T.D., Gowdy, T.E., Stewart, H.E., and Pease, J.W. 1991. Lifeline performance and ground deformation in the Marina During 1989 Loma Prieta Earthquake. *In* Proceedings of the Third Japan-U.S. Workshop on Earthquake

- Resistant Design of Lifeline Facilities and Countermeasures for Soil Liquefaction, Tech. Report NCEER-91-0001, pp.129-146.**
- O'Rourke, T.D., and Hamada, M. 1992. Case studies of liquefaction and lifeline performance during past earthquakes. Volume 2, United States Case Studies, Technical Report NCEER-92-0002, National Center for Earthquake Engineering Research, Buffalo, NY.**
- O'Rourke, T.D., and Lane, P.A. 1989. Liquefaction hazards and their effects on buried pipelines. Technical Report NCEER-89-0007, National Center for Earthquake Engineering Research, Buffalo, NY, February.**
- O'Rourke, T.D., and Pease, J.W. 1992. Large ground deformations and their effects on lifeline facilities: 1989 Loma Prieta Earthquake. Case Studies of Liquefaction and Lifeline Performance during Past Earthquakes, Vol. 2: United States case studies Ed. By O'Rourke and Hamada, Technical report NCEER-92-0002, Feb. 17, pp. 5-1 – 5-79.**
- O'Rourke, T.D., and Pease, J.W. 1997. Mapping liquefaction layer thickness for seismic hazard assessment. Journal of Geotechnical and Geoenvironmental Engineering, ASCE, 123(1): 46-56.**
- O'Rourke, T.D., Roth, B.L., and Hamada, M. 1992b. Large ground deformations and their effects on lifeline facilities: 1971 San Fernando earthquake. Case Studies of Liquefaction and Lifeline Performance During Past Earthquakes, Vol. 2, Technical Report NCEER-92-0002, National Center for Earthquake Engineering Research, Buffalo, NY.**
- Parra, E. 1996. Numerical modeling of liquefaction and lateral ground deformation including cyclic mobility and dilative behavior in soil systems. Ph.D. dissertation, Department of Civil Engineering, Rensselaer Polytechnic Institute.**
- Peacock, W.H., and Seed, H.B. 1968. Sand liquefaction under cyclic loading simple shear conditions. Journal of Soil Mechanics and Foundations Division, ASCE, 94(SM3): 689-708.**
- Pease, J.W., and Bureau, G. 1998. Influence of site geometry on dynamic liquefaction displacements. Geotechnical Earthquake Engineering and Soil Dynamics III, Geotechnical Special Publication No. 75, Vol. 1, pp.726-738.**

- Pease, J.W., and O'Rourke, T.D. 1993. Liquefaction hazards in the Mission District and South of Market areas, San Francisco, California. Liquefaction and Ground Failure in San Francisco: Site Investigation, Modeling, and Hazard Assessment for the Urban Environment, Grant No. 14-08-0001-G2128, Cornell University.
- Pease, J.W., and O'Rourke, T.D. 1998. Liquefaction hazards in the Mission District and South of Market area, San Francisco. The Loma Prieta, California, Earthquake of October 17, 1989 - liquefaction, U.S. Geological Survey Professional Paper 1551-B, pp. B25 - B60.
- Poulos, S.J., Castro, G., and France, J.W. 1985. Liquefaction evaluation procedure. *Journal of Geotechnical Engineering, ASCE*, **111**(6): 772 – 792.
- Power, M.S., Egan, J.A., Shewbridge, S.E., deBacker, J., and Faris, J.R. 1998. Analysis of liquefaction-induced damage on Treasure Island. The Loma Prieta, California, Earthquake of October 17, 1989 - Liquefaction, U. S. Geological Survey Professional Paper 1551-B, pp. B87-B120.
- Prevost, J.H. 1981. DYNAFLOW: a nonlinear transient finite element analysis program. Department of Civil Engineering, Princeton University, Princeton, New Jersey.
- Prevost, J.H. 1985. A simple plasticity theory for frictional cohesionless soils. *Soil Dynamics and Earthquake Engineering*, **4**(1): 9 – 17.
- Rauch, A.F. 1997. EPOLLS: an empirical method for predicting surface displacements due to liquefaction-induced lateral spreading in earthquakes. Ph.D. thesis, Virginia Polytechnic Institute and State University, Blacksburg, Virginia, May.
- Rauch, A.F., and Martin, J.R. 2000. EPOLLS model for predicting average displacements on lateral spreads. *Journal of Geotechnical and Geoenvironmental Engineering, ASCE*, **126**(4): 360-371.
- Robertson, P.K. 1990. Soil classification using the CPT. *Canadian Geotechnical Journal*, **27**(1): 151-158.
- Robertson, P.K. 1994. Suggested terminology for liquefaction. 47th Canadian Geotechnical Conference, September 21-23, Halifax, Nova Scotia, pp. 277-286.
- Robertson, P.K. 1998. Cone penetration testing geotechnical applications guide. Produced by ConeTec Inc. & Gregg In Situ Inc., Second Edition, October.
- Robertson, P.K., Campanella, R.G., and Wightman, A. 1983. SPT-CPT correlations.

- Journal of Geotechnical Engineering, **109**(11): 1449-1459.
- Robertson, P.K., and Campanella, R.G. 1985. Liquefaction potential of sands using the cone penetration test. *Journal of Geotechnical Engineering, ASCE*, **22**(3): 298-307.
- Robertson, P.K., and Campanella, R.G. 1986. Estimating liquefaction potential of sands using the flat dilatometer. *Geotechnical Testing Journal, ASTM*, **9**(1): 38 – 40.
- Robertson, P.K., and Fear, C.E. 1995. Liquefaction of sands and its evaluation. *In Proceedings, IS Tokyo '95, 1st International Conference on Earthquake Geotechnical Engineering, Keynote Lecture.*
- Robertson, P.K., and Wride, C.E. 1997. Cyclic liquefaction and its evaluation based on the SPT and CPT. *In Proceedings of the NCEER Workshop on Evaluation of Liquefaction Resistance of Soils, Edited by T. L. Youd and I. M. Idriss, Technical Report NCEER-97-0022, Salt Lake, Utah, December 31, pp. 41-87.*
- Robertson, P.K., and Wride C.E. 1998. Evaluating cyclic liquefaction potential using the CPT. *Canadian Geotechnical Journal*, **35**(3): 442-459.
- Rollins, K.M., and McHood, M.D. 1998. Comparison of computed and measured liquefaction-induced settlements in the Marina District, San Francisco. *The Loma Prieta, California, Earthquake of October 17, 1989 - Liquefaction, U. S. Geological Survey Professional Paper 1551-B, pp. B223-B240.*
- Sanglerat, G. 1972. *The penetrometer and soil exploration.* Elsevier Scientific Publishing Company, Amsterdam-Oxford-New York.
- Sarma, S.K. 1975. Seismic stability of earth dams and embankments. *Geotechnique*, **25** (4).
- Sasaki, Y., Tokida, K., Matsumoto, H., and Saya, Y. 1991. Shake table tests on lateral ground flow induced by soil liquefaction. *In Proceedings, Third Japan-U.S. Workshop on Earthquake Resistant Design of Lifeline Facilities and Countermeasures for Soil Liquefaction, San Francisco, CA, T. D. O'Rourke and M. Hamada (eds.), National Center for Earthquake Engineering Research, SUNY-Buffalo, pp. 371-385.*
- Sasaki, Y., Towhata, I., Tokida, K., Yamada, K., Matsumoto, H., Tamari, Y., and Saya, S. 1992. Mechanism of permanent displacement of ground caused by seismic liquefaction. *Soils and Foundations*, **32**(3): 79-96.

- Seed, H.B. 1976. Evaluation of soil liquefaction effects on level ground during earthquakes. *Liquefaction Problems in Geotechnical Engineering*, ASCE Annual Convention, Philadelphia, Sep. 27- Oct. 1, pp. 1-104.
- Seed, H.B. 1979a. Soil liquefaction and cyclic mobility evaluation for level ground during earthquakes. *Journal of Geotechnical Engineering Division*, ASCE, **105**(GT2): 201-255.
- Seed, H.B. 1979b. Considerations in the earthquake-resistant design of earth and rockfill dams. 19th Rankine Lecture of the British Geotechnical Society, *Geotechnique*, Vol. XXIX, No. 3, September, pp. 215-263.
- Seed, H.B. 1983. Earthquake resistant design of earth dams. *Symposium on Seismic Design of Earth Dams and Caverns*, ASCE, New York, pp. 41 – 64.
- Seed, R.B., Dickenson, S., and Mok, C.M. 1994. Site effects on strong shaking and seismic risk: recent developments and their impact on seismic design codes and practice. *Structural Congress XII*, Vol. 1, ASCE, New York, pp.573-578.
- Seed, R.B., and Harder, L.F. 1990. SPT-based analysis of cyclic pore pressure generation and undrained residual strength. *In Proceedings H. B. Seed Memorial Symp.*, Vol. 2, BiTech Publishers, Vancouver, BC, May, pp.351-376.
- Seed, H.B., and Idriss, I.M. 1971. Simplified procedure for evaluation soil liquefaction potential. *Journal of the Soil Mechanics and Foundations Division*, ASCE, **97**(SM9): 1249-1273.
- Seed, H.B., and Idriss, I.M. 1982. Ground motions and soil liquefaction during earthquakes. *Earthquake Engineering Research Institute*, 134p.
- Seed, H.B., Idriss, I.M., and Arango, I. 1983. Evaluation of liquefaction potential using field performance data. *Journal of Geotechnical Engineering*, ASCE, **109**(3): 458 – 482.
- Seed, H.B., and Lee, K.L. 1966. Liquefaction of saturated sands during cyclic loading. *Journal of the Soil Mechanics and Foundations Division*, ASCE, **92**(SM6): 105 – 134.
- Seed, H.B., Lee, K.L., Idriss, I.M., and Makdisi, F.I. 1975. The slides in the San Fernando dams during the earthquake of February 9, 1971. *Journal of Geotechnical Engineering Division*, ASCE, **101**(GT7).

- Seed, H.B., Tokimatsu, K., Harder, L.F., and Chung, R.M. 1985. Influence of SPT procedures in soil liquefaction resistance evaluations. *Journal of Geotechnical Engineering*, **111**(12): 1425-
- Shamoto, Y., Sato, M., and Zhang, J.M. 1996. Simplified estimation of earthquake-induced settlements in saturated sand deposits. *Soils and Foundations*, **36**(1): 39-50.
- Shamoto, Y., Zhang, J.M., and Goto, S. 1997. Mechanism of large post-liquefaction deformation in saturated sand. *Soils and Foundations*, **37**(2): 71-80.
- Shamoto, Y., Zhang, J., and Tokimatsu, K. 1998. New charts for predicting large residual post-liquefaction ground deformation. *Soil Dynamics and Earthquake Engineering*, Vol. 17, pp. 427-438.
- Skempton, A.K. 1986. Standard penetration test procedures and the effects in sands of overburden pressure, relative density, particle size, aging and overconsolidation. *Geotechnique*, **36**(3): 425 – 447.
- Stark, T.D., and Mesri, G. 1992. Undrained shear strength of liquefied sands for stability analysis. *Journal of Geotechnical Engineering*, **118**(11): 1727-1747.
- Stokoe, K.H., Roesset, J.M., Bierschwale, J.G., and Aouad, M. 1988. Liquefaction potential of sands from shear wave velocity. *In Proceedings, 9th World Conference on Earthquake Engineering*, Tokyo, Vol. 3, pp. 213 - 218.
- Taboada, V. 1995. Centrifuge modeling of earthquake-induced lateral spreading in sand using a laminar box. Ph.D. thesis, Department of Civil Engineering, Rensselaer Polytechnic Institute, Troy, N.Y.
- Taboada, V.M., Abdoun, T., and Dobry, R. 1996. Prediction of liquefaction-induced lateral spreading by dilatant sliding block model calibrated by centrifuge tests. *Proc. 11th World Conference on Earthquake Engineering*, Acapulco, Mexico, Paper No. 1037.
- Taboada, V.M., and Dobry, R. 1998. Centrifuge modeling of earthquake-induced lateral spreading in sand. *Journal of Geotechnical and Geoenvironmental Engineering*, ASCE, **124**(12): 1195-1206.
- Tan, C.K., and Duncan, J.M. 1991. Settlement of footings on sands-accuracy and reliability, in *Geotechnical Engineering Congress*, Boulder, Colo., 1991, *Proceedings: American Society of Civil Engineerings Special Publication 27*, V. 1, pp. 446-455.

- Tatsuoka, F., Iwasaki, T., Tokida, K., Yasuda, S., Hirose, M., Imai, T., and Kon-no, M. 1980. Standard penetration tests and soil liquefaction potential evaluation. *Soils and Foundations, JSSMFE*, **20**(4): 95-111.
- Tatsuoka, F., Toki, S., Miura, S., Kato, H., Okamoto, M., Yamada, S., Yasuda, S., and Tanizawa, F. 1986. Some factors affecting cyclic undrained triaxial strength of sand. *Soils and Foundations*, **26**(3): 99-116.
- Tatsuoka, F., Zhou, S., Sato, T., and Shibuya, S. 1990. Method of evaluating liquefaction potential and its application. *Seismic Hazards in the Soil Deposits in Urban Areas*, pp. 75-109 (in Japanese)
- Taylor, H.T., Cameron, J.T., Vahdani, S., and Yap, H. 1992. Behavior of the seawalls and shoreline during the earthquake. The Loma Prieta, California, Earthquake of October 17, 1989 - Marina District, U. S. Geological Survey Professional Paper 1551-F, pp. F141-F153.
- Tika-Vassilikos, T.E., Sarma, S.K., and Ambraseys, N.N. 1993. Seismic displacement on shear surfaces in cohesive soils. *Earthquake Engineering and Structural Dynamics*, Vol. 22.
- Tokimatsu, K., Kojima, H., Kuwayama, S., Abe, A., Midorikawa, S. 1994. Liquefaction-induced damage to buildings in 1990 Luzon earthquake. *Journal of Geotechnical Engineering, ASCE*, **120**(2): 290 - 307.
- Tokimatsu, K., and Seed, H.B. 1987. Evaluation of settlements in sands due to earthquake shaking. *Journal of Geotechnical Engineering, ASCE*, **113**(8): 861-879.
- Tokimatsu, K. and Yoshimi, Y. 1981. Field correlation of soil liquefaction with SPT and grain size. *In Proceedings of Eight World Conference on Earthquake Engineering, San Francisco, CA*, 95-102.
- Tokimatsu, K. and Yoshimi, Y. 1983. Empirical correlation of soil liquefaction based on SPT N-value and fines content. *Soils and Foundations*, **23**(4): 56 - 74.
- Tokimatsu, K., and Yoshimi, Y. 1984. Criteria of soil liquefaction with SPT and fines content. *In Proceedings of the 8th World Conference on Earthquake Engineering, San Francisco, CA, July, Vol. 3*, pp. 255 - 262.
- Towhata, I., Ghalandarzadeh, A., Sundarraj, K.P., and Monge, W.V. 1996. Dynamic failures of subsoils observed in waterfront areas. *Soils and Foundations, Special*

- Issue on Geotechnical Aspects of the January 17 1995 Hyogoken-Nambu Earthquake, January, Japanese Geotechnical Society, pp. 149-160.
- Towhata, I., Orense, R.P., and Toyota H. 1999. Mathematical principles in prediction of lateral ground displacement induced by seismic liquefaction. *Soils and Foundations*, **39**(2): 1-19.
- Towhata, I., Sasaki, Y., Tokida, K., Matsumoto, H., Tamari, Y., and Yamada, K. 1992. Prediction of permanent displacement of liquefied ground by means of minimum energy principle. *Soils and Foundations*, **32**(3): 97-116.
- Towhata, I., Tokida, K., Tomari, Y., Matsumoto, H., and Yamada, K. 1991. Prediction of permanent lateral displacement of liquefied ground by means of variational principle. *In Proceedings of the Third Japan-U.S. Workshop on Earthquake Resistant Design of Lifeline Facilities and Countermeasures for Soil Liquefaction*, Tech. Report NCEER-91-0001, pp.237-251.
- Towhata, I., and Toyota, H. 1994. Dynamic analysis of lateral flow of liquefied ground. *5th US-Japan Workshop on Earthquake Resistant Design of Lifeline Facilities and Countermeasures Against Soil Liquefaction*, O'Rourke, T. D. and Hamada, M., Eds., Snowbird, Utah, Report NCEER-94-0026, Buffalo, NY.
- Toyota, H., and Towhata, I. 1994. Post-liquefaction ground flow in shaking table tests. *In Proceedings from the Fifth U.S.-Japan Workshop on Earthquake Resistant Design of Lifeline Facilities and Countermeasures Against Soil Liquefaction*, September 29 - October 1, Snowbird, Utah, Technical Report NCEER-94-0026.
- Vaid, Y.P. and Sivathayalan, S. 2000. Fundamental factors affecting liquefaction susceptibility of sands. *Can. Geotech. J.* **37**: 592 – 606.
- Vaid, Y.P., Uthayakumar, M., Sivathayalan, S., Pobertson, P.K., and Hofmann, B. 1995. Laboratory testing of Syncrude sand. *In Proceedings of the 48th Canadian Geotechnical Conference*, Vancouver, Vol. 1, pp. 223-232.
- Vreugdenhil, R.A. 1995. Interperation of poezocone data and its use in estimating seismic oil liquefaction potential. Ph.D. Thesis, University of Canterbury, New Zealand, May, p. 183.
- Wakamatsu, K., Yoshida, N., Suzuki, N., and Tazoh, T. 1992. Liquefaction-induced large ground deformations and their effects on lifelines during the 1990 Luzon,

- Philippines earthquake. *Case Studies of Liquefaction and Lifeline Performance During Past Earthquakes*, Vol. 1, Technical Report NCEER-92-0001, National Center for Earthquake Engineering Research, Buffalo, NY.
- Yasuda, S., Nagase, H., Kiku, H., and Uchida, Y. 1991. A simplified procedure for the analysis of the permanent ground displacement. *In Proceedings of the Third Japan-U.S. Workshop on Earthquake Resistant Design of Lifeline Facilities and Countermeasures for Soil Liquefaction*, Tech. Report NCEER-91-0001, pp.225-236.
- Yasuda, S., Nagase, H., Kiku, H., and Uchida, Y. 1992. The mechanism and a simplified procedure for the analysis of permanent ground displacement due to liquefaction. *Soils and Foundations*, **32**(1): 149-160.
- Yegian, M.K., Marciano, E.A., Ghahraman, V.G. 1991. Earthquake-induced permanent deformations: probabilistic approach. *Journal of Geotechnical Engineering, ASCE*, **117**(1): 35 - 49.
- Yoshimi, Y. and Oh-oka, H. 1975. Influence of degree of shear stress reversal on the liquefaction potential of saturated sand. *Soils and Foundations*, **15**(3): 27 – 40.
- Yoshimi, Y., Tokimatsu, K., and Hosaka, Y. 1989. Evaluation of liquefaction resistance of clean sands based on high-quality undisturbed samples. *Soils and Foundations*, **29**(1): 93-104.
- Youd, T.L. 1978. Major cause of earthquake damage is ground failure. *Civil Engineering, ASCE*, April, pp. 47-51.
- Youd, T.L., and Bartlett, S.F. 1988. US case histories of liquefaction-induced ground displacement. *1st Japan-United States Workshop on Liquefaction, Large Ground Deformation and Their Effects on Lifeline Facilities*, Tokyo, Japan, Nov. 16-19, pp. 22-31.
- Youd, T.L., and Bennett, M.J. 1983. Liquefaction sites, Imperial Valley, California. *Journal of Geotechnical Engineering*, **109**(3): 440-457.
- Youd, T.L., and Garris, C.T. 1995. Liquefaction-induced ground-surface disruption. *Journal of Geotechnical and Geoenvironmental Engineering, ASCE*, **121**(11): 805-808.
- Youd, T.L., Hansen, C.M., and Bartlett, S.F. 1999. Revised MLR equations for predicting lateral spread displacement. *In Proceedings of the Seventh U.S.-Japan*

- Workshop on Earthquake Resistant Design of Lifeline Facilities and Countermeasures Against Soil Liquefaction, Seattle, August 15-17, Technical Report MCEER-99-0019, pp. 99-114.
- Youd, T.L., and Hoose, S.N. 1976. Liquefaction during 1906 San Francisco Earthquake. *Journal of Geotechnical Engineering, ASCE*, **102**(GT5): 425 - 439.
- Youd, T.L., and Hoose, S.N. 1977. Liquefaction susceptibility and geologic setting. *In Proceedings of the 6th World Conference on Earthquake Engineering*, Prentice-Hall, Inc., Vol. 3, pp. 2189-2194.
- Youd, T.L., and Hoose, S.N. 1978. Historic ground failures in Northern California triggered by earthquakes. U. S. Geological survey Professional paper 993, U.S. Geological Survey, 177p.
- Youd, T.L., Idriss, I.M., et al. 2001. Liquefaction resistance of soils: summary report from the 1996 NCEER and 1998 NCEER/NSF Workshops on evaluation of liquefaction resistance of soils. *Journal of Geotechnical and Geoenvironmental Engineering*, **127**(4): 297 – 313.
- Youd, T.L., and Kiehl, S.J. 1996. Distribution of ground displacements and strains induced by lateral spread during the 1964 Niigata earthquake. *In Proceedings of the sixth U.S. - Japan Workshop on Earthquake Resistant Design of Lifeline Facilities and Countermeasures against Soil Liquefaction*, Technical Report NCEER-96-0012, M. Hamada and T. D. O'Rourke (eds.), September 11, pp. 205 - 219.
- Youd, T.L., and Perkins, D.M. 1987. Mapping of liquefaction severity index. *Journal of Geotechnical Engineering*, **113**(11): 1374-1392.
- Youd, T.L., and Wiczorek, G.F. 1982. Liquefaction and secondary ground failure. The Imperial Valley, California, Earthquake of October 15, 1979, U.S. Geological Survey, Geological survey Professional Paper 1254, pp. 223-250.
- Youd, T.L., and Wiczorek, G.F. 1984. Liquefaction during the 1981 and previous earthquakes Near Westmorland, California. U. S. Geological Survey, Open-file Report 84-680, pp. 1-36.
- Zeghal, M., and Elgamal, A. 1994. Analysis of site liquefaction using earthquake records. *Journal of Geotechnical Engineering*, **120**(6): 996-1017.
- Zeghal, M., Elgamal, A.W., Zeng, X., and Arulmoli, K. 1999. Mechanism of

liquefaction response in sand-silt dynamic centrifuge tests. *Soil Dynamics and Earthquake Engineering*, Vol. 18, pp. 71-85.

Zhou, S.G. 1981. Influence of fines on evaluating liquefaction of sand by CPT. *In Proceedings of International Conference on Recent Advances in Geotechnical Earthquake Engineering and Soil Dynamics*, St. Louis, MO, 1, 167-172.

APPENDIX A: LISTING OF THE DATABASES IN THIS RESEARCH

A listing of the data used for this research is presented in this appendix.

Table A1 presents the data used in developing the proposed approach, as developed in Chapter 7, to estimate liquefaction-induced lateral displacements for gently sloping ground without a free face. Table A2 lists the data used in developing the proposed approach, as proposed in Chapter 8, to estimate liquefaction-induced lateral displacements for level ground with a free face. The data used in developing the proposed approach, as introduced in Chapter 9, to estimate liquefaction-induced lateral displacements for gently sloping ground with a free face are presented in Table A3.

The definition of the symbols in Tables A1, A2 and A3 are as follows:

S: ground slope as a percentage;

L: the distance to the toe of a free face in meter;

H: the height of a free face in meter;

LD: measured lateral displacement in centimeter;

LDI_{SPT}: the lateral displacement index calculated using the SPT-based procedures and the SPT data;

LDI_{CPT}: the lateral displacement index calculated using the CPT-based procedures and the CPT data or the equivalent CPT data converted from the SPT data;

LDI_{SPT&CPT}: the lateral displacement index calculated either using the SPT-based procedures and the SPT data or using the CPT-based procedures and the CPT data;

M_w: the moment magnitude of an earthquake;

a_{max}: the peak surface acceleration at a site for a given earthquake.

Table A1 A summary of the data used in this research for gently sloping ground without a free face

NO.	SITE	LOCATION	S (%)	LD (cm)	LD _{SPT} (cm)	LD _{CPT} (cm)	EARTHQUAKE	M _w	a _{max} (g)
1	Mission Creek Zone, San Francisco	19th Street at Mission Playground	1.8	180		64.5	1906 San Francisco	7.9	0.6
2	Mission Creek Zone, San Francisco	Valencia at 18th to 19th Streets	1.8	210		173.1	1906 San Francisco	7.9	0.6
3	Mission Creek Zone, San Francisco	Capp Street at 17th to 18th Streets	1	100		73.1	1906 San Francisco	7.9	0.6
4	Mission Creek Zone, San Francisco	South Van Ness Avenue at 17th to 18th Streets	1.2	120		73.1	1906 San Francisco	7.9	0.6
5	South of Market Area, San Francisco	Seventh Street at Market to Mission Streets	1	60		32.7	1906 San Francisco	7.9	0.6
6	South of Market Area, San Francisco	Mission and 7th Streets	1.7	150		44.3	1906 San Francisco	7.9	0.6
7	South of Market Area, San Francisco	Seventh Street at Mission to Howard Streets	2.3	210		44.3	1906 San Francisco	7.9	0.6
8	South of Market Area, San Francisco	Columbia Street at Folsom Street	1	100		61.9	1906 San Francisco	7.9	0.6
9	Furu-Sumida Creek area in Tokyo	B-B' Section, Site E	1.6	250	208.4	190.1	1923 Kanto	7.9	0.25
10	Fukui Plain, Japan	4-4' Section, East Zone	2.3	300	118.2	90.6	1948 Fukui	7	0.25
11	Fukui Plain, Japan	5-5' Section, West Zone	3.4	350	134.4	136.8	1948 Fukui	7	0.25
12	Fukui Plain, Japan	5-5' Section, West Zone	1.8	250	134.4	136.8	1948 Fukui	7	0.25
13	Fukui Plain, Japan	5-5' Section, West Zone	0.4	100	134.4	136.8	1948 Fukui	7	0.25
14	Niigata, Japan	F-10, K-K'	0.9	340	380.6	385.4	1964 Niigata	7.5	0.19
15	Niigata, Japan	F-10, K-K'	0.89	275	380.6	385.4	1964 Niigata	7.5	0.19
16	Niigata, Japan	F-10, K-K'	0.77	257	380.6	385.4	1964 Niigata	7.5	0.19
17	Niigata, Japan	F-10, K-K'	0.87	239	380.6	385.4	1964 Niigata	7.5	0.19

Table A1 continued

NO.	SITE	LOCATION	S (%)	LD (cm)	LD _{SPT} (cm)	LD _{CPT} (cm)	EARTHQUAKE	M _w	a _{max} (g)
18	Niigata, Japan	F-10, K-K'	0.77	254	380.6	385.4	1964 Niigata	7.5	0.19
19	Niigata, Japan	G-10, L-L'	0.21	151	173.4	220.2	1964 Niigata	7.5	0.19
20	Niigata, Japan	G-10, L-L'	0.35	145	173.4	220.2	1964 Niigata	7.5	0.19
21	Niigata, Japan	G-10, L-L'	0.24	115	173.4	220.2	1964 Niigata	7.5	0.19
22	Niigata, Japan	G-10, L-L'	0.24	146	173.4	220.2	1964 Niigata	7.5	0.19
23	Niigata, Japan	G-10, L-L'	0.24	111	173.4	220.2	1964 Niigata	7.5	0.19
24	Niigata, Japan	G-10, L-L'	0.24	118	173.4	220.2	1964 Niigata	7.5	0.19
25	Niigata, Japan	G-10, L-L'	0.24	81	173.4	220.2	1964 Niigata	7.5	0.19
26	Niigata, Japan	G-10, L-L'	0.27	153	173.4	220.2	1964 Niigata	7.5	0.19
27	Niigata, Japan	G-10, L-L'	0.27	82	173.4	220.2	1964 Niigata	7.5	0.19
28	Niigata, Japan	G-10, L-L'	0.27	146	173.4	220.2	1964 Niigata	7.5	0.19
29	Niigata, Japan	G-10, L-L'	0.21	81	173.4	220.2	1964 Niigata	7.5	0.19
30	Niigata, Japan	H-10, N-N'	0.54	75	289.0	304.4	1964 Niigata	7.5	0.19
31	Niigata, Japan	H-10, N-N'	0.71	229	289.0	304.4	1964 Niigata	7.5	0.19
32	Niigata, Japan	H-10, N-N'	0.63	78	289.0	304.4	1964 Niigata	7.5	0.19
33	Niigata, Japan	H-10, N-N'	0.54	135	289.0	304.4	1964 Niigata	7.5	0.19
34	Niigata, Japan	H-10, N-N'	0.63	80	337.2	350.4	1964 Niigata	7.5	0.19
35	Niigata, Japan	H-10, N-N'	0.34	115	293.9	302.4	1964 Niigata	7.5	0.19
36	Niigata, Japan	H-10, N-N'	0.36	130	293.9	302.4	1964 Niigata	7.5	0.19
37	Niigata, Japan	H-10, N-N'	0.32	115	293.9	302.4	1964 Niigata	7.5	0.19
38	Niigata, Japan	H-10, N-N'	0.39	170	293.9	302.4	1964 Niigata	7.5	0.19
39	Niigata, Japan	H-10, N-N'	0.41	192	293.9	302.4	1964 Niigata	7.5	0.19
40	Niigata, Japan	H-10, N-N'	0.45	207	293.9	302.4	1964 Niigata	7.5	0.19
41	Niigata, Japan	H-10, N-N'	0.46	100	422.4	424.1	1964 Niigata	7.5	0.19
42	Niigata, Japan	H-10, N-N'	0.33	120	422.4	424.1	1964 Niigata	7.5	0.19
43	Niigata, Japan	H-10, N-N'	0.37	140	422.4	424.1	1964 Niigata	7.5	0.19
44	Niigata, Japan	H-10, N-N'	0.38	140	422.4	424.1	1964 Niigata	7.5	0.19

Table A1 continued

NO.	SITE	LOCATION	S (%)	LD (cm)	LD _{SPT} (cm)	LD _{CPT} (cm)	EARTHQUAKE	M _w	a _{max} (g)
45	Niigata, Japan	H-10, N-N'	0.37	100	422.4	424.1	1964 Niigata	7.5	0.19
46	Niigata, Japan	H-10, N-N'	0.48	137	422.4	424.1	1964 Niigata	7.5	0.19
47	Niigata, Japan	H-10, N-N'	0.42	120	422.4	424.1	1964 Niigata	7.5	0.19
48	Niigata, Japan	H-10, N-N'	0.54	203	501.7	532.7	1964 Niigata	7.5	0.19
49	Niigata, Japan	H-10, N-N'	0.51	150	345.8	356.1	1964 Niigata	7.5	0.19
50	Niigata, Japan	H-10, N-N'	0.37	130	345.8	356.1	1964 Niigata	7.5	0.19
51	Niigata, Japan	H-10, N-N'	0.46	110	345.8	356.1	1964 Niigata	7.5	0.19
52	Niigata, Japan	H-10, N-N'	0.46	130	345.8	356.1	1964 Niigata	7.5	0.19
53	Niigata, Japan	H-10, N-N'	0.46	140	345.8	356.1	1964 Niigata	7.5	0.19
54	Niigata, Japan	H-10, M-M'	0.63	426	319.2	316.3	1964 Niigata	7.5	0.19
55	Niigata, Japan	H-10, M-M'	0.63	465	319.2	316.3	1964 Niigata	7.5	0.19
56	Niigata, Japan	H-10, M-M'	0.81	353	319.2	316.3	1964 Niigata	7.5	0.19
57	Niigata, Japan	H-10, M-M'	0.63	333	319.2	316.3	1964 Niigata	7.5	0.19
58	Niigata, Japan	H-10, M-M'	0.63	332	319.2	316.3	1964 Niigata	7.5	0.19
59	Niigata, Japan	H-10, M-M'	0.51	296	319.2	316.3	1964 Niigata	7.5	0.19
60	Niigata, Japan	H-10, M-M'	0.63	316	319.2	316.3	1964 Niigata	7.5	0.19
61	Niigata, Japan	H-10, M-M'	0.51	333	319.2	316.3	1964 Niigata	7.5	0.19
62	Niigata, Japan	H-10, M-M'	0.41	112	414.0	419.9	1964 Niigata	7.5	0.19
63	Niigata, Japan	H-10, M-M'	0.52	308	414.0	419.9	1964 Niigata	7.5	0.19
64	Niigata, Japan	H-10, M-M'	0.4	273	414.0	419.9	1964 Niigata	7.5	0.19
65	Niigata, Japan	H-10, M-M'	0.4	253	414.0	419.9	1964 Niigata	7.5	0.19
66	Niigata, Japan	H-10, M-M'	0.56	292	414.0	419.9	1964 Niigata	7.5	0.19
67	Niigata, Japan	H-10, M-M'	0.55	317	414.0	419.9	1964 Niigata	7.5	0.19
68	Niigata, Japan	H-10, M-M'	0.34	233	414.0	419.9	1964 Niigata	7.5	0.19
69	Niigata, Japan	H-10, M-M'	0.33	227	414.0	419.9	1964 Niigata	7.5	0.19
70	Niigata, Japan	H-10, M-M'	0.55	235	414.0	419.9	1964 Niigata	7.5	0.19
71	Niigata, Japan	H-10, M-M'	0.52	321	414.0	419.9	1964 Niigata	7.5	0.19
72	Niigata, Japan	H-10, M-M'	0.66	306	414.0	419.9	1964 Niigata	7.5	0.19

Table A1 continued

NO.	SITE	LOCATION	S (%)	LD (cm)	LD _{SPT} (cm)	LD _{CPT} (cm)	EARTHQUAKE	M _w	a _{max} (g)
73	Niigata, Japan	H-10, M-M'	0.47	223	414.0	419.9	1964 Niigata	7.5	0.19
74	Niigata, Japan	H-10, M-M'	0.64	294	414.0	419.9	1964 Niigata	7.5	0.19
75	Niigata, Japan	H-10, M-M'	0.64	297	414.0	419.9	1964 Niigata	7.5	0.19
76	Niigata, Japan	H-10, M-M'	0.4	175	360.5	358.4	1964 Niigata	7.5	0.19
77	Niigata, Japan	H-10, M-M'	0.38	328	438.4	442.4	1964 Niigata	7.5	0.19
78	Niigata, Japan	H-10, M-M'	0.46	318	438.4	442.4	1964 Niigata	7.5	0.19
79	Niigata, Japan	H-10, M-M'	0.47	351	438.4	442.4	1964 Niigata	7.5	0.19
80	Niigata, Japan	H-10, M-M'	0.27	197	438.4	442.4	1964 Niigata	7.5	0.19
81	Niigata, Japan	H-10, M-M'	0.35	170	438.4	442.4	1964 Niigata	7.5	0.19
82	Niigata, Japan	H-10, M-M'	0.38	327	438.4	442.4	1964 Niigata	7.5	0.19
83	Niigata, Japan	H-10, M-M'	0.27	199	438.4	442.4	1964 Niigata	7.5	0.19
84	Niigata, Japan	H-10, M-M'	0.29	162	317.7	320.3	1964 Niigata	7.5	0.19
85	Niigata, Japan	H-10, M-M'	0.36	309	317.7	320.3	1964 Niigata	7.5	0.19
86	Niigata, Japan	H-10, M-M'	0.43	153	317.7	320.3	1964 Niigata	7.5	0.19
87	Niigata, Japan	H-10, M-M'	0.43	323	420.6	427.4	1964 Niigata	7.5	0.19
88	Niigata, Japan	H-10, M-M'	0.48	150	255.0	259.2	1964 Niigata	7.5	0.19
89	Niigata, Japan	H-10, M-M'	0.64	142	255.0	259.2	1964 Niigata	7.5	0.19
90	Niigata, Japan	H-10, M-M'	0.48	189	255.0	259.2	1964 Niigata	7.5	0.19
91	Niigata, Japan	H-10, M-M'	0.38	161	255.0	259.2	1964 Niigata	7.5	0.19
92	Niigata, Japan	H-10, M-M'	0.48	149	255.0	259.2	1964 Niigata	7.5	0.19
93	Niigata, Japan	F-10, K-K'	0.48	149	243.2	242.8	1964 Niigata	7.5	0.19
94	Niigata, Japan	F-10, K-K'	0.54	155	243.2	242.8	1964 Niigata	7.5	0.19
95	Niigata, Japan	F-10, K-K'	0.42	163	243.2	242.8	1964 Niigata	7.5	0.19
96	Niigata, Japan	F-10, K-K'	0.84	247	373.0	362.5	1964 Niigata	7.5	0.19
97	Niigata, Japan	F-10, K-K'	0.75	196	373.0	362.5	1964 Niigata	7.5	0.19
98	Niigata, Japan	F-10, K-K'	0.65	134	370.9	353.4	1964 Niigata	7.5	0.19
99	Niigata, Japan	F-10, J-J'	0.31	109	307.8	280.8	1964 Niigata	7.5	0.19
100	Niigata, Japan	F-10, J-J'	0.25	283	307.8	280.8	1964 Niigata	7.5	0.19

Table A1 continued

NO.	SITE	LOCATION	S (%)	LD (cm)	LDI _{SPT} (cm)	LDI _{CPT} (cm)	EARTHQUAKE	M _w	a _{max} (g)
101	Niigata, Japan	F-10, J-J'	0.32	169	306.8	315.3	1964 Niigata	7.5	0.19
102	Niigata, Japan	F-10, J-J'	0.27	160	306.8	315.3	1964 Niigata	7.5	0.19
103	Niigata, Japan	F-10, J-J'	0.38	127	306.8	315.3	1964 Niigata	7.5	0.19
104	Niigata, Japan	F-10, J-J'	0.47	172	306.8	315.3	1964 Niigata	7.5	0.19
105	Niigata, Japan	F-10, J-J'	0.36	152	306.8	315.3	1964 Niigata	7.5	0.19
106	Niigata, Japan	F-10, J-J'	0.32	156	306.8	315.3	1964 Niigata	7.5	0.19
107	Niigata, Japan	F-10, J-J'	0.29	135	306.8	315.3	1964 Niigata	7.5	0.19
108	Niigata, Japan	F-10, J-J'	0.24	123	306.8	315.3	1964 Niigata	7.5	0.19
109	Niigata, Japan	F-10, J-J'	0.27	275	306.8	315.3	1964 Niigata	7.5	0.19
110	Niigata, Japan	F-10, J-J'	0.25	179	306.8	315.3	1964 Niigata	7.5	0.19
111	Niigata, Japan	G-10, L-L'	0.38	130	123.3	161.0	1964 Niigata	7.5	0.19
112	Niigata, Japan	G-10, L-L'	0.26	191	123.3	161.0	1964 Niigata	7.5	0.19
113	Niigata, Japan	G-10, L-L'	0.29	350	123.3	161.0	1964 Niigata	7.5	0.19
114	Niigata, Japan	G-10, L-L'	0.38	157	123.3	161.0	1964 Niigata	7.5	0.19
115	Niigata, Japan	G-10, L-L'	0.35	276	123.3	161.0	1964 Niigata	7.5	0.19
116	Niigata, Japan	G-10, L-L'	0.61	218	171.6	221.1	1964 Niigata	7.5	0.19
117	Juvenile Hall, San Fernando Valley, California	San Fernando Road	1.2	168	59.8	18.3	1971 San Fernando	6.4	0.55
118	Noshiro, Japan	N-1, 1	0.64	105	86.2	81.5	1983 Nihonkai-Chubu	7.7	0.25
119	Noshiro, Japan	N-2, 2	2.22	224	111.8	113.7	1983 Nihonkai-Chubu	7.7	0.25
120	Noshiro, Japan	N-2, 2	2.27	298	103.5	85.4	1983 Nihonkai-Chubu	7.7	0.25
121	Noshiro, Japan	N-3, 3	6.19	292	54.9	56.6	1983 Nihonkai-Chubu	7.7	0.25
122	Noshiro, Japan	N-3, 3	1.59	78	31.4	33.5	1983 Nihonkai-Chubu	7.7	0.25

Table A1 continued

NO.	SITE	LOCATION	S (%)	LD (cm)	LD _{ISPT} (cm)	LD _{ICPT} (cm)	EARTHQUAKE	M _w	a _{max} (g)
123	Noshiro, Japan	N-4, 4	2.6	211	85.5	101.1	1983 Nihonkai-Chubu	7.7	0.25
124	Noshiro, Japan	N-4, 4	5.9	292	50.0	45.8	1983 Nihonkai-Chubu	7.7	0.25
125	Noshiro, Japan	N-4, 4	0.17	65	82.2	71.2	1983 Nihonkai-Chubu	7.7	0.25
126	Noshiro, Japan	N-5, 5	1.4	250	164.2	145.2	1983 Nihonkai-Chubu	7.7	0.25
127	Noshiro, Japan	N-6, 6	1.48	236	143.5	134.7	1983 Nihonkai-Chubu	7.7	0.25
128	Noshiro, Japan	N-7, 7	0.76	180	106.7	98.0	1983 Nihonkai-Chubu	7.7	0.25
129	Noshiro, Japan	N-7, 7	1.57	258	67.6	63.6	1983 Nihonkai-Chubu	7.7	0.25
130	Noshiro, Japan	S-4, 4	1.49	240	155.2	150.9	1983 Nihonkai-Chubu	7.7	0.25
131	Noshiro, Japan	S-5, 5	1.47	194	81.4	95.8	1983 Nihonkai-Chubu	7.7	0.25
132	Noshiro, Japan	S-5, 5	1	110	81.4	95.8	1983 Nihonkai-Chubu	7.7	0.25
133	Noshiro, Japan	S-6, 6	3.18	238	71.3	83.3	1983 Nihonkai-Chubu	7.7	0.25
134	Noshiro, Japan	S-6, 6	1.42	153	71.3	83.3	1983 Nihonkai-Chubu	7.7	0.25
135	Noshiro, Japan	S-7, 7	1.98	237	111.4	111.3	1983 Nihonkai-Chubu	7.7	0.25
136	Noshiro, Japan	S-7, 7	0.77	114	140.0	134.3	1983 Nihonkai-Chubu	7.7	0.25
137	Noshiro, Japan	S-9, 9	3.33	217	82.9	70.8	1983 Nihonkai-Chubu	7.7	0.25
138	Noshiro, Japan	S-9, 9	1.89	128	82.9	70.8	1983 Nihonkai-Chubu	7.7	0.25
139	Noshiro, Japan	S-11, 11	7.48	139	17.2	20.1	1983 Nihonkai-Chubu	7.7	0.25
140	Noshiro, Japan	S-12, 12	5.71	208	31.7	34.2	1983 Nihonkai-Chubu	7.7	0.25

Table A2 A summary of the data used in this research for level ground with a free face

NO.	SITE	LOCATION	L (m)	H (m)	LD (cm)	LD _{SPT} (cm)	LD _{CPT} (cm)	EARTHQUAKE	M _w	a _{max} (g)
1	Portage Creek #1, Alaska	MP 63.0	4.9	2.4	191	69.3	23.3	1964 Alaska	9.2	0.31
2	Twenty Mile River, Alaska	MP 64.7	30.5	4.9	157	172.9	129.4	1964 Alaska	9.2	0.31
3	Niigata, Japan	G-10, B-B'	34.1	5.2	224	463.5	463.6	1964 Niigata	7.5	0.19
4	Niigata, Japan	G-10, B-B'	31.7	5.2	649	463.5	463.6	1964 Niigata	7.5	0.19
5	Niigata, Japan	G-10, B-B'	89	5.2	185	463.5	463.6	1964 Niigata	7.5	0.19
6	Niigata, Japan	G-10, B-B'	171.3	5.2	41	495.7	439.9	1964 Niigata	7.5	0.19
7	Niigata, Japan	G-10, B-B'	167.7	5.2	55	495.7	439.9	1964 Niigata	7.5	0.19
8	Niigata, Japan	G-10, B-B'	109.1	5.2	80	537.3	544.5	1964 Niigata	7.5	0.19
9	Niigata, Japan	G-10, B-B'	174.1	5.2	130	420.3	413.2	1964 Niigata	7.5	0.19
10	Niigata, Japan	G-10, B-B'	188.1	5.2	100	601.7	497.0	1964 Niigata	7.5	0.19
11	Niigata, Japan	G-10, E-E'	61	5.2	476	486.6	492.4	1964 Niigata	7.5	0.19
12	Niigata, Japan	G-10, E-E'	43.3	5.2	872	477.7	503.5	1964 Niigata	7.5	0.19
13	Niigata, Japan	H-10, A-A'	102.7	5.2	397	472.6	438.2	1964 Niigata	7.5	0.19
14	Niigata, Japan	H-10, A-A'	47	5.2	818	472.6	438.2	1964 Niigata	7.5	0.19
15	Niigata, Japan	H-10, A-A'	116.8	5.2	337	472.6	438.2	1964 Niigata	7.5	0.19
16	Niigata, Japan	H-10, A-A'	30.5	5.2	828	472.6	438.2	1964 Niigata	7.5	0.19
17	Niigata, Japan	H-10, A-A'	106.7	5.2	189	383.6	360.5	1964 Niigata	7.5	0.19
18	Niigata, Japan	G-10, A-A'	101.5	5.2	135	383.6	360.5	1964 Niigata	7.5	0.19
19	Niigata, Japan	H-10, A-A'	26.5	5.2	1015	411.3	423.6	1964 Niigata	7.5	0.19
20	Niigata, Japan	G-10, H-H'	29.3	4.9	487	440.0	418.8	1964 Niigata	7.5	0.19
21	Niigata, Japan	G-10, H-H'	97.9	4.9	235	440.0	418.8	1964 Niigata	7.5	0.19
22	Niigata, Japan	G-10, H-H'	39.3	4.9	482	440.0	418.8	1964 Niigata	7.5	0.19
23	Niigata, Japan	G-10, H-H'	123.2	4.9	182	440.0	418.8	1964 Niigata	7.5	0.19
24	Niigata, Japan	G-10, H-H'	78.7	4.9	186	440.0	418.8	1964 Niigata	7.5	0.19

Table A2 continued

NO.	SITE	LOCATION	L (m)	H (m)	LD (cm)	LD _{SP} T (cm)	LD _{CP} T (cm)	EARTHQUAKE	M _w	a _{max} (g)
25	Niigata, Japan	G-10, H-H'	8.8	4.9	712	440.0	418.8	1964 Niigata	7.5	0.19
26	Niigata, Japan	G-10, H-H'	91.5	4.9	237	440.0	418.8	1964 Niigata	7.5	0.19
27	Niigata, Japan	G-10, H-H'	30.5	4.9	705	440.0	418.8	1964 Niigata	7.5	0.19
28	Niigata, Japan	G-10, H-H'	97.9	4.9	174	440.0	418.8	1964 Niigata	7.5	0.19
29	Niigata, Japan	G-10, H-H'	75	4.9	250	440.0	418.8	1964 Niigata	7.5	0.19
30	Niigata, Japan	G-10, H-H'	14	4.9	766	440.0	418.8	1964 Niigata	7.5	0.19
31	Niigata, Japan	G-10, H-H'	53.4	4.9	439	440.0	418.8	1964 Niigata	7.5	0.19
32	Niigata, Japan	G-10, H-H'	85.1	4.9	148	440.0	418.8	1964 Niigata	7.5	0.19
33	Niigata, Japan	G-10, H-H'	30.5	4.9	739	440.0	418.8	1964 Niigata	7.5	0.19
34	Niigata, Japan	G-10, H-H'	39.3	4.9	320	440.0	418.8	1964 Niigata	7.5	0.19
35	Niigata, Japan	G-10, H-H'	158.8	4.9	165	440.0	418.8	1964 Niigata	7.5	0.19
36	Niigata, Japan	G-10, H-H'	82.6	4.9	296	440.0	418.8	1964 Niigata	7.5	0.19
37	Niigata, Japan	G-10, H-H'	35.7	4.9	626	440.0	418.8	1964 Niigata	7.5	0.19
38	Niigata, Japan	G-10, H-H'	127.1	4.9	192	440.0	418.8	1964 Niigata	7.5	0.19
39	Niigata, Japan	G-10, H-H'	43.3	4.9	350	440.0	418.8	1964 Niigata	7.5	0.19
40	Niigata, Japan	G-10, H-H'	144.8	4.9	182	440.0	418.8	1964 Niigata	7.5	0.19
41	Niigata, Japan	G-10, H-H'	133.2	4.9	208	440.0	418.8	1964 Niigata	7.5	0.19
42	Niigata, Japan	G-10, H-H'	168.9	4.9	164	440.0	418.8	1964 Niigata	7.5	0.19
43	Niigata, Japan	G-10, H-H'	25.3	4.9	427	440.0	418.8	1964 Niigata	7.5	0.19
44	Niigata, Japan	G-10, H-H'	101.5	4.9	183	440.0	418.8	1964 Niigata	7.5	0.19
45	Niigata, Japan	G-10, H-H'	43.3	4.9	377	440.0	418.8	1964 Niigata	7.5	0.19
46	Niigata, Japan	G-10, H-H'	170.1	4.9	155	440.0	418.8	1964 Niigata	7.5	0.19
47	Niigata, Japan	G-10, H-H'	16.5	4.9	502	440.0	418.8	1964 Niigata	7.5	0.19
48	Niigata, Japan	G-10, H-H'	165.2	4.9	148	440.0	418.8	1964 Niigata	7.5	0.19
49	Niigata, Japan	G-10, E-E'	106.7	5.2	185	415.2	395.3	1964 Niigata	7.5	0.19
50	Niigata, Japan	G-10, E-E'	47	5.2	290	636.7	664.8	1964 Niigata	7.5	0.19

Table A2 continued

NO.	SITE	LOCATION	L (m)	H (m)	LD (cm)	LD _{SPT} (cm)	LD _{CPT} (cm)	EARTHQUAKE	M _w	a _{max} (g)
51	Niigata, Japan	G-10, E-E'	73.8	5.2	353	526.0	530.0	1964 Niigata	7.5	0.19
52	Niigata, Japan	G-10, E-E'	41.8	5.2	629	619.9	640.2	1964 Niigata	7.5	0.19
53	Niigata, Japan	G-10, E-E'	52.1	5.2	601	619.9	640.2	1964 Niigata	7.5	0.19
54	Niigata, Japan	G-10, E-E'	139.6	5.2	325	375.0	371.9	1964 Niigata	7.5	0.19
55	Niigata, Japan	G-10, E-E'	79.9	5.2	360	603.1	615.6	1964 Niigata	7.5	0.19
56	Niigata, Japan	G-10, E-E'	107.9	5.2	365	489.1	493.7	1964 Niigata	7.5	0.19
57	Niigata, Japan	G-10, E-E'	154.9	5.2	345	504.5	524.5	1964 Niigata	7.5	0.19
58	Niigata, Japan	G-10, E-E'	90.2	5.2	457	468.7	514.6	1964 Niigata	7.5	0.19
59	Niigata, Japan	G-10, E-E'	165.2	5.2	519	504.5	524.5	1964 Niigata	7.5	0.19
60	Niigata, Japan	G-10, E-E'	128.4	5.2	475	540.3	534.3	1964 Niigata	7.5	0.19
61	Niigata, Japan	G-10, E-E'	38.1	5.2	534	362.8	375.6	1964 Niigata	7.5	0.19
62	Niigata, Japan	G-10, E-E'	68.6	5.2	456	362.8	375.6	1964 Niigata	7.5	0.19
63	Niigata, Japan	G-10, E-E'	58.5	5.2	475	362.8	375.6	1964 Niigata	7.5	0.19
64	Niigata, Japan	G-10, B-B'	167.7	5.2	208	470.9	438.4	1964 Niigata	7.5	0.19
65	Niigata, Japan	G-10, B-B'	115.5	5.2	52	383.2	368.4	1964 Niigata	7.5	0.19
66	Niigata, Japan	G-10, B-B'	133.2	5.2	286	383.2	368.4	1964 Niigata	7.5	0.19
67	Niigata, Japan	H-10, A-A'	186.6	5.2	100	478.9	502.8	1964 Niigata	7.5	0.19
68	Niigata, Japan	H-10, A-A'	170.1	5.2	100	478.9	502.8	1964 Niigata	7.5	0.19
69	Niigata, Japan	H-10, A-A'	57	5.2	599	478.9	502.8	1964 Niigata	7.5	0.19
70	Niigata, Japan	H-10, A-A'	188.1	5.2	122	246.4	260.0	1964 Niigata	7.5	0.19
71	Niigata, Japan	H-10, A-A'	144.8	5.2	145	246.4	260.0	1964 Niigata	7.5	0.19
72	Jensen Plant, San Fernando	B-B' Section	433.6	14.2	16	57.2	68.5	1971 San Fernando	6.4	0.55
73	Jensen Plant, San Fernando	B-B' Section	276	16	46	76.9	95.4	1971 San Fernando	6.4	0.55
74	Jensen Plant, San Fernando	B-B' Section	228.1	14.2	54	76.9	95.4	1971 San Fernando	6.4	0.55
75	Jensen Plant, San Fernando	B-B' Section	190.4	11.4	62	61.2	79.0	1971 San Fernando	6.4	0.55
76	Jensen Plant, San Fernando	B-B' Section	118.5	11.4	70	49.8	61.2	1971 San Fernando	6.4	0.55
77	Jensen Plant, San Fernando	B-B' Section	28.1	11.4	207	72.1	54.7	1971 San Fernando	6.4	0.55

Table A2 continued

NO.	SITE	LOCATION	L (m)	H (m)	LD (cm)	LD _{SPT} (cm)	LD _{CPT} (cm)	EARTHQUAKE	M _w	a _{max} (g)
78	Jensen Plant, San Fernando	C-C' Section	467	16.6	2	9.7	2.4	1971 San Fernando	6.4	0.55
79	Jensen Plant, San Fernando	C-C' Section	299	16.6	30	52.7	93.8	1971 San Fernando	6.4	0.55
80	Jensen Plant, San Fernando	C-C' Section	203	16.6	40	56.1	89.7	1971 San Fernando	6.4	0.55
81	Jensen Plant, San Fernando	C-C' Section	124	10.4	100	119.8	140.8	1971 San Fernando	6.4	0.55
82	Jensen Plant, San Fernando	C-C' Section	20.5	10.4	300	105.3	122.3	1971 San Fernando	6.4	0.55
83	Jensen Plant, San Fernando	D-D' Section	413.4	17.2	3	5.0	14.4	1971 San Fernando	6.4	0.55
84	Jensen Plant, San Fernando	D-D' Section	286.7	17.2	10	16.1	25.2	1971 San Fernando	6.4	0.55
85	Jensen Plant, San Fernando	D-D' Section	211.3	17.2	14	16.1	25.2	1971 San Fernando	6.4	0.55
86	Jensen Plant, San Fernando	D-D' Section	150	17.2	35	43.7	59.3	1971 San Fernando	6.4	0.55
87	Jensen Plant, San Fernando	D-D' Section	21.5	17.2	114	61.0	83.5	1971 San Fernando	6.4	0.55
88	Moss Landing, California	State Beach	15	1.9	100		113.8	1989 Loma Prieta	7	0.25
89	Moss Landing, California	State Beach	15	2.4	30		27.8	1989 Loma Prieta	7	0.25
90	Moss Landing, California	MBARI Facilities	15	5.75	28		36.6	1989 Loma Prieta	7	0.25
91	Moss Landing, California	MBARI Facilities	15	5.75	8		69.6	1989 Loma Prieta	7	0.25
92	Moss Landing, California	MBARI Facilities	18.5	5.75	25		20.8	1989 Loma Prieta	7	0.25
93	Moss Landing, California	Marine Lab	5	2	140		103.9	1989 Loma Prieta	7	0.25
94	Moss Landing, California	Marine Lab	40	2	46		103.9	1989 Loma Prieta	7	0.25
95	Moss Landing, California	Marine Lab	15	2	125		81.5	1989 Loma Prieta	7	0.25
96	Moss Landing, California	Marine Lab	18	2	80		59.1	1989 Loma Prieta	7	0.25
97	Moss Landing, California	Marine Lab	47	2	46		51.2	1989 Loma Prieta	7	0.25
98	Dagupan, Philippines	North of Fernandez Ave.	20	4.5	300	148.4	159.1	1990 Luzon	7.6	0.2
99	Dagupan, Philippines	North of Fernandez Ave.	83	4.5	100	148.4	159.1	1990 Luzon	7.6	0.2
100	Dagupan, Philippines	West of Magsaysay Br.	15	4	600	219.6	215.5	1990 Luzon	7.6	0.2

Table A2 continued

NO.	SITE	LOCATION	L (m)	H (m)	LD (cm)	LD _{ISPT} (cm)	LD _{CPT} (cm)	EARTHQUAKE	M _w	a _{max} (g)
101	Dagupan, Philippines	West of Magsaysay Br.	53	4	250	219.6	215.5	1990 Luzon	7.6	0.2
102	Dagupan, Philippines	West of Magsaysay Br.	88	4	150	219.6	215.5	1990 Luzon	7.6	0.2
103	Dagupan, Philippines	West of Magsaysay Br.	109	4	50	219.6	215.5	1990 Luzon	7.6	0.2
104	Dagupan, Philippines	East of Magsaysay Br.	10	11.5	500	78.9	81.5	1990 Luzon	7.6	0.2
105	Dagupan, Philippines	East of Magsaysay Br.	76	11.5	200	78.9	81.5	1990 Luzon	7.6	0.2
106	Kobe Port Area, Japan	1-1', Nishinomiya-hama	0	13	210	282.9	263.9	1995 Kobe	7.6	0.2
107	Kobe Port Area, Japan	1-1', Nishinomiya-hama	116	13	117	282.9	263.9	1995 Kobe	6.9	0.54
108	Kobe Port Area, Japan	1-1', Nishinomiya-hama	172	13	57	282.9	263.9	1995 Kobe	6.9	0.54
109	Kobe Port Area, Japan	1-1', Nishinomiya-hama	320	13	62	282.9	263.9	1995 Kobe	6.9	0.54
110	Kobe Port Area, Japan	2-2', Nishinomiya-hama	0	13	300	408.8	433.2	1995 Kobe	6.9	0.54
111	Kobe Port Area, Japan	2-2', Nishinomiya-hama	70	13	194	408.8	433.2	1995 Kobe	6.9	0.54
112	Kobe Port Area, Japan	2-2', Nishinomiya-hama	200	13	100	408.8	433.2	1995 Kobe	6.9	0.54
113	Kobe Port Area, Japan	2-2', Nishinomiya-hama	268	13	85	408.8	433.2	1995 Kobe	6.9	0.54

Table A2 continued

NO.	SITE	LOCATION	L (m)	H (m)	LD (cm)	LDI _{SPT} (cm)	LDI _{CPT} (cm)	EARTHQUAKE	M _w	a _{max} (g)
114	Kobe Port Area, Japan	1-1', Uozaki-hama	0	15.2	300	494.6	524.8	1995 Kobe	6.9	0.54
115	Kobe Port Area, Japan	1-1', Uozaki-hama	76	15.2	174	494.6	524.8	1995 Kobe	6.9	0.54
116	Kobe Port Area, Japan	1-1', Uozaki-hama	120	15.2	62	494.6	524.8	1995 Kobe	6.9	0.54
117	Kobe Port Area, Japan	1-1', Fukae-hama	0	12	426	443.6	418.0	1995 Kobe	6.9	0.54
118	Kobe Port Area, Japan	1-1', Fukae-hama	76	12	156	443.6	418.0	1995 Kobe	6.9	0.54
119	Kobe Port Area, Japan	1-1', Fukae-hama	106	12	117	443.6	418.0	1995 Kobe	6.9	0.54
120	Kobe Port Area, Japan	1-1', Fukae-hama	220	12	76	443.6	418.0	1995 Kobe	6.9	0.54
121	Kobe Port Area, Japan	2-2', Fukae-hama	0	12	472	357.1	325.8	1995 Kobe	6.9	0.54
122	Kobe Port Area, Japan	2-2', Fukae-hama	80	12	145	357.1	325.8	1995 Kobe	6.9	0.54
123	Kobe Port Area, Japan	2-2', Fukae-hama	168	12	106	357.1	325.8	1995 Kobe	6.9	0.54
124	Kobe Port Area, Japan	2-2', Fukae-hama	236	12	40	357.1	325.8	1995 Kobe	6.9	0.54
125	Kobe Port Area, Japan	1-1', Ashiya-hama	0	14.8	230	359.0	383.1	1995 Kobe	6.9	0.54
126	Kobe Port Area, Japan	1-1', Ashiya-hama	100	14.8	140	359.0	383.1	1995 Kobe	6.9	0.54
127	Kobe Port Area, Japan	1-1', Ashiya-hama	212	14.8	70	359.0	383.1	1995 Kobe	6.9	0.54
128	Kobe Port Area, Japan	1-1', Ashiya-hama	248	14.8	40	359.0	383.1	1995 Kobe	6.9	0.54
129	Kobe Port Area, Japan	1-1', Port Island	0	16	400	465.1	456.3	1995 Kobe	6.9	0.54
130	Kobe Port Area, Japan	1-1', Port Island	48	16	174	465.1	456.3	1995 Kobe	6.9	0.54
131	Kobe Port Area, Japan	1-1', Port Island	54	16	132	465.1	456.3	1995 Kobe	6.9	0.54
132	Kobe Port Area, Japan	1-1', Port Island	128	16	117	465.1	456.3	1995 Kobe	6.9	0.54
133	Kobe Port Area, Japan	1-1', Port Island	172	16	88	465.1	456.3	1995 Kobe	6.9	0.54
134	Kobe Port Area, Japan	1-1', Port Island	216	16	49	465.1	456.3	1995 Kobe	6.9	0.54
135	Kobe Port Area, Japan	2-2', Port Island	0	15.1	350	436.2	418.8	1995 Kobe	6.9	0.54
136	Kobe Port Area, Japan	2-2', Port Island	32	15.1	179	436.2	418.8	1995 Kobe	6.9	0.54
137	Kobe Port Area, Japan	2-2', Port Island	80	15.1	140	436.2	418.8	1995 Kobe	6.9	0.54
138	Kobe Port Area, Japan	2-2', Port Island	180	15.1	55	436.2	418.8	1995 Kobe	6.9	0.54

Table A2 continued

NO.	SITE	LOCATION	L (m)	H (m)	LD (cm)	LD _{SPT} (cm)	LD _{CPT} (cm)	EARTHQUAKE	M _w	a _{max} (g)
139	Kobe Port Area, Japan	3-3', Port Island	0	16	400	422.7	386.2	1995 Kobe	6.9	0.54
140	Kobe Port Area, Japan	3-3', Port Island	88	16	147	422.7	386.2	1995 Kobe	6.9	0.54
141	Kobe Port Area, Japan	3-3', Port Island	144	16	100	422.7	386.2	1995 Kobe	6.9	0.54
142	Kobe Port Area, Japan	3-3', Port Island	284	16	45	422.7	386.2	1995 Kobe	6.9	0.54
143	Kobe Port Area, Japan	4-4', Port Island	0	16	285	262.6	233.4	1995 Kobe	6.9	0.54
144	Kobe Port Area, Japan	4-4', Port Island	32	16	210	262.6	233.4	1995 Kobe	6.9	0.54
145	Kobe Port Area, Japan	4-4', Port Island	120	16	146	262.6	233.4	1995 Kobe	6.9	0.54
146	Kobe Port Area, Japan	4-4', Port Island	210	16	43	262.6	233.4	1995 Kobe	6.9	0.54
147	Kobe Port Area, Japan	4-4', Port Island	280	16	37	262.6	233.4	1995 Kobe	6.9	0.54
148	Kobe Port Area, Japan	5-5', Port Island	8	17.3	225	361.0	360.7	1995 Kobe	6.9	0.54
149	Kobe Port Area, Japan	5-5', Port Island	68	17.3	81	361.0	360.7	1995 Kobe	6.9	0.54
150	Kobe Port Area, Japan	5-5', Port Island	152	17.3	79	361.0	360.7	1995 Kobe	6.9	0.54
151	Kobe Port Area, Japan	1-1', Rokko Island	0	18.4	250	433.1	433.5	1995 Kobe	6.9	0.54
152	Kobe Port Area, Japan	1-1', Rokko Island	28	18.4	128	433.1	433.5	1995 Kobe	6.9	0.54
153	Kobe Port Area, Japan	1-1', Rokko Island	100	18.4	90	433.1	433.5	1995 Kobe	6.9	0.54
154	Kobe Port Area, Japan	1-1', Rokko Island	176	18.4	66	433.1	433.5	1995 Kobe	6.9	0.54
155	Kobe Port Area, Japan	1-1', Rokko Island	264	18.4	40	433.1	433.5	1995 Kobe	6.9	0.54
156	Kobe Port Area, Japan	2-2', Rokko Island	0	16	270	360.0	338.4	1995 Kobe	6.9	0.54
157	Kobe Port Area, Japan	2-2', Rokko Island	32	16	177	360.0	338.4	1995 Kobe	6.9	0.54
158	Kobe Port Area, Japan	2-2', Rokko Island	104	16	80	360.0	338.4	1995 Kobe	6.9	0.54
159	Kobe Port Area, Japan	2-2', Rokko Island	212	16	40	360.0	338.4	1995 Kobe	6.9	0.54
160	Kobe Port Area, Japan	3-3', Rokko Island	0	18.7	330	452.1	477.2	1995 Kobe	6.9	0.54
161	Kobe Port Area, Japan	3-3', Rokko Island	108	18.7	96	452.1	477.2	1995 Kobe	6.9	0.54
162	Kobe Port Area, Japan	3-3', Rokko Island	224	18.7	60	452.1	477.2	1995 Kobe	6.9	0.54

Table A2 continued

NO.	SITE	LOCATION	L (m)	H (m)	LD (cm)	LD _{ISPT} (cm)	LD _{ICPT} (cm)	EARTHQUAKE	M _w	a _{max} (g)
163	Kobe Port Area, Japan	4-4', Rokko Island	0	18	310	476.9	519.0	1995 Kobe	6.9	0.54
164	Kobe Port Area, Japan	4-4', Rokko Island	32	18	80	476.9	519.0	1995 Kobe	6.9	0.54
165	Kobe Port Area, Japan	4-4', Rokko Island	256	18	40	476.9	519.0	1995 Kobe	6.9	0.54
166	Kobe Port Area, Japan	5-5', Rokko Island	0	14	177	249.3	195.6	1995 Kobe	6.9	0.54
167	Kobe Port Area, Japan	5-5', Rokko Island	20	14	119	249.3	195.6	1995 Kobe	6.9	0.54
168	Kobe Port Area, Japan	5-5', Rokko Island	64	14	34	249.3	195.6	1995 Kobe	6.9	0.54
169	Kobe Port Area, Japan	5-5', Rokko Island	200	14	10	249.3	195.6	1995 Kobe	6.9	0.54
170	Kobe Port Area, Japan	6-6', Rokko Island	0	20	500	664.8	715.2	1995 Kobe	6.9	0.54
171	Kobe Port Area, Japan	6-6', Rokko Island	44	20	147	664.8	715.2	1995 Kobe	6.9	0.54
172	Kobe Port Area, Japan	6-6', Rokko Island	280	20	79	664.8	715.2	1995 Kobe	6.9	0.54
173	Kobe Port Area, Japan	6-6', Rokko Island	364	20	60	664.8	715.2	1995 Kobe	6.9	0.54
174	Kobe Port Area, Japan	1-1', Mikage-hama	0	12.7	350	432.2	487.6	1995 Kobe	6.9	0.54
175	Kobe Port Area, Japan	1-1', Mikage-hama	116	12.7	146	432.2	487.6	1995 Kobe	6.9	0.54
176	Kobe Port Area, Japan	1-1', Mikage-hama	192	12.7	118	432.2	487.6	1995 Kobe	6.9	0.54
177	Kobe Port Area, Japan	1-1', Mikage-hama	304	12.7	66	432.2	487.6	1995 Kobe	6.9	0.54

Table A3 A summary of the data used in this research for gently sloping ground with a free face

NO.	SITE	LOCATION	S (%)	L (m)	H (m)	LD (cm)	LD _{SPT&CPT} (cm)	EARTHQUAKE	M _w	a _{max} (g)
1	Niigata, Japan	G-10, G-G	0.24	16.5	3.4	105	78.8	1964 Niigata	7.5	0.19
2	Niigata, Japan	G-10, G-G	0.48	81.4	3.4	67	78.8	1964 Niigata	7.5	0.19
3	Niigata, Japan	G-10, G-G	0.36	104.3	3.4	124	133.1	1964 Niigata	7.5	0.19
4	Niigata, Japan	G-10, G-G	0.24	71	3.4	87	78.8	1964 Niigata	7.5	0.19
5	Niigata, Japan	G-10, G-G	0.24	16.5	3.4	90	78.8	1964 Niigata	7.5	0.19
6	Niigata, Japan	G-10, G-G	0.48	101.5	3.4	68	78.8	1964 Niigata	7.5	0.19
7	Niigata, Japan	G-10, D-D'	0.45	116.8	5.2	89	330.0	1964 Niigata	7.5	0.19
8	Niigata, Japan	G-10, D-D'	0.45	122	5.2	136	330.0	1964 Niigata	7.5	0.19
9	Niigata, Japan	G-10, D-D'	0.45	67.4	5.2	191	330.0	1964 Niigata	7.5	0.19
10	Niigata, Japan	G-10, F-F'	-0.22	181.7	5.2	181	371.9	1964 Niigata	7.5	0.19
11	Niigata, Japan	G-10, F-F'	-0.22	161.3	5.2	270	401.8	1964 Niigata	7.5	0.19
12	Niigata, Japan	G-10, F-F'	-0.22	184.1	5.2	122	400.7	1964 Niigata	7.5	0.19
13	Niigata, Japan	G-10, F-F'	-0.22	158.8	5.2	247	375.3	1964 Niigata	7.5	0.19
14	Niigata, Japan	G-10, F-F'	-0.22	139.6	5.2	195	375.3	1964 Niigata	7.5	0.19
15	Niigata, Japan	G-10, I-I'	-0.34	38.1	4.9	273	278.5	1964 Niigata	7.5	0.19
16	Niigata, Japan	G-10, I-I'	-0.34	55.8	4.9	92	278.5	1964 Niigata	7.5	0.19
17	Niigata, Japan	G-10, I-I'	-0.34	68.6	4.9	214	278.5	1964 Niigata	7.5	0.19
18	Niigata, Japan	G-10, I-I'	-0.34	85.1	4.9	126	278.5	1964 Niigata	7.5	0.19
19	Niigata, Japan	G-10, I-I'	-0.34	26.5	4.9	177	278.5	1964 Niigata	7.5	0.19
20	Niigata, Japan	G-10, I-I'	-0.34	91.5	4.9	81	278.5	1964 Niigata	7.5	0.19
21	Niigata, Japan	G-10, I-I'	-0.34	59.8	4.9	219	278.5	1964 Niigata	7.5	0.19
22	Niigata, Japan	G-10, I-I'	-0.34	95.1	4.9	105	278.5	1964 Niigata	7.5	0.19

Table A3 continued

NO.	SITE	LOCATION	S (%)	L (m)	H (m)	LD (cm)	LDISPT&CPT (cm)	EARTHQUAKE	M _w	a _{max} (g)
23	Niigata, Japan	G-10, I-I'	-0.34	160.1	4.9	129	351.8	1964 Niigata	7.5	0.19
24	Niigata, Japan	G-10, I-I'	-0.34	133.2	4.9	70	351.8	1964 Niigata	7.5	0.19
25	Niigata, Japan	G-10, I-I'	-0.34	171.3	4.9	140	351.8	1964 Niigata	7.5	0.19
26	Niigata, Japan	G-10, I-I'	-0.34	171.3	4.9	110	351.8	1964 Niigata	7.5	0.19
27	Niigata, Japan	G-10, F-F'	-0.22	194.2	5.2	188	366.9	1964 Niigata	7.5	0.19
28	Niigata, Japan	G-10, F-F'	-0.22	171.3	5.2	267	366.9	1964 Niigata	7.5	0.19
29	Niigata, Japan	G-10, F-F'	-0.22	170.1	5.2	240	366.9	1964 Niigata	7.5	0.19
30	Niigata, Japan	G-10, F-F'	-0.22	30.5	5.2	617	387.6	1964 Niigata	7.5	0.19
31	Niigata, Japan	G-10, F-F'	-0.22	30.5	5.2	538	387.6	1964 Niigata	7.5	0.19
32	Niigata, Japan	G-10, F-F'	-0.22	71	5.2	374	387.6	1964 Niigata	7.5	0.19
33	Imperial Valley, California	Heber Road	1.5	15.2	1.56	203	95.2	1979 Imperial Valley	6.5	0.6
34	Imperial Valley, California	Heber Road	1.5	39	1.56	91	134.0	1979 Imperial Valley	6.5	0.6
35	Imperial Valley, California	Heber Road	1.5	18.3	1.56	147	168.0	1979 Imperial Valley	6.5	0.6
36	Imperial Valley, California	Heber Road	1.5	12.5	1.56	399	192.4	1979 Imperial Valley	6.5	0.6
37	Imperial Valley, California	Heber Road	1.5	32.6	1.56	30	82.6	1979 Imperial Valley	6.5	0.6
38	Imperial Valley, California	Heber Road	1.5	13.1	1.56	381	134.0	1979 Imperial Valley	6.5	0.6
39	Imperial Valley, California	Heber Road	1.5	14	1.56	262	136.4	1979 Imperial Valley	6.5	0.6
40	Imperial Valley, California	Heber Road	1.5	17.7	1.56	229	186.4	1979 Imperial Valley	6.5	0.6
41	Imperial Valley, California	Heber Road	1.5	18.6	1.56	152	104.4	1979 Imperial Valley	6.5	0.6
42	Imperial Valley, California	Heber Road	1.5	14.9	1.56	211	137.9	1979 Imperial Valley	6.5	0.6
43	Imperial Valley, California	Heber Road	1.5	18.9	1.56	140	96.8	1979 Imperial Valley	6.5	0.6
44	Imperial Valley, California	Heber Road	1.5	19.5	1.56	150	99.9	1979 Imperial Valley	6.5	0.6
45	Imperial Valley, California	Heber Road	1.5	12.8	1.56	424	186.4	1979 Imperial Valley	6.5	0.6

Table A3 continued

NO.	SITE	LOCATION	S (%)	L (m)	H (m)	LD (cm)	LD _{SPT&CPT} (cm)	EARTHQUAKE	M _w	a _{max} (g)
46	Imperial Valley, California	Heber Road	1.5	18.3	1.56	201	134.0	1979 Imperial Valley	6.5	0.6
47	Imperial Valley, California	Heber Road	1.5	11.9	1.56	320	144.3	1979 Imperial Valley	6.5	0.6
48	Imperial Valley, California	Heber Road	1.5	12.2	1.56	262	110.7	1979 Imperial Valley	6.5	0.6
49	Imperial Valley, California	Heber Road	1.5	17.1	1.56	142	104.4	1979 Imperial Valley	6.5	0.6
50	Imperial Valley, California	Wildlife	-0.47	5.8	2.4	20.7	26.6	1987 Superstition Hills	6.5	0.21
51	Imperial Valley, California	Wildlife	-0.47	18.6	2.4	18	34.9	1987 Superstition Hills	6.5	0.21
52	Imperial Valley, California	Wildlife	-0.47	5.8	2.4	23.2	26.6	1987 Superstition Hills	6.5	0.21
53	Imperial Valley, California	Wildlife	-0.47	24.4	2.4	10.7	31.3	1987 Superstition Hills	6.5	0.21
54	Imperial Valley, California	Wildlife	-0.47	16.5	2.4	10.7	23.8	1987 Superstition Hills	6.5	0.21
55	Shiribeshi River, Japan	Area D	0.7	36.8	1.9	184	130.2	1993 Hokkaido	7.7	0.25
56	Shiribeshi River, Japan	Area D	0.7	33.4	1.9	137	130.2	1993 Hokkaido	7.7	0.25
57	Shiribeshi River, Japan	Area D	0.7	55.2	1.9	96	149.6	1993 Hokkaido	7.7	0.25
58	Shiribeshi River, Japan	Area D	0.8	50.2	2.5	286	210.6	1993 Hokkaido	7.7	0.25
59	Shiribeshi River, Japan	Area D	0.8	56.8	2.5	250	210.6	1993 Hokkaido	7.7	0.25
60	Shiribeshi River, Japan	Area D	0.8	90.3	2.5	149	210.6	1993 Hokkaido	7.7	0.25

**APPENDIX B: FIGURES SHOWING ESTIMATED LIQUEFACTION-INDUCED
LATERAL DISPLACEMENTS WITH DEPTH FOR THE THREE SITES AT THE
MOSS LANDING CASE HISTORY**

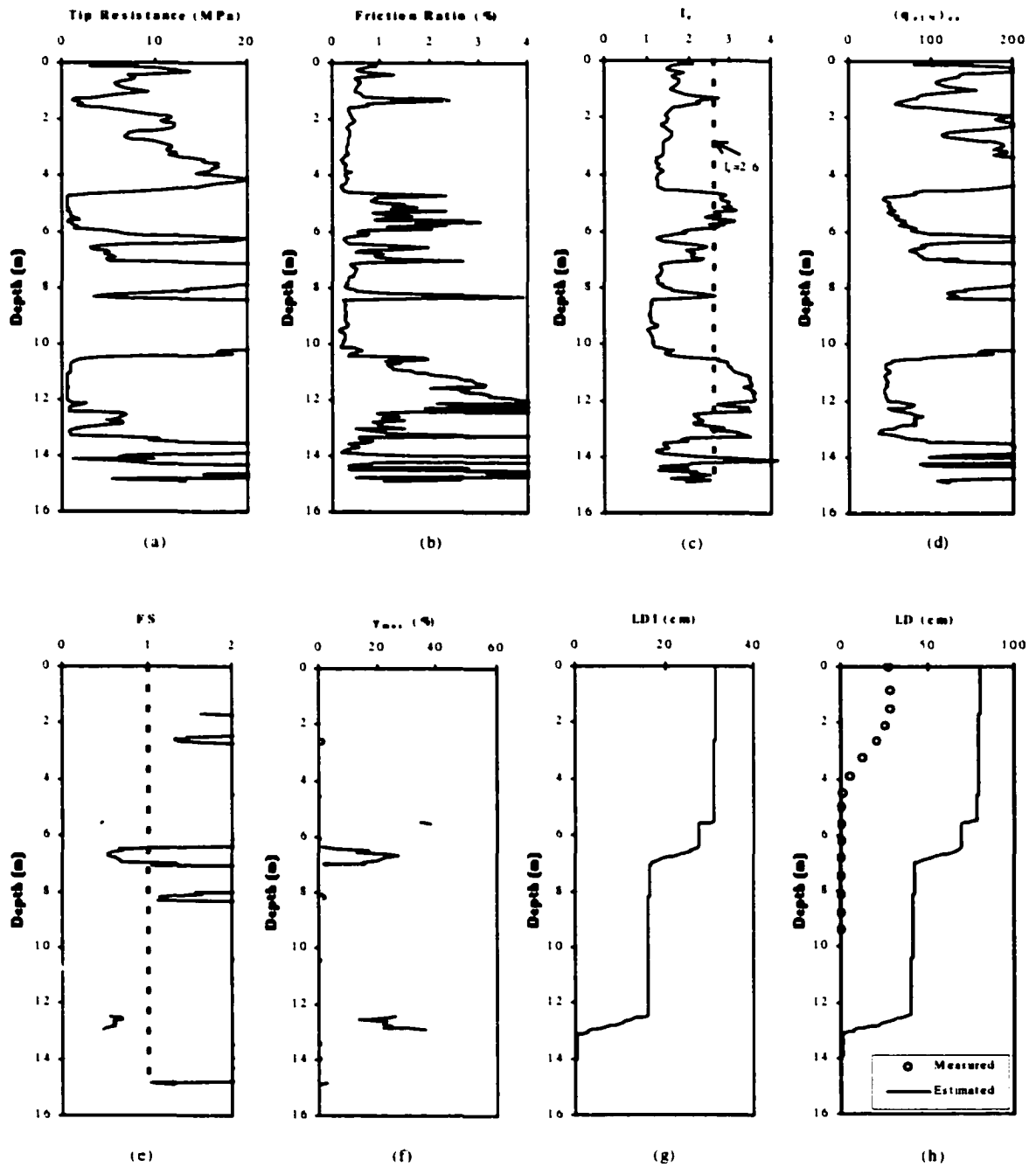


Figure B1 Liquefaction potential analysis using the NCEER CPT-based method and CPT data from CPT UC-3 and comparison of the estimated profile of lateral displacement with depth with the measured one by the inclinometer SI-2 (16m to UC-3) at Moss Landing

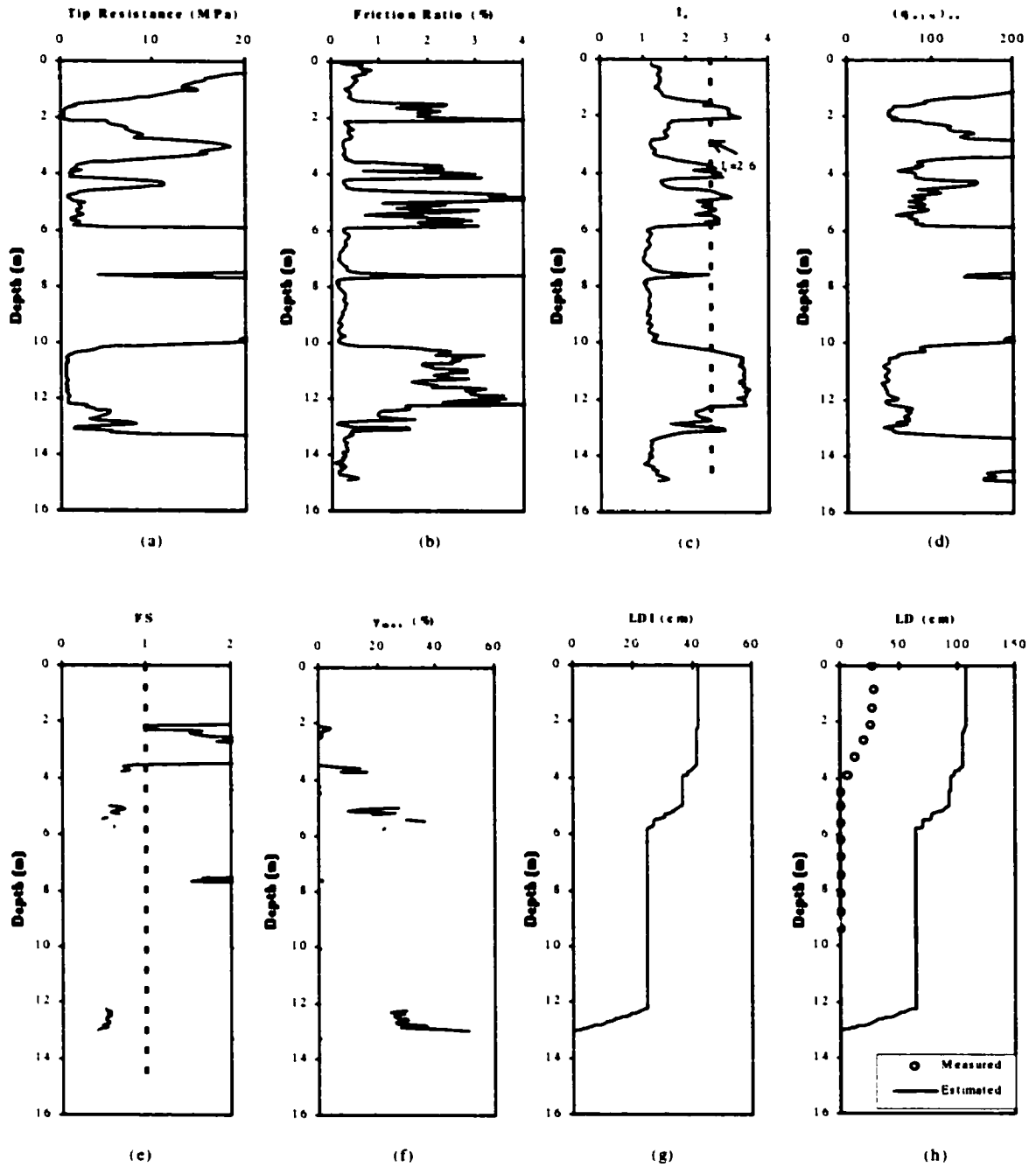


Figure B2 Liquefaction potential analysis using the NCEER CPT-based method and CPT data from CPT UC-4 and comparison of the estimated profile of lateral displacement with depth with the measured one by the inclinometer SI-2 (close to UC-4) at Moss Landing

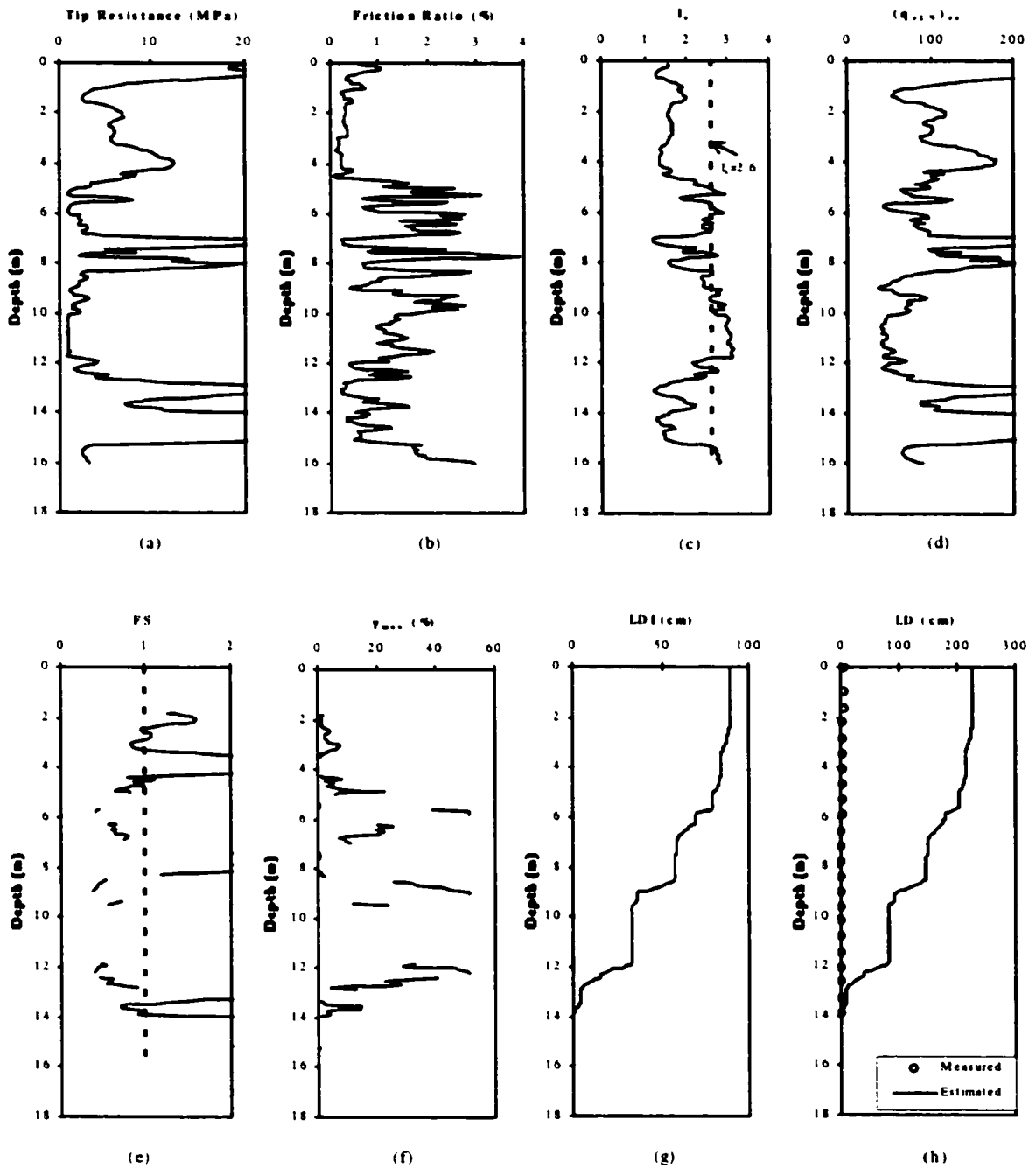


Figure B3 Liquefaction potential analysis using the NCEER CPT-based method and CPT data from CPT RC-1 and comparison of the estimated profile of lateral displacement with depth with the measured one by the inclinometer SI-4 (close to RC-1) at Moss Landing

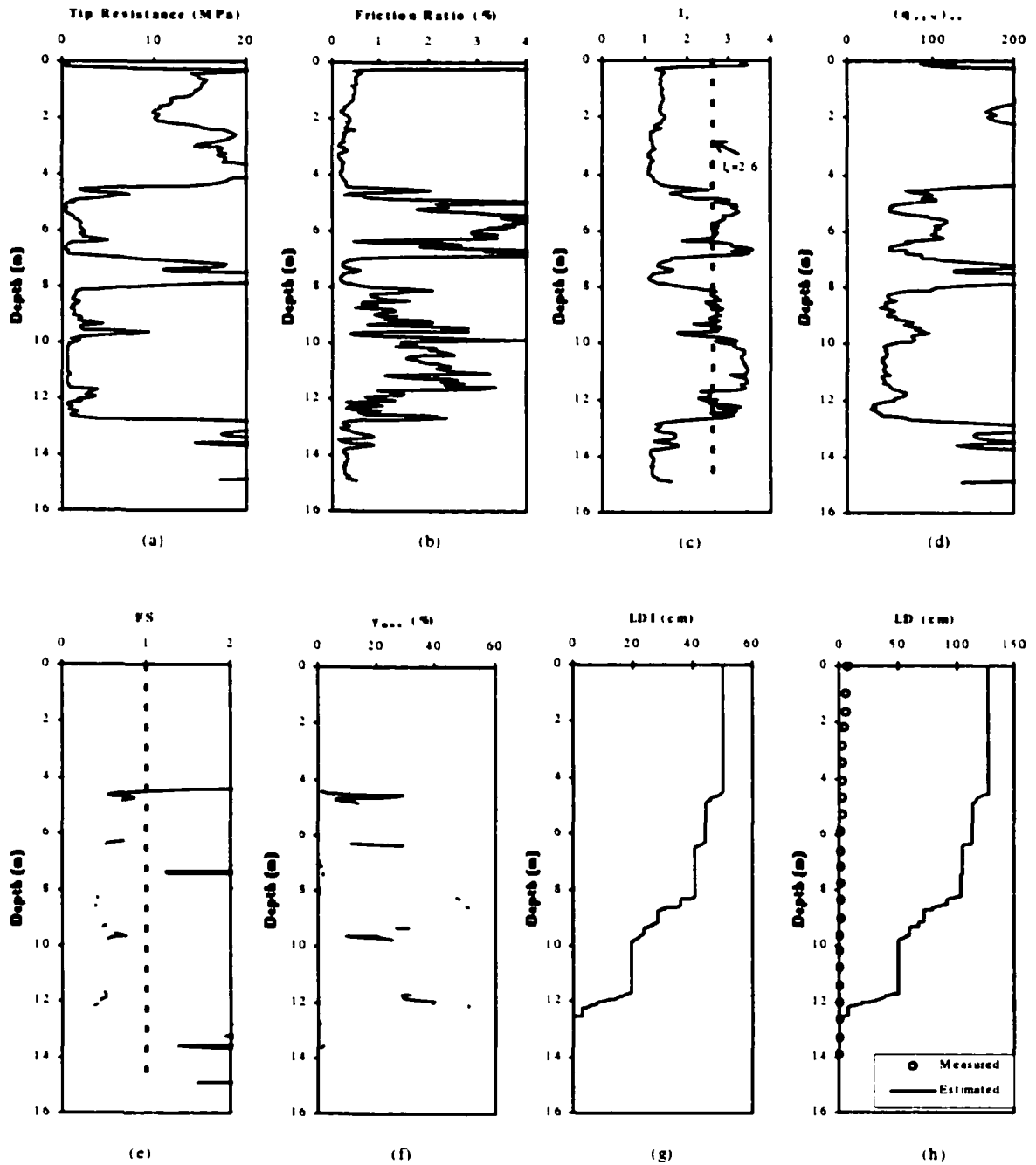


Figure B4 Liquefaction potential analysis using the NCEER CPT-based method and CPT data from CPT UC-2 and comparison of the estimated profile of lateral displacement with depth with the measured one by the inclinometer SI-4 (13 m to UC-2) at Moss Landing

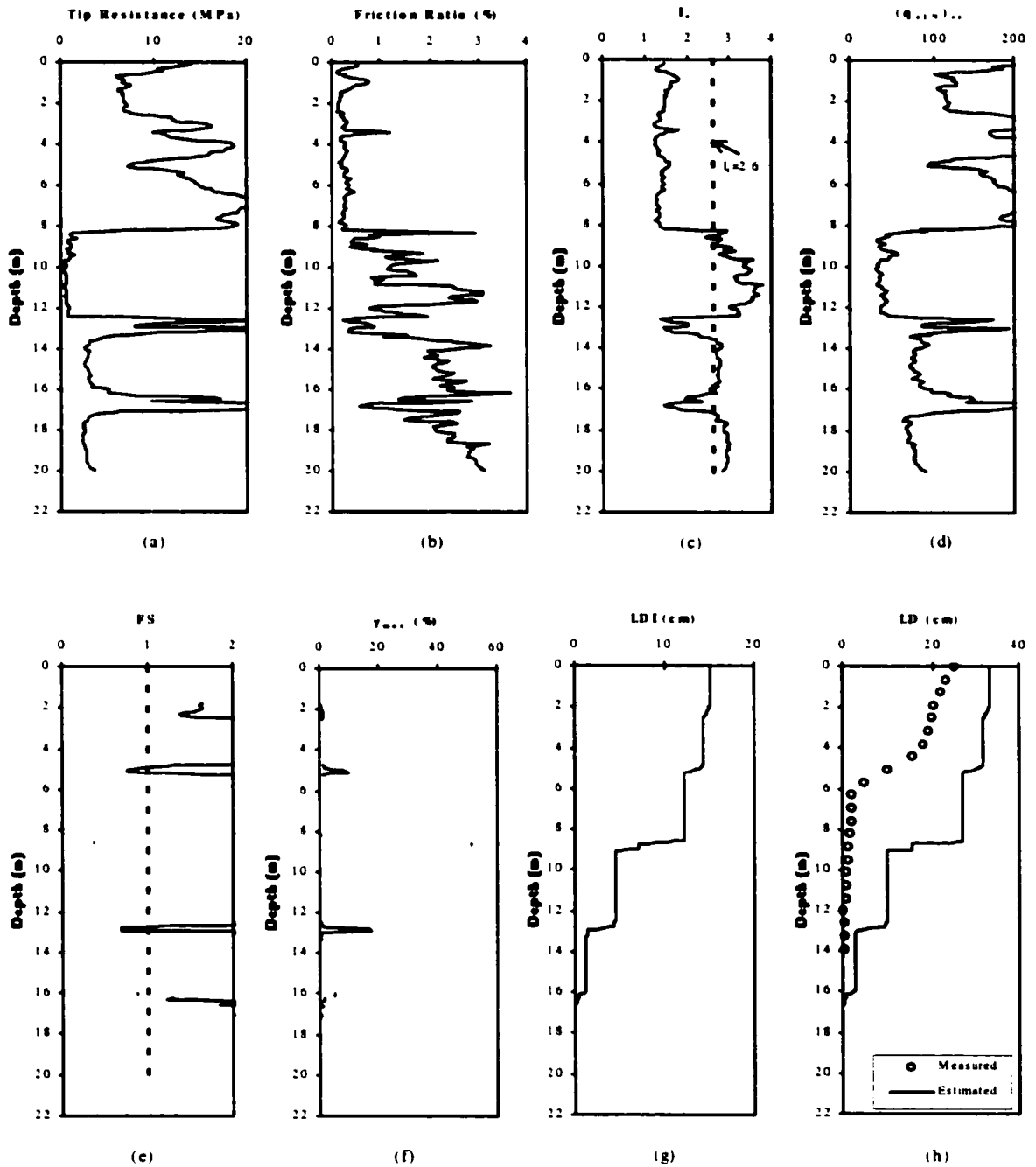


Figure B5 Liquefaction potential analysis using the NCEER CPT-based method and CPT data from CPT RC-4 and comparison of the estimated profile of lateral displacement with depth with the measured one by the inclinometer SI-5 (close to RC-4) at Moss Landing

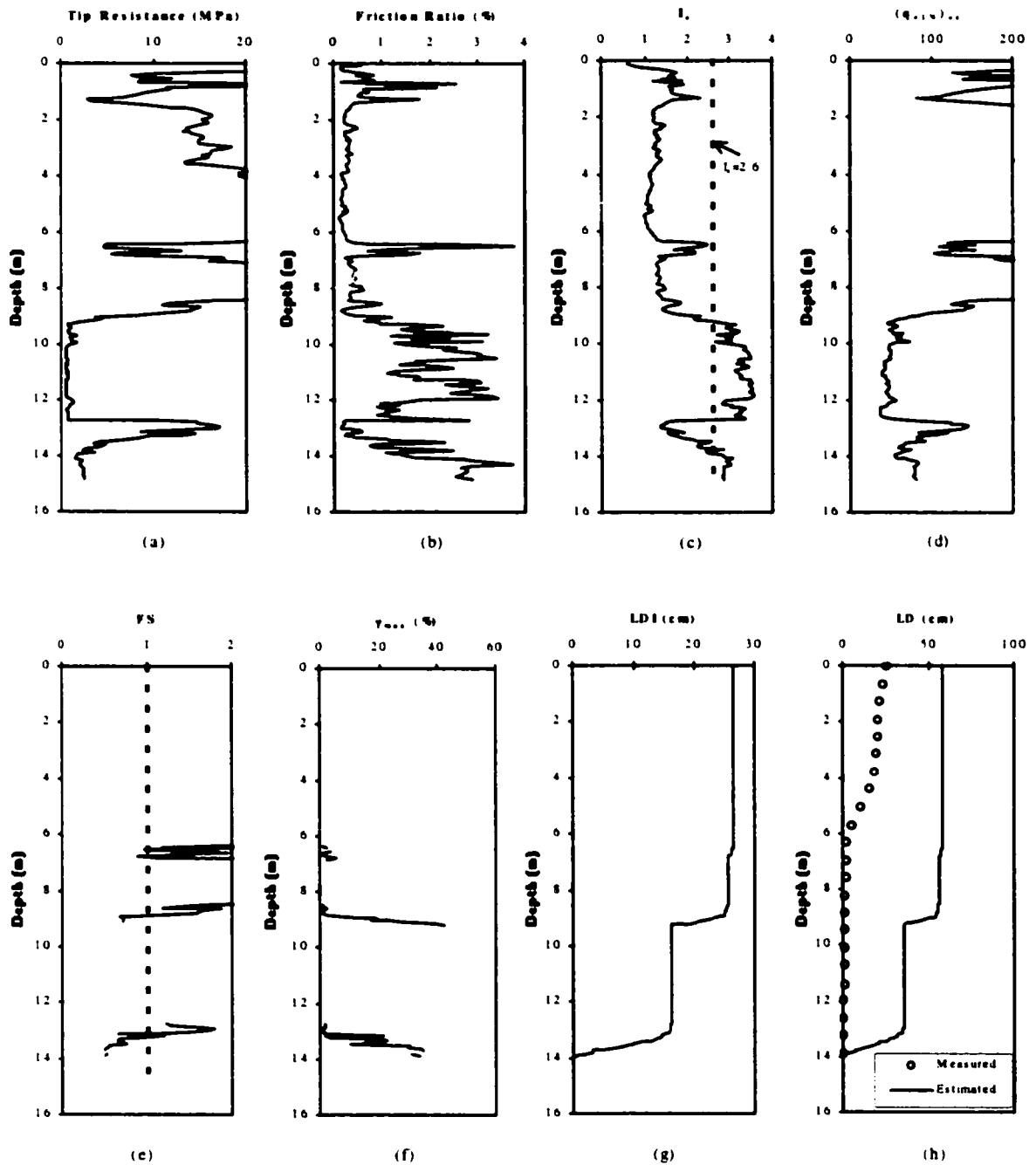


Figure B6 Liquefaction potential analysis using the NCEER CPT-based method and CPT data from CPT UC-5 and comparison of the estimated profile of lateral displacement with depth with the measured one by the inclinometer SI-5 (close to UC-5) at Moss Landing